



UNIVERSITAT
POLITÈCNICA
DE VALÈNCIA

Departamento de Máquinas y Motores Térmicos

DOCTORAL THESIS:

**“Methodology for the Numerical
Characterization of a Radial
Turbine under Steady and
Pulsating Flow”**

Presented by: D. PABLO FAJARDO
Supervised by: DR. D. JOSÉ GALINDO

in fulfillment of the requisites for the degree of

Doctor of Philosophy

Valencia, July 2012

PhD. Thesis

**“Methodology for the Numerical Characterization of a Radial
Turbine under Steady and Pulsating Flow”**

AUTHORS

Presented by: D. PABLO FAJARDO
Supervised by: DR. D. JOSÉ GALINDO

DEFENSE COMMITTEE

Chairman: DR. D. JOSÉ MARÍA DESANTES FERNÁNDEZ
Secretary: DR. D. PEDRO ACISCLO RODRÍGUEZ AUMENTE
Members: DR. D. JESÚS LÓPEZ DÍEZ
DR. D. JESÚS MARÍA FERNÁNDEZ DEL ORO
DR. D. GREGORIO LÓPEZ JUSTE

Valencia, July 2012

Abstract

The increasing use of turbochargers is leading to an outstanding research to understand the internal flow in turbomachines. In this frame, computational fluid dynamics (CFD) is one of the tools that can be applied to contribute to the analysis of the fluid-dynamic processes occurring in a turbine. The objective of this thesis is the development of a methodology for performing simulations of radial turbomachinery optimizing the available computational resources. This methodology is used for the characterization of a vaned-nozzle turbine under steady and pulsating flow conditions.

An important effort has been devoted in adjusting the case configuration to maximize the accuracy achievable with a certain computational cost. Concerning the cell size, a local mesh independence analysis is proposed as a procedure to optimize the distribution of cells in the domain, thus allowing to use a finer mesh in the most suitable places. Particularly important in turbomachinery simulations is the influence of the approach for simulating rotor motion. In this thesis two models have been compared: *multiple reference frame* and *sliding mesh*. The differences obtained using both methods were found to be significant in off-design regions. Steady flow CFD results have been validated against global measurements taken on a gas-stand.

The modeling of a turbine, installed either on a turbocharger test rig or an engine, requires the calculation of the flow in the ducts composing the system. Those ducts could be simulated assuming a one-dimensional (1D) approximation, and thus reducing the computational cost. In this frame of ideas, two CFD boundary conditions have been developed. The first one allows performing coupled 1D-3D simulations, communicating the flow variables from each domain through the boundary. The second boundary condition is based in a new formulation for a stand-alone anechoic end, which intends to represent the flow behavior of an infinite duct.

Finally, the turbine was simulated under engine-like pulsating conditions. The pulsating effects are analyzed separately in the different components of the turbine and are compared with the results obtained in equivalent steady simulations, in order to evaluate their quasi-steadiness. The information from the computations is used to describe the unsteady flow in the turbine components, and thus, contribute to engine modeling by the implementation of a new turbine model for its use in 1D codes.

Resumen

La alta implantación de la sobrealimentación está propiciando un enorme avance en la comprensión del flujo interno en turbomaquinas . La mecánica de fluidos computacional (CFD) es una de las herramientas que pueden aplicarse para contribuir al análisis de los fenómenos fluido-dinámicos en la turbina. El objetivo de la presente tesis es el desarrollo de una metodología para realizar simulaciones de turbomaquinaria radial, optimizando los recursos computacionales disponibles. Esta metodología se emplea para caracterizar una turbina con un estator alabeado en condiciones de flujo estacionario y pulsante.

Se ha dedicado un esfuerzo importante a la optimización de la configuración del caso para conseguir maximizar la precisión alcanzable con un cierto coste computacional. Respecto al tamaño de malla, se ha propuesto un análisis local de independencia de malla como procedimiento para optimizar la distribución de celdas en el dominio, permitiendo el uso de un mallado más fino donde sea más eficiente. De especial importancia en simulaciones de turbomaquinaria es la influencia del método escogido para el movimiento del rotor. En esta tesis se han comparado dos modelos: *multiple reference frame* y *sliding mesh*. Las diferencias encontradas entre ambos son significativas principalmente en condiciones fuera de diseño. Los resultados obtenidos para flujo estacionario se han validado frente a medidas adquiridas en un banco de ensayos.

El modelado de una turbina, ya esté instalada en un banco de ensayos o en motor, requiere calcular los conductos que componen el sistema. Los cuales pueden ser calculados empleando aproximaciones unidimensionales (1D) lo que reduce el coste computacional. Por esta razón, se han desarrollado dos condiciones de contorno para su uso en CFD. La primera de ellas permite realizar cálculos acoplados 1D-3D, mediante la transferencia de las variables fluidas a través de la frontera entre los dominios. En la segunda se presenta una nueva formulación para una condición de contorno anecoica.

Por último, la turbina se ha simulado en condiciones pulsantes similares a las que aparecen en motor. Con ello se analizan los efectos pulsantes por separado en cada componente de la turbina y se comparan con los resultados de simulaciones estacionarias equivalentes, con el objetivo de evaluar su cuasi-estacionariedad. La información obtenida de las simulaciones permite contribuir al modelado de motores mediante el desarrollo de un nuevo modelo de turbina para su empleo en códigos 1D.

Resum

L'alta implementació de la sobrealimentació està propiciant un enorme avanç en la comprensió del flux intern en turbomàquines. La mecànica de fluids computacional (CFD) és una de les eines que poden aplicar-se per a contribuir a l'anàlisi dels fenòmens fluid-dinàmics en la turbina. L'objectiu de la present tesi és el desenvolupament d'una metodologia per a realitzar simulacions de turbomaquinària radial, optimitzant els recursos computacionals disponibles. Aquesta metodologia s'empra per a caracteritzar una turbina amb un estator amb àleps en condicions de flux estacionari i polsant.

S'ha dedicat prou esforç a l'optimització de la configuració del cas per a aconseguir maximitzar la precisió que es pot esbrinar amb un cert cost computacional. Respecte a la grandària de la malla, s'ha proposat un anàlisi local d'independència de malla a mena de procediment per a optimitzar la distribució de les cel·les al domini, permetent l'ús d'un mallatge més fi on siga més eficient. D'especial importància en simulacions de turbomaquinària és la influència del mètode elegit per al moviment del rotor. En aquesta tesi s'han comparat dos models: *multiple reference frame* i *sliding mesh*. Les diferències encontrades entre ambdós són significatives principalment en condicions fora de disseny. Els resultats obtinguts per a flux estacionari s'han validat front a mesures adquirides a un banc d'assajos.

El modelatge d'una turbina, ja siga instal·lada a un banc d'assajos o en un motor, requereix el càlcul del flux intern dels conductes que componen el sistema. Els quals poden ser calculats emprant aproximacions unidimensionals (1D) cosa que redueix el cost computacional. Per aquesta raó, s'han desenvolupat dues condicions de contorn per al seu ús en CFD. La primera d'elles permet realitzar càlculs acoblats 1D-3D, mitjançant la transferència de les variables fluïdes a través de la frontera entre els dos dominis. En la segona se presenta una nova formulació per a una condició de contorn anecoica que funciona de manera autònoma.

Per últim, la turbina s'ha simulat en condicions polsants similars a les que apareixen en motor. D'aquesta manera s'analitzen els efectes polsants per separat en cada component de la turbina i se comparen amb els resultats de simulacions estacionàries equivalents, amb l'objectiu d'avaluar la seua quasi-estacionareitat. La informació obtinguda de les simulacions permet contribuir al modelatge de motors mitjançant el desenvolupament d'un nou model de turbina per a emprar-lo en codis 1D.

Acknowledgments

It is quite difficult to individually thank every single person that has collaborated or supported me during this period.

I would like to thank CMT-Motores Térmicos and Universitat Politècnica de València as for allowing me to become part of this research group. Also, I would like to thank all the people from this department and the rest of people that I have worked with.

Special thanks to Prof. Galindo for his guidance and support and to Roberto Navarro, my officemate, for his help, support, company, and the *useful* (at least most of the times) technical discussions. We have learned a lot together. I am also indebted to my evaluation committee members for their helpful comments.

During this endeavor the presence of some special people has helped me to overcome the gloomiest times and hardest days in these last years. One person in particular deserves to be cited here... *ella lo sabe*. I would like to thank my family and friends for always being there.

Valencia, July 2012.

*“To everyone who has helped me in one way or another to be successful in
this project.”*

Contents

1	Introduction	1
1.1	Introduction	2
1.1.1	CFD codes	3
1.1.2	Turbomachinery modeling	4
1.2	Objectives	6
1.3	Methodology	7
	Chapter 1 bibliography	11
2	Set-up analysis and optimization of numerical simulations for radial turbines	13
2.1	Introduction	14
2.1.1	CFD in turbomachinery	14
2.2	Computational methodology. Definition of a reference case. . .	16
2.2.1	Experimental methodology	17
2.2.2	Computational domain	21
2.2.3	Boundary conditions	23
2.2.4	Wheel rotation strategies	24
2.2.5	Viscous model	25
2.3	Mesh independence	27
2.3.1	Volute	29
2.3.2	Stator	30
2.3.3	Rotor	33
2.3.4	Outlet section	36
2.3.5	Final considerations and selected mesh	37
2.4	Set-up Comparison	40
2.4.1	Type of solver	40
2.4.2	Mesh motion strategy	43
2.4.3	Temporal discretization	46
2.5	Summary of the results: Turbine map	49

2.6	Summary and conclusions	51
	Chapter 2 bibliography	59
3	Implementation of a 1D-3D coupling computational fluid dynamic boundary condition	61
3.1	Introduction	62
3.2	Coupling methodology	64
	3.2.1 The method of characteristics	64
	3.2.2 Homentropic flow	67
	3.2.3 Non-Homentropic flow	67
3.3	Implementation	68
	3.3.1 OpenWAM	69
	3.3.2 ANSYS-FLUENT	70
3.4	Validation	71
	3.4.1 Sod's problem	71
	3.4.2 Impulse test rig	72
3.5	Conclusions	76
	Chapter 3 bibliography	78
4	Development of an anechoic boundary condition for compu- tational fluid dynamic codes	79
4.1	Introduction	80
4.2	Non-reflecting boundary conditions	82
	4.2.1 Assessment of NRBCs available in ANSYS-FLUENT . .	83
	4.2.2 Implementing a boundary condition in a CFD commer- cial code	86
4.3	Proposal of a new non-reflecting boundary condition for non- homentropic flow	89
	4.3.1 Modifications for non-homentropic flow	89
	4.3.2 Implementation of an anechoic condition	90
	4.3.3 Incident pressure condition	94
4.4	Application to the analysis of the acoustic response of a muffler	95
	4.4.1 Experimental facility	95
	4.4.2 Full three-dimensional simulation	96
	4.4.3 Proposed Methodology	97
4.5	Summary and conclusions	99
	Chapter 4 bibliography	105

5	Analysis of the influence of real flow effects in computational fluid dynamics boundary conditions based on the method of characteristics	107
5.1	Introduction	108
5.2	Non-perfect gas	109
5.3	Viscous flow	110
5.4	Swirling flow	114
5.5	Possible applications of the developed boundary conditions . .	118
5.5.1	Anechoic BC	118
5.5.2	Coupled 1D-3D simulation	118
5.6	Conclusions	120
	Chapter 5 bibliography	123
6	Computational analysis of pulsating flow in radial turbomachinery and its application to engine modelling	125
6.1	Introduction	126
6.2	Computational methodology and steady flow results	127
6.3	Pulsating flow results	129
6.3.1	Overall behavior	130
6.3.2	Local behavior of the different components	131
6.4	Discussion of results	133
6.5	Application to engine modeling	139
6.5.1	Proposed model	141
6.5.2	Model calibration	146
6.5.3	Pulsating results	147
6.6	Conclusions	151
	Chapter 6 bibliography	155
7	Conclusions and future works	157
7.1	Conclusions	158
7.1.1	Computational methodology: Case configuration	158
7.1.2	Developed boundary conditions	161
7.1.3	Pulsating flow	163
7.2	Original contributions	165
7.3	Future works	167
	Chapter 7 Bibliography	170
	Global bibliography	171

Appendix 1: UDF code	185
Appendix 2: OpenWAM CFD connection	213

List of symbols

Latin letters

a	sound speed.
A	cross sectional area.
$A(f)$	complex amplitude of the incident pulse.
A_a	entropy level.
c_i	flow velocity in absolute frame in section i .
c_p	specific heat at constant pressure.
c_v	specific heat at constant volume.
C	characteristic line.
$C(f)$	complex amplitude of the transmitted pulse.
D	hydraulic diameter.
f	friction coefficient.
G	specific momentum loss due to friction.
\dot{m}	mass flow rate.
M	mass.
N	rotational speed.
p	pressure.
P	power.
q	specific heat transfer rate.
r	radial coordinate.
R	specific gas constant.
Re	Reynolds number.
s	specific entropy.
S	cross sectional area.
t	time.
Δt	time step size.
T	temperature and torque.
T_T	turbine torque.

TL	transmission loss.
u	axial velocity.
u_τ	friction velocity.
v_θ	tangential velocity.

Greek letters

β	backward Riemann variable (C^-).
β_i	Flow velocity angle in section i .
ϵ	roughness height.
γ	specific heats ratio.
λ	forward Riemann variable (C^+).
ν	cinematic viscosity.
π	pressure ratio.
ρ	density.
τ_w	wall shear stress.

Subscript

b	backward pressure.
f	forward pressure.
eff	effective.
ref	reference.
t	total.
$+$	forward direction.
$-$	backward direction.
0	flow.
∞	value at infinity.
in	value reaching the boundary.

Superscript

$*$	corrected variable.
k	polytropic coefficient for process in the stator.

n polytropic coefficient for process in the rotor.
 N value at the N^{th} time step.

Abbreviations

1D one-dimensional.
3D three-dimensional.
BC boundary condition.
CFD computational fluid dynamics.
ICE internal combustion engine.
MoC method of characteristics.
NRBC non-reflecting boundary condition.

Chapter 1

Introduction

Contents

1.1	Introduction	2
1.2	Objectives	6
1.3	Methodology	7
	Chapter 1 bibliography	11

1.1 Introduction

A COMPRESSIBLE FLOW TURBINE is a flow device that extracts energy from a fluid by expanding it through a stator and rotor system. When the flow passes through the rotor, it has a high tangential velocity that causes the rotation of the blades. The fluid can be a gas or a liquid depending on the applications. Turbines, depending of their geometry, can be classified in various types: axial, radial, or mixed flow ones, are used in all kinds of power-plants. Different scales of turbines are used, from the large turbines usually used in aircraft propulsion or the steam turbines for electricity generation to the smaller ones used in micro gas turbines. The most common application of radial turbomachinery is probably as part of a turbocharger for internal combustion engines (ICEs).

In the last decades, the legislation on internal combustion engines has severely reduced the limits for pollutant and noise emissions. This fact, combined with the necessity to keep production costs bounded, has driven researchers to optimize the efficiency of ICEs. These requirements have established the research activity at design phase as a key stage in the engine production process. Therefore, an intensive investigation on ICEs has been carried out, focusing on the optimization of performances and fuel consumption. In particular, the improvement of gas exchange processes has been thoroughly investigated [100, 26, 110].

Turbocharging is one of the most important technologies for the automotive industry, and particularly for diesel engines [5]. In an ICE, the energy of the exhaust gases is about 30-40 percent of the chemical energy released by the combustion [85]. These gases are expanded through the turbine of the turbocharger which drives the compressor connected through shaft. The compressor is used to increase the density of the air admitted to the cylinder. Thereby the power output of the engine can be increased or alternatively the engine size can be reduced, without decreasing the power output. This technique is known as *downsizing*. The use of turbochargers allows one to reduce the engine cylinder volume and weight, without reducing the power and torque produced. At the same time, this technology decreases the fuel consumption and reduces emissions [71, 85], which is vital for successfully fulfilling the current restrictions imposed by legislation.

The increasing use of turbochargers is leading to an outstanding develop-

ment of turbocharging technology. For instance, turbine vanes have evolved greatly over the last years, from being just a flat plate to the aerodynamically-shaped profiles used in the most recent designs. Another development in turbochargers industry that has been rapidly introduced in the market are variable geometry turbines (VGT), which improve transient performance of the engine [2, 25]. In order to keep improving the efficiency of turbochargers, it is necessary to understand and fully characterize its internal flow behavior.

Unfortunately, the effect on an ICE performance due to modifications in gas exchange components cannot be predicted beforehand, since the interactions between the acoustic responses of the different elements involved (intake or exhaust systems, turbomachinery, etc.) are quite strong [91, 77]. In this way, the use of computational fluid dynamics (CFD) has helped researchers in understanding flow behavior inside these components [20, 72] and also in allowing predictions of the results of different configurations without the cost of testing them experimentally [9]. CFD simulations allow researchers to understand flow behavior and quantify important flow parameters such as mass flow rates or pressure drops, provided that the CFD tools had been properly validated against experimental results. For reasons such as the aforementioned, CFD simulations have become a valuable tool in helping both the analysis and design of the intake and exhaust systems of an ICE.

1.1.1 CFD codes

The CFD codes are usually used in a wide range of engineering applications. Probably the most used ones are the one-dimensional and the three dimensional CFD models. One-dimensional CFD codes allow to understand global behavior of a flow system in terms of flow rates and pressure, having a good resolution in unsteady compressible problems. These codes solve a simplified version of the fluid flow governing equations in cases that have a dominant direction. Their main advantage is their low computational cost. However, if a good geometrical resolution or a more detailed flow field is needed, 3D simulations become essential. Three-dimensional CFD codes allow one to obtain an accurate solution of the flow field of the studied system, but with a extremely higher computational cost, moreover if non-steady simulations are considered.

CMT-Motores Térmicos has developed a 1D CFD code, particularly design

for the calculation of pressure waves in the intake and exhausts systems of an ICE. OpenWAM is an open source one-dimensional gas dynamic model able to compute the air management of internal combustion engine [79]. The code is based in assuming a one-dimensional flow and neglecting the effect of viscosity. The resulting system of equations is solved in the time domain using a Finite Difference 2-step Lax-Wendroff scheme. The code also includes lumped models to compute the filling and emptying process of other ICE elements as cylinders, plenums, heat exchanges, etc.

Dealing with three-dimensional computations, CMT-Motores Térmicos has experience with several commercial codes. In the current work, the computations have been performed using the code ANSYS-FLUENT. ANSYS-FLUENT is a finite volume code, capable of simulating viscous 3-dimensional flows. ANSYS-FLUENT is used extensively in industries such as automotive, aerospace, chemical, etc. The use of a commercial code has the advantage of having been extensively validated, but it has the inconvenience of its lack of accessibility to the flow variables and to the code itself.

1.1.2 Turbomachinery modeling

As previously commented CMT-Motores Térmicos has a in-house open source 1D code called OpenWAM. This code computes the pipes composing an ICE by means of a discretization of the Navier-Stokes equations. Additionally, the code includes some zero dimensional subcomponents which allow to model the rest of the elements of an ICE, acting as boundary conditions, and thus acquiring the capacity of simulating the behavior of a whole engine. Particularly interesting for this thesis are the models of the compressor [44], and specially, turbine [99]. The turbine model is based on two nozzles in series, separated by an intermediate reservoir, which reproduces mass accumulation in the system. The reaction degree is calculated by means of geometrical parameters and the corrected variables, obtained from the turbine maps. Once reaction degree is determined, the pressure drops produced at the stator and at the rotor can be computed taking into account the turbine efficiency, and the type and the position of the stator vanes. The model has proved to give good results for fixed and variable geometry turbines. As input, the model requires the turbine maps. Those can be supplied by the manufacturer or measured in a turbocharger test rig. CMT-Motores Térmicos has the capability of experimentally testing turbochargers in steady or pulsating flow conditions.

Currently two different types of testing rigs are available, a steady flow test bench which uses a rotary screw compressor or those based in mounting the turbo on a truck engine. The first ones allow testing in steady flow conditions, as it is commonly done by turbomachinery manufacturers. However, pulsating conditions can be achieved using a rotatory valve. On the contrary, the second type allow to test the turbocharger working on engine conditions. The current measurement techniques commonly used in radial turbomachinery only allow obtaining global values of the flow variables, but not a complete description of the flow field. In this frame of ideas, the use of three dimensional CFD turbomachinery computations seems interesting.

For the case of 3D simulations, CMT-Motores Térmicos has experience in this field, mostly on aspects dealing with the air management in cylinder, combustion process, and flow in diesel injectors and jets. However, this thesis is among the firsts works in the group dealing with CFD computations of turbomachinery.

Modeling turbomachinery poses particular problems: their geometrical complexity requires the use of viscous compressible three dimensional (3D) codes to capture the flow behavior properly. Additionally, a mesh motion procedure is needed in order to truthfully reproduce the rotor flow. This mesh motion can be obtained using a steady approach (multiple reference frame) in which the mesh does not really moves or a fully transient procedure (sliding mesh model). The first approach has the advantage of its lower computational cost, but typically unsteady flow effects are missed in the process and can only be captured if the mesh is really moved. However this makes the computational cost even higher, and additionally, an oscillation is induced in the flow variables. These fluctuations travel along the domain, and eventually are reflected when reaching the boundaries. These reflections increase the computational time required to achieve a periodic solution.

Regarding CFD simulation, it is worth clarifying the difference between the type of solver used and the dependence with time of the boundary conditions. The solver can be steady or transient. In a steady solver the equations terms related to the temporal variation are not included, while the transient one does include these terms. If a sliding mesh model is used, then the solver must be transient. However, in a transient simulation the boundary conditions can be either steady or time dependent, depending on whether the turbine is analyzed under steady flow conditions or pulsating conditions.

If the objective of the computation is to obtain the acoustic response of a system the use of long ducts is needed in order to avoid any interference produced by the boundaries. This fact can be easily understood when compared to the experimental procedure used to obtain the acoustic response in an impulse test rig, such as the one simulated in [20]. Including these long ducts in the computational domain leads to a dramatic increase of the computational cost [46].

In this frame, the idea of developing a non-reflecting boundary condition (NRBC) that behaves as a long duct seems interesting. Since the acoustic response of these long ducts is supposed to be the lack of wave reflection, several researchers [87, 7, 29] have tried to develop the so-called non-reflecting or anechoic boundary conditions (BCs), to be able to eliminate these components without any penalty in the accuracy. A similar reasoning can be followed if a turbocharger test rig has to be simulated, in which long ducts are needed in order to have uniform flow at the measurement sections. Their inclusion in the computational domain could represent even doubling the number of cells in some configurations.

1.2 Objectives

Since this is the first thesis in CMT-Motores Térmicos which has as a main core a CFD analysis of turbomachinery, the main objective of the present thesis is to develop a methodology to characterize the behavior of a radial turbine by means of CFD. Additionally, the methodology intends to optimize the use of the current computational resources available, obtaining the best resolution possible and reducing the total computational time required.

A second objective is to analyze the performances of a radial turbine under steady and pulsating flow conditions. The testing at steady flow conditions is the most common procedure followed by turbochargers manufacturers, while pulsating flow is more similar to the real conditions when the turbine is working on a reciprocating engine. The steady flow results are used to validate the numerical procedure and afterwards obtain the pulsating results to have a better understanding of the transient flow effects in the radial turbine.

The main advantage of the use of CFD is that the complete flow field can be analyzed, in contrast to the current experimental measurements, in which

only global variables are obtained. The last objective is the use of this new information available to improve the turbine models that are currently in use, particularly for the transient flow regimen.

1.3 Methodology

Once the main objectives of the thesis have been established, the methodology followed in this thesis is now described.

Since this is the first thesis in the group whose based on CFD computations of turbomachinery, the first task was to develop a methodology of performing those computations using ANSYS-FLUENT. Additionally, an optimization of the case with the objective of obtain the best resolution possible with the available computational resources was conducted. In this frame the computational domain, the mesh and the different configuration models need to be defined as done in chapter 2. In order to evaluate the mesh independence, and thus be able to optimize the cell distribution, an analysis was performed. The different models used in the simulations were described. Particularly, a comparison of the solver types and the moving mesh strategies was shown. In this chapter, an experimental test-stand for turbochargers is also describes. The measurements obtained in this facility are used to evaluate the results obtained with numerical simulations in steady flow conditions.

Generally, the test facilities employed for testing radial turbines have long inlet and outlet ducts. If these ducts need to be simulated, the computational cost can be severely increased. Similar argument might be done if a simulation of the turbine installed in a complete engine model is required. Due to the expected one-dimensionality of the internal flow in the ducts and the availability on a one-dimensional numerical code, which can model a whole turbine, as OpenWAM, the development of a boundary condition to connect the 3D domain in ANSYS-FLUENT with the domain in OpenWAM seems interesting. The use of this boundary condition will allow to perform 1D-3D coupled computations, where good geometrical resolution is achieved where required, while the rest of the domain can be computed using a less computationally expensive code. The development and implementation of this boundary condition is presented in chapter 3. Following the same criteria, some problems can be found in which the modeling of a semi-infinite duct could be interesting. This could be the case of the analysis of the acoustic response of a system,

in which the reflections of the pressure waves at the boundaries need to be avoided. In this case, the use of a so-called anechoic or non-reflecting boundary condition could reduce the computational requirements of the simulation. The non-reflecting conditions available in ANSYS-FLUENT were assessed and afterwards a new formulation has been proposed and implemented in chapter 4. The two developed boundary conditions are based in the method of characteristics. However, their use of this method relies on some assumptions that are not always fulfilled in turbomachinery simulations. Therefore, an analysis of the influence of real flow effects on them was conducted in chapter 5. The computational tools developed in this thesis could be used to optimize the use of the requirements of a simulation, allowing to increase the effort in the most interesting regions of the domain and reducing the resources needed in the rest on them.

The turbine has been characterized under steady flow conditions in chapter 2, as it has been traditionally done for testing turbomachinery. This tradition probably comes from the aeronautic field, where it is common to obtain the performance of turbomachinery under these conditions. However, when the turbine is installed in a reciprocating engine, the flow at the turbine inlet is modulated by the piston movement. In order to evaluate the behavior of the turbine under pulsating conditions, numerical simulations using sinusoidal pressure pulses at the inlet are presented in chapter 6. These data are used to increase the knowledge of the unsteady internal flow in the turbine, and in this way, contribute to radial turbine modeling.

Finally, in chapter 7 the main contributions and conclusions of the thesis are summarized. These conclusions lead to a series of future work to continue with the current research in turbomachinery modeling. For the sake of clarity and to make easier the review of the bibliography, the references cited on each chapter are collected at the end of the respective chapter in order of appearance; while the whole bibliography is included in alphabetic order after chapter 7. The code developed implementing the boundary conditions presented in chapters 3 and 4 is included as appendix at the end of the present document.

Chapter Bibliography 1

- [2] J. Andersen, E. Karlsson, and A. Gawell. “Variable turbine geometry on SI engines”. In: *SAE 2006 World Congress*. SAE 2006-01-0020. 2006 (cit. on pp. 3, 16).
- [5] E. Arcaklioglu and I. Çelikten. “A diesel engine’s performance and exhaust emissions”. In: *Applied Energy* 80.1 (2005), pp. 11–22 (cit. on p. 2).
- [7] O. V. Atassi. “Nonreflecting boundary conditions for the time-dependent convective wave equation in a duct”. In: *Journal of Computational Physics* 197.2 (2004), pp. 737–758. ISSN: 0021-9991 (cit. on pp. 6, 81, 108).
- [9] N. C. Baines. “A meanline prediction method for radial turbine efficiency”. In: *6th International Conference on Turbocharging and Air Management Systems, I Mech E*. C554-6. Concepts ETI, Inc. Institution of Mechanical Engineers, 1998 (cit. on p. 3).
- [20] A. Broatch, X. Margot, A. Gil, and F. D. Denia. “A CFD Approach to the Computation of the Acoustic Response of Exhaust Mufflers”. In: *Journal of Computational Acoustic* 13.2 (2005), pp. 301–316. DOI: 10.1142/S0218396X05002682 (cit. on pp. 3, 6, 72, 80, 95, 97).
- [25] H. Chen. “Turbine wheel design for Garrett advanced variable geometry turbines for commercial vehicle applications”. In: *8th International Conference on Turbochargers and Turbocharging, Institution of Mechanical Engineers*. 2006 (cit. on pp. 3, 16).
- [26] C. D. Copeland, R. Martinez-Botas, and M. Seiler. “Comparison Between Steady and Unsteady Double-Entry Turbine Performance Using the Quasi-Steady Assumption”. In: *Journal of Turbomachinery* 133 (2011), pp. 031001–1/031001–10 (cit. on pp. 2, 126, 130).
- [29] J. R. Dea, F. X. Giraldo, and B. Neta. “High-order non-reflecting boundary conditions for the linearized 2-D Euler equations: No mean flow case”. In: *Wave Motion* 46.3 (2009), pp. 210–220 (cit. on pp. 6, 81, 108).
- [44] J. Galindo, JR Serrano, H. Climent, and A. Tiseira. “Experiments and modelling of surge in small centrifugal compressor for automotive engines”. In: *Experimental Thermal and Fluid Science* 32.3 (2008), pp. 818–826 (cit. on p. 4).

- [46] J. Galindo, A. Tiseira, P. Fajardo, and R. Navarro. “Coupling methodology of 1D finite difference and 3D finite volume CFD codes based on the Method of Characteristics”. In: *Mathematical and Computer Modelling* 54.7-8 (2011), pp. 1738–1746. DOI: <http://dx.doi.org/10.1016/j.mcm.2010.11.078> (cit. on pp. 6, 15, 62, 81, 88, 93, 112, 118, 167).
- [71] K. Mollenhauer and H. Tschoeke. *Handbook of Diesel Engines*. Springer, 2010 (cit. on p. 2).
- [72] G. Montenegro and A. Onorati. “Modeling of Silencers for IC Engine Intake and Exhaust Systems by Means of an Integrated 1D-multiD Approach”. In: *SAE International Journal of Engines* 1.1 (2009), p. 466. DOI: 10.4271/2008-01-0677 (cit. on pp. 3, 62, 80).
- [77] M. L. Munjal. *Acoustics of ducts and mufflers with application to exhaust and ventilation system design*. Wiley-Interscience, 1987. ISBN: 0471847380 (cit. on pp. 3, 95).
- [79] OpenWAM. CMT- Motores Térmicos. Universidad Politécnica de Valencia. URL: <http://www.OpenWAM.org> (cit. on pp. 4, 14, 63, 87, 98).
- [85] F. Payri and J. M. Desantes, eds. *Motores de combustión interna alternativos*. Reverté, 2011 (cit. on p. 2).
- [87] F. Payri, J. M. Desantes, and A. J. Torregrosa. “Acoustic boundary condition for unsteady one-dimensional flow calculations”. In: *Journal of Sound and Vibration* 188.1 (1995), pp. 85–110. ISSN: 0022-460X (cit. on pp. 6, 15, 83, 87, 108).
- [91] K. S. Peat, A. J. Torregrosa, A. Broatch, and T. Fernández. “An investigation into the passive acoustic effect of the turbine in an automotive turbocharger”. In: *Journal of Sound and Vibration* 295.1-2 (2006), pp. 60–75 (cit. on p. 3).
- [99] J. R. Serrano, F. J. Arnau, V. Dolz, A. Tiseira, and C. Cervelló. “A model of turbocharger radial turbines appropriate to be used in zero-and one-dimensional gas dynamics codes for internal combustion engines modelling”. In: *Energy Conversion and Management* 49.12 (2008), pp. 3729–3745 (cit. on pp. 4, 120, 141, 144, 149).

- [100] J. R. Serrano, F. J. Arnau, P. Piqueras, A. Onorati, and G. Montenegro. “1D gas dynamic modelling of mass conservation in engine duct systems with thermal contact discontinuities”. In: *Mathematical and Computer Modelling* 49.5-6 (2009), pp. 1078–1088. DOI: 10.1016/j.mcm.2008.03.015 (cit. on pp. 2, 64, 69).
- [110] M. Tancrez, J. Galindo, C. Guardiola, P. Fajardo, and O. Varnier. “Turbine adapted maps for turbocharger engine matching”. In: *Experimental Thermal and Fluid Science* 35.1 (2011), pp. 146–153. DOI: 10.1016/j.expthermflusci.2010.07.018 (cit. on p. 2).

Chapter 2

Set-up analysis and optimization of numerical simulations for radial turbines

Contents

2.1	Introduction	14
2.2	Computational methodology. Definition of a reference case.	16
2.3	Mesh independence	27
2.4	Set-up Comparison	40
2.5	Summary of the results: Turbine map	49
2.6	Summary and conclusions	51
	Chapter 2 bibliography	59

2.1 Introduction

OVER THE LAST YEARS, researchers have focused in trying to understand the fluid dynamic processes in a turbomachine [55, 11]. The research can be done in two different ways: experimental or computational. Experimental research is carried out by testing the turbo in a test rig [43, 106, 96]. Other researchers use CFD in order to analyze and understand the internal flow in the turbine [53], therefore it is becoming a valuable tool for studying this kind of systems [119]. There have been some studies in order to characterize the internal flow in a radial turbine under steady flow conditions [31, 112, 51]. In order to increase the efficiency of radial turbines some improvements are used as the variable geometry stator, which allow having a better performance in a wider flow range [53].

There are 0D-1D models which allow to simulate a fluid system obtaining good temporal response even in supersonic regime [79, 88]. However there are some conditions in which a good geometrical resolution is needed and therefore 3D simulations are needed. 3D-CFD codes allow to obtain an accurate solution of the flow field of the studied system, but with considerable computational cost [1, 102]. In this chapter, a methodology to configure the computational case of a turbine is presented, focusing on the definition of the computational model, in terms of meshing, mesh movement algorithm and computational algorithm.

In this chapter, an analysis of the main works found on CFD in turbomachinery are analyzed next. Afterwards the procedures followed to define the case configuration used are presented.

2.1.1 CFD in turbomachinery

CFD is a valuable tool for researchers in all disciplines of fluid mechanics and particularly in turbomachinery. Its use is growing constantly due to the advances in development of numerical methods and computational power. However, concerning the design process of a new turbomachine, the direct use of CFD tools is still unfeasible with the current computational capabilities [6]. The problem of designing a turbine (or the optimization of an existing one) reduces to the selection of reasonable values for the different geometric parameters. Nowadays the know-how of the designer is still the main tool for

designing and optimizing turbomachines [123, 10].

Generally, 1D approaches to design and analyze turbomachines can be considered well adapted and powerful enough for most applications, such as turbocharger matching with the ICE. However, design and research are reaching a point in which it is necessary to fully understand the internal flow of the turbine. In the literature, there are some papers showing a good correspondence between CFD computations and experimental results [28, 112, 102, 58]. It is possible to find more works concerning CFD in turbomachinery, Blanco-Marigorta et al. [16] studied the influence of the volute geometry and relative position between impeller and volute casing by means of an unsteady simulation, but with steady boundary conditions, using FLUENT. Palfreyman et al. studied the aerodynamic characteristics of a mixed-flow turbine [81, 97] or other CFD works on radial turbomachines [51].

When turbochargers are tested in an experimental rig, long ducts at the inlet and exit are needed, mainly when it comes to pulsating flow, in order to avoid spurious reflections on the boundaries and being able to decompose the pressure waves depending on their traveling direction [87]. In the same way, long distances are needed in the computational model, increasing the size of the mesh and therefore the computational requirements. There are some situations in which the turbomachine works at highly unsteady conditions, requiring transient simulations, which increase the computational cost furthermore. In this case, it is necessary to simulate enough time in order to allow the different pressure waves to cross the domain. In order to minimize computational requirements the idea of performing 1D-3D co-simulations seems clear [46], which allows to simulate a complex system by using 3D simulations just in the zones of the domain where it is needed, while keeping most of the piping system with a 1D model.

The objective of this chapter is to optimize the set-up of a 3D simulation for a turbocharger turbine in order to maximize the efficiency of the computations, that is, to achieve the higher resolution possible with the available computational resources. A second objective could be to present a list of good working practices to perform CFD simulations in turbomachinery for industry. Different aspects must be considered. An introduction of the uses of CFD in turbomachinery has been presented. The first thing that must be analyzed when dealing with 3D simulations is the geometry considered and more precisely the mesh. The mesh should be fine enough to truthfully reproduce the wanted geometry, this is usually achieved by searching the in-

dependence of the solution with the mesh. This analysis is done later on the chapter. A commercial code as ANSYS-FLUENT has different discretization schemes implemented. A discussion on them is also presented on the chapter. A CFD turbomachinery simulation must also deal with other models as the viscous model and more importantly in the case of rotating machines, the mesh movement model, which will be also analyzed and discussed. As part of this methodology, the results obtained in the simulation should be compared with experimental result, in order to check, at least in a global way, the validity of the simulation.

2.2 Computational methodology. Definition of a reference case.

In this chapter, 3D CFD simulations have been performed using the real geometry of a Garret GT15 Turbocharger's radial variable geometry turbine. As it was mentioned before, the idea of this chapter is to analyze and optimize the set-up of a 3D CFD simulation of a radial turbine. In this particular case, the simulations have been performed using the commercial code ANSYS-FLUENT. In the process of setting-up the case, there are a lot of different parameters that must be considered, and therefore it seems reasonable to analyze the different effects one at a time. For this reason, a reference case is defined and it is used as reference for the different configurations.

In order to validate the computations some experimental measurements are taken in an experimental test rig, as the one shown in [89]. The experimental methodology is described in 2.2.1 and the measurements will be used in the following sections to calibrate the validity of the simulations. In this work, the computational domain is going to be considered as the one that can be found if the turbine is set in a turbocharger test rig.

The turbine used is a variable geometry turbine (VGT) [2, 25], this fact introduces a new uncertainty in the simulation since it is not clear how to determine the actual aperture of the stator nozzle once the turbine is set in the test rig both at high or low temperatures condition. At low temperatures there is some uncertainty due to the existence of *mechanical play* in the different elements of the mechanism. While at high temperatures the deformation of the elements that form the mechanism is unknown. In addition the existence

of turbine vanes has influence in the operating conditions of the turbine and particularly the interaction between stator and rotor may have some influence in the simulation set-up as it will be commented later on.

In order to determine the requirements of the computational mesh used and to compare the different case set-ups a reference case is defined. In this way the results obtained with the different simulation methodologies could be compared. In this work, all the computations were performed using ideal gas model with variable thermal properties as air model, more information can be found in [4].

In the rest of the current section, the reference case is going to be described. First, the computational domain and the boundary conditions used are described, followed by some comments of two important aspects to deal with when performing turbomachinery simulation as the moving mesh strategy and the viscous model.

2.2.1 Experimental methodology

The test bench in which the experimental data were obtained is similar to the one developed in [24]. This experimental facility is a steady or constant flow test bench which is used to test the whole turbo system. Therefore, this bench is formed by two separated flow lines: the one feeding the turbine at controlled pressure and temperature; and the second is the compressor feeding system.

2.2.1.1 Experimental facility

The turbine line supplies hot and pressurized air flow to the turbine. Air flow is pressurized using a rotary screw compressor, which produces up to $9.84 \text{ m}^3 \cdot \text{s}^{-1}$ at a maximum pressure of 3.5 bar. After the compressor, the air passes through a group of 5 concentric electric resistances of 12.5 kW each. In this way, the generated flow is supplied at a similar thermodynamic conditions to those found in the exhaust manifold of an ICE. The flow passes through the turbine, inducing its rotation, driving the compressor. The compressor takes the air at atmospheric conditions from the inlet duct, and this flow is compressed as it passes through the compressor.

Both lines are instrumented to measure the mass-flow rate passing through

Table 2.1: Characteristic of the measurements sensors in the facility.

Variable	Type	Trade	Model	Range	Accuracy
p	Piezoelec.	Kistler	RA5	0-6 bar -20-85° C	0.1%
	Piezoresist.	Kistler	4053A5	0-5 bar -20-50° C	0.1%
T	Thermoc.	-	K	0-1260° C	0.75%
	Thermores.	-	PT100	-150-300° C	0.5°
\dot{m}	Hot-wire.	Sensyflow	DN150	0-720 kg/h	0.72 kg/h
	Hot-film	Hitachi	AFH70	-	-
N	Eddy c.	Picoturn	BM-V6	≤ 320 krpm -20-230° C	0.009%

them. Additionally, measurements of flow pressure and temperature at the ducts at the inlet and outlet of both compressor and turbine are taken [109]. In the duct at the compressor outlet a valve is set to allow one to modify the compressor operating point (back-pressure). A control system to regulate the power injected to the turbine was developed. The system evaluates power from the measurements of the mass flow rate, the flow thermodynamic variables, and the rotational speed, which is also measured, and thus regulates the inflow conditions.

The flow variables of interest have been: pressure, temperature, mass flow rate, and rotational speed. The main characteristics in terms of range and accuracy of the different measurement sensors used in the facility are shown in table 2.1. Pressure measurements have been taken at different sections of the ducts and using two different types of sensors depending on the required temporal response.

Since the simulations were performed assuming adiabatic walls, when the measurements are taken in the test rig, the turbocharger is insulated to minimize heat losses through the walls. Additionally, to reduce the internal heat transfer some *adiabatic* tests were performed, in which the temperature at the inlet of the turbine, compressor and oil are maintained at a similar value.

The small size of turbocharger turbines, and particularly for the case of the vaned ones, makes difficult the acquisition of measurements of the internal flow variables, and generally only global measures are available. This means that

only pressure ratio, corrected mass-flow rate, rotational speed and enthalpy jump between the inlet and outlet of the turbine are available. The corrected mass flow rate is defined as:

$$\dot{m}^* = \frac{\dot{m} \sqrt{\frac{T_0}{T_{ref}}}}{\frac{p_0}{p_{ref}}}, \quad (2.1)$$

in this work, 101325 Pa and 288.15 K are taken as reference values to compute the corrected mass.

2.2.1.2 Angular position

It is worth to mention again that there exists an additional uncertainty when comparing the measurements and the simulations that is the position of the nozzle vanes of the VGT. The positioning system of the vanes presents some clearance in the mechanism, which introduces some uncertainty in the real position that is being tested. The problem here lays in the impossibility to view the position once the turbine is mounted.

In order to have an estimation of the position of the vanes during the test, a calibrated screw is used to move the rack mechanism of the stator vanes. In this way, the vanes are moved by rotating the screw. The position is then measured via the displacement of the rack. In order to calibrate the model some tests have been done dismounting the turbine, and measuring the vane angle in different positions. Figure 2.1 shows a picture the stator vanes for the most open position. Pictures can be taken at different positions and used to obtain the correspondent position.

The position of the vanes is measured with respect the radial coordinate passing through the rotation axis, as indicated in figure 2.1. The results obtained of the angular position of the vanes versus the rack position are presented in Fig. 2.2.

From the results of the angular position, it seems that a linear trend will fit well the behavior of the positing system. However, some comments about this positioning system should be made. The first one is about the dispersion found in the value of the angle for different stator vanes for a given position, which was of about $\pm 1^\circ$. This effect was not included in the CFD model, in which all the vanes are set at the same angle. The second comment is about the

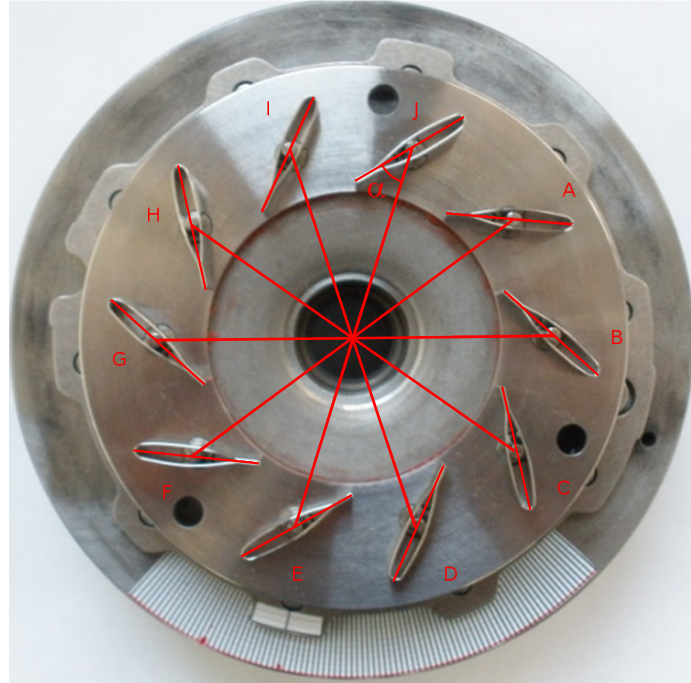


Figure 2.1: Picture of the stator vanes in the most open position. The reference radial direction is indicated for each vane.

previously mentioned mechanical play of the positioning mechanism. Once the position of the screw was set, the vanes cloud still be moved by hand about $\pm 5^\circ$, this means that during the operation the angular position of the vanes might change due to the aerodynamic forces. The mechanism has been probably designed with this play in order to be fixed one the turbine is working in real temperature conditions. The thermal behavior of the different materials increases this uncertainty, since it is not clear that the mechanism works in the same way in hot and cold flow.

All the above reasons introduce an uncertainty when comparing experimental measurements with simulations, and thus will make difficult the validation on the computational results as it will discussed later on. In the following, in order to reduce the number of parameters the stator position was kept constant at a value of 75 %.

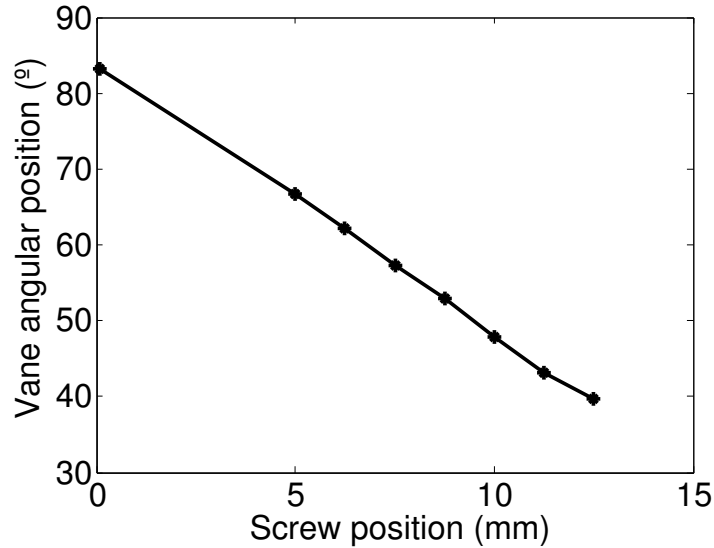


Figure 2.2: Evolution of the angular position of the stator vanes as a function of the position of the screw.

2.2.2 Computational domain

The turbine was considered as it was installed in the turbocharger test rig, as the one showed in [65] so that straight ducts were set at the inlet and at the outlet of the turbine. These ducts are also used to minimize the influence of the computational boundary conditions in the operation of the turbine. In figure 2.3 a sketch of the radial turbine is shown with one of the meshes used in this analysis. In figure 2.3 only part of the domain presenting the turbine is shown. However, as it was mentioned before two straight ducts are used, a 120 mm (about 4 diameters) one upstream of the volute inlet (section 1) and a 500 mm (about 12 diameters) one at the turbine outlet (section 5). Due to the complexity of the system, in the following analyses the turbine is going to be divided in different regions: volute, nozzles, rotor, and outlet. The interfaces between two consecutive regions, which also indicated in figure 2.3, are used as post-processing surfaces. These post-processing surfaces are numbered correlatively as identified in Table 2.2 and are used in all this work to analyze the computational results.

As previously stated, the simulations are performed neglecting the heat

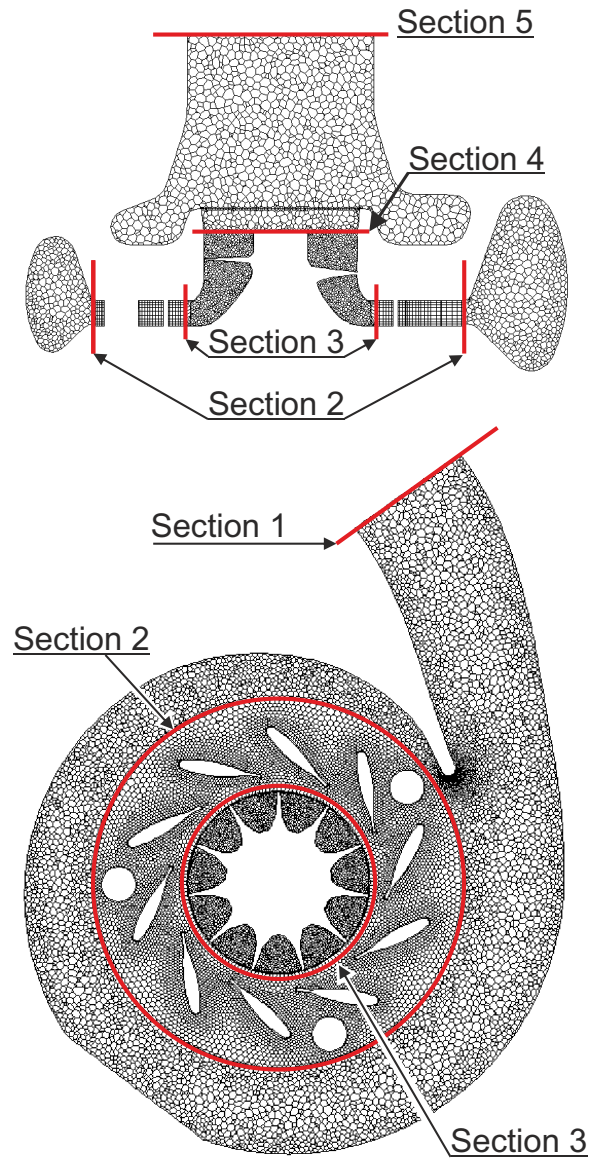


Figure 2.3: Schematic representation of the turbine geometry and 3D computational mesh for turbine simulations. The different post-processing stations are included.

Table 2.2: Situation of the different sections considered in the computational domain

Section number	Description
0	Domain Inlet
1	Volute Inlet
2	Volute Outlet-Nozzle Inlet
3	Nozzle Outlet-Rotor Inlet
4	Rotor Outlet
5	Turbine Outlet
6	Domain Outlet

transfer through the walls. The effect of heat transfer in turbomachinery has been studied in the literature, mainly for axial turbomachinery as [104]. The works described in [18, 101] also studied the heat transfer effects on the turbocharger performance, focusing on the effect on the performance of the compressor and on the results from a one dimensional model. In the current work, the heat transfer from the turbine is going to be considered negligible, mainly due to the insulation of the turbine case, and therefore the walls are going to be considered as adiabatic.

2.2.3 Boundary conditions

Testing turbochargers under steady flow conditions, although it does not truthfully represent the actual operational conditions when the turbine is installed on engine, is the standard procedure followed by manufacturers. In this chapter, all the simulations are performed at steady inflow conditions, using as boundary conditions the total pressure and temperature at the inlet section and static pressure at the outlet. Another option could have been to impose mass flow rate at the inlet, instead of using total pressure. However, the combination of total pressure at the inlet and static pressure at the outlet has been found to provide good numerical stability and convergence rates in radial turbine simulations [102].

The pressure outlet boundary condition allows one to specify the gauge pressure at the outlet section of the computational domain when the flow is subsonic, while the pressure is extrapolated from the interior if supersonic

regime is reached [3].

2.2.4 Wheel rotation strategies

One of the main topics to deal with is the strategy of simulating the rotor motion. There are basically two different approaches: Multiple Reference Frame (MRF) and Sliding Mesh Model (SMM).

In the first one of them the mesh does not really move. Instead, it uses a coordinate system that rotates with the rotor and the equations are solved in this rotation reference frame. Therefore the Coriolis and centrifugal forces are introduced in the Navier-Stokes equations as source terms. The rest of the turbine, that does not rotate, and the ducts are expressed in a non-rotational (inertial) coordinate system. Some works on the literature as [59] used this approach, which implies that some effects such as the blade passing and the interaction stator-rotor are not considered.

The main advantage of using the MRF approach is its reduced computational cost. However, it cannot take into account typical unsteady flow effects, as for example, the vortex shedding. For the case of turbomachinery simulations, the multiple reference frame approach may have some impact on the results, as it was stated in [82]. A similar conclusion was obtained by the work of Liu and Hill [64] in which different turbocompressors were analyzed, finding evidences of the importance of the mesh motion model in the cases in which the stator-rotor interaction needed to be considered. Additionally, Liu and Hill analyzed two different MRF methods, concluding that the differences found when using the *frozen rotor* one were larger than the ones when the *circumferential averaging* was considered. Other work [54] stated the frozen rotor model was not the most appropriate for radial compressor simulations. In the present work, the MRF simulations were performed using the *frozen rotor* approach available in ANSYS-FLUENT. Since the circumferential averaging approach was not considered, hereinafter frozen rotor and MRF are used indistinctly.

The second approach consists in using the Sliding Mesh Model (SMM), also known as moving mesh, in which one part of the mesh is rotating with respect to the stationary part. The connection between the two zones is done by means of sliding interfaces. This means that the connectivity for cells on either side of the interface changes at each time step. The SMM has been

proved to give good results as reported in [50]. With the SSM approach the blade passing effect is captured. This fact can be notice in the pressure wave fluctuations propagating both upstream and downstream the rotor.

In this work, the rotational speed of the turbine has been kept constant in order to reduce the amount of parameters under study. The selected rotational speed for the analysis was $18953 \text{ rad} \cdot \text{s}^{-1}$.

2.2.5 Viscous model

A variety of papers can be found in the literature dealing with the different viscous models for turbomachinery simulations. With the current computational capacities a Direct Numerical Simulation, in which the whole Navier-Stokes equations are computed, is only affordable in simple cases (flat plate, pipes, ...). For the rest of the cases turbulence needs to be modeled. Turbulence modeling is a main issue in CFD simulations [121]. At this step different approaches can be followed: the use of an Unsteady Reynolds Averaged method (URANS) or the use of a Detached Eddy Simulation (DES) [107] or even a Large Eddy Simulation (LES) [103, 30].

In LES simulations the large eddies are explicitly resolved. This means that only the small scales need to be modeled, which results in a more accurate solution, since small scales are usually more isotropic and less affected by macroscopic flow effects. On the other hand in the Reynolds Averaging approach, Navier-Stokes equations are time averaged, thus an instantaneous quantity can be decomposed into a time-averaged plus a fluctuating quantity. With this approach RANS equations govern the averaged flow quantities, while the fluctuations terms are being modeled, thus defining the Reynolds stresses. Therefore a closure model is needed to define and compute this new unknowns and, in this way, to close the system of equations. The most common closure models available in CFD commercial codes might be classified as models based on Boussinesq approach and Reynolds Stress Model (RSM).

DES model is a mixture between LES simulation for the free stream flow, while the boundary layer is modeled using a RANS approach. More information about the turbulence modeling can be found in the book of Versteeg and Malalasekera [119].

DES and LES models are expected to be more precise, however they re-

quire much higher computational cost which is unaffordable for this kind of calculations of a whole radial turbine with the current computational capabilities. In the framework of URANS models, the most commonly used for engineering applications are those based on the Boussinesq approach, which establishes the proportionality between Reynolds stresses and mean rates of deformation (mean velocity gradient), thus creating the turbulence viscosity concept. The main difference between models based on the Boussinesq approach and the RSM is that the latter one solves an equation for each term of the Reynolds Stress Tensor. Therefore, RSM is more suitable for problems in which the anisotropy of turbulence is important. However, the additional computational cost of the Reynolds Stress Model is generally not justified.

There have been many works dealing with the analysis of turbulence models in turbomachinery simulations. In [116] an analysis of different RANS turbulence models in CFD computations of radial turbomachinery is performed. Among the RANS closure models, the more commonly used for internal flow problems are those defined with two equations. The main advantage of these models is their good performance, with just a small increase on the CPU time of about a 10 % when compared to the laminar solution. The most important two-equations turbulence models use the turbulent kinetic energy k . These models can be divided in those based on the turbulence dissipation rate, ϵ , based on the development of [56], or, the specific dissipation rate, ω , based on the work of Wilcox [121]. $k - \omega$ model is more accurate than the $k - \epsilon$ in computing the near wall layers, since the ω function might be integrated to the viscous sublayer. These kind of models are commonly known as *Low-Re*, referring to the turbulent Reynolds number. The main problem of the standard $k - \omega$ model by Wilcox is the strong sensitivity of the ω -function to the free stream properties [70].

Turbomachines are complex fluid dynamic systems in which adverse pressure gradients and flow separation might occur. In order to capture those phenomena and avoid the sensitivity of Wilcox's $k - \omega$ model, without using more complex and more computationally expensive models, SST turbulence model developed by Menter [67] is used. The SST model blends the robust and accurate formulation of the $\kappa - \omega$ model in the near-wall region with the free-stream independence of the $\kappa - \epsilon$ model in the far field. In SST turbulence model the transport of the principal turbulent shear stress is taken into account, which allows obtaining the correct response to adverse pressure gradients.

The SST model has been applied over a wide range of validation cases [68] and, particularly, it has been used in most turbomachinery applications found in the literature. Menter et al. [69] applied the SST model for turbomachinery simulations, showing a good agreement between the computations and the experimental data for all the cases considered. These cases showed the ability of the model to capture the effects of the variations of Reynolds number and flow separation in a wide range of conditions. In [60] the SST model is used to perform CFD simulations in an axial fan. Other application of the SST model in turbomachinery simulations is found in [92] in which the uncertainty of transition prediction is analyzed. Simpson et al. [102] used the SST in CFD simulations of a vaned and a vaneless radial turbine showing good results. In view of the results found in the literature in which the $\kappa - \omega$ SST model has been proved to provide good results, this model is used for the computations performed in this work.

2.3 Mesh independence

The 3D meshes used for the computations are similar to that shown in Fig. 2.3. The main difficulty when dealing with real geometries is the achievement of an appropriate mesh. In this work a non-conformal mesh was used. The mesh has been built using a mixed polyhedral and extruded-polygonal mesh. FLUENT offers the possibility of generating a polyhedral mesh from a tetrahedral one using the algorithm described in [3]. The main advantage of using polyhedral meshes is that they have better accuracy than the equivalent tetrahedral one or, in other words, is possible to achieve the same resolution with a reduced number of cells [38]. Polyhedral meshes have been used in computational problems in engineering, as for example in the work of Tritthart et al. [117], in which a method for solving Reynolds equations with polyhedral cells was developed, showing a better behavior in some problems than the quadrilateral cells. Once the mesh typology has been chosen, a mesh independence analysis should be performed.

The mesh independence analysis is usually done by considering that the finer is the mesh the better are the results obtained. This can be explained analyzing the discretization error, which decreases with the cell size. The usual procedure when dealing with turbomachinery simulations consists in using different meshes each one of them with a smaller cell size. This procedure

has been used in the work of Zachos et al. [124] and Li et al. [61]. The explained procedure may seem straight forward in the case of a simple system, particularly if the cells are more or less uniformly distributed. However for a more complex system, and moreover if a real geometry is considered, this procedure may be not the most appropriate since not all the subdomains of the system need the same amount of cells. This can be illustrated in the case of the turbine, in which it could seem interesting to have a smaller cell size in the rotor section, where the momentum interchange occurs, than in the ducts, which could even be computed with a one-dimensional approximation. The procedure shown here intends to optimize the resources in terms of cell distribution.

Additionally it is worth to mention that even though in the ideal case the smaller the cells are, the better is the result, there are other issues that have not been taken into account. On the one hand, if the cell refinement is not properly done, it may cause an increase of cells aspect ratio, and the use of distorted cells can introduce convergence errors and even spurious solutions. On the other hand, it is well known that RANS turbulence models are usually applied in combination of wall-functions, which model the flow behavior near the wall. Although the $k - \omega$ turbulence model was chosen, and its *automatic wall treatment* [37] has the advantage of ensuring as high degree of grid independence as possible, it is necessary to evaluate that the value of y^+ is in the range of application of the wall-function [3]. The y^+ is a function of the mesh size, its definition can be found in the book of Versteeg and Malalasekera [119]:

$$y^+ \equiv \frac{u_\tau y}{\nu} \quad (2.2)$$

where u_τ represents the so called friction velocity, which is defined as:

$$u_\tau = \sqrt{\frac{\tau_w}{\rho}} \quad (2.3)$$

This might become a problem if the mesh is too refined during the mesh independence analysis. As previously stated, the turbine was divided in 4 different regions, namely: volute, stator, rotor, and outlet section. The process followed in this work to perform the mesh independence analysis is based in defining a reference case: geometry, mesh, and configuration. Starting with this case, each of the turbine zones were refined separately, substituting in the reference case just the region being analyzed. Several simulations are performed, each one with a finer mesh and the process continues until variation the solution

of two consecutive cases is sufficiently small, as it is usually done in standard mesh independence analysis. At this point, the increase of the computational cost of an additional refinement will not be justified by the increase in resolution. The process continues with the refinement of the following turbine zone. Once all the sections are analyzed the information obtained can be used to determine the regions in which the refinement is more worthwhile.

In order to study the mesh refinement effect two parameters are going to be studied for all the different refinements: the mass-flow through the current element and the total torque developed by the turbine. In the following subsections, the meshing procedure of each one of the turbine regions and the local mesh independence analysis in each one of them are shown.

2.3.1 Volute

The objective of the volute is to feed the stator in the most uniform way as possible. For this reason, the volute should be design as a convergent duct, in order to compensate the mass-flow towards the stator and keep the pressure at the volute-stator interface as constant as possible. As it was previously mentioned, a polyhedric mesh is used in the volute. Due to the importance of the volute's tongue, a smaller cell size in this region might be of interest. An ANSYS-FLUENT size function was used centered in the tongue's edge, as shown in Fig. 2.4. The size function was configured with a minimum size of half the default meshing size used for the original tetrahedral mesh, and a growth rate of 1.1. Therefore, all the meshes are size is defined by just one size parameter, the default meshing size.

Different volute sizes where analyzed, each one of them having about twice number of cells. The information about the size of the volute meshes used is gathered in Table 2.3. In the table, the reference case is also indicated.

As previously mentioned, each of the volutes was replaced in the reference. The results obtained with each one of them are plotted in figure 2.5. The figure shows the evolution of mass-flow and torque in percentage with the number of elements in the volute.

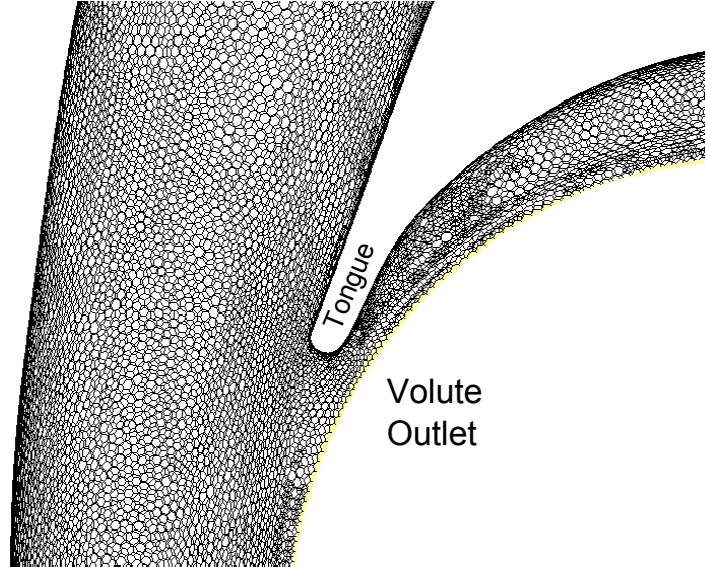


Figure 2.4: Close-up of the mesh in the volute's tongue.

Table 2.3: Size of the volute meshes used in the mesh independence analysis

Volute number	Number of polyhedric cells
V0	26491
V1	40267
V2	71613
V3	141022
V4	242443 (reference case)
V5	444760
V6	646077
V7	1034209

2.3.2 Stator

As previously mentioned, the turbine subjected to study was a vaned turbine. In the current analysis the vanes were kept at a constant position. Due to the particular shape of the nozzle section, it has two different characteristic lengths which are important for the meshing procedure. On one hand, the faces that

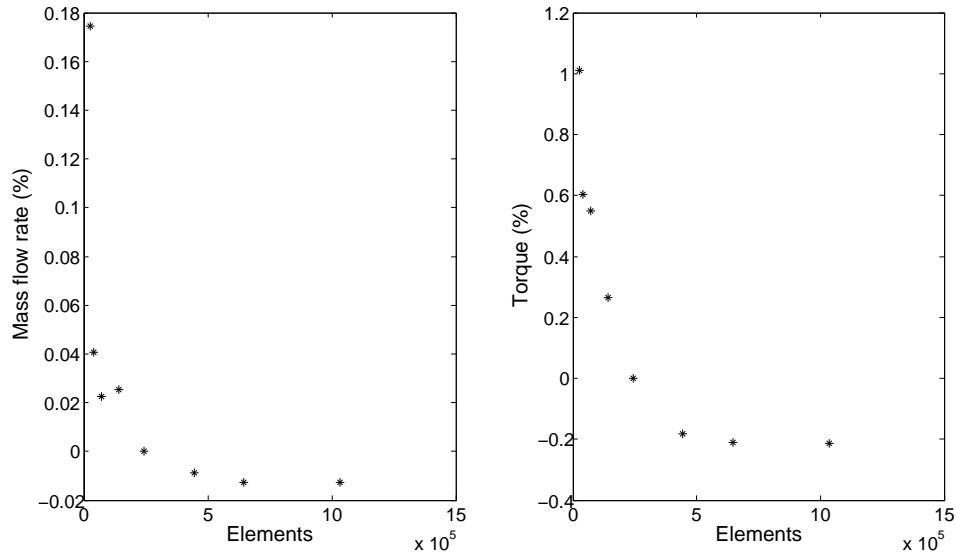


Figure 2.5: Mesh independence analysis for the volute section.

form the stator wall, whose mesh will define the resolution obtained in the stator vanes. On the other hand, the transversal length or stator thickness that is important to describe the profiles in the stator. Due to this reason, the chosen topology for the stator mesh was extruded polygons.

This means that the faces forming the stator wall were meshed using triangular cells, which were extruded in the transversal direction. Afterwards, ANSYS-FLUENT converts these triangles in polygons. Therefore, the mesh of the stator is defined with the cell size used in the stator walls, both upper and lower faces were meshed in the same way, and the number of rows in the transversal direction. Dealing with the stator wall meshes, it may seem interesting to have a better resolution, finer mesh, in the regions close to the stator vanes and screws, therefore a size function with the same configuration than in the volute was used.

In the following analysis two different parameters are used to describe the mesh: the number of cells in the stator wall and the number of rows in the transversal direction. The combinations used are gathered in Table 2.4.

Table 2.4: Size of the stator meshes used in the mesh independence analysis

Number of cells in the wall	Number of rows	Case Number
8743	11 (reference case)	S0
14159	10	S1
	15	S2
	22	S3
24490	10	S4
	15	S5
	22	S6
	30	S7
43396	6	S8
	10	S9
	15	S10
	22	S11
79302	30	S12
	15	S13
	22	S14
	30	S15

First, the mesh independence is directly performed using the total number of cells, some trends can be seen in Fig. 2.6 showing that if the number of cells is increased the dispersion of the values decreases. However it is not clear whether it is worthier to increase the number of cells in the face or the number of rows.

In Fig. 2.7, the evolution of the analyzed parameters with the number of rows is shown. The different curves are grouped together according to the number of elements in the stator wall.

From the previous results, it is clear that for the face meshes with 43396 and 79302 elements, the evolution with the number of cells is almost the same. Additionally, the increase in computational cost from 15 to 30 transversal rows does not justify the change in the solution of about 0.4% in the torque developed by the turbine. In any case, the intermediate value of 22 rows might represent a good trade-off solution.

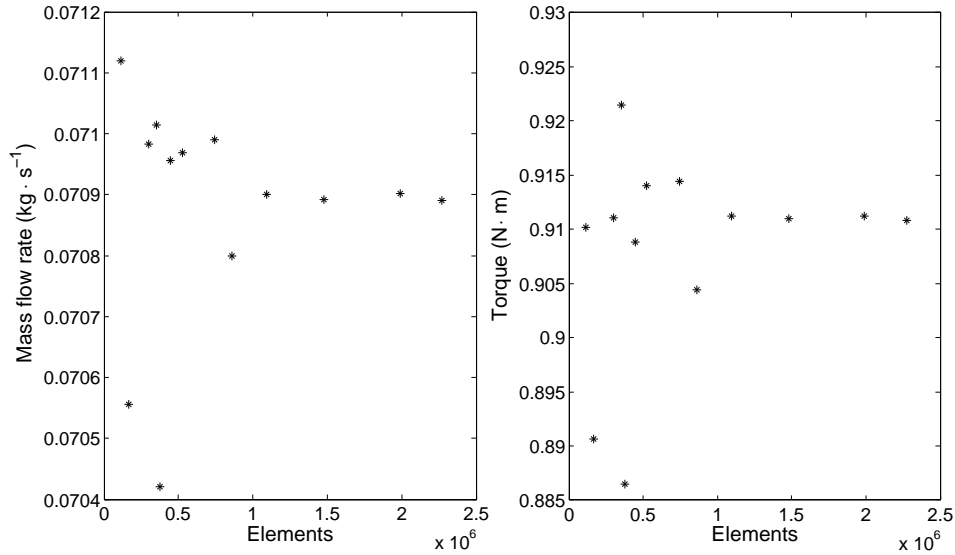


Figure 2.6: Mesh independence analysis for the stator section using the total number of cells.

A small volume is used between the stator and rotor sections. This volume goes from the end of the stator vanes until the rotor inlet section, as can be seen in 2.3. This volume is meshed with hexahedral using the same face size than in the stator. In the final mesh, the number of elements in this transition stator rotor section is included as being part of the stator.

2.3.3 Rotor

The rotor section is, due to its shape, the part of the original geometry where the effects of working with real digitalized geometries are more noticeable 2.8. This may be seen in the different fillet radius in the rotor blades. Therefore, the polyhedral mesh is appropriate for the rotor region. Following the same criteria than with the previous turbine regions, a size function was used to increase the resolution closer to the walls. The configuration was similar to that used for the case of the volute and stator. Therefore, the total number of elements is defined with the default meshing size, as it happened in the volute.

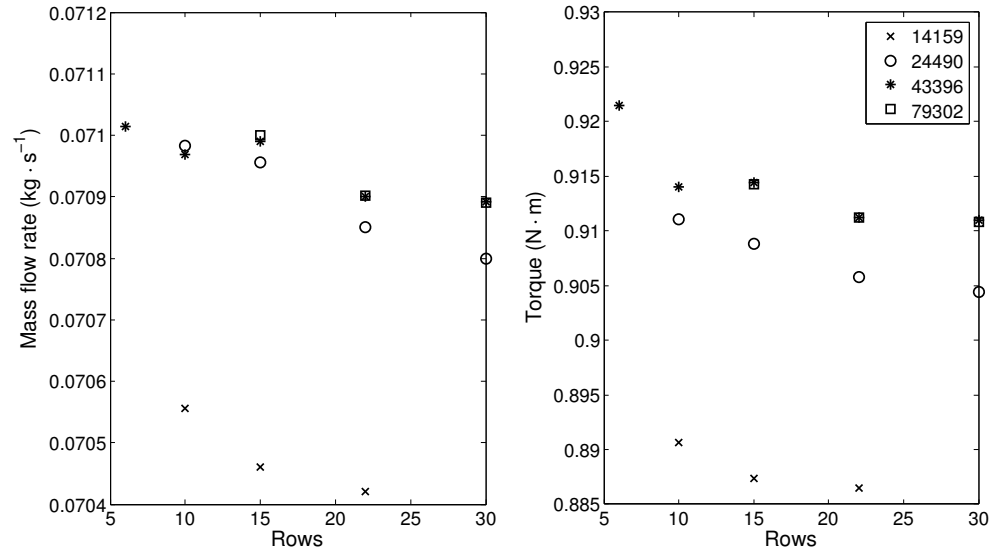


Figure 2.7: Mesh independence analysis for the stator section using the number of rows.

The different rotor meshes used in the analysis are presented in Table 2.5.

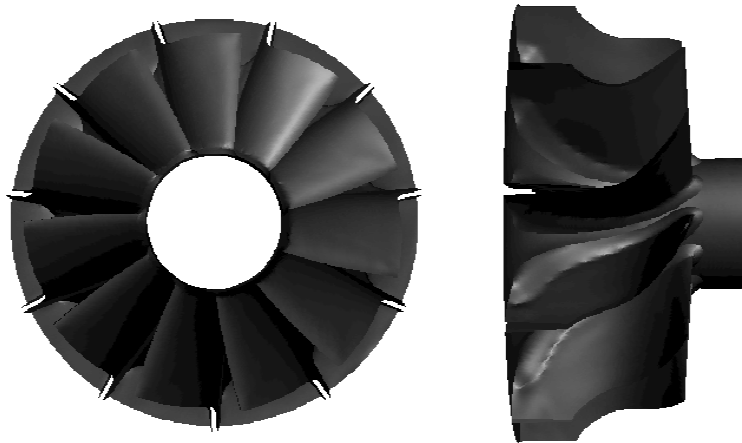


Figure 2.8: Close-up of the geometry of the rotor zone.

Table 2.5: Size of the rotor meshes used in the mesh independence analysis

Rotor number	Number of polyhedric cells
R0	64655
R1	99662
R2	285001 (reference case)
R3	315943
R4	423821
R5	518067
R6	657259
R7	810716

The results obtained for the rotor mesh independence in terms of mass flow rate through the rotor and generated torque are shown in Fig 2.9. In this case, the independence curve has a different shape than the previous ones. The curve obtained in volute had a typical *overdamped* shape. However for the case of the rotor presents a higher oscillating behavior and the curve *overshots*, i.e. exceeds the equilibrium level at each oscillation, but at the same time reducing the total amplitude.

This oscillating behavior made necessary to increase the number of points in this analysis in order to ensure that not spurious aliasing effect is obtained. If only 4 points would have been acquired, the behavior obtained could have been completely different, leading to an erroneous result. The difference obtained between the last points of the analysis is of about 0.2%. The oscillations are probably due to accumulation of different flow effects and not directly the mesh. In fact, if a torque parameter is defined relating the torque to the flow variables at the rotor inlet as

$$C_m = \frac{T_T}{1/2\rho U_{rotor}^2}, \quad (2.4)$$

and it is used as parameter for the mesh independence analysis, these oscillations do not appear. This result can be seen in figure 2.10. The reason might be that using the torque parameter, reduces the influence of the inlet conditions in torque, thus being only influenced by the exchange of momentum with the rotor walls.

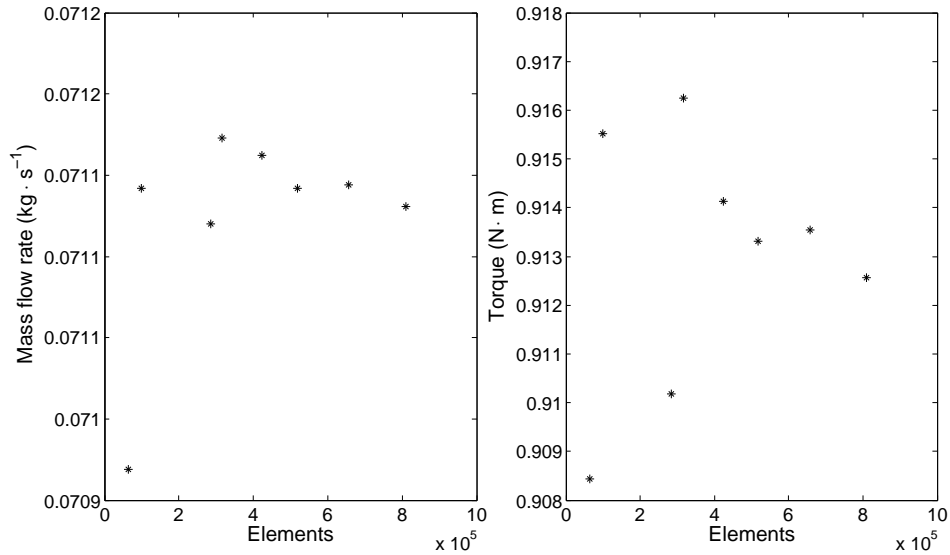


Figure 2.9: Mesh independence analysis for the rotor section using the number of cells.

2.3.4 Outlet section

The outlet section of the turbine is the one comprised between the outlet section and the turbine outlet (section 4 and 5 of Fig. 2.3). In the turbine subjected to study, the cross-sectional area was more or less constant in the section after the expansion at the end of the rotor. However, there was a non-uniform surrounding cavity around this section which may act as a resonator 2.3. As in the previous cases, different mesh sizes were used in the outlet region. In this case, a uniform tetrahedral mesh, for its posterior conversion to polyhedrons, was used. The different meshes used are presented in Table 2.6.

The results obtained for the outlet section mesh independence in terms of mass flow rate through the section and the generated torque of the turbine are shown in Fig 2.11. Figure shows a very pronounced trend. In meshes with more than 10^5 elements the parameters do not change much. However, for meshes with fewer elements the variation is important. One point that must

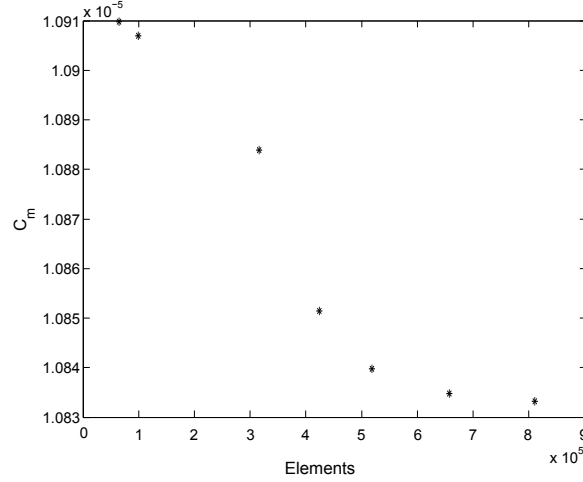


Figure 2.10: Evolution of the torque coefficient with the number of cells in the rotor section of the turbine.

Table 2.6: Size of the outlet section meshes used in the mesh independence analysis

Outlet section number	Number of polyhedral cells
O0	29281
O1	56392
O2	128671 (reference case)
O3	207451
O4	432179

be considered is the possible variation of the independence analysis with the operating point. For this reason it may be interesting to select the mesh with a certain security margin if a given resolution is needed.

2.3.5 Final considerations and selected mesh

In the previous subsections, the local mesh independence of the different turbine components was analyzed. From those results it is possible to establish which distribution of cells between the different turbine zones is more

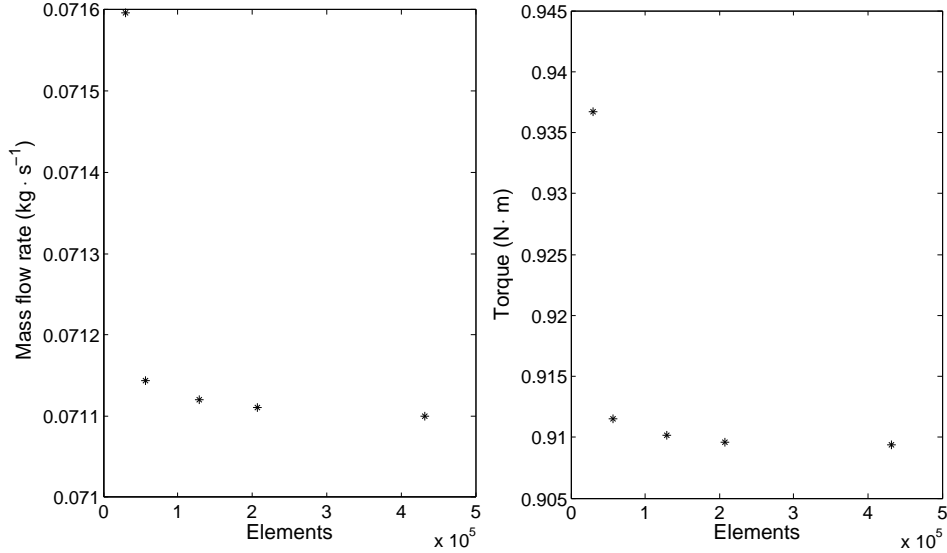


Figure 2.11: Local mesh independence analysis of the outlet section of turbine. Evolution of mass-flow through the outlet section and torque with the number of cells.

interesting according to the actual computational resources. However some considerations should be done before proceeding.

First of all, since the current analysis has been performed separating the influence of the different components, if a final mesh resolution of about a 1 % accuracy is sought, in order to be conservative the relative error in each of the components should be lower (about a 0.2% was considered in this work).

The previous analysis was performed assuming that the behavior of the different components was independent. This was needed to justify the procedure that was followed. In that procedure, the local mesh independence of each component was studied by replacing only that region of the mesh in a reference case, and thus all the variations between the different simulations were attributed to the replaced zone. However, it is not obvious that if mesh independence has been achieved using the rest of the regions from the reference case; it will also be independent once all the regions have changed to the refined mesh. In order to ensure the independence final mesh, some additional

simulations were performed substituting one of the mesh components for the finer one used in the previous analysis. In this way the effect of the reference case was assessed. The solutions obtained matched the ones with the reference case, therefore the mesh independence is ensured. In the same way, the effect of the operational point may affect the mesh independence. Although this effect is not expected to be important and it is not analyzed in the current work, it should be considered if a given relative error is required.

Finally, the inlet and outlet ducts were not included in the mesh independence analysis. The inlet and outlet were meshed using a similar cell size than the one used in the volute and a copper scheme was used to mesh the volume.

2.3.5.1 Final mesh

From the results of the mesh independence analysis, the following meshes were chosen for each of the components:

Table 2.7: Number of elements in the mesh of the different turbine components for the mesh selected using the mesh independence analysis.

Zone	Number of polyhedric cells (%)	Average cell volume (mm ³ /cell)
Volute	646077 (23.3 %)	0.21
Stator	1094812 (39.5 %)	0.017
Rotor	657259 (23.6 %)	0.017
Outlet section	207451 (7.5 %)	0.40
Total number of elements	2777122	0.090

It is important to remark that the mesh selected for the stator is the one with 43396 cells in the stator wall and 22 rows in transversal direction. The number of elements in the ducts is not included in Table 2.7, but the cells are counted in the total number of elements. The inlet duct represents about a 1.2 % of the total amount of cells, while the outlet duct is about a 4.9 %. The total number of cells if only the turbine is considered is 2605599. The last column in Table 2.7 represents the average cell size in each turbine zone. As expected, the cell size required in the volute is bigger than the one obtained in stator and rotor.

2.4 Set-up Comparison

Once the mesh to be used in the simulations was selected, the configuration of the computational cases must be done. There are different factors that should be considered during the configuration of the case. The most important are: the moving mesh strategy, the solver used in the simulations and the temporal discretization. In this section, a comparison of the different configuration is done in order to check the behavior of the different configurations.

2.4.1 Type of solver

ANSYS-FLUENT offers two different numerical methods [38, 4]: the pressure-based and the density-based solvers. Historically speaking, the density-based approach was mainly used for high-speed compressible flows, while the pressure-based approach was developed for incompressible and mildly compressible flow. However, recently both methods have been extended to solve a wide range of flow conditions beyond their traditional intent.

In both methods the momentum equations are used to obtain the velocity field. In the density-based approach, the continuity equation is used to obtain the density field while the pressure field is determined from the equation of state. While in the pressure-based one, continuity and momentum equations are combined to obtain a pressure or pressure correction equation, from which the pressure field is extracted. The two numerical methods employ a similar discretization process (finite-volume), but the approach used to linearize and solve the discretized equations is different. Additionally, the origins of the density-based formulation may give an accuracy (i.e. shock resolution) advantage over the pressure-based solver for high-speed compressible flows.

2.4.1.1 Pressure-based

As stated above, the pressure equation is derived from the continuity and the momentum equations in such a way that the velocity field, corrected by the pressure, satisfies the continuity. Since the governing equations are nonlinear and coupled to another one, the solution process involves iterations. This means that the entire set of governing equations (continuity for the velocity field and pressure equation) is solved repeatedly until the solution converges.

Two pressure based algorithms are available at ANSYS-FLUENT: segregated and coupled [4]. In the segregated algorithm, the individual governing equations for the solution variables are solved one after another. Therefore, they are solved decoupled or segregated from other equations, hence its name. Secondly, in the coupled algorithm the momentum equations and the pressure-based continuity equation are solved simultaneously. In general, the coupled algorithm significantly improves the convergence speed over the segregated algorithm. However, the memory requirement for the coupled algorithm is higher than for the segregated algorithm. Additionally, coupled solver has a better resolution in compressible flow effects.

2.4.1.2 Density-based

In the same way, two formulations exist under the density-based solver: implicit and explicit [4]. The density-based explicit and implicit formulations solve the equations for additional scalars sequentially. The implicit and explicit density-based formulations differ in the way that they linearize the coupled equations. In the implicit formulation, for a given variable, the unknown value in each cell is computed using a relation that includes both existing and unknown values from neighboring cells. Therefore, each unknown will appear in more than one equation in the system, and these equations must be solved simultaneously to give the unknown quantities. In contrast, in the explicit formulation, for a given variable, the unknown value in each cell is computed using a relation that includes only the existing values. Therefore, each unknown will appear in only one equation in the system and the equations for the unknown value in each cell can be solved one at a time to give the unknown quantities.

In summary, the coupled implicit approach solves for all flow variables in all cells at the same time, while the density-based explicit approach solves for all variables one cell at a time. The choice of the implicit or explicit solver applies only to the coupled set of governing equations. Transport equations for additional scalars are solved segregated from the coupled set. Due to broader stability characteristics of the implicit formulation, a converged steady-state solution can be obtained much faster using the implicit formulation rather than the explicit formulation. However, the implicit formulation requires more memory than the explicit formulation.

When a density-based numerical method is used to obtain steady-state flow solutions the temporal terms are maintained in the equation. Therefore, the solution is computed assuming that time marching proceeds until a steady-state solution is reached, that is commonly known as time-marching algorithm. This procedure differs from the one followed when using pressure-based methods, in which the terms dealing with temporal variation are not included in the discretized equations.

2.4.1.3 Comparison

In this work, some simulations to compare the behavior of pressure-based and density-based numerical methods were carried out. The calculations were performed using the Multiple Reference Frame approach to simulate rotor motion. The first conclusion obtained is that the computational cost of the cases computed with the density-based solver was about 5-10 times greater than with the pressure based coupled solver. Simulations have been performed with different mesh sizes using the two formulations. The results have been compared in terms of corrected mass flow and power developed by the turbine. Hereinafter, whenever corrected mass flow is mentioned, it is referred to a pressure (p_0) of 101325 Pa and a temperature (T_0) of 288.15 K. The results from the different simulations are shown in 2.12.

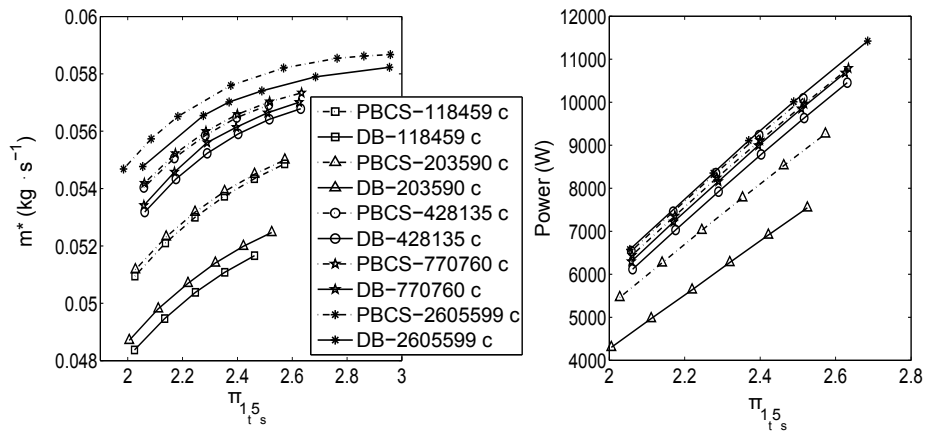


Figure 2.12: Comparison Pressure Based Coupled (PBCS) and DB solvers. In terms of flow-capacity (left) and turbine power vs pressure ratio (right) for different meshes

In view of the results, some conclusions can be extracted. On the one hand, it can be stated that even though the ANSYS-FLUENT user's manual says that nowadays both solvers are valid for all flow regimes, the results obtained are quite different. It is interesting to observe that for the different mesh sizes the pressure based coupled solver gives higher flow capacity than the density based. On the other hand, it seems that the relative error between the pressure and density solvers is reduced as the number of cells increases. In the same way, the relative difference between two consecutive mesh sizes also decreases. The mesh with 2605599 cells is the one obtained from the mesh independence analysis of the previous section, and for this mesh, the relative error between the results with the PBCS and the DB one is less than a 1%. Finally, it is interesting to remark that a single steady (MRF) point with the DB solver for the finest mesh required about 1 month of computations with the current computational resources at our disposal, while the PBCS solver needed about 1/10 of that time. This fact justifies the use of the PBCS in the following simulations included in this work.

Concerning the spatial discretization, in all the simulations a second order scheme was used for all integration variables. The spatial discretization scheme is needed to compute the face values required for the convection terms from the discrete values stored at the cells centers.

2.4.2 Mesh motion strategy

Previously, a description of the different moving mesh strategies was given. In this section, the results using both rotor motion approaches are presented. In the multiple reference frame (MRF) approach, the relative positions of the stationary and rotating domains throughout the calculation are fixed, only a frame transformation is performed across the boundary. Therefore, it is a steady-state approximation of the rotor movement. On the other hand, in the sliding mesh model the mesh of the rotor is actually moved, and therefore it is inherently unsteady, which means that the flow variables will always keep an oscillating behavior caused by the blade passing (among other effects). The simulation has to be calculated until a periodic solution is found. This unsteadiness generates pressure waves due to the rotor movement.

These pressure waves will increase time averaged pressure upstream of the turbine, but they will also introduce viscous losses, but this is most probably a

secondary effect. Additionally, these waves will cause spurious reflections when reaching the outlet boundary. These reflections increase the computational time needed to reach a periodic solution. Another solution could be the use of a sufficiently long duct at the outlet boundary, this solution will be analyzed deeply in the following chapters. For the MRF cases, where the wheel is stationary, the dynamics of the blade passing effects are of course not captured.

Some works found on literature on simulation of turbomachinery were done using the MRF approach [59]. The movement of the mesh highly increases the computational cost, but it might be necessary if rotor-stator interaction is strong. This effect was analyzed by [64] in the case of a turbocompressor. For the case of a radial turbine, the work of Simpson et al. [102] showed that the SMM solutions gave better results than the MRF. Other authors in the literature support this conclusion [52, 82, 57].

Figure 2.13 shows the results obtained with both moving mesh approaches: MRF and SMM. In this case, the two computations have been performed using the same mesh and the same solver (PBCS) in order to isolate this effect. The results are compared with the experimental measurements taken in the testing facility. In the figure, π_{1t5s} stands for the ratio between the total pressure at section 1 (see Fig. 2.3) and the static pressure at section 5; and \dot{m}_1^* is the corrected mass-flow computed at section 1. This notation is used hereinafter in other graphs of the thesis.

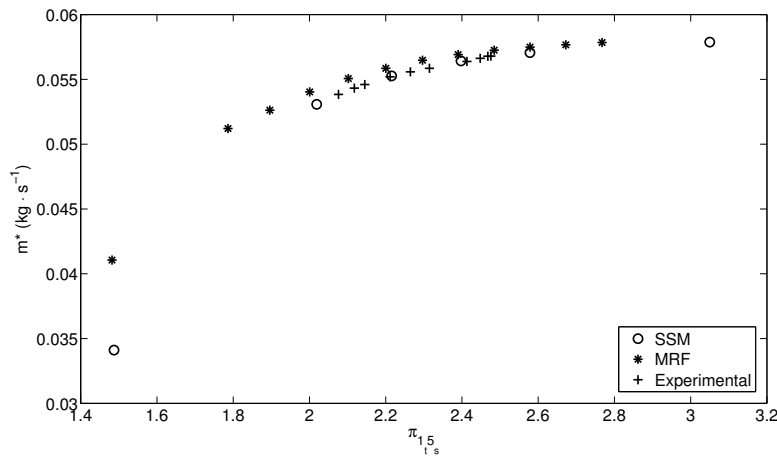


Figure 2.13: Flow capacity curves of a radial turbine. Corrected mass flow vs overall pressure ratio.

From the results showed in Figure 2.13, concerning the flow capacity it seems that both methods give similar results for the points at higher pressure ratio (design points). However, the curves vary for points in off-design conditions, these points might be more affected by the stator-rotor interaction. This points will be particularly interesting when the turbine is studied under pulsating flow conditions as done in chapter 6.

As previously said, there is an uncertainty in positioning the stator at the desired aperture. This fact made difficult the acquisition of experimental data to validate the computations. The methodology that has been followed to measure the points was as followed. The turbine installed the facility was set in a given pressure ratio and the stator aperture was changed, using the rack of the positioning system, until the corrected mass flow matched the one previously computed. Once the stator position is set, a complete curve is obtained. Figure 2.14, shows the evolution of the power developed by the turbine as a function of pressure ratio. Once again some difference is found between the results computed using both moving mesh techniques. Although in the graph, the power generated has been used, it is equivalent to representing the torque since the rotational speed was kept constant.

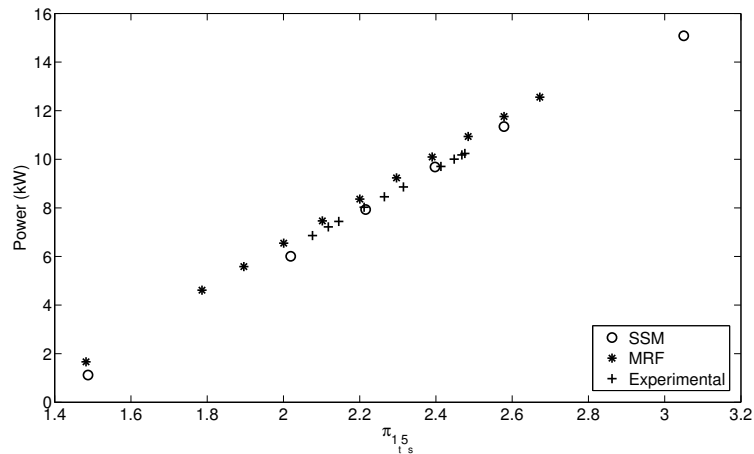


Figure 2.14: Performance curves of a radial turbine in terms of the power developed.

In view of the previous graphs, there is an additional difficulty when trying to validate the computational results since only a narrow range of experimental data might be obtained and therefore the off-design points, where the differences are bigger, are not evaluated. As a conclusion from the results

obtained it seems that there is a better correlation between the experiments and the computations performed using the SMM than with the MRF ones. Thus, it seems necessary to use sliding mesh model, especially in situations in which stator-rotor interaction effects are important. As a final comment, it is worth to mention that for a single SSM computation to reach periodic regime about 50 rotor revolutions were required, which took over two months of computational time.

2.4.3 Temporal discretization

The last topic that is going to be covered in this section is about the temporal discretization of the equations. The SMM requires performing the simulation in transient conditions since the mesh is actually moved, and therefore a transient discretization of the equations is needed. Temporal discretization involves the integration of the terms of the differential equations over a time step Δt , which needs to be defined. More information about the temporal discretization schemes might be found in [83].

Among the time-discretization options available in ANSYS-FLUENT, the first decision is selecting whether to use an implicit or an explicit approach. In an explicit time discretization, the time step, Δt , is restricted to the stability limit of the underlying solver (i.e. CFL condition). This criterion will give a different time step in each cell of the domain. However, in order to be time-accurate, all the cells in the domain should use the same time step, thus, the selected time step must be the minimum of all the local time steps in the domain. The use of explicit time stepping is quite restrictive, and leads to time steps of the order of 10^{-9} for the case of the turbine which is unaffordable for the current computational resources available. Moreover, explicit time discretization is only available for the density based solver, which represents a further increase of the computational time. For all the previous reasons the implicit time discretization was used in the current work.

On the other hand, the advantage of the fully implicit scheme is that it is unconditionally stable with respect to time step size [4]. In this case, the time step is not obtained from the application of a stability criterion, but instead it has to be selected. The influence of the time step size is analyzed in the following.

2.4.3.1 Time step size

As a general criterion, in order to resolve the transient behavior of the blade passing about 10-20 time steps per blade passing should be taken [3]. This time step size is of the same order than other time steps adopted in the literature, as in the work of Simpson et al. [102] who took a time step size of 1 degree per time step. Other works used a time step size ranging from 0.6° [51], 1° [80] up to 5° per time-step [58] was used. In the current simulations a time step size of 200 time steps per rotor revolution was considered as first approach. Therefore, given the rotational speed of the impeller of $18953 \text{ rad}\cdot\text{s}^{-1}$, a time step size $1.6576\cdot 10^{-6}$ seconds. In this subsection, a sensitivity analysis of the effect of the time step size is performed.

The unsteadiness of the SMM simulation can be seen plotting the torque history developed by the turbine, as shown in the left side of Figure 2.15. The oscillations correspond to the unsteady behavior of the internal flow in the turbine. In particular, the oscillations due to the impeller rotation and the blade passing can be identified in the frequency spectrum. The main frequency of the impeller rotation can be computed as:

$$f_{Rotor} = \frac{\omega}{2\pi} = 3016.46 \text{ Hz} \quad (2.5)$$

This line is marked in the frequency spectrum plotted on the right side of Figure 2.15. The firsts cycles of the signal are discarded, as indicated in the right side of Figure 2.15, in order to take into account only the periodic part of the signal. Additionally, the FFT was computed applying a Hamming window to the signal. The other characteristic frequency, which is in fact the one with higher amplitude, is the one depending on the rotor blade passing. Since there are 11 blades, the frequency is 33181.1 Hz. In this work an analysis of the variation of the mean value of torque and the amplitude of the oscillations with respect to the time step size is done. The results are presented in Table 2.8.

The results are presented in terms of the variation in percentage of the mean value of the torque developed by the turbine with respect to the torque obtained with the initial time step size. The oscillations are also presented in percentage relative to the respective mean value. The error of the mean value tends to decrease with the time step size. However, it is clear that dividing by two the time step size doubles the computational requirements, and as stated above a single computation in SMM took over two months. Therefore, a time step size of $1.6576\cdot 10^{-6}$ seconds was selected for the rest of the transient

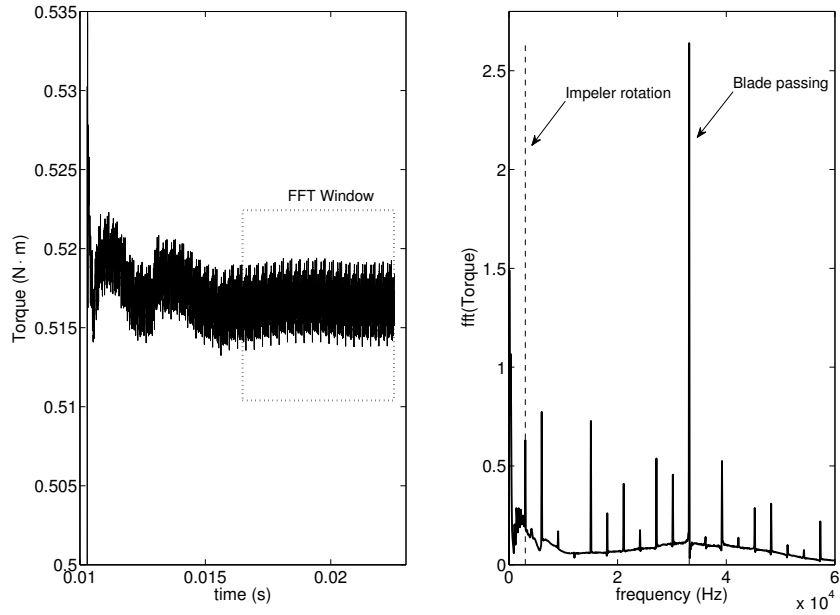


Figure 2.15: Temporal evolution of torque developed by the turbine (left) and FFT (right).

Table 2.8: Analysis of the influence of the time step size.

Time step (s)	Mean value variation (%)	Amplitude of oscillations (%)
$1.6576 \cdot 10^{-6}$	-	1.05 %
$3.3152 \cdot 10^{-6}$	1.45 %	0.77 %
$8.288 \cdot 10^{-7}$	1.24 %	1.42 %

computations, since doubling the computational time was unaffordable with the current computational capabilities.

2.5 Summary of the results: Turbine map

In the previous sections, a mesh independence analysis 2.3 and the optimization of the case configuration 2.4 were performed. The analysis of the set-up has shown that pressure-based and density based solvers give different results, but they tend to converge as the mesh is refined. When dealing with the mesh motion strategy to different approaches were analyzed. The results showed that the results are similar in the design range. However, the differences increase as point separates from the design region as shown in Figure 2.13. It can be concluded that the MRF, due to its low computational cost, represents a good choice to obtain a first approach of the solution if the considered points are close to the design conditions. On the contrary, if off-design points are evaluated the rotor-stator interactions effects are higher and thus a fully unsteady SMM simulation is required.

The turbine analyzed is a VGT, this means that the angle of the stator vanes can be varied in order to change its effective area. This effect increases the transient performance of the turbocharger. The analysis was done using a constant aperture angle in the stator. In this section, the turbine maps are obtained for different apertures in order to analyze the effect on the turbine behavior. Numerical results are compared to those acquired on the test bench. Experimental measurements could only be taken in a narrow range close to the design conditions. Therefore, in order to reduce the computational cost, the simulations are performed using MRF strategy. The results obtained in terms of flow capacity are presented in Figure 2.16.

The nozzle aperture increases the flow capacity for the same pressure ratio. As stated before, there is an additional uncertainty in the actual value of the angle of the stator vanes, which makes difficult to compare the experimental and numerical results. However, it seems that all the curves obtained follow the same trend. The results from experimental opening A and the simulations with a 50 % opening are in good accordance.

In order to describe the behavior of a turbine, generally two different curves should be given: one representing the flow capacity of the turbine, as the one shown in Figure 2.16, and another one dealing with the torque or power generated by the turbine. Figure 2.17 shows the power developed by the turbine versus the mass flow parameter. The use of the mass flow parameter is equivalent to the corrected mass flow since the only differences are the

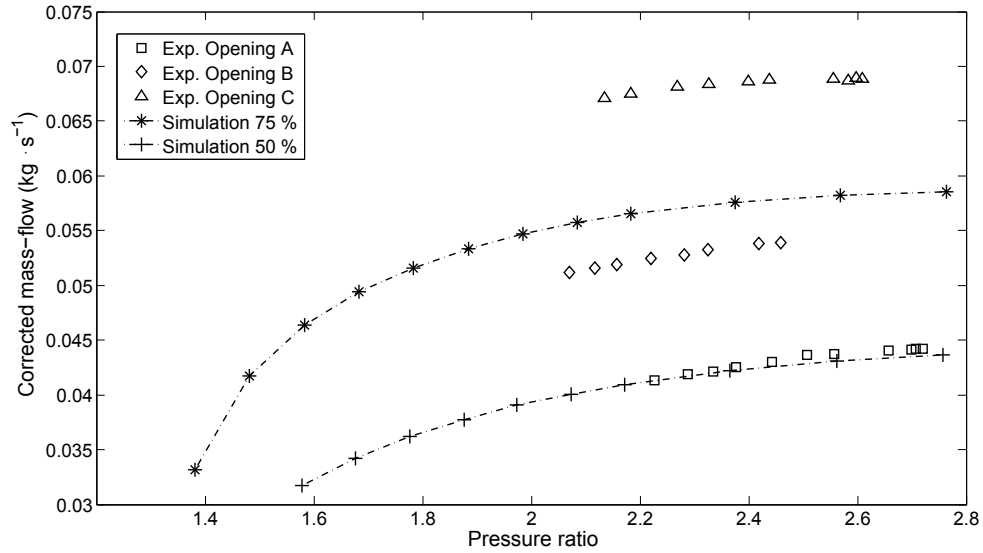


Figure 2.16: Turbine flow capacity for different nozzle apertures. Three experimental apertures and two simulated ones are shown.

reference pressure (101325 Pa) and temperature (288.15 K).

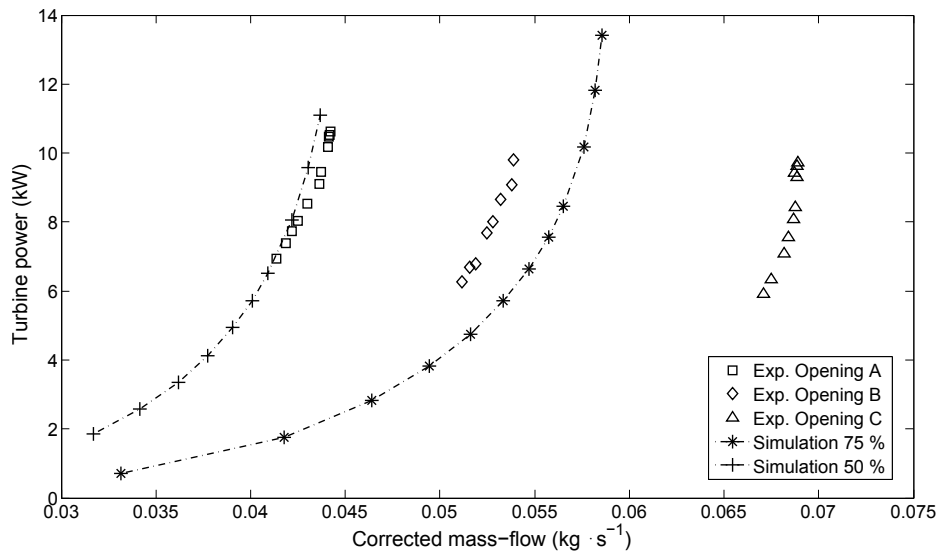


Figure 2.17: Turbine performance in terms of power versus mass flow parameter. Three experimental apertures and two simulated ones are shown.

Since the curves are normally acquired at constant speed, torque and power are equivalent quantities. The results show that all the curves have similar trend only varying the effective section. Also, the curves obtained for the experimental opening A and the simulation at 50 % aperture show good agreement. It is convenient to remember that the corrected mass flow and power obtained with the MRF approach were a bit over estimated (about a 7 % for the power) as presented in Figures 2.13 and 2.14. If this fact is taken into account, the agreement would be even better if SMM was considered. Due to the good agreement found between experimental and numerical result, the validity of the simulations can be established.

In this work all the performance results have been presented in terms of torque or power developed. However, probably the most common presentation is in terms of an efficiency defined as:

$$\eta = \frac{P}{P_{is}}, \quad (2.6)$$

where P is the actual power developed by the turbine and P_{is} is the isentropic power, that is the maximum power that can be develop the turbine at the given conditions. The definition of the efficiency is clear for a steady case, but it is not so obvious when dealing with pulsating flows, as will de discussed in chapter 6. For this reason and in order to be coherent the same procedure has been applied in this chapter.

2.6 Summary and conclusions

In this chapter, the description of the CFD methodology that has been used in this work has been presented. First, an assessment of different CFD models have been performed, focusing on the description of the turbine used, the boundary conditions and the viscous model. The selection of the viscous model has been based on several works found in the literature which successfully applied the $\kappa - \omega$ SST model to turbomachinery simulations. As boundary conditions, trough all this work total pressure and temperature are imposed in the inlet section, and static pressure at the outlet of the domain. A description of the experimental facility and the measurement sensors used to acquire the validation data was presented.

In order to optimize the distribution of cells in the mesh, a local mesh

independence analysis was developed. The general mesh independence procedure is based in analyzing the global amount of cells in the mesh. In this work, the analysis has been performed dividing the turbine in zones, namely: volute, nozzles section, rotor and outlet section. The cell size of each of the zones was varied and replaced in a reference case, until the independence of the current region was achieved. The same procedure was repeated for the different regions.

Afterwards, the different options available in ANSYS-FLUENT for the case configuration have been analyzed. These options deal with the solver type, the moving mesh strategy and the time step size. The density based and the pressure based solvers give different results. However, the relative error decreases as the number of cells in the mesh increases. Concerning the rotor motion strategy, two different approaches were considered: the multiple reference frame and the sliding mesh model. The first approach has a much lower computational cost and gives a good approximation (about a 7% error in torque) if the operating point is close to the design conditions, thus it has been applied to obtain the characteristics curves of the turbine. However, if off-design points are considered the error increases, since the transient effects as the rotor-stator interaction become more important, and thus, it is necessary to perform a fully transient simulation, actually rotating the mesh, to capture this behavior.

The rotation of the impeller blades creates pressure fluctuations that propagate through the domain. When a pressure fluctuation reaches the boundary, it is reflected and returns towards the turbine, changing the flow field. This process continues until a converged periodic solution is obtained. For this reason, it is important to separate the boundaries from the region of interest to avoid spurious perturbations of the solution. However, increasing the length of ducts will increase the already high computational time or employ computational resources in the computation of ducts that could even be computed using a one-dimensional approach. In this frame of ideas the possibility of performing a one-dimensional-three-dimensional computation or the development of a boundary condition that behaves as an infinite duct seems interesting. This possibility will be further analyzed in chapters 3 and 4.

Finally, since the turbine analyzed is a VGT the effect of nozzles aperture in the turbine flow capacity and performance curve is studied. The results are compared with experimental measurements taken in a turbocharger test rig. The agreement found between the results allows to establish the validity of

the computations performed.

Chapter Bibliography 2

- [1] M. Abidat, M. K. Hamidou, M. Hachemi, and M. Hamel. “Design and flow analysis of radial and mixed flow turbine volutes”. In: *European Conference on Computational Fluid Dynamics*. 2006 (cit. on p. 14).
- [2] J. Andersen, E. Karlsson, and A. Gawell. “Variable turbine geometry on SI engines”. In: *SAE 2006 World Congress*. SAE 2006-01-0020. 2006 (cit. on pp. 3, 16).
- [3] ANSYS Inc. *Ansys Fluent 12.0 User’s Guide*. Canonsburg, PA 15317, 2009 (cit. on pp. 24, 27, 28, 47, 83, 85).
- [4] ANSYS Inc. *ANSYS FLUENT Theory Guide*. 2011 (cit. on pp. 17, 40, 41, 46).
- [6] A. Arnone and R. Pacciani. “Rotor-stator interaction analysis using the Navier–Stokes equations and a multigrid method”. In: *Journal of Turbomachinery* 118 (1996), p. 679 (cit. on p. 14).
- [10] N. C. Baines. “Radial Turbines - An Integrated Design Approach”. In: *6th European Conference on Turbomachinery - Fluid Dynamics and Thermodynamics*. Lille, France, 2005 (cit. on p. 15).
- [11] N. C. Baines, G. B. Ingénieur-mécanicien, N. C. Baines, and N. C. Baines. *Fundamentals of turbocharging*. Ed. by Concepts NREC. Concepts NREC, 2005 (cit. on p. 14).
- [16] E. Blanco-Marigorta, J. Fernández-Francos, J. González-Pérez, and C. Santolaria-Morros. “Numerical flow simulation in a centrifugal pump with impeller-volute interaction”. In: *ASME 2000 Fluids Engineering Division Summer Meeting*. 2000, pp. 1–6 (cit. on p. 15).
- [18] D. Bohn, T. Heuer, and K. Kusterer. “Conjugate flow and heat transfer investigation of a turbo charger”. In: *Journal of engineering for gas turbines and power* 127 (2005), p. 663 (cit. on p. 23).
- [24] C. Cervelló. “Contribución a la Caracterización Experimental y al Modelado de Turbinas de Geometría Variable en Grupos de Sobrealimentación”. PhD thesis. Tesis Doctoral UPV, 2005 (cit. on p. 17).

- [25] H. Chen. “Turbine wheel design for Garrett advanced variable geometry turbines for commercial vehicle applications”. In: *8th International Conference on Turbochargers and Turbocharging, Institution of Mechanical Engineers*. 2006 (cit. on pp. 3, 16).
- [28] J. Dai, N. Ijichi, H. Tange, H. Shibata, H. Tamaki, and S. Yamaguchi. “Comparison of internal flow field between experiment and computation in a radial turbine impeller”. In: *JSME International Journal Series B* 47.1 (2004), pp. 48–56 (cit. on p. 15).
- [30] J. W. Deardorff. “A numerical study of three-dimensional turbulent channel flow at large Reynolds numbers”. In: *Journal of Fluid Mechanics* 41.02 (1970), pp. 453–480 (cit. on p. 25).
- [31] G. Decombes, J. F. Pichouron, F. Maroteaux, N. Moreno, and J. Julien. “Simulation of the performance of a variable geometry turbocharger for Diesel engine road propulsion”. In: *International Journal of Thermodynamics* 5.3 (2010), pp. 139–149 (cit. on pp. 14, 158).
- [37] T. Esch and FR Menter. “Heat transfer predictions based on two-equation turbulence models with advanced wall treatment”. In: *Proceedings of the 4th international symposium on turbulence, heat & mass transfer, Antalya, Turkey*. 2003, pp. 614–621 (cit. on p. 28).
- [38] FLUENT. *FLUENT 6.3 Validation Guide*. 2006 (cit. on pp. 27, 40).
- [43] J. Galindo, J. R. Serrano, C. Guardiola, and C. Cervelló. “Surge limit definition in a specific test bench for the characterization of automotive turbochargers”. In: *Experimental thermal and fluid science* 30.5 (2006), pp. 449–462 (cit. on p. 14).
- [46] J. Galindo, A. Tiseira, P. Fajardo, and R. Navarro. “Coupling methodology of 1D finite difference and 3D finite volume CFD codes based on the Method of Characteristics”. In: *Mathematical and Computer Modelling* 54.7-8 (2011), pp. 1738–1746. DOI: <http://dx.doi.org/10.1016/j.mcm.2010.11.078> (cit. on pp. 6, 15, 62, 81, 88, 93, 112, 118, 167).
- [50] F. Hellström. “Numerical computations of the unsteady flow in turbochargers”. PhD thesis. Royal Institute of Technology KTH Mechanics, 2010 (cit. on pp. 25, 129).

- [51] F. Hellstrom and L. Fuchs. “Effects of inlet conditions on the turbine performance of a radial turbine”. In: *PROCEEDINGS OF THE ASME TURBO EXPO 2008: Power for Land, Sea and Air*. Berlin: New York: AMER SOC MECHANICAL ENGINEERS, 2008 (cit. on pp. 14, 15, 47, 158).
- [52] F. Hellstrom and L. Fuchs. “Numerical Computation of the Pulsatile Flow in a Turbocharger With Realistic Inflow Conditions From an Exhaust Manifold”. In: *Proceedings of ASME Turbo Expo 2009: Power for Land, Sea and Air*. GT2009-5961. ASME. 2009 (cit. on pp. 44, 126, 158).
- [53] H. Hiereth and P. Prenninger. *Charging the internal combustion engine*. Ed. by SpringerWienNewYork. Springer Verlag, 2007 (cit. on pp. 14, 158).
- [54] K. Hillewaert and RA Van den Braembussche. “Numerical simulation of impeller–volute interaction in centrifugal compressors”. In: *Journal of Turbomachinery* 121 (1999), p. 603 (cit. on p. 24).
- [55] D. Japikse and N. C. Baines. *Introduction to turbomachinery*. Ed. by Oxford University Press. Concepts Eti, 1997 (cit. on p. 14).
- [56] WP Jones and B.E. Launder. “The prediction of laminarization with a two-equation model of turbulence”. In: *International Journal of Heat and Mass Transfer* 15.2 (1972), pp. 301–314 (cit. on p. 26).
- [57] T. Kawakubo. “Unsteady Rotor-Stator Interaction of a Radial-Inflow Turbine With Variable Nozzle Vanes”. In: *Proceedings of ASME Turbo Expo 2010: Power for Land, Sea and Air*. ASME. 2010 (cit. on pp. 44, 126, 129, 158).
- [58] T. Kreuz-Ihli, D. Filsinger, A. Schulz, and S. Wittig. “Numerical and experimental study of unsteady flow field and vibration in radial inflow turbines”. In: *Journal of Turbomachinery* 122 (2000), pp. 247–254 (cit. on pp. 15, 47).
- [59] J. K. W. Lam, Q. D. H. Roberts, and G. T. McDonnell. “Flow modelling of a turbocharger turbine under pulsating flow”. In: *ImechE Conference Transactions from 7th International Conference on Turbochargers and Turbocharging*. 2002, pp. 14–15 (cit. on pp. 24, 44, 126, 158).

- [60] K. S. Lee, K. Y. Kim, and A. Samad. “Design optimization of low-speed axial flow fan blade with three-dimensional RANS analysis”. In: *Journal of mechanical science and technology* 22.10 (2008), pp. 1864–1869 (cit. on p. 27).
- [61] H. Li. “Fluid flow analysis of a single-stage centrifugal fan with a ported diffuser”. In: *Engineering Applications of Computational Fluid Mechanics* 3 (2009), pp. 147–163 (cit. on p. 28).
- [64] Z. Liu and D.L. Hill. “Issues surrounding multiple frames of reference models for turbo compressor applications”. In: *Fifteenth International Compressor Engineering Conference*. Purdue University. 2000 (cit. on pp. 24, 44, 127, 129).
- [65] J. M. Luján, V. Bermúdez, J. R. Serrano, and C. Cervelló. “Test bench for turbocharger groups characterization”. In: *SAE Paper 2002-01-0163* (2002) (cit. on pp. 21, 82).
- [67] F. R. Menter. “Two-equation eddy-viscosity turbulence models for engineering applications”. In: *AIAA journal* 32.8 (1994), pp. 1598–1605 (cit. on p. 26).
- [68] F. R. Menter, M. Kuntz, and R. Langtry. “Ten years of industrial experience with the SST turbulence model”. In: *Turbulence, heat and mass transfer* 4 (2003), pp. 625–632 (cit. on p. 27).
- [69] F. R. Menter, R. Langtry, and T. Hansen. “CFD simulation of turbomachinery flows—verification, validation and modeling”. In: *European Congress on Computational Methods in Applied Sciences and Engineering, ECCOMAS*. 2004 (cit. on p. 27).
- [70] FR Menter. “Influence of freestream values on k-omega turbulence model predictions”. In: *AIAA journal* 30 (1992), pp. 1657–1659 (cit. on p. 26).
- [79] OpenWAM. CMT- Motores Térmicos. Universidad Politécnica de Valencia. URL: <http://www.OpenWAM.org> (cit. on pp. 4, 14, 63, 87, 98).
- [80] M.H. Padzillah, Rajoo S., and Martinez-Botas R.F. “Numerical Assessment of Unsteady Flow Effects on a Nozzled Turbocharger Turbine”. In: *Proceedings of ASME Turbo Expo 2012*. GT2012-69062. 2012 (cit. on p. 47).

- [81] D. Palfreyman, R. F. Martinez-Botas, and N. Karamanis. “Computational and experimental investigation of the aerodynamics of turbocharger mixed-flow turbines”. In: *ImechE Conference Transactions from 7th International Conference on Turbochargers and Turbocharging, 14-15 May London UK*. 2002, pp. 45–59 (cit. on pp. 15, 126, 131, 158).
- [82] D. Palfreyman and RF Martinez-Botas. “The pulsating flow field in a mixed flow turbocharger turbine: An experimental and computational study”. In: *Journal of Turbomachinery* 127 (2005), p. 144 (cit. on pp. 24, 44, 127).
- [83] S.V. Patankar. *Numerical heat transfer and fluid flow*. Hemisphere Pub, 1980 (cit. on p. 46).
- [87] F. Payri, J. M. Desantes, and A. J. Torregrosa. “Acoustic boundary condition for unsteady one-dimensional flow calculations”. In: *Journal of Sound and Vibration* 188.1 (1995), pp. 85–110. ISSN: 0022-460X (cit. on pp. 6, 15, 83, 87, 108).
- [88] F. Payri, J. Galindo, J. R. Serrano, and F. J. Arnau. “Analysis of numerical methods to solve one-dimensional fluid-dynamic governing equations under impulsive flow in tapered ducts”. In: *International Journal of Mechanical Sciences* 46.7 (2004), pp. 981–1004 (cit. on pp. 14, 72).
- [89] F. Payri, J. Galindo, J. R. Serrano, and M. A. Reyes-Belmonte. “Experimental methodology to a comprehensive characterization of automotive turbochargers”. In: *EAEC2011-A17*. Valencia, 2011 (cit. on pp. 16, 128).
- [92] R. Pecnik, J. A. S. Witteveen, and G. Iaccarino. “Uncertainty quantification for laminar-turbulent transition prediction in RANS turbomachinery applications”. In: *49th AIAA Aerospace Sciences Meeting including the New Horizons Forum and Aerospace Exposition*. AIAA 2011-660. 2011 (cit. on p. 27).
- [96] S. Rajoo and R. M. Botas. “Variable geometry mixed flow turbine for turbochargers: an experimental study”. In: *International Journal of Fluid Machinery and Systems* 1.1 (2008), pp. 155–168 (cit. on p. 14).
- [97] S. Rajoo and R. Martinez-Botas. “Mixed flow turbine research: A Review”. In: *Journal of Turbomachinery* 130 (2008), p. 044001 (cit. on pp. 15, 126).

- [101] S. Shaaban and J. Seume. “Analysis of turbocharger non-adiabatic performance”. In: *ImechE Conference Transactions from 8th International Conference on Turbochargers and Turbocharging*. 2006, pp. 119–130 (cit. on p. 23).
- [102] A. T. Simpson, S. W. T. Spence, and J. K. Watterson. “A comparison of the flow structures and losses within vaned and vaneless stators for radial turbines”. In: *Journal of Turbomachinery* 131 (2009), p. 031010 (cit. on pp. 14, 15, 23, 27, 44, 47, 129, 158).
- [103] J. Smagorinsky. “General circulation experiments with the primitive equations”. In: *Monthly weather review* 91.3 (1963), pp. 99–164 (cit. on p. 25).
- [104] E.M. Smirnov. “Recent Progress in Numerical Simulation of Highly Three-Dimensional Turbulent Flows and Endwall Heat Transfer in Turbine Blade Cascades”. In: *Heat Transfer Research* 42.1 (2011), pp. 25–44 (cit. on p. 23).
- [106] S. W. T. Spence, R. S. E. Rosborough, D. Artt, and G. McCullough. “A direct performance comparison of vaned and vaneless stators for radial turbines”. In: *Journal of Turbomachinery* 129 (2007), p. 53 (cit. on p. 14).
- [107] M. Strelets. “Detached eddy simulation of massively separated flows”. In: *In 39th AIAA Aerospace Sciences Meeting and Exhibit*. AIAA 2001-0879. American Institute of Aeronautics & Astronautics, 2001 (cit. on p. 25).
- [109] *Supercharging Testing Standards*. Engine Power Test Code Committee, Issued August, 1995. (Cit. on p. 18).
- [112] A. Thakker and F. Hourigan. “Computational fluid dynamics analysis of a 0.6 m, 0.6 hub-to-tip ratio impulse turbine with fixed guide vanes”. In: *Renewable energy* 30.9 (2005), pp. 1387–1399 (cit. on pp. 14, 15).
- [116] A. M. Tousi, A. Tourani, et al. “Comparison of turbulence methods in CFD analysis of compressible flows in radial turbomachines”. In: *Aircraft Engineering and Aerospace Technology: An International Journal* 80.6 (2008), pp. 657–665 (cit. on p. 26).
- [117] M. Tritthart and D. Gutknecht. “Three-dimensional Simulation of Free-Surface Flows using Polyhedral Finite Volumes”. In: *Engineering Applications of Computational Fluid Mechanics* 1 (2007), pp. 1–14 (cit. on p. 27).

- [119] H. K. Versteeg and W. Malalasekera. *An introduction to computational fluid dynamics: the finite volume method*. Prentice Hall, 2007 (cit. on pp. 14, 25, 28, 72).
- [121] D. C. Wilcox. *Turbulence Modeling for CFD (Hardcover)*. Dcw Industries, Incorporated; 3rd edition, 2006 (cit. on pp. 25, 26).
- [123] S. Yedidiah. *Centrifugal pump user's guidebook: problems and solutions*. Kluwer Academic Publishers, 1996 (cit. on p. 15).
- [124] P.K. Zachos, N. Grech, B. Charnley, V. Pachidis, and R. Singh. "Experimental and numerical investigation of a compressor cascade at highly negative incidence". In: *Engineering Applications of Computational Fluid Mechanics* 5.1 (2011), pp. 26–36 (cit. on p. 28).

Chapter 3

Implementation of a 1D-3D coupling computational fluid dynamic boundary condition

Contents

3.1	Introduction	62
3.2	Coupling methodology	64
3.3	Implementation	68
3.4	Validation	71
3.5	Conclusions	76
	Chapter 3 bibliography	78

3.1 Introduction

IN THE PREVIOUS CHAPTER¹ a description of the turbine CFD model has been presented. A particular effort has been made to optimize the limited computational resources so that the best resolution can be achieved. The aim has been to allocate the finest mesh only where it is necessary. This methodology has yielded to a mesh distribution within the turbine domain. However, a part of the calculation domain was not taken into account in that analysis, the turbine inlet and outlet ducts. These ducts are included in the calculation for several reasons. First, the boundary conditions are set away from the turbine in order minimize its spurious influence in the internal flow of the turbine. Secondly, radial turbines are typically tested on gas-stands with long straight inlet and outlet ducts or flow straighteners. To include these pipes or at least a part of them in the domain eases the comparison with tests results taken at locations far away from the turbine. Finally, the turbine model developed in chapter 2 can be implemented into a complete engine model. These models include the calculation of the exhaust and intake systems where the turbocharger is connected.

In order to perform a CFD simulation some assumptions or models are needed. Generally, the less restrictive are the hypothesis made, the more accurate the results will be. However, assumptions can imply a significant reduction in the time consumption without a loss in the accuracy, as long as the physical problem that is being modeled meets the requirements made.

The engine exhaust and exhaust systems are mainly composed of ducts, which can be accurately simulated by means of one-dimensional, non-viscous codes. However, there are several components that manifest a complex three-dimensional flow behavior, such as turbomachinery or manifolds junctions, therefore being unable to be simulated properly by 1D codes, and thus requiring viscous, 3D codes. Hence, it is a right choice to save computational time by simulating the complex components by means of a 3D code and modeling with a 1D code the rest of the system, i.e. the ducts. In this way, a coupling methodology between the 1D and the 3D code in the respective interfaces is required, being the objective of numerous authors [78, 72, 73].

¹This chapter has been published as: *Coupling methodology of 1D finite difference and 3D finite volumes CFD codes based on the method of characteristics*. Mathematical and Computer Modelling. 2011. [46]

In this chapter, a coupling methodology between the in-house 1D code OpenWAM [79] and the 3D commercial code ANSYS-FLUENT by means of the method of characteristics has been developed and validated.

OpenWAM calculates the internal flow in pipes under the assumption of non-linear inviscid one-dimensional flow. As it was indicated in the previous chapter, the model includes some zero dimensional elements to simulate the filling and emptying process of other ICE components. The connection between the different pipes and reservoirs and also the calculation of elements where the flow is not one-dimensional is carried out using simplified conservation equations without spacial resolution and usually quasi-steady.

OpenWAM is particularly suitable for the calculation of pressure wave movement in the pipes of the intake and exhaust systems and their effects on engine performance and also intake and exhaust noise emissions. However, the simplification of the boundary conditions can lead to low accuracy results. These elements could be more properly calculated with a detailed multidimensional calculation.

ANSYS-FLUENT is a commercial code, which makes impossible the modification of the code to perform certain tasks which are not implemented by default. Nevertheless, the program offers the so-called *User Defined Functions* (UDFs) for that purpose, allowing the user to write a function in the C programming language that can be dynamically loaded with the ANSYS-FLUENT solver, in order to perform the desired tasks. In this chapter, a methodology to perform a 1D-3D-proprietary-code coupling is going to be developed. An introduction to the problem and the codes used has been presented.

In the next section, the methodology followed to perform the coupling is shown, focusing on the explanation of the method of characteristics, which is used to allow the transfer of information between the two codes. Later, the procedure that has been developed for obtaining and transferring necessary information from each of the codes is explained. The coupling methodology has been validated using two different tests shown in section 3.4. Finally, in section 3.5 the conclusions are presented.

3.2 Coupling methodology

In the introduction, it was established the need for the development of a coupling methodology in order to perform a simulation combining a 1D and a 3D code. The main differences between both codes have been described, including the difficulties to modify the commercial 3D software, ANSYS-FLUENT. Therefore, the chosen approach must allow an implementation in terms of the available tools of ANSYS-FLUENT (i.e. UDFs and *monitors*), without overlooking the accuracy in managing the transient problems that have been scoped. Eventually, the well-known method of characteristics was found to meet these requirements, and so was used as a means of solving the coupling problem. Some references [21] performed the coupling directly transferring the flow field variables, or by means of a Riemann solver [78]. In contrast to those, the use of the MoC is a physically based methodology that will give the exact solution if the hypotheses are satisfied. Moreover, the implementation of boundary conditions by means of the MoC for different elements, such as volume, has been the subject of a wide analysis in the past years and OpenWAM has already a set of them implemented in [41], [100] and [42].

3.2.1 The method of characteristics

The method of characteristics (MoC) is a mathematical technique for solving hyperbolic partial differential equations. The method allows to reduce a partial differential equation into a family of ordinary differential equations (ODE) enabling to integrate a solution from some initial data. It is interesting to notice that this method gives the exact solution of the flow equations, provided that the conditions needed to obtain a hyperbolic system of PDEs are fulfilled. In this chapter, the MoC is going to be applied to the particular case of fluid dynamics Navier-Stokes equations.

Euler equations are a simplified form of Navier-Stokes equations for an inviscid compressible flow. Therefore, Euler equations are applicable in high Reynolds number flows, such as those found in ICEs, in which viscosity can be neglected. In the case of an unsteady 1D adiabatic flow, being x the direction of the flow, continuity equation establishes:

$$\frac{\partial \rho}{\partial t} + u \frac{\partial \rho}{\partial x} + \rho \frac{\partial u}{\partial x} = 0. \quad (3.1)$$

The second equation to be considered is the momentum equation in the x direction, which could be written as:

$$\rho \frac{\partial u}{\partial t} + \rho u \frac{\partial u}{\partial x} + \frac{\partial p}{\partial x} = 0 \quad (3.2)$$

and for the entropy:

$$\frac{\partial s}{\partial t} + u \frac{\partial s}{\partial x} = 0. \quad (3.3)$$

The previous set of equations is closed with an equation of state, as:

$$s = s(\rho, p). \quad (3.4)$$

Differentiating equation (3.4):

$$ds = \left(\frac{\partial s}{\partial p} \right) \Big|_{\rho=\text{const.}} dp + \left(\frac{\partial s}{\partial \rho} \right) \Big|_{p=\text{const.}} d\rho \quad (3.5)$$

and applying that $a = \sqrt{-\frac{(\partial s/\partial \rho)_p}{(\partial s/\partial p)_\rho}} = \sqrt{\left(\frac{\partial p}{\partial \rho} \right)_s}$, eq. (3.3) can be rewritten as:

$$\frac{\partial p}{\partial t} + u \frac{\partial p}{\partial x} - a^2 \left(\frac{\partial \rho}{\partial t} + u \frac{\partial \rho}{\partial x} \right) = 0. \quad (3.6)$$

Equations (3.1), (3.2) and (3.6) form a hyperbolic system. Equation (3.6) is already written in its characteristic form and its meaning is clear: entropy remains constant along a path-line, which is a line in the plane (x, t) that fulfills $\frac{\partial x}{\partial t} = u$.

It is possible to rearrange equations (3.1) and (3.2) to find its characteristic form. In order to do that equation (3.6) is used to substitute the variable density from (3.1). Equation (3.1) then becomes:

$$\frac{\partial p}{\partial t} + u \frac{\partial p}{\partial x} + \rho a^2 \frac{\partial u}{\partial x} = 0. \quad (3.7)$$

Adding to this equation, equation (3.2) times an undetermined factor, κ , obtaining:

$$\frac{\partial p}{\partial t} + (u + \kappa) \frac{\partial p}{\partial x} + \rho \kappa \left[\frac{\partial u}{\partial t} + \left(u + \frac{a^2}{\kappa} \right) \frac{\partial u}{\partial x} \right] = 0. \quad (3.8)$$

For equation (3.8) to acquire its characteristic form, the derivatives of p and u must have the same direction in the plane (x, t) . This means that:

$$u + \kappa = u + \frac{a^2}{\kappa} \Rightarrow \kappa = \pm a. \quad (3.9)$$

Substituting the previous condition in eq. (3.8), the two equations required to close the system of hyperbolic equations are obtained:

$$\frac{\partial p}{\partial t} + (u + a) \frac{\partial p}{\partial x} + \rho a \left[\frac{\partial u}{\partial t} + (u + a) \frac{\partial u}{\partial x} \right] = 0 \quad (3.10)$$

$$\frac{\partial p}{\partial t} + (u - a) \frac{\partial p}{\partial x} + \rho a \left[\frac{\partial u}{\partial t} + (u - a) \frac{\partial u}{\partial x} \right] = 0. \quad (3.11)$$

The characteristic lines from the system of eqs. (3.6), (3.10) and (3.11), are the family of curves that satisfy the conditions: $\frac{dx}{dt} = u$ and $\frac{dx}{dt} = a \pm u$. For each one of these curves, there is one variable that will remain constant along it. Those variables are known as Riemann invariants and are defined as:

$$\frac{d\lambda}{dt} = \frac{dp}{dt} + \rho a \frac{du}{dt} = 0 \Rightarrow C^+: \frac{dx}{dt} = a + u \quad (3.12)$$

$$\frac{d\beta}{dt} = \frac{dp}{dt} - \rho a \frac{du}{dt} = 0 \Rightarrow C^-: \frac{dx}{dt} = a - u \quad (3.13)$$

$$\frac{dA_a}{dt} = \frac{dp}{dt} - a^2 \frac{d\rho}{dt} = 0 \Rightarrow C^0: \frac{dx}{dt} = u. \quad (3.14)$$

The previous set of equations is a coupled system of three equations. Notice that the partial derivatives have been replaced by ordinary derivatives, since they are performed in the same direction of the plane (x, t) , which is also the local direction of the correspondent characteristic line. This system of equations will allow to compute the solution in any point of the plane (x, t) from the solution at the previous time, as it is shown in Figure 3.1.

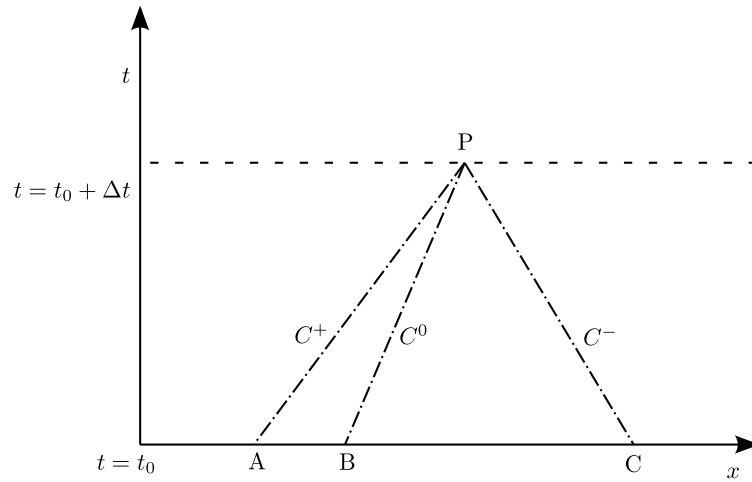


Figure 3.1: Characteristic lines in the plane (x, t)

3.2.2 Homentropic flow

For an ideal gas, in the particular case of a homentropic flow, in which the entropy is uniform in the whole flow field, equation (3.6) or (3.14) becomes trivial, and the Riemann invariants may be computed as:

$$\lambda = a + \frac{\gamma - 1}{2}u, \quad (3.15)$$

$$\beta = a - \frac{\gamma - 1}{2}u. \quad (3.16)$$

Note that in this chapter a dimensional form of the Riemann invariant has been used, in order to highlight its physical interpretation.

3.2.3 Non-Homentropic flow

If the entropy of the flow is not initially uniform, the entropy across a line C^+ and C^- will change, and the values of the Riemann invariants will be modified along the characteristic lines. The value of A_a is not affected by this variation, since entropy is exactly what is constant through a characteristic of the family

C^0 . In this situation, A_a may be defined as:

$$A_a = a \cdot \left(\frac{p}{p_{ref}} \right)^{-\frac{\gamma-1}{2\gamma}}. \quad (3.17)$$

In eq. (3.17), the value of p_{ref} must be the initial pressure of the domain. All along this development the assumptions of inviscid flow and negligible heat transfer have been used. The values of the Riemann invariants, from equations (3.15), (3.16) and (3.17), can be modified taking into account the non-uniformity in entropy in the flow field, the existence of friction with the walls or heat transfer through the walls. This modification is done by means of assuming a deviation of the value of the Riemann invariant due to each one of these effects [13] along the characteristic line considered. The existence of these variations means that the value will not be the same at two different points of the characteristic line. As an example of this fact, the variation of the λ invariant is provided in the following equations:

$$\begin{aligned} \lambda|_2 &= \lambda|_1 + d\lambda \\ &= a + \frac{\gamma-1}{2}u + d\lambda|_f + d\lambda|_Q + d\lambda|_S \end{aligned} \quad (3.18)$$

where,

$$\begin{aligned} d\lambda|_f &= -(\gamma-1) \left[1 - (\gamma-1) \frac{u}{a} \right] \frac{f}{D} u^2 \frac{u}{|u|} dt \\ d\lambda|_Q &= \frac{(\gamma-1)^2}{2} q \frac{1}{a} dt \\ d\lambda|_S &= a \frac{dA_a}{A_a}. \end{aligned} \quad (3.19)$$

The expressions of the modifiers are similar for the other two Riemann invariants, as can be seen in reference [14].

3.3 Implementation

In order to update the boundary condition in the interface of the two domains in each time step, the characteristics and the corresponding entropy level must be extracted from the two domains to allow the transfer of information between the codes. The information needed as input in the boundary condition is also

different in each one of the codes. The necessary variables that need to be extracted from the flow field in order to compute the Riemann invariants can be derived by means of equations (3.18) and (3.19). The way in which these variables are obtained depends on the code considered. Since the time-step size in each one of the codes could be different, a time interpolation procedure is needed, as shown in Figure 3.2.

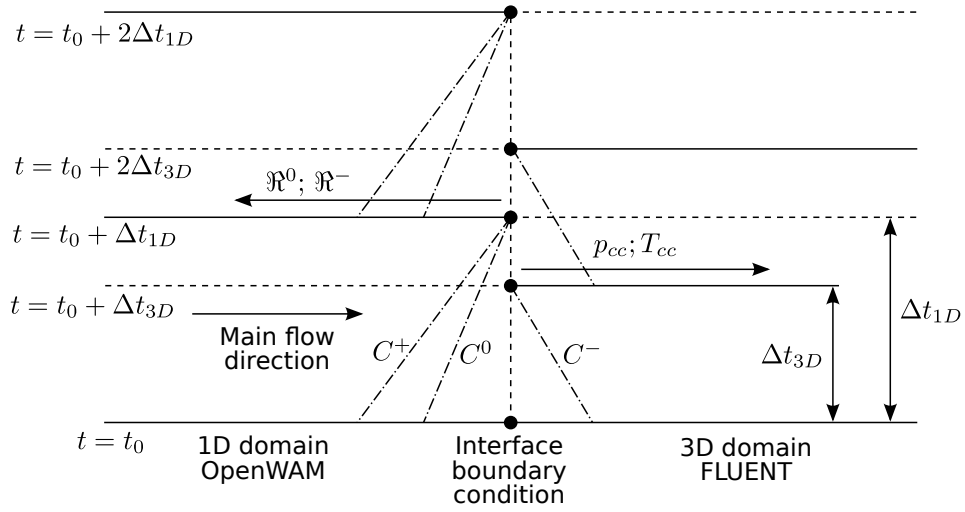


Figure 3.2: Characteristic lines in the plane (x,t) in two successive time steps

The interchange of information between the two codes is done by means of two text files. A routine has been implemented in the codes in order to wait until the correspondent file is update to a higher time than the one needed.

3.3.1 OpenWAM

In the case of OpenWAM, the input variables needed as BC are directly the Riemann invariants. This code previously had a function to connect two ducts by means of the MoC [41, 100, 42]. Basically, the function allows to send the value of the invariants that arrive to the end of the duct at the next time step and receives the reciprocal invariants on the other side of the boundary. In order to take into account the possibility of changes in the flow direction, a decision loop is used to determine the appropriate entropy level. With the

values of the invariants and the entropy level, the function obtains the variables needed to update the boundary condition.

3.3.2 ANSYS-FLUENT

As stated before, the variables that ANSYS-FLUENT needs as input are not the Riemann invariants. If the coupling boundary is an inlet boundary, the code requires as an input the value of the total pressure and total temperature, whereas if the coupling boundary is an outlet boundary, it will need the static pressure and total temperature (only used if there is recirculating flow). It is important to notice that the surface in which the necessary flow variables should be obtained, varies with the flow field and therefore with time. The impossibility to modify this code required a particular approach to obtain the desired invariants. First of all, a so-called *custom field function* is defined as follows:

$$\begin{aligned} pos_{\lambda} &= x + (u + a) \cdot \Delta t_{MoC} \\ pos_{\beta} &= x + (u - a) \cdot \Delta t_{MoC} \\ pos_{A_a} &= u \cdot \Delta t_{MoC}. \end{aligned} \tag{3.20}$$

These *custom field functions* indicate the position that the information (Riemann invariant) of a given flow particle will reach in the considered time (Δt_{MoC}). Then, one must define an *isosurface* of the fluid particles whose information will reach the boundary condition of the considered domain for each one of the characteristic lines. This condition is applied by setting $pos_{\mathfrak{R}} = x_{BC}$, where x_{BC} is the x -position of the boundary condition. Where \mathfrak{R} represents any of the Riemann invariants: λ , β and A_a .

ANSYS-FLUENT manages *isosurfaces* in a dynamic way, so that the values of the *isosurface* are those corresponding to the current time step. This approach allows obtaininig the invariants which will arrive to the boundary condition after a Δt_{MoC} . Since the *isosurface* holds the proper position of the corresponding characteristic, one only needs to write with a *monitor* the involved variables (a, u, p, T, γ) at the *isosurface* and apply equation (3.18) in order to obtain the value of the invariant. Finally, from equations (3.15), (3.16) and (3.17), it can be easily derived that the variables needed to define

the boundary condition are:

$$\begin{aligned}
 a_{BC} &= \frac{\lambda + \beta}{2} \\
 u_{BC} &= \frac{\lambda - \beta}{\gamma_{BC} - 1} \\
 p_{BC} &= p_{ref} \left(\frac{a_{BC}}{A_a} \right)^{\frac{2\gamma_{BC}}{\gamma_{BC} - 1}}.
 \end{aligned} \tag{3.21}$$

The values of the Riemann invariants must be taken at the boundary condition in order to recover the proper values. Even though γ_{BC} is a function of temperature, an explicit set of equations can be obtained by using the value of γ_{BC} corresponding to the temperature at the BC at the previous time step.

Finally, a *User Defined Function*(UDF) has been written in order to manage all the information, such as reading the monitors and the file supplied by OpenWAM, computing the invariants, writing them into a file for OpenWAM to read and applying the proper boundary condition.

3.4 Validation

In order to validate the coupling procedure, it is going to be applied to two different problems. The first one is a well-known analytical test-case, known as Sod's problem. The second problem will allow checking that the fluid-dynamic variables are transferred correctly in a real case, using a configuration equivalent to an impulse test rig.

3.4.1 Sod's problem

Sod's problem [105] is a shock tube test problem commonly used to test the accuracy of computational fluid codes. The test consists in the transient evolution of a shock tube divided initially by a membrane into two separate regions which are set at different pressures and temperatures. For the sake of simplicity, the test has been used only with a pressure difference. At time zero this membrane is eliminated and the flow inside the tube starts to evolve. In our case, the simulation consisted in a 2 meters tube divided into two computational domains. The first one is a 1D domain computed with OpenWAM,

whereas the second one is simulated with FLUENT. The aforementioned membrane is situated at 0.8 m, as shown in Figure 3.3. The region of the domain at the left side of the membrane is initially set at a pressure of 3 bar and a temperature of 293 K, while the right side is set at a pressure of 1 bar and a temperature of 293 K.

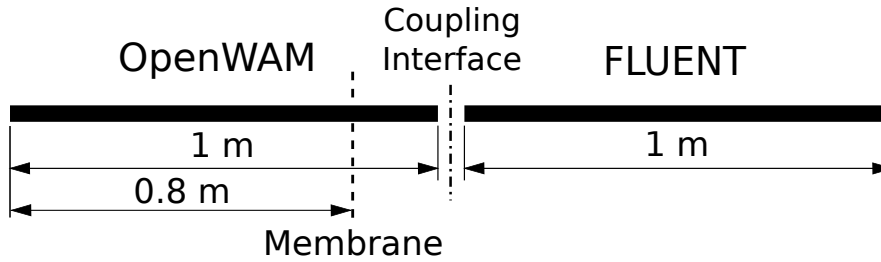


Figure 3.3: Computational domain of Sod's Problem

This problem is interesting assuming an inviscid flow and neglecting the heat transfer through the walls, since it has analytical solution. Therefore, the solution obtained with the coupling can be validated.

It is important to notice that the two regions start with a different entropy level, so that the correction for the variation of entropy for the Riemann invariants λ and β must be applied. A distribution of the pressure, velocity and temperature in the tube is obtained for a time of 2 ms. Figures. 3.4, 3.5 and 3.6 show a comparison between the analytical solution for a two meter tube and the results obtained with the coupling procedure using a 1 meter 1D tube and 1 meter 3D tube.

As can be seen, the results obtained using the two codes coupled and the analytical solution are quite correlated, meaning that the coupling methodology is transferring the information properly. The small peaks that appear in the curves are due to numerical disturbances induced by the scheme [119].

3.4.2 Impulse test rig

An impulse test rig is a device used for measuring the acoustic response of a system [20, 88]. Mainly, it consists of two long ducts (each one about 20 meters long) at the inlet and the outlet of the element whose acoustic response

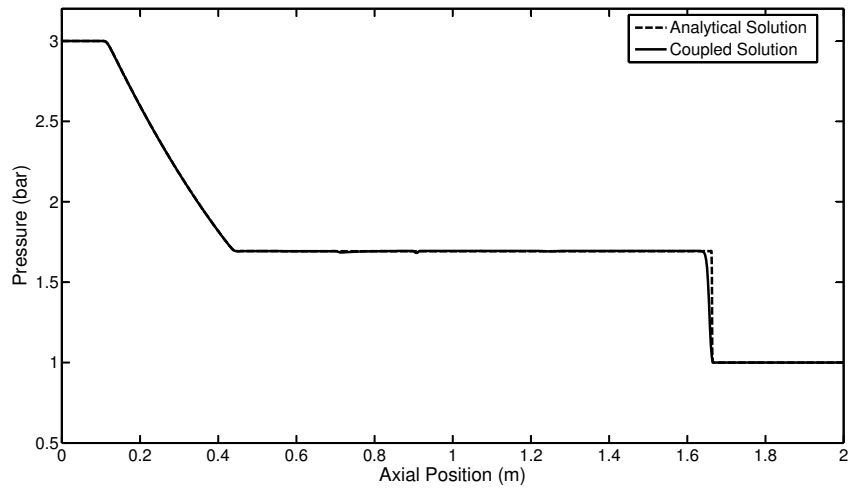


Figure 3.4: Distribution of the pressure inside the shock tube for $t=2$ ms

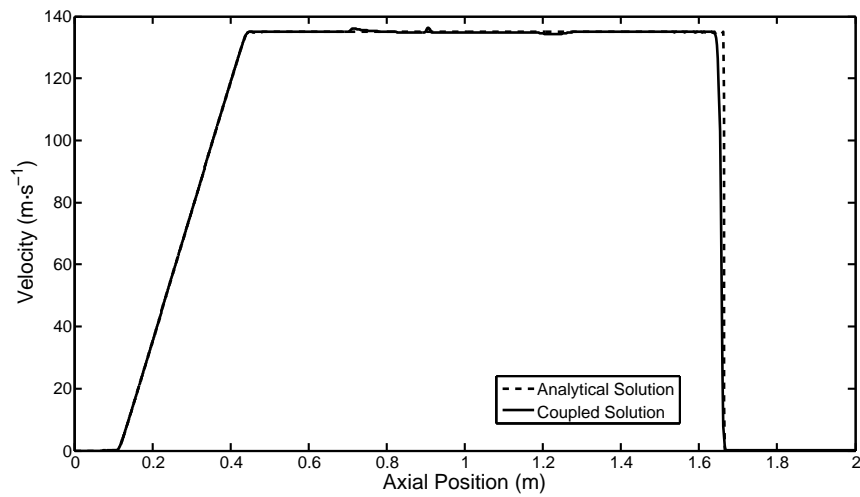


Figure 3.5: Distribution of the velocity inside the shock tube for $t=2$ ms

is meant to be measured. Such long ducts are required so that the pressure waves going out of the system (reflected at the inlet and transmitted at the

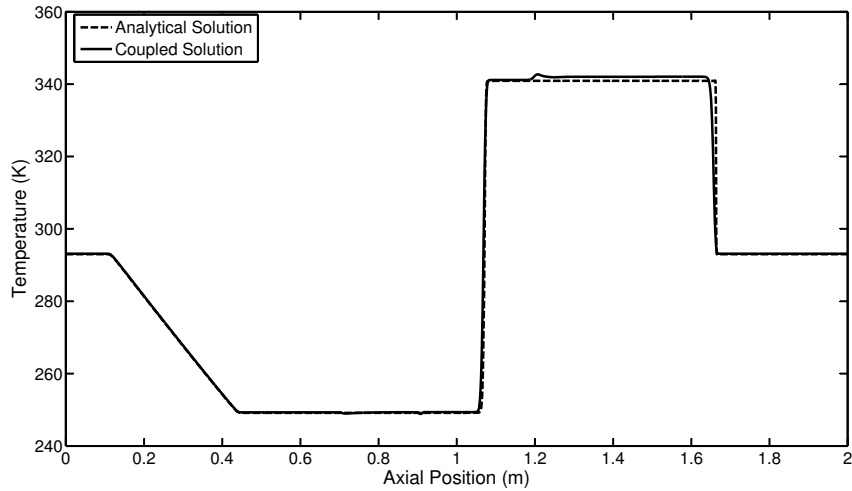


Figure 3.6: Distribution of the temperature inside the shock tube for $t=2$ ms

outlet) do not come back to it during the experiment.

This test case is interesting since it represents the main utility that this coupling BC has, i.e., reducing the size of a 3D computational domain and therefore its computational cost. This is performed by computing an important and geometrically simpler part of a domain, i.e. the ducts, with a 1D code and using the 3D code to simulate just the complex section of the domain.

The performed simulation consists of a 20.1 m long duct in which the first 19.9 m are simulated with OpenWAM and the last 0.2 m with FLUENT, as shown in Figure 3.7.

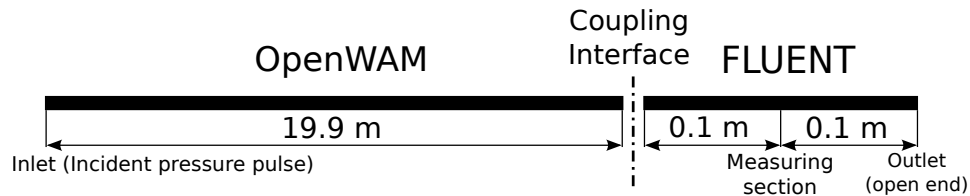


Figure 3.7: Computational domain of the impulse test rig

A pressure pulse corresponding to a measured one is set at the inlet, with the outlet being an open end with zero gauge pressure. The incident pressure arriving at a measuring section set at 20 m is monitored. Therefore, the evolution with time of the incident pressure at the measuring section is plotted together with the pressure pulse set at the inlet Figure 3.8.

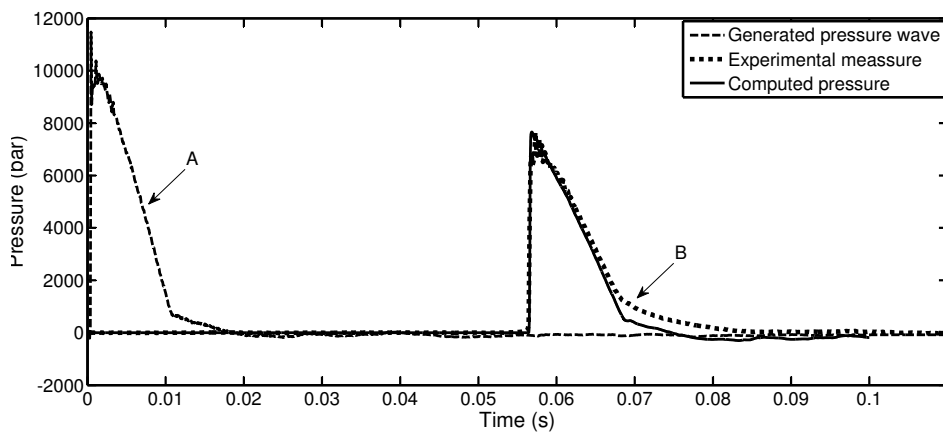


Figure 3.8: Time evolution of the incident pressure at the inlet and measuring section

The solution obtained using the 1D-3D simulation is quite similar to the experimental measure in terms of incident pressure. However, a small difference appears in the change of slope of the triangular peak. In the experimental results, the transition is smooth (mark B in Figure 3.8). On the other hand, the simulation provides a sharper shape, similar to that which had the inlet (mark A in Figure 3.8). This is due to the lack of a turbulence model in OpenWAM. Therefore, the diffusive effect of turbulence, which smoothes the change in the slopes of the curve, is neglected.

Moreover, if this simulation is performed entirely with the 3D solver, it takes 20 times more than the simulation using the coupled 1D-3D boundary condition. The increase of computational cost is due to two different aspects: the time required for the flow to pass through the ducts and the increase time per computational time step due to the higher number of cells.

3.5 Conclusions

A methodology to perform a combined 1D-3D simulation has been developed. The main advantage of this kind of modeling is that it allows achieving a good geometric resolution (3D) where required, but with a reduced computational cost if compared to a 3D simulation of the whole domain.

The procedure of interchanging information between the two domains is done by means of the method of characteristics. It is interesting to remark that the MoC gives the exact solution for a hyperbolic system of PDEs. It has been implemented for a 3D commercial code, with the difficulties inherent to this process due to the lack of accessibility of those kind of codes.

Two different validation procedures have been followed. In the first one, a theoretical case (Sod's problem) has been calculated and compared with the analytical solution. The results show that the corrections on the entropy level associated to temperature discontinuities. The second validation was based on tests in an impulse test rig. The comparison of calculated and measured results shows that the 1D-3D boundary condition predicts properly the information transfer between the codes, although the 1D code does not account for diffusive flow effects.

Finally, the boundary condition developed in this chapter has several benefices. First, it reduces the calculation time up to 1-2 orders of magnitude depending on the relative sizes of turbine and pipes mesh. Second, the boundary condition allows implementing the turbine model within whole engine 1D models such as OpenWAM. Also, the boundary condition avoids the spurious reflections at the boundary condition.

On this last point further work has been carried out in the thesis. Following the method of characteristics method a stand-alone anechoic boundary condition has been developed and is presented in chapter 4. Also, further investigation on real flow effects not considered in this chapter has been carried out. This is presented in chapter 5.

Chapter Bibliography 3

- [13] R. S. Benson, R. D. Garg, and D. Woollatt. "A numerical solution of unsteady flow problems". In: *International Journal of Mechanical*

- Sciences* 6.1 (1964), pp. 117–144. DOI: 10.1016/0020-7403(64)90009-8 (cit. on pp. 68, 87, 109).
- [14] R. S. Benson, J. H. Horlock, and D. E. Winterbone. *The thermodynamics and gas dynamics of internal combustion engines*. Ed. by Oxford University Press. Vol. 1. Oxford University Press, 1982 (cit. on pp. 68, 89, 109).
- [20] A. Broatch, X. Margot, A. Gil, and F. D. Denia. “A CFD Approach to the Computation of the Acoustic Response of Exhaust Mufflers”. In: *Journal of Computational Acoustic* 13.2 (2005), pp. 301–316. DOI: 10.1142/S0218396X05002682 (cit. on pp. 3, 6, 72, 80, 95, 97).
- [21] M. Brück, B. Michaelis, M. Awasthi, and R. Reinelt. “1D/3D-Coupling GT-POWER/FLUENT to Predict Species Transport in Exhaust Oxygen Sensors at Engine Operating Conditions”. In: *European Automotive CFD Conference*. 2007 (cit. on p. 64).
- [41] J. Galindo, J. R. Serrano, F. J. Arnau, and P. Piqueras. “Description of a Semi-Independent Time Discretization Methodology for a One-Dimensional Gas Dynamics Model”. In: *Journal of Engineering for Gas Turbines and Power* 131 (2009), p. 034504. DOI: 10.1115/1.2983015 (cit. on pp. 64, 69, 98).
- [42] J. Galindo, J. R. Serrano, F. J. Arnau, and P. Piqueras. “High-frequency response of a calculation methodology for gas dynamics based on Independent Time Discretisation”. In: *Mathematical and Computer Modelling* 50.5-6 (2009), pp. 812–822. DOI: 10.1016/j.mcm.2009.05.011 (cit. on pp. 64, 69).
- [46] J. Galindo, A. Tiseira, P. Fajardo, and R. Navarro. “Coupling methodology of 1D finite difference and 3D finite volume CFD codes based on the Method of Characteristics”. In: *Mathematical and Computer Modelling* 54.7-8 (2011), pp. 1738–1746. DOI: <http://dx.doi.org/10.1016/j.mcm.2010.11.078> (cit. on pp. 6, 15, 62, 81, 88, 93, 112, 118, 167).
- [72] G. Montenegro and A. Onorati. “Modeling of Silencers for IC Engine Intake and Exhaust Systems by Means of an Integrated 1D-multiD Approach”. In: *SAE International Journal of Engines* 1.1 (2009), p. 466. DOI: 10.4271/2008-01-0677 (cit. on pp. 3, 62, 80).

- [73] G. Montenegro, A. Onorati, F. Piscaglia, and G. D’Errico. *Integrated 1D-Multi-D Fluid Dynamic Models for the Simulation of ICE Intake and Exhaust Systems*. Tech. rep. 2007-01-0495. SAE Technical Paper Series, 2007. DOI: 10.4271/2007-01-0495 (cit. on p. 62).
- [78] A. Onorati, G. Montenegro, and G. D’Errico. *Prediction of the Attenuation Characteristics of IC Engine Silencers by 1-D and Multi-D Simulation Models*. Tech. rep. 2006-01-1541. SAE Technical Paper Series, 2006. DOI: 10.4271/2006-01-1541 (cit. on pp. 62, 64, 81).
- [79] OpenWAM. CMT- Motores Térmicos. Universidad Politécnica de Valencia. URL: <http://www.OpenWAM.org> (cit. on pp. 4, 14, 63, 87, 98).
- [88] F. Payri, J. Galindo, J. R. Serrano, and F. J. Arnau. “Analysis of numerical methods to solve one-dimensional fluid-dynamic governing equations under impulsive flow in tapered ducts”. In: *International Journal of Mechanical Sciences* 46.7 (2004), pp. 981–1004 (cit. on pp. 14, 72).
- [100] J. R. Serrano, F. J. Arnau, P. Piqueras, A. Onorati, and G. Montenegro. “1D gas dynamic modelling of mass conservation in engine duct systems with thermal contact discontinuities”. In: *Mathematical and Computer Modelling* 49.5-6 (2009), pp. 1078–1088. DOI: 10.1016/j.mcm.2008.03.015 (cit. on pp. 2, 64, 69).
- [105] G. A. Sod. “A survey of several finite difference methods for systems of nonlinear hyperbolic conservation laws”. In: *Journal of Computational Physics* 27.1 (1978), pp. 1–31. DOI: 10.1016/0021-9991(78)90023-2 (cit. on pp. 71, 84).
- [119] H. K. Versteeg and W. Malalasekera. *An introduction to computational fluid dynamics: the finite volume method*. Prentice Hall, 2007 (cit. on pp. 14, 25, 28, 72).

Chapter 4

Development of an anechoic boundary condition for computational fluid dynamic codes

Contents

4.1	Introduction	80
4.2	Non-reflecting boundary conditions	82
4.3	Proposal of a new non-reflecting boundary condition for non-homentropic flow	89
4.4	Application to the analysis of the acoustic response of a muffler	95
4.5	Summary and conclusions	99
	Chapter 4 bibliography	105

4.1 Introduction

THE NEED TO REDUCE¹ development costs of internal combustion engines (ICE) have led to considerable efforts seeking the improvement of the fluid-dynamic and acoustic behavior of the different components of an ICE. In particular, the use of numerical simulations for muffler evaluation and design has become common practice.

Among the different techniques available, those most used are based upon a one-dimensional (plane-wave) approach, due to their extremely low computational cost. Such codes are particularly well suited for the computation of wave action in the ducts of intake and exhaust systems and its effects on ICE performance and noise emissions. However, these do not deal with the actual geometry and rely upon quasi-steady assumptions. In cases in which the geometry is relatively simple, one-dimensional (1D) codes provide good resolution even in compressible unsteady flows. However, for more realistic geometries, it is imperative to resort to the numerical solution of the three-dimensional (3D) wave propagation.

3D analyses are usually achieved in the linear regime, by means of the finite element method (FEM), as described in [84], or the boundary element method (BEM), in order to obtain magnitudes in the frequency domain, such as the transmission loss. These methods have been extensively used for design purposes, even if they present some limitations when handling anisotropy or when describing the coupling between the mean flow and the fluctuations [118].

A further step is the use of full 3D-CFD simulations in order to describe the unsteady flow behavior of a system. In these codes, the full flow equations are solved in the time domain, and then the information can be transformed into the frequency domain for its analysis. The main advantage of these methods is that, since turbulence is modeled, its dissipative effects are also taken into account. Some previous work by [20] and [72] show the potential benefits of CFD, with good agreement with experiments when modeling both mean and pulsating flow in actual exhaust mufflers. The main problem when using 3D-CFD codes is the CPU time consumed during the computations given that an extension of the computational domain, by means of long ducts, is required

¹This chapter has been accepted for publication as: *Development of a non-reflecting boundary condition for its application in 3D computational fluid dynamic codes*. Engineering Applications of Computational Fluid Mechanics. Date of acceptance 16/04/2012. [115]

in order to capture isolated pressure signals upstream and downstream of the system under study in order to compute its acoustic response. In the previous chapter, a 1D-3D boundary condition has been developed with the idea of reducing the total computational cost. The same idea was followed by [78] and [46] solved this problem by performing coupled 1D-3D CFD computations, which allow for the use of 1D codes in some regions of the domain while still conserving a good geometrical resolution where required.

In this frame of ideas, the development of non-reflecting boundary conditions (NRBCs) for their use in 3D-CFD acoustic computations appears to be a suitable alternative. With these boundary conditions the use of long ducts to capture the acoustic response of the system analyzed is not necessary, so that the CPU-time required is considerably reduced. This methodology has similar advantages to those of using 1D models to simulate the flow in the ducts, and the full 3D-CFD calculations are performed where required to take into account the singularity of complex geometries. Of course, NRBCs are used in a wide range of different applications [47, 62].

The literature on the implementation of NRBCs usually groups the boundary conditions into three categories. The first one comprises the methods based on a decomposition into Fourier modes [7, 49, 34]. In the second category the conservation equations are extrapolated in order to obtain asymptotic solutions [111, 17, 29]. Methods that follow the classical absorbing boundary condition developed by [36] fall into this category. Finally, the third category includes methods based on the method of characteristics (MoC) [113, 114, 63], which is also the basis of the work presented here.

While some NRBCs have been developed for internal flow problems [7, 74], most of the existing NRBCs were conceived for their application to external flow problems [49], and cannot be used in a straightforward manner in internal flow simulations. CFD commercial codes usually include some boundary conditions claimed to be non-reflecting. However, as will be shown later, the performance of those included in ANSYS-FLUENT is not the most appropriate for the problem under consideration. The objective of this chapter is to develop and implement a new non-reflecting boundary condition for its use in ANSYS-FLUENT. The main difficulty involved arises from the dependence of the implementation on the flow variables arriving at the boundary.

The chapter is organized as follows: First, the theoretical definition of NRBCs is described. Then, the non-reflecting boundary conditions avail-

able in ANSYS-FLUENT are analyzed, showing their limitations when a non-homentropic problem is considered. In order to overcome those limitations, the issues associated with the inclusion of a new boundary condition in a commercial 3D-CFD code are addressed, and a first validation of the procedure for an existing NRBC is shown. An improved NRBC is proposed and implemented for its use in ANSYS-FLUENT. In the last section, this boundary condition is applied to reproduce the acoustic behavior of a real 3D muffler. The results obtained, comprising both the pressure evolution in the time domain and the transmission loss in the frequency domain, are evaluated by comparison with experimental measurements and with the results from conventional full 3D CFD calculations indicating, in view of the quality of the results and the substantial reduction achieved in the computation time, the suitability of the proposed methodology for design and evaluation purposes.

4.2 Non-reflecting boundary conditions

As stated in the previous section, an NRBC renders unnecessary the use of a long duct in order to avoid the reflection of pressure waves at the boundary, and therefore it may be expected to work as an infinite duct. The implementation of such a boundary condition in a 3D-CFD code will reduce considerably the computation time.

This reduction gains importance if the main interest of the problem lies in a particular section of the domain and the rest of the elements are geometrically simple, such as ducts. A good example of this kind of application could be the simulation of an impulse test rig (with about 20 m of ducts both at the inlet and outlet) [86] or a turbocharger test rig [65]. The reduction in computation time achieved when the ducts are removed is related to two different aspects. First, the number of cells in the domain is reduced and hence the CPU time per time step. Secondly, and even more important, one may save all the time required for the information to propagate along the ducts and reach the system under study.

Once the flow variables are known, it is possible and convenient to decompose them in order to identify separately the information propagating in both forward (p_f) and backward (p_b) directions. Such a decomposition might be

performed by applying eq. (4.1), as shown by [87]:

$$\begin{aligned}
 p_f &= p_0 \left[\frac{1}{2} \left(1 + \left(\frac{p}{p_0} \right)^{\frac{\gamma-1}{2\gamma}} \left(1 + \frac{\gamma-1}{2} \frac{u}{a} \right) \right) \right]^{\frac{2\gamma}{\gamma-1}} \\
 p_b &= p_0 \left[\frac{1}{2} \left(1 + \left(\frac{p}{p_0} \right)^{\frac{\gamma-1}{2\gamma}} \left(1 - \frac{\gamma-1}{2} \frac{u}{a} \right) \right) \right]^{\frac{2\gamma}{\gamma-1}}
 \end{aligned} \tag{4.1}$$

Then it is possible, according to [76], to recover the pressure from its forward and backward components as follows:

$$\left(\frac{p}{p_0} \right)^{\frac{\gamma-1}{2\gamma}} = \left(\frac{p_f}{p_0} \right)^{\frac{\gamma-1}{2\gamma}} + \left(\frac{p_b}{p_0} \right)^{\frac{\gamma-1}{2\gamma}} - 1. \tag{4.2}$$

This decomposition will be referred to frequently in the rest of the discussion. Returning to the NRBCs, two different kinds can be defined:

- The incident pressure boundary condition, which is an inlet condition in which the flow variables at the boundary are not known, but instead information is available on the pressure component coming from upstream of the boundary (p_f). Therefore, computing the flow field is required in order to recover the pressure at the boundary condition by means of eq. (4.2).
- An anechoic end, which is an outlet boundary condition in which information does not propagate upstream of the boundary.

In view of eq. (4.1) the previous definition of an anechoic end may suggest setting $p = p_f$ (whence $p_b = p_0$) at the boundary. However, it will be shown later that this is incorrect. It is remarkable that an anechoic end is physically meaningful only when the flow goes out of the domain. The main contributions of this chapter are related with the anechoic condition, but the conclusions may be easily extended to the incident pressure boundary condition.

4.2.1 Assessment of NRBCs available in ANSYS-FLUENT

Three different kinds of NRBC are currently available in ANSYS-FLUENT [3]:

1. *Turbo-specific non-reflecting boundary condition*, which is not considered in this chapter as it can only be used for steady-state calculations with the density-based solver and structured meshes.
2. *General non-reflecting boundary condition*, which is applicable only with the density-based solver but can be used in both steady and unsteady simulations without any geometric restrictions. This boundary condition is based on the characteristic analysis developed by [113, 114], after which the Linear Relaxation Method (LRM) is used to determine the value of the incoming wave amplitude, as shown by [94] and [98]. There are two versions of this boundary condition:
 - (a) *Pressure at infinity*, in which the pressure at the boundary is relaxed toward the imposed pressure at infinity.
 - (b) *Average boundary pressure*, in which the average pressure on the boundary is forced to approach the exit pressure value.
3. *Pressure far-field boundary condition*, which uses Riemann invariants to determine the flow variables at the boundaries and has no constraints regarding solver or mesh type.

In order to check the validity of the NRBCs available in ANSYS-FLUENT, they were checked against the well-known Sod's shock tube. The solver used for these simulations was a density based solver with an explicit time discretization. Sod's problem [105] is a shock tube problem commonly used to test the accuracy of computational fluid codes [120, 35, 95]. The interest of this problem lies in the fact that an analytical solution is available when viscosity is neglected. The test consists in the transient evolution in a shock tube, divided initially by means of a membrane into two separate regions which are set to different pressures and temperatures (for the sake of simplicity, here the same temperature was initially set in both regions). At time zero, the membrane is removed and the flow inside the tube starts to evolve. Sod's shock tube is quite a challenging problem, since the boundary has to deal with changes in entropy, which are not present in homentropic flow but are likely to be found in the conditions expected in an ICE. In the case studied, a tube of 1 m length was simulated with an outlet NRBC, as can be seen in fig. 4.1. The membrane was located at $x = 0.8$ m and fluid-flow variables were registered at a measuring section at $x = 0.9$ m. The behavior of the NRBCs previously described was then checked.

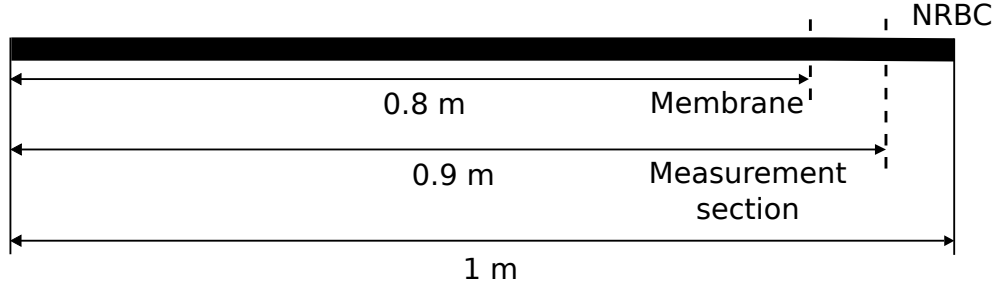


Figure 4.1: Computational domain of Sod's Problem used to validate the NRBCs.

As indicated above, an anechoic end is expected to behave as an *infinite* duct. Therefore, the results obtained in the simulations were compared with the results of simulating a duct sufficiently long so as to avoid any possible reflection at the boundary, thus behaving *locally* as an infinite duct. In fig. 4.2, the pressure decomposition and the Riemann variables at the measuring section of the long duct are shown. At 0.22×10^{-3} s, a λ -wave arrives and pressure rises. Then, at 0.69×10^{-3} s, the entropy discontinuity modifies p_f and p_b without any change in the static pressure. The other Riemann variables (λ and β) are also modified due to the entropy variation. After that, everything remains unchanged.

Performance of the different NRBCs is presented in figure 4.3. It appears that none of them can be regarded as a proper anechoic boundary condition, since they do not represent satisfactorily the behavior of a long duct. Both *general non-reflecting boundary conditions* produce a spurious β rise at 0.77×10^{-3} s when the λ -wave reaches the boundary. As a consequence, a non-physical pressure jump is produced. Moreover, the *pressure at infinity* version, even if it is considered as more adequate for unsteady flow simulations than its counterpart [3], actually exhibits some noise after the spurious rise in pressure. Finally, the *pressure far field* version does not produce any reflection upon arrival of a λ -wave. However, it produces an unreal pressure rise at 1.87×10^{-3} s, due to the spurious β variation originated when the entropy discontinuity reaches the boundary, as shown in fig. 4.3. The error underlying this boundary condition is that the backward invariant, i.e., β , is regarded as constant, whereas in fig. 4.2 it can be seen that it is modified due to variations in the entropy level. This consideration is taken into account

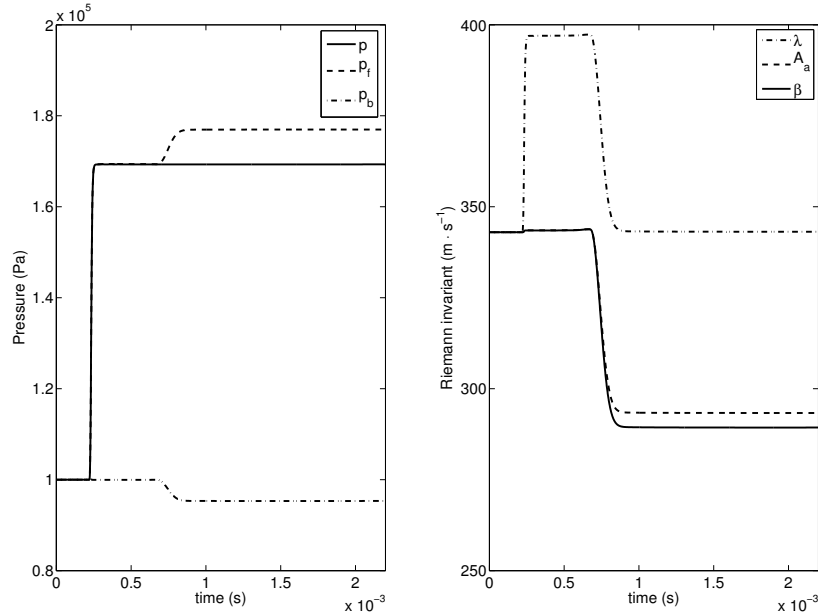


Figure 4.2: Values of flow variables: pressure and decomposed pressure (left) and Riemann variables (right) in an ideal infinite tube.

in section 4.3 below for the development of the proposed anechoic boundary condition.

4.2.2 Implementing a boundary condition in a CFD commercial code

One of the main drawbacks when dealing with commercial CFD codes is the lack of access to the fluid variables in the entire domain, as they are necessary to compute the proper values at the boundary. The methodology used in the following to account for information exchange across the boundary is based on that described in chapter 3, where the method of characteristics (MoC) was applied in order to perform a coupled 1D-3D CFD simulation. The MoC is a mathematical technique for solving hyperbolic systems of partial differential equations (PDEs), in which the system of PDEs is reduced to a family of ordinary differential equations (ODEs), thus enabling one to obtain a solution

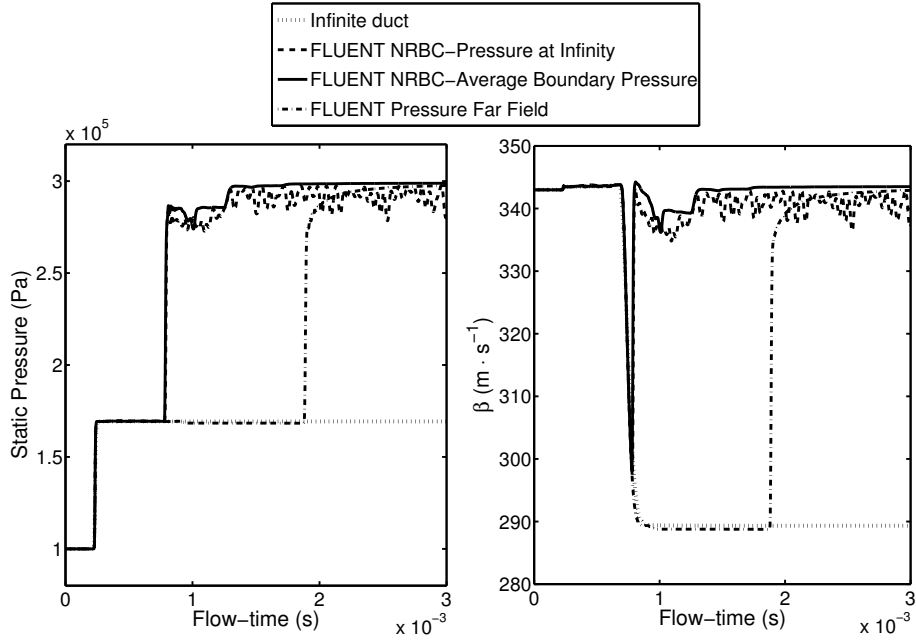


Figure 4.3: Values of flow variables: pressure (left) and β (right) in a short tube using the different NRBCs implemented in ANSYS-FLUENT and in an ideal infinite tube.

from some initial data. The MoC establishes that there are certain flow variables, known as Riemann invariants (λ , β , and A_a), which remain constant along certain lines, known as characteristic lines. The approach used in the present chapter is similar, but there is no need to perform the coupled simulation, since the problem is *decoupled*, i.e. different elements of the domain can be calculated independently, given that the direction of the flow does not change and that the incident conditions are known. In order to check the viability of the implementation of an NRBC, the anechoic end implemented in [79] was considered. This boundary condition is based on the developments of [87], which lead to the condition $\beta = A_a$ at the boundary. Once the values of the flow variables are obtained for the domain, it is possible to compute the Riemann invariants λ and A_a . The value of β is then obtained from the application of the non-reflecting condition, as shown by [13].

The results obtained from such a procedure are shown in figs.4.2 and 4.4, where it is clear that the relevant information has been successfully transferred

from and to the computational domain. Nevertheless, a certain numerical error is found (marked with an A in fig. 4.4), which might be attributed to the discretization, as suggested by [46]. However, it is interesting to remark that this error vanishes after few time steps and therefore it only affects the solution momentarily. Comparing the result computed with this anechoic condition, plotted in fig. 4.4, with the expected result presented in fig. 4.2, it is possible to observe that this boundary condition does not truthfully represent an anechoic condition, since a pressure wave is reflected from the boundary. This can be seen in the changes that appear in the curves representing the reflected pressure, p_b and β , which follow from setting $\beta = A_a$ at the boundary (mark B in fig. 4.4).

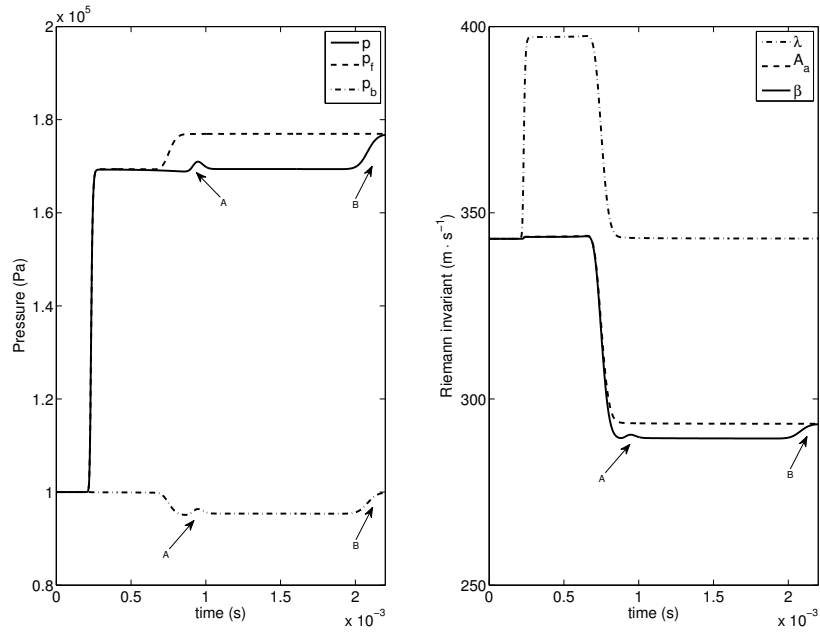


Figure 4.4: Values of flow variables: pressure and pressure components (left) and Riemann variables (right) using former implementation of an anechoic end, $\beta = A_a$.

4.3 Proposal of a new non-reflecting boundary condition for non-homentropic flow

4.3.1 Modifications for non-homentropic flow

In the previous chapter was presented that for each Riemann invariant to remain constant along its characteristic line, the flow must be assumed to be not only isentropic (i.e. inviscid and with negligible heat transfer) but also homentropic. If these assumptions do not hold, then the value of the Riemann invariants is not the same at two different points along their respective characteristic line and, therefore, they are referred to as Riemann *variables* instead of Riemann *invariants*. The corresponding expressions can be modified to account for entropy non-uniformity in the flow-field, and for the existence of wall friction or heat transfer through the walls by means of the modifiers presented in chapter 3 for the λ variable. In the present case, the interest relies on the variation of β between two points of a characteristic line, which can be computed with the following modifiers, which take into account friction (f), heat transfer (Q) and entropy variation (S), respectively:

$$\begin{aligned}\beta|_2 &= \beta|_1 + \Delta\beta \\ &= a - \frac{\gamma-1}{2}u + \Delta\beta|_f + \Delta\beta|_Q + \Delta\beta|_S\end{aligned}\quad (4.3)$$

where

$$\begin{aligned}\Delta\beta|_f &= \int_1^2 d\beta|_f = \\ &= - \int_1^2 (\gamma-1) \left[1 - (\gamma-1) \frac{u}{a} \right] \frac{f}{D} u^2 \frac{u}{|u|} dt \\ \Delta\beta|_Q &= \int_1^2 d\beta|_Q = \int_1^2 \frac{(\gamma-1)^2}{2} q \frac{1}{a} dt \\ \Delta\beta|_S &= \int_1^2 d\beta|_S = \int_1^2 a \frac{dA_a}{A_a}.\end{aligned}\quad (4.4)$$

Similar expressions may be obtained for the modifiers of the other two Riemann variables, as can be seen in [14]. Particularly interesting in the case under consideration is the modification of the Riemann variables due to a change in the entropy of the flow along a characteristic line. The expression

which allows one to compute such a variation may be discretized as:

$$\Delta\beta|_{S_1 \rightarrow 2} = \int_1^2 a \frac{dA_a}{A_a} \approx \frac{a_1 + a_2}{2} \ln \left(\frac{A_{a_2}}{A_{a_1}} \right). \quad (4.5)$$

4.3.2 Implementation of an anechoic condition

As previously stated, an anechoic end is expected to behave as an infinite duct. In terms of the MoC, such an infinite duct would always send back the same value of β_{out} , corresponding to the initial value of β at the boundary, which hereinafter will be denoted as β_∞ . Thus, in the homentropic case one must keep the value of β_{in} constant and equal to its value at the start of the simulation, i.e. β_∞ . Should a change of the entropy level happen, the actual value of β_{in} would be no longer β_∞ . In this case, β_{in} would be obtained by adding to β_∞ the modifiers associated with the variation of the entropy level, corresponding to equation (4.4).

Therefore, the value of β along the characteristic line (C^-) will be modified every time a different entropy level reaches this line. It is interesting to note that entropy levels are transported along the C^0 characteristic lines and thus the changes of entropy occur at the crossing points of the two characteristic lines (see fig. 4.5). The corresponding changes in β can be computed by applying eqs. (4.3), (4.4) and (4.5). In this way, the value of β at the C^- characteristic line that will arrive at the boundary condition at the N -th time step, just after crossing the C^0 characteristic line that passed through the boundary condition at the j -th time step, is given by:

$$\beta_j^N = \beta_\infty + \sum_{i=1}^j \Delta\beta|_{s_{i-1} \rightarrow i}^N \quad (4.6)$$

where subscript i represents the time step at which the different C^0 characteristic lines crossed the boundary condition. This can be seen in figure 4.5, where the characteristic lines have been represented as straight and parallel lines for the sake of simplicity. It is important to remark that β_N^N , which will be referred to as β_{in}^N , corresponds to the value of β that arrives at the boundary condition at the N -th time step. For $i = 0$, the values of the Riemann variables are those computed at the boundary condition at $t = 0$, which are marked with subscript ∞ .

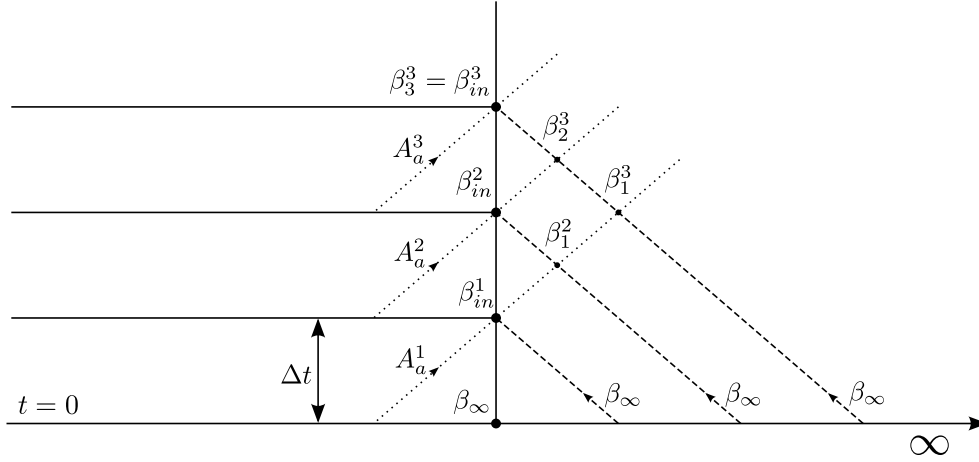


Figure 4.5: Modification of the β values due to changes of entropy occurring at the crossing points of the two characteristic lines.

Equation (4.6) represents all the evolution along a characteristic line, from the downstream infinity to the boundary condition, so that it would be necessary in principle to compute the flow in the whole duct. Nevertheless, if the first time steps are examined carefully (figure 4.6), an approximate procedure can be devised. This is described next.

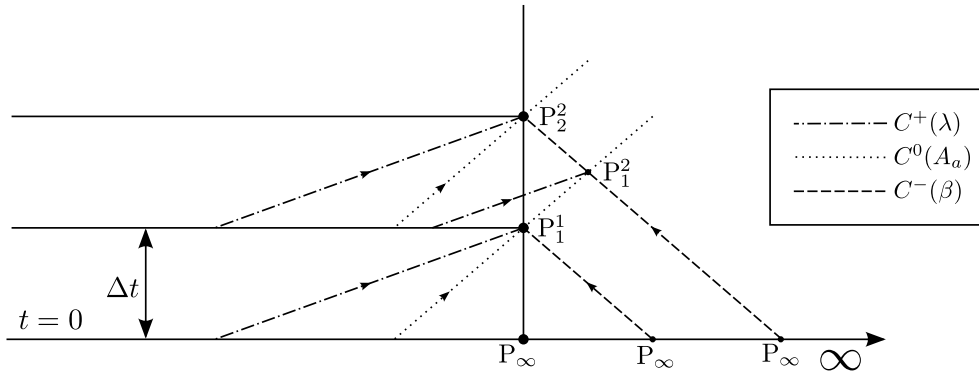


Figure 4.6: Schematic representation of the characteristic lines at an anechoic end. The points P_j^N are defined following the criteria used in eq. (4.6).

Applying eq. (4.6) to the first time step ($N = 1$) and discretizing the

modifiers according to eq. (4.5), one gets

$$\beta_{in}^1 = \beta_1^1 = \beta_\infty + \frac{a_1^1 + a_\infty}{2} \ln \frac{A_a^1}{A_a^\infty}. \quad (4.7)$$

Now, since $a_1^1 = (\lambda_1^1 + \beta_1^1)/2$, the following condition is readily obtained:

$$\beta_{in}^1 = \left[\beta_\infty + \frac{a_\infty}{2} \ln \frac{A_a^1}{A_a^\infty} + \frac{\lambda_1^1}{4} \ln \frac{A_a^1}{A_a^\infty} \right] \left[1 - \frac{1}{4} \ln \frac{A_a^1}{A_a^\infty} \right]^{-1}. \quad (4.8)$$

If the same reasoning is applied to λ_{in}^1 , one obtains a linear system of two equations that allows one to compute β_{in}^1 and λ_{in}^1 . In the same way, for the second time step, it is possible to show that

$$\beta_1^2 = \left[\beta_\infty + \frac{a_\infty}{2} \ln \frac{A_a^1}{A_a^\infty} + \frac{\lambda_1^2}{4} \ln \frac{A_a^1}{A_a^\infty} \right] \left[1 - \frac{1}{4} \ln \frac{A_a^1}{A_a^\infty} \right]^{-1} \quad (4.9)$$

and that

$$\beta_2^2 = \left[\beta_1^2 + \frac{a_1^2}{2} \ln \frac{A_a^2}{A_a^1} + \frac{\lambda_2^2}{4} \ln \frac{A_a^2}{A_a^1} \right] \left[1 - \frac{1}{4} \ln \frac{A_a^2}{A_a^1} \right]^{-1}. \quad (4.10)$$

In order to obtain an equation for β_2^2 involving only the variables arriving at the boundary condition, it may be assumed that

$$\begin{aligned} \lambda_1^2 &\simeq \lambda_1^1 \\ a_1^2 &\simeq a_1^1 \end{aligned} \quad (4.11)$$

which, taking into account eqs. (4.8), (4.9) and (4.10), gives the following approximation for β_2^2 :

$$\widetilde{\beta}_2^2 = \left[\beta_1^1 + \frac{a_1^1}{2} \ln \frac{A_a^2}{A_a^1} + \frac{\lambda_2^2}{4} \ln \frac{A_a^2}{A_a^1} \right] \left[1 - \frac{1}{4} \ln \frac{A_a^2}{A_a^1} \right]^{-1}. \quad (4.12)$$

Recalling eqs. (4.9), (4.10) and (4.12), the relative error of this approximation can be written as:

$$\begin{aligned} \frac{\beta_2^2 - \widetilde{\beta}_2^2}{\beta_2^2} &= \left[(\lambda_1^2 - \lambda_1^1) \ln \frac{A_a^1}{A_a^\infty} \left(4 - \ln \frac{A_a^1}{A_a^\infty} \right)^{-1} + \right. \\ &+ \left. \frac{a_1^2 - a_1^1}{2} \ln \frac{A_a^2}{A_a^1} \right] \\ &\times \left[\beta_1^2 + \frac{a_1^2}{2} \ln \frac{A_a^2}{A_a^1} + \frac{\lambda_2^2}{4} \ln \frac{A_a^2}{A_a^1} \right]^{-1}. \end{aligned} \quad (4.13)$$

A detailed analysis of eq. (4.13) indicates that the worst-case scenario corresponds to the presence of discontinuities in A_a . Within the expected application scope of this new NRBC, such a case could be the simulation of the exhaust system of an ICE. According to [15], the maximum value along the whole cycle of the logarithm of the entropy level ratio at the exhaust pipe is 0.3 at $N = 2500$ rpm. Considering this upper bound, eq. (4.13) becomes:

$$\begin{aligned} \frac{\beta_2^2 - \widetilde{\beta}_2^2}{\beta_2^2} &= [0.08(\lambda_1^2 - \lambda_1^1) + 0.15(a_1^2 - a_1^1)] \\ &\times \left[\beta_1^2 + \frac{a_1^2}{2} \ln \frac{A_a^2}{A_a^1} + \frac{\lambda_2^2}{4} \ln \frac{A_a^2}{A_a^1} \right]^{-1} \end{aligned} \quad (4.14)$$

showing that the importance of the error committed when assuming eq. (4.11) is relatively small, since the corresponding differences are multiplied by coefficients much smaller than unity.

Therefore, it can be concluded that, for an anechoic case, the value of β arriving at the boundary condition at the N -th time step can be computed as:

$$\begin{aligned} \widetilde{\beta}_{in}^N &= \left[\beta_{in}^{N-1} + \frac{a_{N-1}}{2} \ln \frac{A_a^N}{A_a^{N-1}} + \frac{\lambda_N}{4} \ln \frac{A_a^N}{A_a^{N-1}} \right] \\ &\times \left[1 - \frac{1}{4} \ln \frac{A_a^N}{A_a^{N-1}} \right]^{-1}. \end{aligned} \quad (4.15)$$

In this way, an anechoic end can be modeled, thus removing the need for computing the flow in the downstream duct. One only needs to know λ and A_a arriving at the boundary at a given time t , the value of β and A_a which arrived at time $t - \Delta t$ and the speed of sound in the boundary at time $t - \Delta t$.

It is remarkable that the proposed approach is quite similar to that used in subsection 4.2.2, since in both cases the value of β is varied only when there is a change in A_a . However, this variation is not directly ΔA_a but the expression given in eq.(4.15). Moreover, stating that $\beta = A_a$ would also be incorrect when having pressure pulses superimposed on a mean flow, since at the initial time step² $\beta = a + u(\gamma - 1)/2 \neq a = A_a$, because u is positive.

The validity of the new implementation was again checked by applying it to Sod's problem. The results obtained with the new NRBC are presented in

²Considering that the reference pressure has been set equal to the initial pressure ($p_0 = p(t = 0)$), as discussed in [46]

figure 4.7. It may be seen that now the behavior is the same as for the ideal infinite duct, shown in fig. 4.2. Again, some small disturbances appear when the discontinuity reaches the boundary (mark A), but these disturbances are damped and tend to disappear within a few time steps.

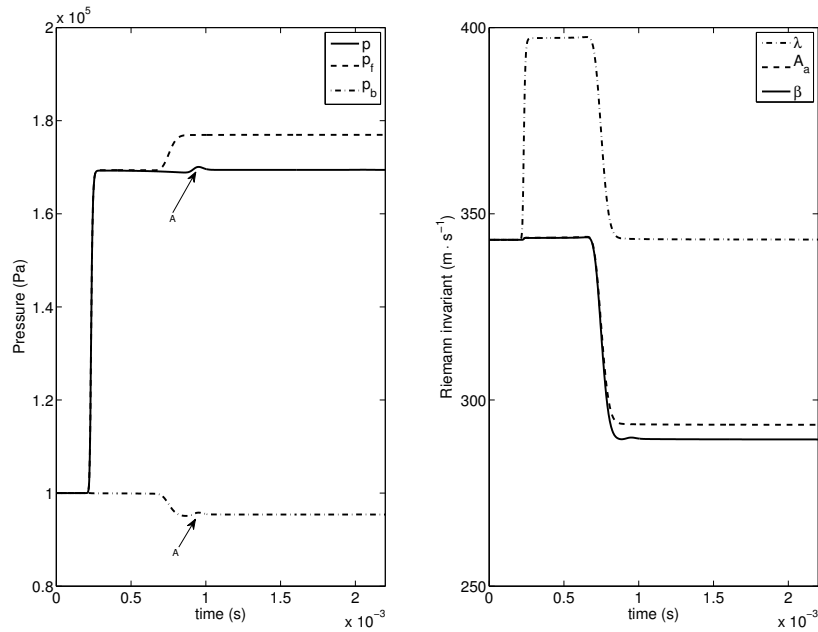


Figure 4.7: Values of flow variables: pressure and pressure components (left) and Riemann variables (right) using the new implementation of the NRBC.

4.3.3 Incident pressure condition

A similar treatment could be applied to an incident pressure boundary condition. However, in this case it is more difficult to find some non-homentropic flow in which the problem could be solved in an independent way (i.e. not in the whole domain, but imposing boundary conditions from previous computations or experiments). A possible example might be a decoupled problem with a domain in which some regions are 1D elements. In such a situation, it would be possible to follow the same approach used for the anechoic end in order to reproduce the behavior of a non-reflecting incident pressure boundary

condition in cases where changes in entropy are present.

4.4 Application to the analysis of the acoustic response of a muffler

In this section, a real application of the proposed NRBC is presented. The case chosen was the computation of the acoustic response of a 3D geometry similar to an exhaust muffler of an ICE. The results of the simulation were compared to experimental data obtained in an impulse test rig as described by [86] and to the results obtained by using long inlet and outlet ducts to isolate the pressure signals [20]. The muffler analyzed (fig. 4.8) was a rectangular parallelepiped with a volume of around 10 liters, which is adequate for the level of excitation imposed in the experiment. Inlet and outlet openings were located on the front and side surfaces, respectively, in order to capture the propagation of transversal modes [77, 32].

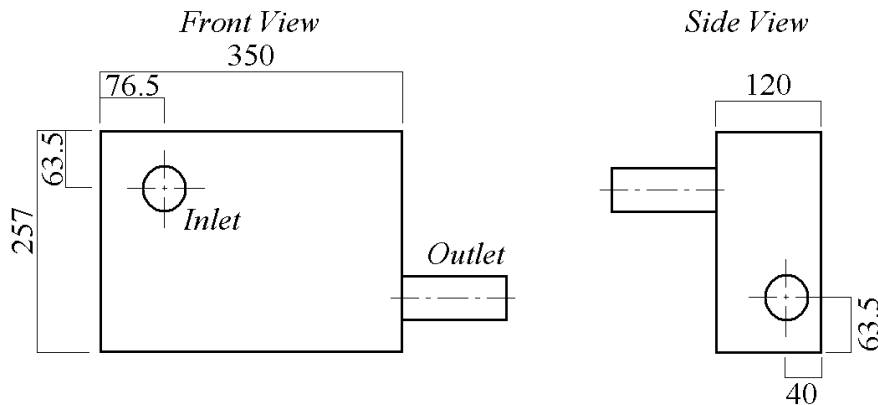


Figure 4.8: Geometry of the 3D muffler.

4.4.1 Experimental facility

In the experiments, the muffler is excited by means of a pressure pulse that provides a similar excitation at all the frequencies of interest. The incident pulse is generated by means of a solenoid valve that controls the discharge

from a high pressure air tank (see figure 4.9). Three transducers are installed upstream and downstream of the muffler: transducer 1 records a reference pulse, while the pulse transmitted by the system is obtained with the third transducer. An additional test has to be carried out by removing the muffler from the set-up in order to obtain the isolated incident pressure pulse from the measurement recorded by transducer 2. Once the incident and transmitted signals are obtained, the fast Fourier transform (FFT) is applied in order to compute different parameters such as the Transmission Loss (TL) of the system tested:

$$TL(f) = 20\log \left| \frac{A(f)}{C(f)} \right| + 10\log \left| \frac{S_u}{S_d} \right|, \quad (4.16)$$

where $A(f)$ and $C(f)$ are the complex amplitudes of the incident and transmitted pulses, respectively, and S_u and S_d are the duct cross-sections upstream and downstream of the muffler, respectively.

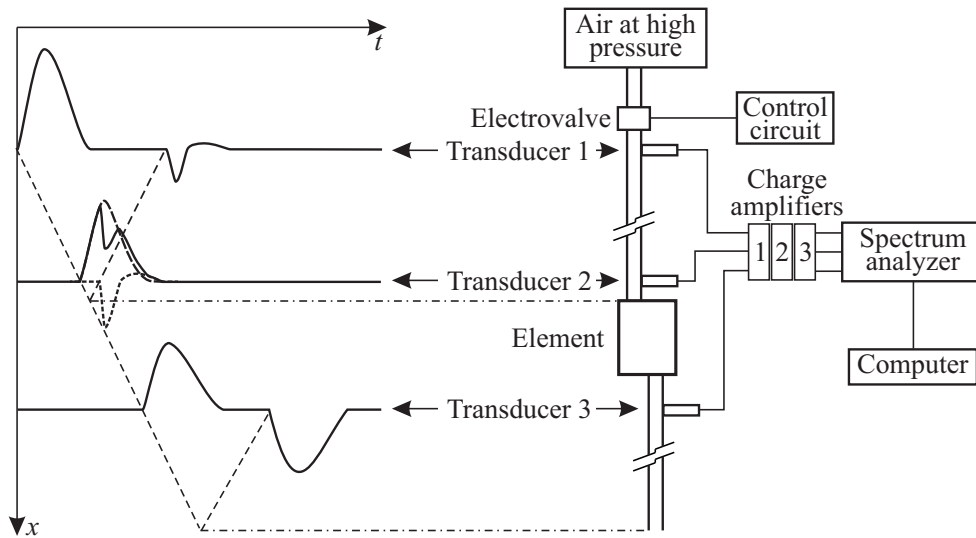


Figure 4.9: Scheme of the measurement setup.

4.4.2 Full three-dimensional simulation

The commercial code ANSYS-FLUENT was used to perform the CFD calculations that simulate the experimental facility described above. ANSYS-

FLUENT is based on a finite-volume discretization of the Navier-Stokes equations which, in this study, were solved with the so-called density-based coupled solver that uses flux-difference splitting. For the time discretization a second order implicit scheme was used. The time step was set to 1×10^{-5} , which is smaller than the sampling frequency used in the test rig. The Realizable $\kappa - \varepsilon$ turbulence model for high Reynolds numbers with wall function was chosen for closure.

The actual geometry and experimental conditions of the impulse test bench, described in the preceding section, were reproduced for the 3D-CFD simulations. The computational domain was a structured hexahedral mesh consisting of the muffler (1.6×10^5 cells) and the inlet and outlet ducts. The length of the inlet and outlet ducts (each 20 m, 0.6×10^5 cells) is the same as that used in the experimental facility in order to avoid reflections and to allow the isolated monitoring of the pulses. At the inlet, the pulse was represented by a temporal variation of the pressure at the inlet boundary condition. The outlet duct is needed to allow for the development of the flow before the pulse reaches the boundary. Since the temperature in the interior of the domain does not differ noticeably from the ambient temperature, the heat transfer through the wall was neglected.

The solution was monitored at the points corresponding to the locations of the transducers in order to obtain the response of the muffler. The methodology is essentially the same as in the experiments. Consequently, an additional simulation in which the muffler was replaced by a straight duct was performed in order to obtain the isolated incident pulse. Finally, the Transmission Loss (TL) was calculated by applying eq. (4.16). [20] proved that this methodology gives very accurate results when compared with the experiments in terms of TL , furthermore providing additional information on the 3D flow features in either the time or the frequency domains. Nevertheless, as previously stated, the computational cost of this methodology in real 3D geometry is high, which justifies the use of an NRBC to speed-up the calculation process.

4.4.3 Proposed Methodology

As already mentioned, the aim of the proposed methodology, based on NRBCs, is to reduce the computational cost by avoiding the 3D flow computation of ducts. Since, in this particular case, the propagation of pressure waves

in the inlet duct is not interesting, the problem was solved in a *decoupled* way, the inlet duct being calculated with a 1D CFD code: [79]. This 1D-code computes the internal flow in pipes under the assumption of non-linear inviscid one-dimensional flow, and has been extensively used [41] to model transient compressible flows in simple geometries with very low computational requirements. The isolated incident pulse was therefore obtained with this simple, low computational cost model, and then incorporated into the 3D model by means of an incident pressure NRBC. Additionally, the anechoic end presented in this chapter was used at the outlet duct, so that a long duct was not required. Other parameters defining the three-dimensional model such as mesh, turbulence or discretization schemes among others were the same as those chosen for the full three-dimensional calculations.

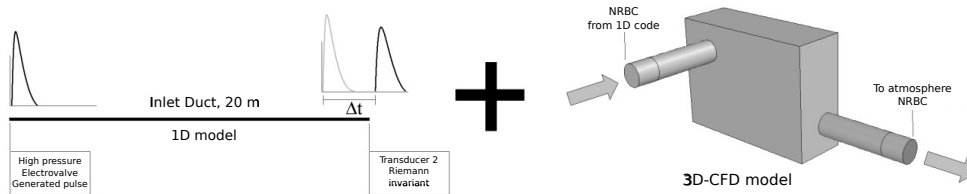


Figure 4.10: Scheme of the combined 1D-3D methodology.

As indicated in section 4.2, the reduction in CPU-time with respect to the full 3D computation is due to two different effects. CPU-time per time step is reduced in this case by around 35% which is fairly close to the corresponding decrease in the number of cells. Of course, the importance of this reduction depends on the number of mesh elements corresponding to the system under study. The second source of CPU-time reduction comes from the reduction in the total simulated time achieved when pulse propagation along the ducts is not computed. Figure 4.11 shows the temporal evolution of the pulses along the system. The reference pulse needs about 0.06 seconds to arrive at the second transducer, where the incident pulse is monitored. During this time the system under study does not receive any pressure excitation, so that no useful information is extracted from the computation in this period, which amounts to about half of the duration of the full 3D computation. Consequently, the CPU-time consumed will decrease down to values close to 50%. Therefore, the overall reduction in computation time due to the combination of both effects in the present case was about 67.5%. This reduction depends on the pulse

duration, and on the characteristic length of the ducts and the element being tested.

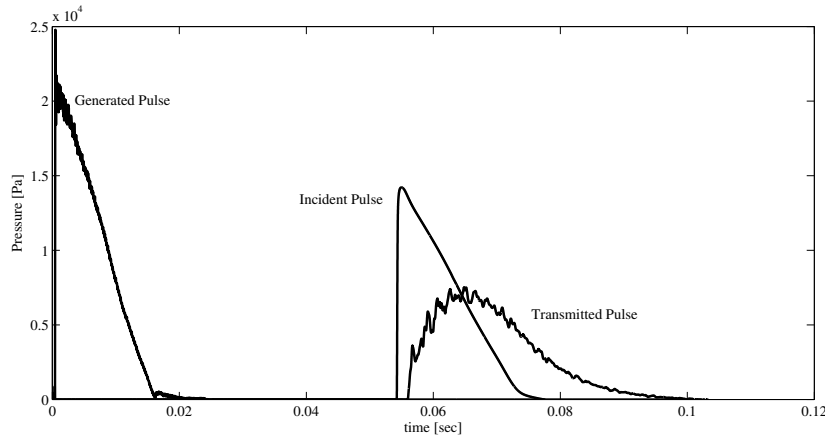


Figure 4.11: Reference, incident and transmitted pulses obtained with the full 3D CFD methodology.

Finally, comparison of the experimental Transmission Loss and the results obtained with both numerical methods (full 3D and combined 1D-3D with NRBCs) is presented in fig. 4.12. Good agreement between measurement and calculations can be observed. Both calculation methods accurately predict the peaks and the pass-band frequencies. The results obtained with the full 3D and the combined 1D-3D simulations are quite similar (less than 1 dB of difference) except in the maximum attenuation of the first narrow peak, in which the error is about 3 dB. It is worth mentioning that recovering the exact value of a peak in an acoustic analysis is not as important as capturing the general behavior. In fact such peaks are not relevant when the muffler is subject to a broadband excitation, which is the most usual case in practice. Additionally, this error is justified in the current application when the savings in CPU-time are considered.

4.5 Summary and conclusions

In this chapter, both a methodology to implement NRBCs in a 3D CFD commercial code (such as ANSYS-FLUENT) for its application to internal flow

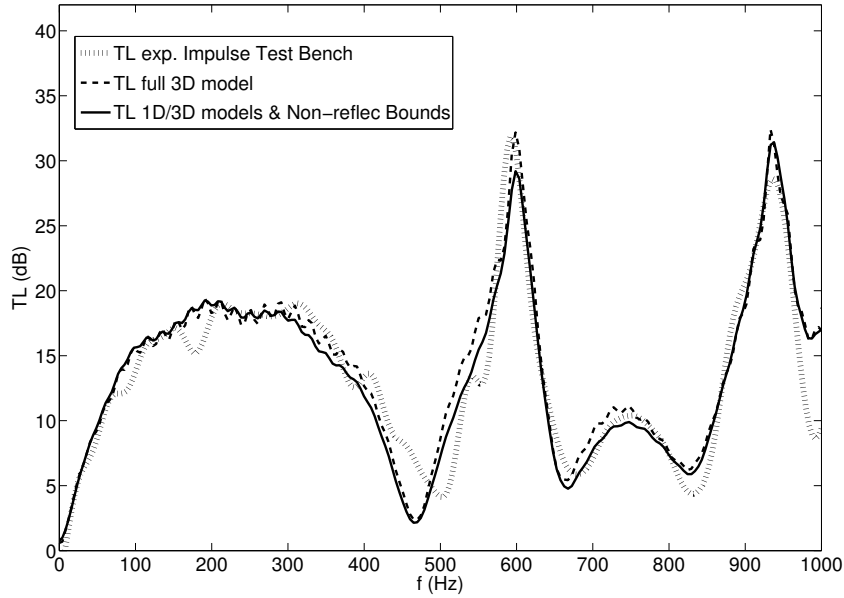


Figure 4.12: Transmission Loss. Comparison of the result measured, using the proposed methodology and full 3D model.

simulations, and the development of a new NRBC, were presented. The transfer of information across the boundary was accounted for by means of the MoC. One of the key points solved in the implementation of a boundary condition in a commercial code was the acquisition of the values of the flow variables in the domain. The performance of the new proposal was compared with a former definition proposed by the authors, and also with the NRBCs available in ANSYS-FLUENT, through their application to Sod's shock tube. Comparison of the solution obtained for an ideal *infinite* tube with the results obtained with the different non-reflecting boundary conditions analyzed, indicated that the non-reflecting boundary conditions available in ANSYS-FLUENT show some spurious reflections, especially when dealing with changes in entropy level. The proposed formulation showed improved performance with respect to the former definition and also to ANSYS-FLUENT built-in boundary conditions. In this chapter, only the particular case of an anechoic end was addressed, however, the same conclusions might be extracted for an incident pressure boundary condition.

Finally, a realistic application to the determination of the acoustic behavior of a 3D muffler was considered, comparing the results obtained with those of experimental tests and a full 3D CFD computation. The comparison indicated that the results in both the time and the frequency domains are very similar to those obtained with the full 3D-CFD simulation. Moreover, the computational cost is reduced by a factor of 3 (67.5%) when simulating an NRBC in the way presented on this chapter. This suggests that the proposed methodology might constitute a suitable tool for design and evaluation purposes.

Two boundary conditions have been developed. The first one, presented in the previous chapter, allows one to perform 1D-3D coupled simulations, while in the present chapter a new stand-alone anechoic formulation was implemented. Those boundary conditions are based in the method of characteristics, and thus rely on some assumptions. In the following chapter 5, the effect of some real flow behavior on the performance of these boundary conditions is evaluated.

Chapter Bibliography 4

- [3] ANSYS Inc. *Ansys Fluent 12.0 User's Guide*. Canonsburg, PA 15317, 2009 (cit. on pp. 24, 27, 28, 47, 83, 85).
- [7] O. V. Atassi. "Nonreflecting boundary conditions for the time-dependent convective wave equation in a duct". In: *Journal of Computational Physics* 197.2 (2004), pp. 737–758. ISSN: 0021-9991 (cit. on pp. 6, 81, 108).
- [13] R. S. Benson, R. D. Garg, and D. Woollatt. "A numerical solution of unsteady flow problems". In: *International Journal of Mechanical Sciences* 6.1 (1964), pp. 117–144. DOI: 10.1016/0020-7403(64)90009-8 (cit. on pp. 68, 87, 109).
- [14] R. S. Benson, J. H. Horlock, and D. E. Winterbone. *The thermodynamics and gas dynamics of internal combustion engines*. Ed. by Oxford University Press. Vol. 1. Oxford University Press, 1982 (cit. on pp. 68, 89, 109).
- [15] V. Bermúdez, J. R. Serrano, P. Piqueras, and O. García-Afonso. "Assessment by means of gas dynamic modelling of a pre-turbo diesel particulate filter configuration in a turbocharged HSDI diesel engine under

- full-load transient operation”. In: *Proceedings of the Institution of Mechanical Engineers, Part D, Journal of Automobile Engineering* 225.9 (2011), pp. 1134–1155 (cit. on p. 93).
- [17] C. Bogey and C. Bailly. “Three-dimensional non-reflective boundary conditions for acoustic simulations: far field formulation and validation test cases”. In: *Acta Acustica united with Acustica* 88 (2002), pp. 463–471. ISSN: 1436-7947 (cit. on p. 81).
- [20] A. Broatch, X. Margot, A. Gil, and F. D. Denia. “A CFD Approach to the Computation of the Acoustic Response of Exhaust Mufflers”. In: *Journal of Computational Acoustic* 13.2 (2005), pp. 301–316. DOI: 10.1142/S0218396X05002682 (cit. on pp. 3, 6, 72, 80, 95, 97).
- [29] J. R. Dea, F. X. Giraldo, and B. Neta. “High-order non-reflecting boundary conditions for the linearized 2-D Euler equations: No mean flow case”. In: *Wave Motion* 46.3 (2009), pp. 210–220 (cit. on pp. 6, 81, 108).
- [32] F. D. Denia, J. Albelda, F. J. Fuenmayor, and A. J. Torregrosa. “Acoustic behaviour of elliptical chamber mufflers”. In: *Journal of Sound and Vibration* 241.3 (2001), pp. 401–421. ISSN: 0022-460X (cit. on p. 95).
- [34] L. W. Dorodnicyn. “Artificial Boundary Conditions for High-Accuracy Aeroacoustic Algorithms”. In: *SIAM Journal on Scientific Computing* 32.4 (2010), pp. 1950–1979 (cit. on p. 81).
- [35] A. M. Elfaghi, W. Asrar, and A. A. Omar. “Higher order compact-flowfield dependent variation (HOC-FDV) solution of one-dimensional problems”. In: *Engineering Applications of Computational Fluid Mechanics* 4.3 (2010), pp. 434–440 (cit. on p. 84).
- [36] B. Engquist and A. Majda. “Absorbing Boundary Conditions for the Numerical Evaluation of Waves”. In: *Math. of Comp.* 31.139 (1977), pp. 629–651 (cit. on p. 81).
- [41] J. Galindo, J. R. Serrano, F. J. Arnau, and P. Piqueras. “Description of a Semi-Independent Time Discretization Methodology for a One-Dimensional Gas Dynamics Model”. In: *Journal of Engineering for Gas Turbines and Power* 131 (2009), p. 034504. DOI: 10.1115/1.2983015 (cit. on pp. 64, 69, 98).

- [46] J. Galindo, A. Tiseira, P. Fajardo, and R. Navarro. “Coupling methodology of 1D finite difference and 3D finite volume CFD codes based on the Method of Characteristics”. In: *Mathematical and Computer Modelling* 54.7-8 (2011), pp. 1738–1746. DOI: <http://dx.doi.org/10.1016/j.mcm.2010.11.078> (cit. on pp. 6, 15, 62, 81, 88, 93, 112, 118, 167).
- [47] D. Givoli. “High-order local non-reflecting boundary conditions: a review”. In: *Wave Motion* 39.4 (2004), pp. 319–326 (cit. on p. 81).
- [49] S. I. Hagstrom T. & Hariharan. “Accurate Boundary Conditions for Exterior Problems in Gas Dynamics”. In: *Mathematics of Computation* 51.184 (1988), pp. 581–597 (cit. on p. 81).
- [62] J. M. Lindquist, B. Neta, and F. X. Giraldo. “A spectral element solution of the Klein-Gordon equation with high-order treatment of time and non-reflecting boundary”. In: *Wave Motion* 47.5 (2010), pp. 289–298 (cit. on p. 81).
- [63] Q. Liu and O. V. Vasilyev. “Nonreflecting boundary conditions based on nonlinear multidimensional characteristics”. In: *International Journal for Numerical Methods in Fluids* 62.1 (2010), pp. 24–55. ISSN: 1097-0363 (cit. on p. 81).
- [65] J. M. Luján, V. Bermúdez, J. R. Serrano, and C. Cervelló. “Test bench for turbocharger groups characterization”. In: *SAE Paper* 2002-01-0163 (2002) (cit. on pp. 21, 82).
- [72] G. Montenegro and A. Onorati. “Modeling of Silencers for IC Engine Intake and Exhaust Systems by Means of an Integrated 1D-multiD Approach”. In: *SAE International Journal of Engines* 1.1 (2009), p. 466. DOI: 10.4271/2008-01-0677 (cit. on pp. 3, 62, 80).
- [74] J. A. Moríñigo and J. J. Salvá. “Robust non-reflecting boundary conditions for the simulation of rocket nozzle flow”. In: *Aerospace Science and Technology* 14 (2010), pp. 429–441. ISSN: 1270-9638 (cit. on p. 81).
- [76] G. F. Mucklow and A. J. Wilson. “Wave-action in gases: the attenuation and reflection of compression waves propagated in pipes”. In: *Proc. I. Mech. Eng.* 1955, pp. 69–80 (cit. on p. 83).
- [77] M. L. Munjal. *Acoustics of ducts and mufflers with application to exhaust and ventilation system design*. Wiley-Interscience, 1987. ISBN: 0471847380 (cit. on pp. 3, 95).

- [78] A. Onorati, G. Montenegro, and G. D’Errico. *Prediction of the Attenuation Characteristics of IC Engine Silencers by 1-D and Multi-D Simulation Models*. Tech. rep. 2006-01-1541. SAE Technical Paper Series, 2006. DOI: 10.4271/2006-01-1541 (cit. on pp. 62, 64, 81).
- [79] OpenWAM. CMT- Motores Térmicos. Universidad Politécnica de Valencia. URL: <http://www.OpenWAM.org> (cit. on pp. 4, 14, 63, 87, 98).
- [84] A. R. Patil, P. R. Sajanpawar, and V. V. Masurekar. *Acoustic Three-Dimensional Finite Element Analysis of a Muffler*. Tech. rep. 960189. SAE Technical Paper Series, 1996 (cit. on p. 80).
- [86] F. Payri, J. M. Desantes, and A. Broatch. “Modified impulse method for the measurement of the frequency response of acoustic filters to weakly nonlinear transient excitations”. In: *The Journal of the Acoustical Society of America* 107 (2000), p. 731 (cit. on pp. 82, 95).
- [87] F. Payri, J. M. Desantes, and A. J. Torregrosa. “Acoustic boundary condition for unsteady one-dimensional flow calculations”. In: *Journal of Sound and Vibration* 188.1 (1995), pp. 85–110. ISSN: 0022-460X (cit. on pp. 6, 15, 83, 87, 108).
- [94] T. J. Poinso and S. K. Lele. “Boundary conditions for direct simulations of compressible viscous flows”. In: *Journal of Computational Physics* 101.1 (1992), pp. 104–129 (cit. on p. 84).
- [95] A. Qamar, N. Hasan, and S. Sanghi. “A new spatial discretization strategy of the convective flux term for the hyperbolic conservation laws”. In: *Engineering Applications of Computational Fluid Mechanics* 4.4 (2010), pp. 593–611 (cit. on p. 84).
- [98] L. Selle, F. Nicoud, and T. Poinso. “Actual impedance of non-reflecting boundary conditions: implications for computation of resonators”. In: *AIAA journal* 42.5 (2004), pp. 958–964 (cit. on p. 84).
- [105] G. A. Sod. “A survey of several finite difference methods for systems of nonlinear hyperbolic conservation laws”. In: *Journal of Computational Physics* 27.1 (1978), pp. 1–31. DOI: 10.1016/0021-9991(78)90023-2 (cit. on pp. 71, 84).
- [111] C. K. W. Tarn. “Computational aeroacoustics: issues and methods”. In: *AIAA Journal* 33.10 (1995), pp. 1788–1796 (cit. on p. 81).

- [113] K. W. Thompson. “Time-dependent boundary conditions for hyperbolic systems”. In: *Journal of Computational Physics* 68 (1987), pp. 1–24 (cit. on pp. 81, 84).
- [114] K. W. Thompson. “Time-dependent boundary conditions for hyperbolic systems, II”. In: *Journal of Computational Physics* 89.2 (1990), pp. 439–461. ISSN: 0021-9991 (cit. on pp. 81, 84).
- [115] A. J. Torregrosa, P. Fajardo, A. Gil, and R. Navarro. “Development of a non-reflecting boundary condition for its application in 3D computational fluid dynamic codes”. In: *Engineering Applications of Computational Fluid Mechanics* (Accepted for publication 16/04/2012) (cit. on pp. 80, 108, 110, 120, 167).
- [118] T. Tsuji, T. Tsuchiya, and Y. Kagawa. “Finite element and boundary element modelling for the acoustic wave transmission in mean flow medium”. In: *Journal of Sound and Vibration* 255.5 (2002), pp. 849–866. ISSN: 0022-460X (cit. on p. 80).
- [120] B. Wang and H. Xu. “A method based on Riemann problem in tracking multi-material interface on unstructured moving grids”. In: *Engineering Applications of Computational Fluid Mechanics* 1.4 (2007), pp. 325–336 (cit. on p. 84).

Chapter 5

Analysis of the influence of real flow effects in computational fluid dynamics boundary conditions based on the method of characteristics

Contents

5.1	Introduction	108
5.2	Non-perfect gas	109
5.3	Viscous flow	110
5.4	Swirling flow	114
5.5	Possible applications of the developed boundary conditions	118
5.6	Conclusions	120
	Chapter 5 bibliography	123

5.1 Introduction

IN THIS CHAPTER¹, the effect of real flow effects on CFD boundary conditions developed by means of the method of characteristics is analyzed. By real flow effects, must be understood some flow conditions that were not taken into account in the development and implementation of the boundary condition. The analysis has been particularized for the case of the anechoic boundary presented in chapter 4, but all the conclusion can be extrapolated to any other CFD boundary condition based on the method of characteristics, as the coupling 1D-3D boundary condition presented in chapter 3.

Several researchers [87, 7, 29] have tried to develop the so-called non-reflecting or anechoic boundary conditions (BCs), to be able to eliminate the ducts sections at the boundaries of the computational domain without any penalty in the accuracy. This reduction of the computational domain can be of use if a turbocharger test rig has to be simulated, in which long ducts are needed in order to have uniform flow at the measurement sections. The inclusion of the ducts in the computational domain could represent even doubling the number of cells in some configurations.

In chapter 4, an anechoic BC was developed, this boundary condition is also described in [115]. An anechoic end is an outlet BC in which information does not travel upstream of the boundary condition (anechoic means literally without echo). This non-reflecting BC should thus behave as a long duct, allowing one to save computational cost. The development is based in the assumption of 1D inviscid flow of a perfect gas with negligible heat transfer is made, the evolution of the flow can be described by means of the method of characteristics (MoC). The MoC identifies the information traveling upstream with the Riemann invariant β . It is known that when non-homentropic flow is considered the Riemann invariants cease being constant. Therefore they are renamed as Riemann variables. Modifications of the Riemann variables can be found in the literature [122, 48]. The effects that change the Riemann invariants that are usually considered are friction, heat transfer, and variations of entropy. It is obvious that friction and heat transfer increase the entropy. However, variations in entropy level are also produced by differences of the initial entropy of the flow field and the entropy flux across the boundaries of

¹This chapter is accepted for publication as: *Analysis of the influence of different real flow effects on computational fluid dynamics boundary conditions based on the method of characteristics*. Mathematical and Computer Modelling. 2012. [45].

the domain.

An infinite duct always sends back the same value of β_{out} . This value corresponds to the initial value of β at the boundary condition, and will be denoted as β_∞ . Therefore, in a homentropic case, one must keep the value of β_{in} constant, and equal to that at the beginning of the simulation, i.e., β_∞ . Should a change of entropy level occur, the actual value of β_{in} would no longer be β_∞ . In this case, β_{in} would be obtained by adding to β_∞ the modifiers associated with the variation of the entropy level ([14]).

In the purposed boundary condition, one only needs to know λ and A_a (Riemann variables) arriving at the boundary at given t , the value of β and A_a that arrived at the boundary at $t - \Delta t$ and the speed of sound at the BC at $t - \Delta t$ in order to compute the flow variables at the boundary. However, as pointed out before, this anechoic BC assumes the existence of a 1D inviscid and adiabatic flow of a perfect gas. In order to assess its ability to be used as the outlet BC in a turbomachinery simulation, the implications of three different real flow effects will be studied in this chapter: non-perfect gas, viscous flow, and swirling flow. In sections 5.2-5.4, these effects will be reviewed, their influence on the anechoic BC will be analyzed, and an implementation improvement (where available) will be proposed. Afterwards, some considerations on the applicability of the boundary conditions developed in the previous chapters are assessed. Finally, in section 5.6, the main conclusions of the work will be presented.

5.2 Non-perfect gas

The MoC was originally developed under the hypothesis of perfect gas behavior [13]. However, if an ideal (but not calorically perfect) gas is considered, the MoC can still be used with some modifications. Following [122], if $c_p = f(T)$, the following variables replace the Riemann variables:

$$\begin{aligned}\lambda' &= \int_{T_{ref}}^T \sqrt{\frac{c_p c_v}{RT}} dT + u \\ \beta' &= \int_{T_{ref}}^T \sqrt{\frac{c_p c_v}{RT}} dT - u \\ s &= \int_{T_{ref}}^T \frac{q+uG}{T} dT\end{aligned}\tag{5.1}$$

The polynomial law stated in [108] or the polynomial function used in ANSYS-FLUENT [39] was used for $c_p(T)$. Following a similar criterion, the first term of the Riemann variables as defined in (5.1) can be expressed as a polynomial of temperature.

The methodology used to impose the boundary condition is the same as the one used in [115]: the fluid variables at the boundary will be recovered from the Riemann variables reaching it. The only difference is that the equations are now nonlinear. From the values of λ' and β' reaching the boundary, it is possible to obtain the value of the flow velocity and a polynomial of temperature. It is necessary to find the roots of the polynomial in order to obtain the temperature. In order to solve this problem, a Newton-Raphson scheme was used to find the value of temperature from the Riemann variables at every time step. Additionally, Horner's algorithm was used in order to efficiently evaluate the polynomial expressions. Finally, the value of the pressure at the boundary was obtained from the entropy and the previously calculated temperature.

The last thing that is worth mentioning when dealing with a non-perfect gas is that the value of the modifier due to changes in entropy used in [115] will not remain the same. The new formulation can be obtained from [122], and it establishes that:

$$d\beta'|_s = \sqrt{\frac{c_v T}{c_p R}} ds \quad (5.2)$$

The application of this new formulation of the modifier due to variations of entropy to the Anechoic BC scheme is straightforward.

To check the influence of this behavior, a simulation was run in which a pressure pulse is applied to a non-calorically perfect gas. In the left side of figure 5.1, one can see how the former Riemann variables A_a and β vary when λ arrives. When the new formulation is implemented, these changes disappear, as can be seen in the right side of figure 5.1.

5.3 Viscous flow

The existence of viscosity in the flow has various effects introducing further complexity in the anechoic BC. First, the diffusive transport induced by viscosity cannot be modeled by the MoC, since it only deals with the hyper-

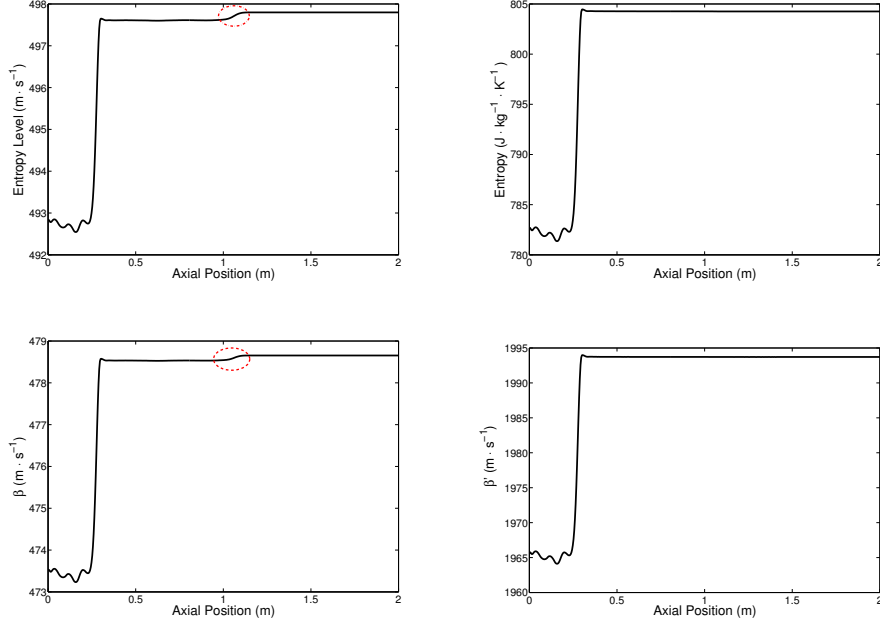


Figure 5.1: First row: Distribution of A_a and s in the axis of the duct after 800 time steps.
Second row: Distribution of β and β' .

bolic part of the Navier-Stokes equations (i.e, the Euler equations). However, since the Reynolds number in the intended applications (flow in ICES) is high ($Re_D \approx 2 \cdot 10^5$ for the considered case), the diffusive transport should be negligible compared to the convection terms. Moreover, there is a loss in momentum due to the existence of friction. This effect is mainly concentrated in the surroundings of the wall. This effect decreases with smoother ducts and higher Reynolds number (until fully developed turbulent flow is reached). As it has been exposed before, there exists a modifier that takes into account this effect in the value of each Riemann variable along its respective characteristic line:

$$d\beta|_f = -(\gamma - 1) \left[1 - (\gamma - 1) \frac{u}{a} \right] \frac{f}{D} u^2 \frac{u}{|u|} dt \quad (5.3)$$

In (5.3), f is the Fanning friction factor, defined as $f = \frac{\tau_w}{\frac{1}{2}\rho u^2}$. In this work, f was estimated by means of the explicit Swamee-Jain equation:

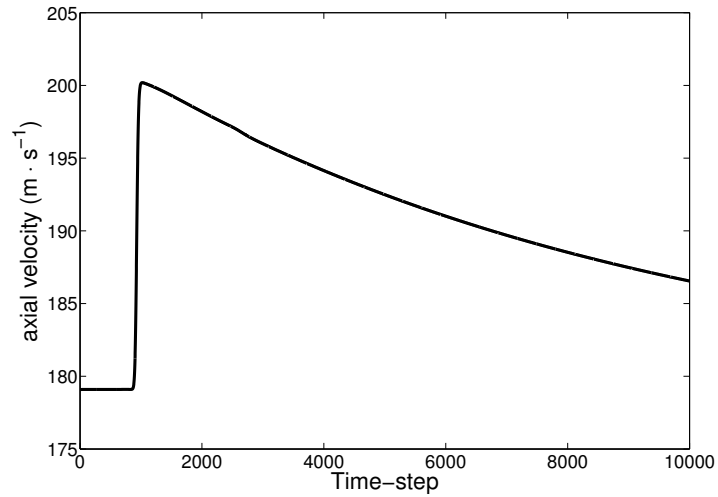
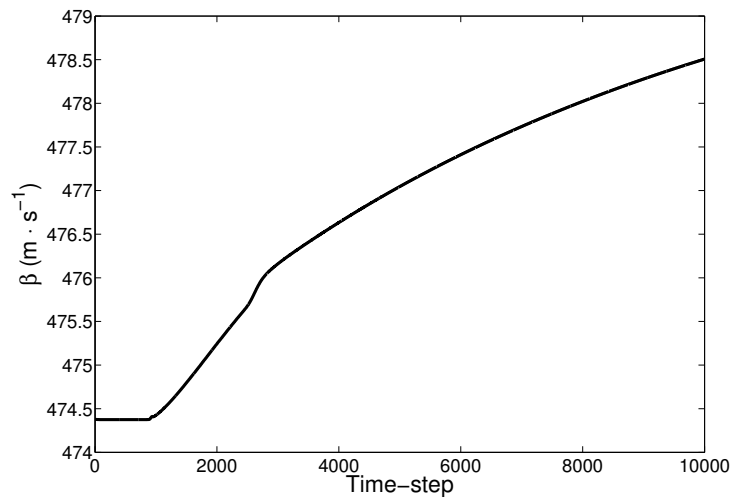
$$f = \frac{0.0625}{\left(\log_{10} \left(\frac{\epsilon}{3.7D} + \frac{5.74}{Re^{0.9}}\right)\right)^2} \quad (5.4)$$

It should be pointed out that eq. (5.4) should not be confused with the more common Swamee-Jain equation for the Darcy friction factor, which is 4 times larger than Fanning's one. It should be mentioned that all the variables needed to evaluate eq. (5.4) are taken from the previous time step, in order to keep the expression explicit.

Besides the previous two effects, friction has another effect that is relevant not because of the use of the MoC but due to the anechoic BC approach. In its development, it was stated that, for inviscid flows, β only had to take into account the entropy changes. However, in viscous flows, when a λ -wave (C^+) arrives, the velocity increases, thus increasing the friction effect and therefore changing the values of the Riemann variables. In order to clarify this fact, a simulation of a long duct with a isentropic step pressure pulse at the inlet of the duct was performed.

The evolution of flow velocity and β were monitored at a given section, which in the case presented in figure 5.2 is the section at $0.9m$ from the inlet. If viscosity were not taken into account, the velocity would increase once the pulse reaches the section considered and afterwards it would remain constant. However, if viscosity were considered, the flow velocity would continue decreasing after the λ -wave had passed, as is shown in 5.2(a). When a wave reaches the boundary, the change of β that still happens at the virtual duct at the right of the boundary is sent backwards. This last fact makes the former anechoic approach invalid to correctly model the acoustic response of an infinite duct with friction, because that duct produces reflections.

Therefore, since the information created at the right of the BC must be taken into account, one should model it, and a 1D-3D coupled simulation such as described in [46] could be helpful. Using this approach would allow one to model the response of a sufficiently long duct but reducing at the same time the computational cost when compared to a fully 3D simulation. It is worth considering how long the duct should be for this approach to be useful. It is well known that in the frictional flow inside a duct the flow velocity increases along the duct. Therefore it will reach a point at which the flow will choke

(a) u_x (b) β Figure 5.2: Evolution with time in a given section of u_x and β .

and will pass to the supersonic regime. After passing to this supersonic, it is obvious that no information will travel upstream. The only thing that has to

be considered is that this point will change with the flow conditions.

Despite the previous comments, one could want to use the developed anechoic BC with viscous flow, if the reduction of computational time was supposed to compensate the loss of accuracy. Thus, a simulation was performed comparing the behavior of a long duct and a short one with the anechoic BC in a turbulent flow, as shown in 5.3(a). The comparison between this simulation and the corresponding long duct is shown in figure 5.3(b).

5.4 Swirling flow

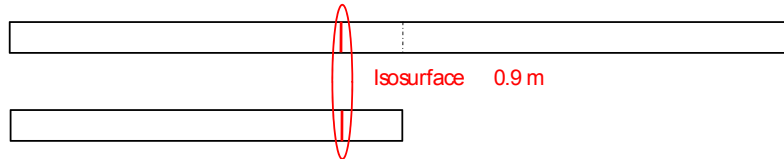
As already noted, among other applications, the anechoic BC is intended to be used as the outlet boundary in a turbine simulation. However, the flow downstream of a turbine is no longer one dimensional, because of the swirl created by the impeller. This swirl is even more important when dealing with off-design points. One of the main problems when using commercial CFD codes is that the BCs available are mainly uniform flow at the boundary. This is normally not a serious issue if the main interest of the computation lies far from the boundary. However, in the case of the development of new BCs, and particularly with the anechoic BC, it is necessary to reproduce the flow behavior close to the boundary. Therefore, a different approach must be followed in order to use the anechoic BC.

If the radial velocity is neglected, a swirling flow is said to be in radial equilibrium ([33]). In such flows, the pressure radial profile satisfies the following equation:

$$\frac{dp}{dr} = \rho(r) \frac{v_{\theta}^2(r)}{r} = F(r) \quad (5.5)$$

Thus, if radial equilibrium is supposed to be achieved at every time step, one can obtain the pressure profile at the BC at a certain time step provided that the pressure at the axis (p_{axis}), in order to obtain the integration constant, and the $F(r)$ profile are known.

Regarding the value of p_{axis} , it can be assumed that the MoC can be still applied to the axis, because $v_{rad} = 0$ due to axial symmetry, and therefore the axis could be assumed to be one dimensional. On the other hand, $F(r)$ is approximated by its value at the previous time step. This explicit approach is



(a) Computational domains

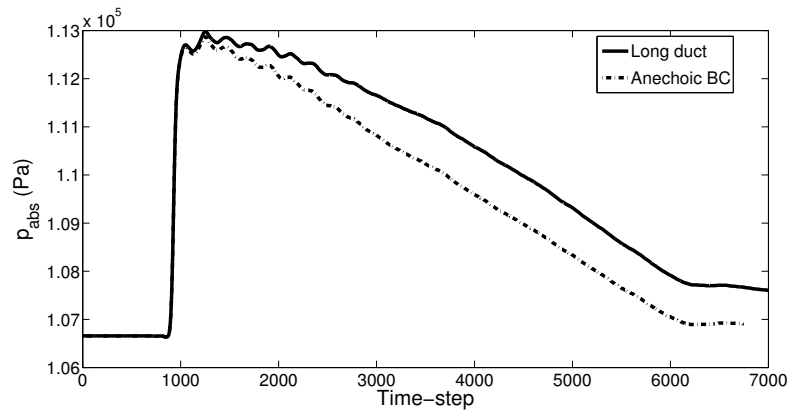
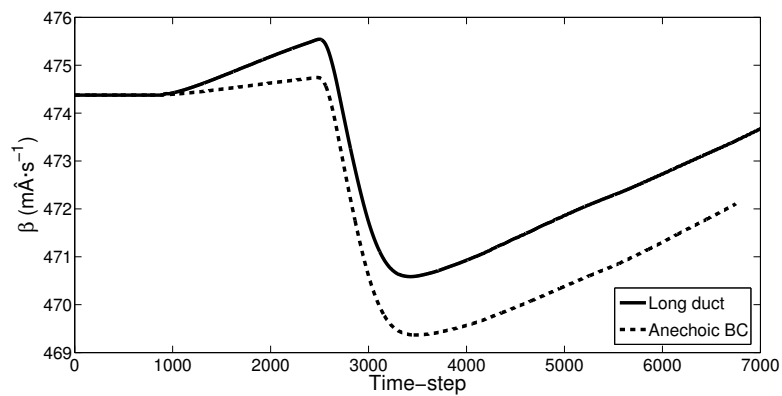
(b) pressure at $x=0.9$ m(c) β at $x=0.9$ m

Figure 5.3: Computational domains used to evaluate the behavior of the Anechoic BC (a) and the evolution of pressure (b) and β (c) in both ducts

used to avoid the iterative process otherwise required to define all the variables at the BC. Therefore, the pressure profile at the BC is computed by integrating

eq. (5.5) between neighboring faces at the BC in increasing radial position, in order to minimize the error, as

$$p(r, t) = p(r - \Delta r, t) + F(r, t - \Delta T) \cdot \Delta r \quad (5.6)$$

The integration process is started with the known value of $p(r = 0) = p_{axis}$ obtained by the application of the MoC to the 1D flow along axis.

The hypothesis of radial equilibrium was checked by running two axisymmetric simulations with a swirling inlet BC: a long duct and a short one with the anechoic BC with radial equilibrium. $p(r)$ profiles of both ducts at the section at 1m (outlet of the short duct) are compared in fig. 5.4. It is shown that the pressure profile is correctly obtained with the radial equilibrium approach.

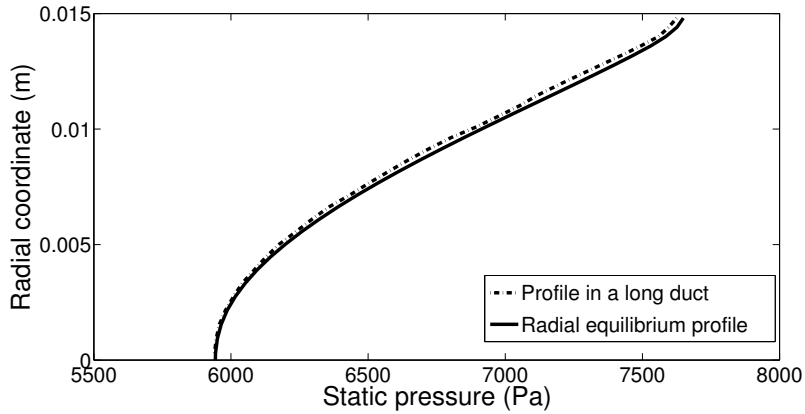


Figure 5.4: Pressure profile at the BC in a long duct (stripped line) compared with the pressure profile obtained imposing radial equilibrium (continuous line)

Then, a transient simulation was run in which a step pressure pulse was set at the inlet of the duct. A comparison between data at the section at $0.9m$ of a long duct and a short one with the anechoic BC was made. The evolution of pressure at the axis is presented in figure 5.5. As expected, the MoC can be satisfactorily applied to the axis.

Regarding the use of the radial equilibrium to obtain the $p(r)$ profile at every time step, an area-weighted average of pressure at the section at $0.9m$ is provided in figure 5.6. Good agreement is found between the values obtained by both simulations.

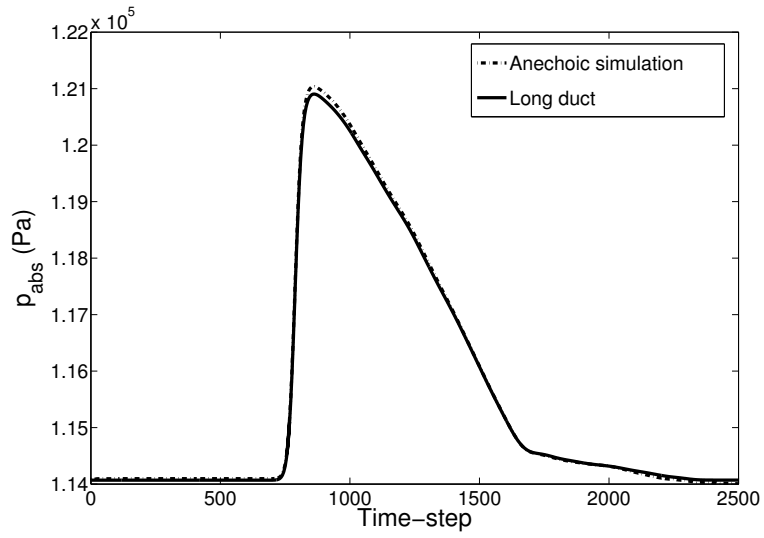


Figure 5.5: Evolution of pressure at the axis of a long duct and a short duct using the anechoic BC

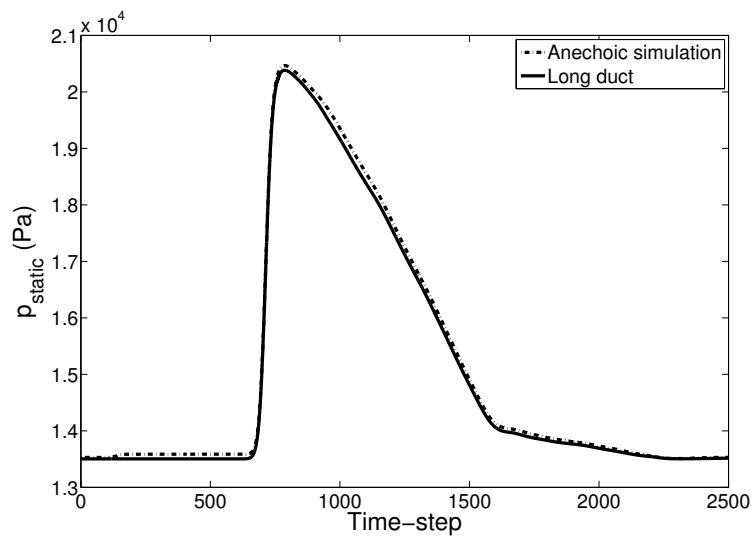


Figure 5.6: Evolution of an area-weighted average of pressure at the section at 0.9m of a long duct and a short duct using the anechoic BC

5.5 Possible applications of the developed boundary conditions

Two different boundary conditions based on the MoC have been developed in this thesis. The first one allowing to perform 1D-3D coupled simulations 3 and the second one appeared with the intent of being a stand alone anechoic end, which acted as a long duct 4. In this section some of the possible uses of the BC are described.

5.5.1 Anechoic BC

In this chapter the effect of real flow effects, as the existence of non-perfect gas behavior, viscous flow or swirling flow, on the performance of the anechoic BC have been analyzed. The anechoic boundary condition have proved to give good results if viscosity is not present in the flow. However, if viscosity is considered, the change friction due to a change in velocity causes the value of the Riemann variables to change, and this means that in a infinite duct the viscous flow does send information backwards (changes in the Riemann variables) after the passing of the pulse. Therefore, as previously mentioned, is this problem is considered the use of the 1D-3D coupled boundary simulation is advisable [46]. Nevertheless, if the case considered is a pressure pulse in a initially stationary flow, as the situation found in a impulse test rig, the effect of viscosity can be neglected. An example of this kind of problem could be the acoustic analysis of system, as the one presented in chapter 4 for a silencer.

Additionally, although it has been established that the developed boundary condition does not behave as a infinite duct if viscous flow is considered, the anechoic condition does reduce the possible reflections in the boundary. Therefore, it could be used to obtained achieve faster the periodic solution in a sliding mesh simulation. In the rest of the situations, it seems more appropriate to use a coupling with a 1D duct.

5.5.2 Coupled 1D-3D simulation

In the frame of the coupled computations, several applications might be of interesting as any of the current simulations performed using the code OpemWAM,

in which a particular section of the domain needs to be resolved with a higher geometrical resolution. The use of the coupled boundary condition allows one to perform a 3D simulation were required, while keeping the rest of the computational domain with a low cost. The main difficulty that must be overlaid is the initialization of the OpenWAM domain, since at the moment it is not possible to restart a simulation from a previous solution.

Since this thesis deals with simulations of turbomachinery, two different applications should be mentioned. The first application is when the turbocharger is considered to be tested in an experimental facility, in which the the pipes at the inlets and outlets of the turbocharger could represent an important part of the domain. On the other hand, one could think of simulating the turbine directly on engine by using the capability of OpenWAM of simulating a whole engine.

5.5.2.1 Simulation of a gas-stand

The ducts of the experimental facility could have a length of 1400 mm and present some expansions (increases in cross-sectional area) that are necessary for a correct fitting with the rest of the additional existing element in the facility, as the duct coming from the rotary screw compressor or the exhaust duct to the atmosphere. Additionally, not all the flow variables are measured in the same points, but instead measurements are taken along the ducts in different positions. Therefore, the simulation of the ducts could make easier the comparison with tests results.

OpenWAM is able to compute the compressible flow in these ducts, considering effects of friction with the walls and changes in the cross-sectional area. In order to evaluate the validity of the procedure, a turbine simulation using the same domain as in chapter 2, but connecting two additional one meter long one-dimensional ducts in the inlet and outlet of the domain.

The intent of this simulation is to demonstrate that this procedure can be applied in future simulations. The process was started from a converged simulation from chapter 2, the objective is to simulate the same operating point in the turbine once the one-dimensional ducts are connected. The main difficulty relays in the initialization of the domain in OpenWAM. Actually, the main problem is in the outlet duct, since the initialization of the inlet duct can be adjusted. In this case, the initialization problem has been overlaid consider-

ing the low computational requirements of the 1D computation. The procedure that was followed is based in consider a phase shift between the starting time of both computations. In this way, the OpenWAM computations start first with constant boundary conditions (actually Riemann variables) from the three-dimensional domain, and the simulation proceed until the domain has reached steady conditions. At this point, the 3D simulation start evolving and from this point on both simulations run coupled. If the simulations and initialization of the OpenWAM simulations are correctly set, then the same solution than the one using just the 3D domain can be obtained, but with longer ducts simulating the behavior of the complete gas-stand. The result current simulation validates the procure which could be used to simulate any one-dimensional dominant region of a complex computational domain.

5.5.2.2 Turbine set on engine

In Figure 5.7 a schematic representation of the different OpenWAM elements used to simulate a 4-strokes turbocharged ICE is shown. The elements composing the turbine are marked in a red box. Models as the one shown in Figure 5.7 are commonly used in engine modeling to obtain engine performances. In this frame, a zero-dimensional model for the turbine, as the one described in [99] is interesting due to its reduced computational cost. However, if the complete geometric description of the turbine is required, the turbine can be replaced by a 3D model by setting the coupling boundary condition at the inlet and outlet ducts of the OpenWAM domain.

The main difficulty relays again in the initialization of OpenWAM. A similar approach than the one presented based on sifting the starting time of the calculations could be applied. However, in this case the boundary conditions are purely unsteady due to the engine strokes, and therefore a proper synchronization is required. This simulation could not be included in the present thesis and is left as future work.

5.6 Conclusions

In a previous work [115], an anechoic BC was developed, based on the assumption of 1D inviscid and adiabatic flow of a perfect gas. In order to be able

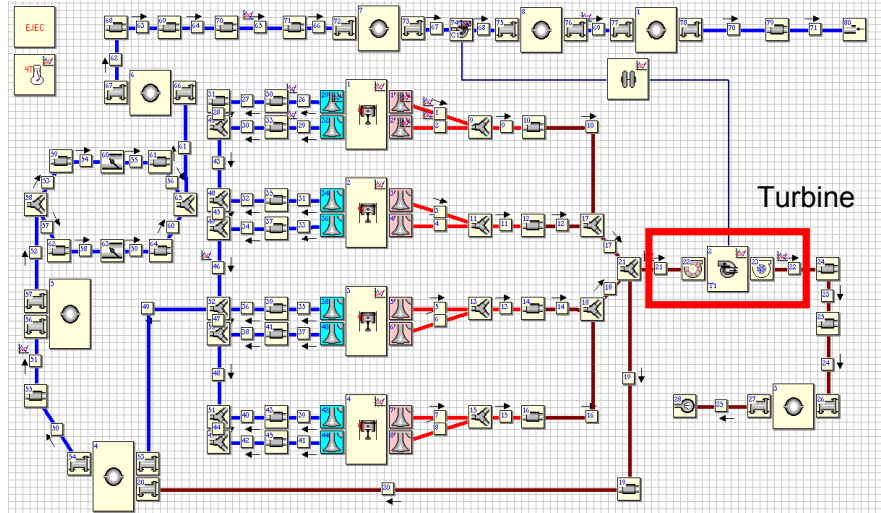


Figure 5.7: Schematic representation of a 4-stroke engine turbocharged OpenWAM model. The turbine submodel is marked in the figure.

to use this anechoic BC in a turbomachinery outlet, three different real flow behaviors have been studied in this chapter. In section 5.2, the hypothesis of ideal instead of perfect gas has been reviewed. A solution has been proposed, and it has been shown to improve significantly the performance of the non-reflecting BC. Then, in section 5.3, the implications of dealing with viscous flow have been investigated. The effect of wall friction has been incorporated into the BC by means of a proper modifier of the Riemann variables and the use of a correlation for the friction factor. It has been shown that an infinite duct does send information backwards when receiving an incoming pressure wave. Therefore, the anechoic approach would never be able to reproduce the behavior of a long duct reliably. However, the anechoic BC could still be used to reduce the time to achieve convergence due to the absence of reflections, but taking into account the lack of accuracy regarding the simulation of the whole duct. In section 5.4, the existence of swirl (characteristic of a turbine's outlet) has been analyzed. An approach to obtain the transversal pressure profile at the outlet has been developed, assuming that the flow is in radial equilibrium.

Although the analysis has been carried out for an anechoic BC, similar conclusions could be established for any other BC developed by means of the

MoC. At the end of this chapter, some comments on the possible applications of the developed boundary conditions are given. A coupled simulation connecting the three-dimensional turbine with two one-dimensional ducts have been performed in order to demonstrate the validity of the initialization procedure. Finally, an additional application of the coupling boundary condition to perform an on engine simulation has been proposed as future work.

Chapter Bibliography 5

- [7] O. V. Atassi. “Nonreflecting boundary conditions for the time-dependent convective wave equation in a duct”. In: *Journal of Computational Physics* 197.2 (2004), pp. 737–758. ISSN: 0021-9991 (cit. on pp. 6, 81, 108).
- [13] R. S. Benson, R. D. Garg, and D. Woollatt. “A numerical solution of unsteady flow problems”. In: *International Journal of Mechanical Sciences* 6.1 (1964), pp. 117–144. DOI: 10.1016/0020-7403(64)90009-8 (cit. on pp. 68, 87, 109).
- [14] R. S. Benson, J. H. Horlock, and D. E. Winterbone. *The thermodynamics and gas dynamics of internal combustion engines*. Ed. by Oxford University Press. Vol. 1. Oxford University Press, 1982 (cit. on pp. 68, 89, 109).
- [29] J. R. Dea, F. X. Giraldo, and B. Neta. “High-order non-reflecting boundary conditions for the linearized 2-D Euler equations: No mean flow case”. In: *Wave Motion* 46.3 (2009), pp. 210–220 (cit. on pp. 6, 81, 108).
- [33] S. L. Dixon and C. Hall. *Fluid mechanics and thermodynamics of turbomachinery*. Butterworth-Heinemann, 2010 (cit. on pp. 114, 144).
- [39] *Fluent 6.3 Getting Started Guide*. Fluent Inc. 2006 (cit. on p. 110).
- [45] J. Galindo, A. Tiseira, P. Fajardo, and R. Navarro. “Analysis of the influence of different real flow effects on computational fluid dynamics boundary conditions based on the method of characteristics”. In: *Mathematical and Computer Modelling* Published online (2012). cited By (since 1996) 0; Article in Press. URL: <http://www.scopus.com/inward/record.url?eid=2-s2.0-84857202860&partnerID=40&md5=d266cfaf6a34fe6010607ad916e6bdd2> (cit. on pp. 108, 167).

- [46] J. Galindo, A. Tiseira, P. Fajardo, and R. Navarro. “Coupling methodology of 1D finite difference and 3D finite volume CFD codes based on the Method of Characteristics”. In: *Mathematical and Computer Modelling* 54.7-8 (2011), pp. 1738–1746. DOI: <http://dx.doi.org/10.1016/j.mcm.2010.11.078> (cit. on pp. 6, 15, 62, 81, 88, 93, 112, 118, 167).
- [48] G. Guderley. *Nonstationary gas flow in thin pipes of variable cross section*. Tech. rep. Washington: NASA Technical Memorandum N.1196, 1948 (cit. on p. 108).
- [87] F. Payri, J. M. Desantes, and A. J. Torregrosa. “Acoustic boundary condition for unsteady one-dimensional flow calculations”. In: *Journal of Sound and Vibration* 188.1 (1995), pp. 85–110. ISSN: 0022-460X (cit. on pp. 6, 15, 83, 87, 108).
- [99] J. R. Serrano, F. J. Arnau, V. Dolz, A. Tiseira, and C. Cervelló. “A model of turbocharger radial turbines appropriate to be used in zero- and one-dimensional gas dynamics codes for internal combustion engines modelling”. In: *Energy Conversion and Management* 49.12 (2008), pp. 3729–3745 (cit. on pp. 4, 120, 141, 144, 149).
- [108] D. R. Stull. *JANAF thermochemical tables*. Tech. rep. DTIC Document, 1971 (cit. on p. 110).
- [115] A. J. Torregrosa, P. Fajardo, A. Gil, and R. Navarro. “Development of a non-reflecting boundary condition for its application in 3D computational fluid dynamic codes”. In: *Engineering Applications of Computational Fluid Mechanics* (Accepted for publication 16/04/2012) (cit. on pp. 80, 108, 110, 120, 167).
- [122] D. E. Winterbone and R. J. Pearson. *Theory of Engine Manifold Design : Wave Action Methods for IC Engines*. John Wiley & Sons, 2000 (cit. on pp. 108–110).

Chapter 6

Computational analysis of pulsating flow in radial turbomachinery and its application to engine modelling

Contents

6.1	Introduction	126
6.2	Computational methodology and steady flow results	127
6.3	Pulsating flow results	129
6.4	Discussion of results	133
6.5	Application to engine modeling	139
6.6	Conclusions	151
	Chapter 6 bibliography	155

6.1 Introduction

THE PREVIOUS CHAPTERS¹ have been focussed on the definition of a computational methodology for the numerical characterization of radial turbomachinery and the optimization of the configuration in order to maximize the capabilities of the computational resources. In this frame, the turbine has been analyzed under steady flow conditions and the results have been validated with global measurements taking on a experimental turbocharger test rig.

When a turbine is installed on a reciprocating engine, the inlet flow is not steady. The turbine receives a highly pulsating flow from the cylinders [57, 59, 52]. These pulses cause the turbine to operate in a wide range of working conditions, reaching extreme off-design points. In the past, most research and characterization of radial turbines was performed at constant flow conditions, using both experimental [97] and numerical [57] approaches. In order to deal with off-design steady conditions, an extrapolation methodology was presented in [90]. In recent times, more attention has been paid to the analysis of pulsating flow in turbines. Baines [12] gives an overview of the different methods used for understanding pulsating flow in a turbine and the factors that influence turbine performance. Papers based on experimental work discuss accumulation and/or wave effects in the turbine and how the signals measured upstream and downstream have to be shifted in order to properly compute performance maps (flow capacity and isentropic efficiency). On the first issue there is general agreement that all the accumulation and wave effects are located in the volute, whereas the impeller can be considered as quasi-steady [26]. There is also a discussion on whether signal shift should be carried out using flow velocity or the speed of sound [66, 22].

Papers using CFD are generally focused on comparing the results against experiments and how the set-up should be defined [81, 52]. One of the points of controversy is how impeller movement is to be reproduced and there are two different approaches on this issue. On one hand, the Multiple Reference Frame (MRF), also known as the frozen rotor, keeps the mesh stationary and simulates the movement by using a rotating coordinate system. The main advantage of the MRF approach is its low computational cost, at the expense

¹This chapter has been submitted for publication as: *Characterization of a radial turbocharger turbine in pulsating flow by means of CFD and its application to engine modeling*. Applied Energy. Date of submission 01/03/2012. [40]

of neglecting the blade passage effect and the stator-rotor interaction. On the other hand, the Sliding Mesh Model (SMM) actually moves the rotor mesh. Palfreiman et al. [82] considered that the frozen rotor approach may have some impact on the results. Similar conclusions might be found for turbocompressors in Liu et al. [64]. However, less attention has been paid to using CFD calculations to compare steady and pulsating flow operating points in order to support the conclusions of other authors. Aymanns et al. [8] recently did this for a waste-gated nozzleless turbine, showing flow capacity and efficiency plots for the turbine impeller which support its quasi-steady behavior.

In this work, CFD simulations were used to analyze the internal pulsating flow in a vaned nozzle, variable geometry turbine (VGT). In order to analyze the effects of pulsating conditions, the different turbine components, i.e. volute, nozzles and rotor, were studied separately. The paper is presented as follows. The numerical model and set-up used are first described. The results obtained using steady boundary conditions are then given. The pulsating flow simulations are presented, with comments on the results, and are compared to the equivalent steady-state points. In the last section, a simplified 1D-0D turbine model is proposed, able to reproduce the unsteady effects previously analyzed.

6.2 Computational methodology and steady flow results

The computational methodology applied in this chapter is based in the work presented in chapter 2. Figure 2.3 shows a schematic view of the turbine used in this work. In this chapter, the different turbine components have been analyzed separately. Thus, it is necessary to correctly identify the post-processing sections, which will be used to express the value of the flow variables. The post-processing sections are marked in Figure 2.3, and are also presented in Table 6.1.

As previously stated in chapter 2, the computational domain included two zones not shown in the figure: two straight ducts which are placed at the turbine inlet (Section 1) and outlet (Section 5). The computational domain was chosen in this way in order to simulate a radial turbine operating in a

turbocharger test-rig, such as the one shown in [89]. These ducts also separate the outlet boundary condition from the turbine. In the paper by Aymanns et al. [8], the outlet boundary condition was directly imposed at the outlet section of the turbine, which was quite close to the impeller, which makes the pressure at the impeller outlet section almost constant. In a waste-gated turbine this procedure is close to reality, due to the typical sudden increase of section at the impeller outlet in this type of turbine. Capobianco and Marelli [23] studied the pressure fluctuations at the impeller outlet of a waste-gated turbine at different opening levels. The results show that at large waste-gate openings, pressure fluctuations downstream of the impeller are not negligible. The hypothesis of constant downstream pressure commonly applied in turbocharger simulations may therefore introduce significant errors.

Table 6.1: Situation of the different sections considered in the computational domain

Section number	Description
0	Domain Inlet
1	Volute Inlet
2	Volute Outlet-Nozzle Inlet
3	Nozzle Outlet-Rotor Inlet
4	Rotor Outlet
5	Turbine Outlet
6	Domain Outlet

The turbine under study does not have an important expansion at the impeller outlet and therefore the validity of the constant pressure approach is not clear. In order to avoid errors when modeling the operating conditions, the outlet boundary was set farther away, thus allowing a certain pressure variation at the impeller outlet. This procedure ensures that the pressure at the turbine outlet is calculated from the flow domain and is not directly imposed.

The mesh size and the case configuration were determined with the analysis performed in chapter 2. Therefore, a pressure based coupled solver with a second-order upwind scheme discretization was used. The time step was chosen to have 200 time steps per rotor revolution. This means a time step size of $1.6576 \cdot 10^{-6}$ seconds. Although the analyzed turbine is a VGT, in the study performed in this chapter, the angle is kept constant to reduce the number of

parameters. In the same way, the rotational speed of the turbocharger was fixed at $18953 \text{ rad}\cdot\text{s}^{-1}$. Although in real pulsating operation the rotational speed would not remain constant, it would change in a narrow range as shown in [66].

In this chapter, the pulsating behavior of the turbine is going to be compared with the steady one. The steady results were represented in Figures 2.13 and 2.14. In view of the results, it was stated that the difference between MRF and SMM calculations is low when the turbine is working close to the design conditions, but in off-design points it increases. The impact that the rotor motion approach has on the solution could be attributed to the stator-rotor interaction [57]. This interaction is important in the present case since the stator is vaned and can also be enhanced by the relatively open VGT position set in this study. Similar conclusions are obtained from other works in the literature [50, 64, 102].

6.3 Pulsating flow results

A parametric study was carried out to quantify the influence of pulse amplitude and frequency on turbine behavior during pulsating conditions. For the sake of simplicity, the pressure pulses set at the inlet were considered to be sinusoidal. The frequencies selected for this study were 50, 90 and 130 Hz. Considering the dominant frequency of a 4-stroke and 4-cylinder engine, these frequencies are equivalent to rotational speeds of 1500, 2700 and 3900 rpm, respectively. It is known that the pressure pulse of one engine cylinder is not sinusoidal. However, since the exhaust flow of each cylinder in a multi-cylinder engine is not synchronized, the pressure response after the collector is more sinusoidal-like. In any case, a general pressure signal can be decomposed into a sum of sinusoidal signals, as has been shown by Costall and Martinez-Botas [27], so that it is of interest to analyze the behavior under sinusoidal signals.

Two different pulse amplitudes were considered in the present work: 50-230 kPa and 90-190 kPa. A mean value of 140 kPa was therefore used in all the calculations. It should be mentioned that all the pressure values given in this thesis are referenced to a constant value of 101325 Pa and are thus *gauge* pressures.

Total temperature was not kept constant at the inlet boundary condition

since pressure and temperature are related in compressible flows. Instead, total temperature was calculated as a function of total pressure, so that an increase in pressure leads to a rise in temperature, according to the isentropic relationship $p_t^{1-\gamma} T_t^\gamma = \text{const.}$ For instance, for the pulse amplitude between 50 and 230 kPa, total temperature ranges from 585 to 725 K. This way of setting exhaust gas temperature is suitable for simulating the pulsating flow produced by a rotating disk in a gas-stand [26]. It is interesting to remark that the steady flow results used hereinafter have been computed setting the inlet total temperature making the equivalent point during the pulse. This was done to ensure that the turbine was working at the same corrected speed. The results are therefore not the same as the ones presented in Figure 2.13.

As stated in chapter 2, the parameters typically analyzed when studying pulsating flow in turbines are the corrected mass-flow rate and efficiency as a function of the total-to-static pressure ratio. However, the definition of the efficiency of the turbine arises some uncertainties [66, 26], due to the possible definitions of the isentropic power. For this reason, in this chapter torque is considered instead of efficiency. Since the rotational speed of the rotor was kept constant, turbine power is proportional to torque.

6.3.1 Overall behavior

The first analysis of the pulsating results was devoted to quantifying the shift in mass flow rate produced by the accumulation and wave effects. Figure 6.1 shows the instantaneous mass flow rate in different sections for the different pulse frequencies and amplitudes analyzed. The pulsating simulations were set-up from a previously converged case using steady boundary conditions (but transient due to the rotor mesh movement). From the figure it can be seen that at least a complete pulse period of the pulse is needed to ensure that a periodic solution is reached.

It can be said that the main source of phase-shift is clearly the volute. This seems a reasonable assumption since it is the section in which the flow spends most time, as it has a larger characteristic length than nozzles or rotor. This effect can be justified using the Strouhal Number, which by definition represents the ratio between a characteristic flow and excitation times.

$$Str = \frac{t_{flow}}{t_{pulse}} = \frac{\frac{L_c}{a+u}}{\frac{1}{f}}. \quad (6.1)$$

The characteristic length of the volute is bigger than that of the rest of the elements. It is therefore clear that the time shift is mainly produced by this element. In fact, Palfreyman et al. [81] proposed that the time-shift is proportional to the average distance traveled by the fluid in the volute. For the simulations in the present work, the mean value of the time-shift varies slightly with the frequency of the pulse, with a value around 0.0011 seconds.

The second effect that can be extracted from the plots is the influence of the plenum in the outlet section of the turbine (see Fig. 2.3). In the 130 Hz case, there is an increase in mass flow between Sections 4 and 5, as shown in Fig. 6.1. The plenum therefore seems to act as a resonator at 130 Hz.

Another fact that has to be pointed out is the pressure found at the turbine outlet. For the 130 Hz and amplitude of 50-230 kPa pulse, the pressure oscillations at the turbine outlet have amplitude of 50 kPa. These fluctuations are possible due to the distance between the outlet boundary and the turbine exit which allows the pressure to evolve with the flow. On the contrary, if the outlet pressure was set close to the turbine outlet, this pressure would have been fixed, and therefore this fluctuation would have been spuriously neglected.

6.3.2 Local behavior of the different components

Flow capacity was then compared in the different turbine components. Figure 6.2 shows the evolution of the corrected mass flow at the volute inlet (Section 1) with the local volute pressure ratio (from Section 1 to 2). As expected, the accumulation and wave effects in the volute make the difference between steady and pulsating results increase with pulse amplitude and frequency. Figure 6.3 shows the same result for the nozzles zone. Due to the smaller nozzle volume and length, the accumulation and wave effects are almost negligible. Figure 6.4 shows the evolution of the flow capacity versus the local pressure ratio in the impeller. The turbine outlet region from Sections 4 to 5 is also included in this plot to take into account the mixing losses at the rotor outlet. The figure also supports the conclusion that the unsteady effects can be neglected within the impeller, due to its small characteristic length. The difference between steady and pulsating flow in the rotor is even lower than in the nozzle section. As has been mentioned above, the definition of isentropic efficiency in transient conditions introduces uncertainties related

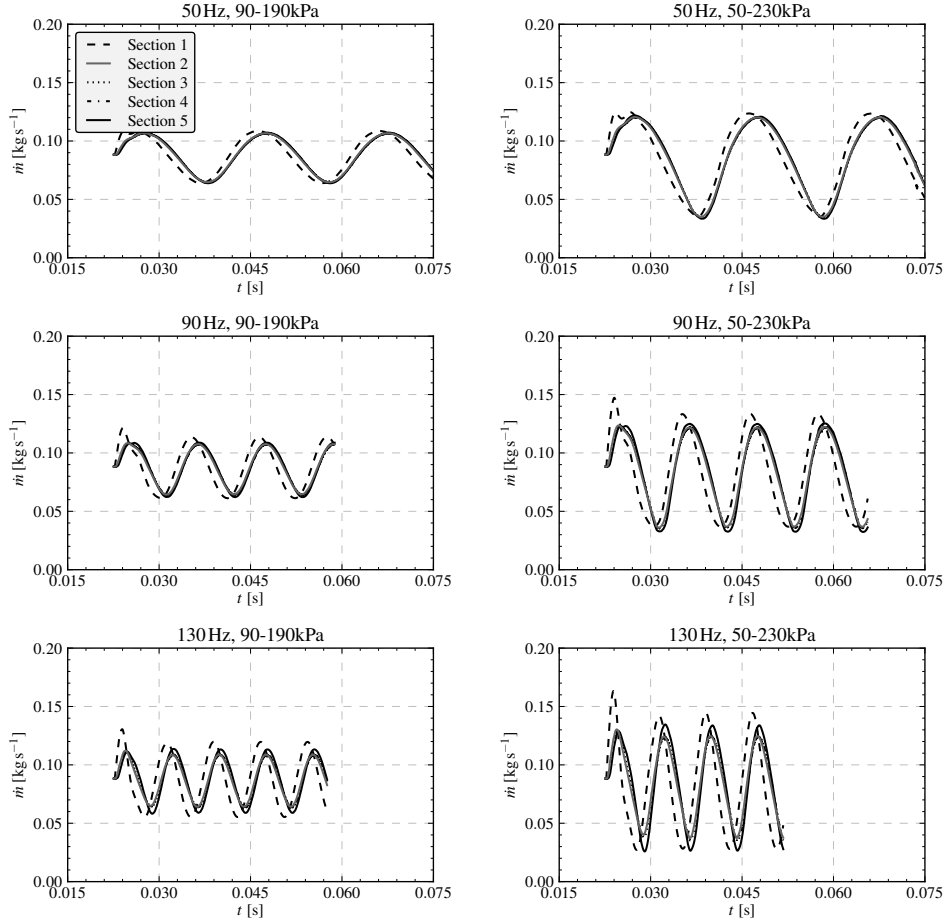


Figure 6.1: Evolution of the mass flow rate with time at different sections for the pulses considered (50 Hz, 90 Hz and 130 Hz) and the two pulse amplitudes (50-230 kPa and 90-190 kPa) are plotted. The time-shift introduced by the volute and the effect of the outlet plenum are indicated.

to the non-synchronized mass flow and pressure ratio [66]. Here instantaneous power was considered instead. Moreover, since the rotational speed of the turbine was kept constant, the torque values (computed from the force acting on the rotor walls) and power are proportional. Fig. 6.5 compares the evolution of the torque obtained under pulsating conditions with the results of the steady simulations. The graphs show that the evolution of torque with

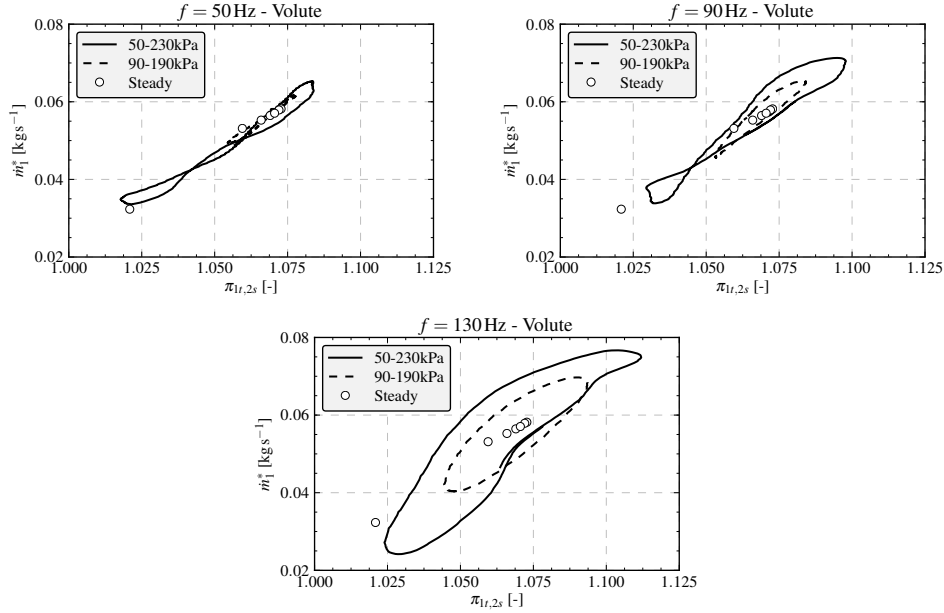


Figure 6.2: Corrected mass flow rate considering conditions at the inlet of the volute vs the expansion ratio in the volute.

pressure ratio cannot be considered as quasi-steady, in contradiction to the conclusion presented in Aymanns et al. [8]. The reason for this disagreement lies in the location of the outlet boundary condition. As previously mentioned, separating the outlet boundary from the impeller ensures that the pressure at the turbine outlet is calculated from the flow field variables, which seems to be a more physical solution. The disagreement is analyzed in further detail in the next section.

6.4 Discussion of results

This section deals with a detailed analysis of the CFD calculations. Besides the time-shift issue discussed in the previous section, there is a pulse *averaging effect* in the volute that can also be analyzed, due to its particular geometry. Figure 6.6 shows the evolution of the velocity magnitude versus the angular coordinate at the volute outlet (Section 2) at a given time. The origin of the

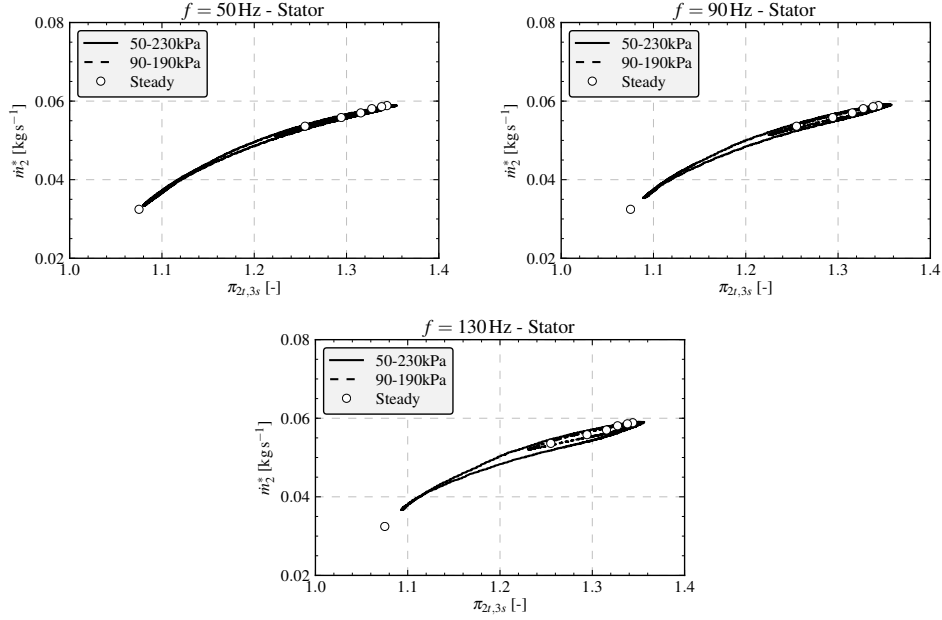


Figure 6.3: Corrected mass flow considering conditions at the inlet of the turbine nozzle vs the expansion ratio in the nozzle.

angular coordinate corresponds to the tongue of the volute. The selected time is close to the pulse minimum of the 130 Hz frequency and amplitude of 50-230 kPa case and is compared with the distribution in the corresponding steady case. From the evolution, it can be established that there is a region in the volute that is effectively behaving as in the 50 kPa case. The rest of the volute is acting as if the pressure was higher, and is thus working under a different operating condition. It can therefore be concluded that the peaks and valleys of the time evolution of the pulsating signal are smoothed out. This effect can be appreciated in Fig. 6.3, in which the nozzles working under pulsating conditions do not reach the minimum mass-flow of the steady points. This effect is more noticeable as the frequency increases, since the volute outlet will be affected by a larger portion of the pulse. Fig. 6.7 shows the velocity flow field in the mid-plane of the nozzles at two different points of the 130 Hz pulse, with the same local pressure ratio (approximately 1.25). Velocity contours in the two situations are similar but not identical. The velocity magnitude is higher in the upper plot. The reason is that even though the pressure ratio is the

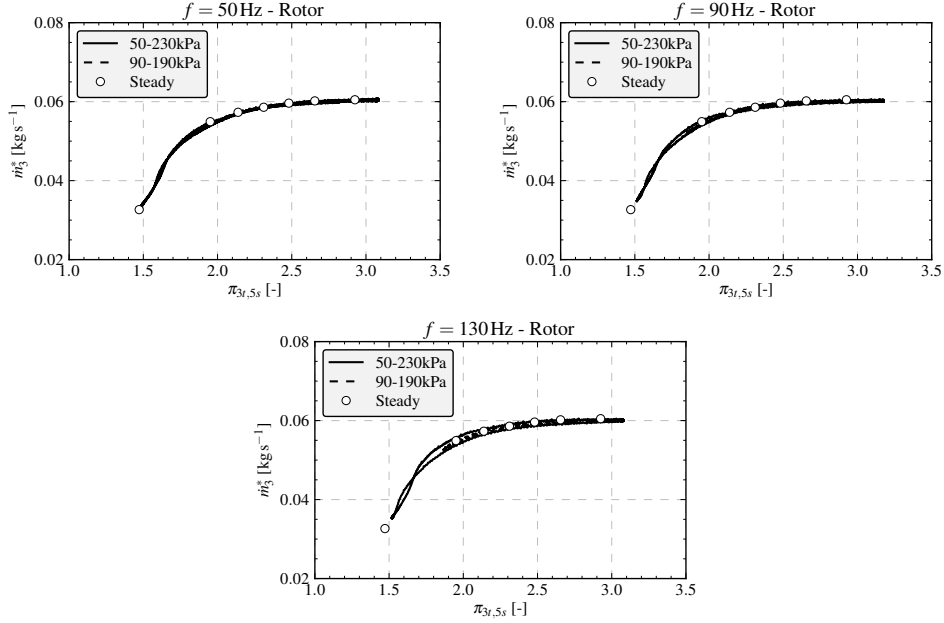


Figure 6.4: Corrected mass flow considering conditions at the inlet of the turbine rotor vs the expansion ratio in the rotor and outlet section of the turbine.

same, the total pressure at the stator inlet is not the same in the two operating conditions. In Fig. 6.7, the flow at the stator inlet is intrinsically non-uniform due to the shape of the volute and the effect of the screws and the vanes of the nozzle. This means the stator flow is not one-dimensional, so that not all the channels will be working under the same conditions. However this aspect is not taken into account in the current analysis, since a circumferential average was taken. During the off-design points, the flow around the stator vanes and screws detaches and reattaches; this does not necessarily happen at the same pressure ratio since it has a certain inertia. This can be seen by analyzing the two flow fields in Fig. 6.7, in which, even though the two cases are at the same pressure ratio, the flow is detached at some vanes in the upper case but not in the lower one. This effect makes the angle at the outlet of this section vary, thus changing the effective area of the nozzles, which can introduce part of the hysteric cycle in the stator. Finally, the same procedure was followed to analyze the flow-field in the rotor. The relative velocity field is shown in Fig. 6.8. Two points are represented with the same local expansion ratio (from

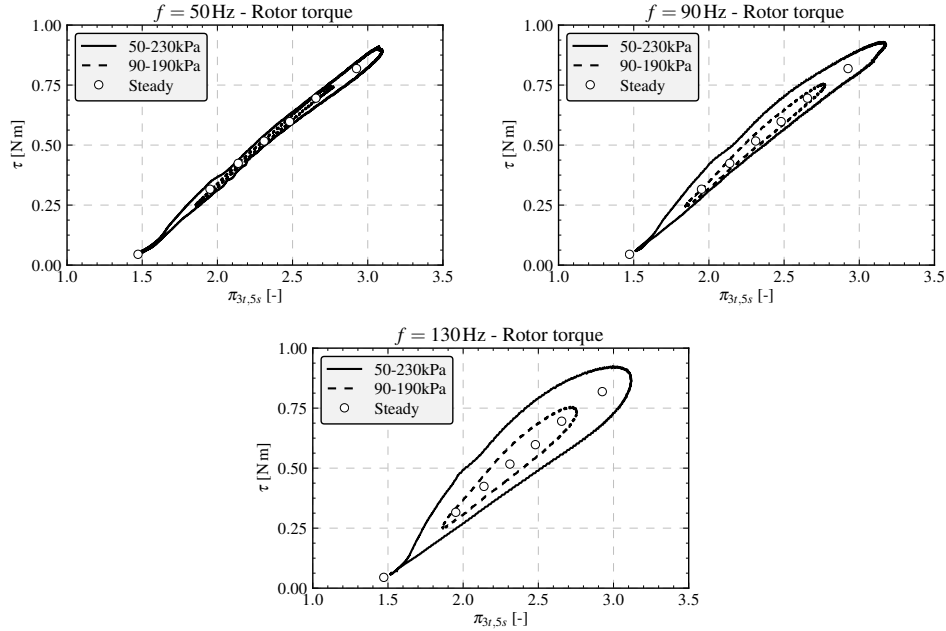


Figure 6.5: Turbine torque vs pressure ratio in the rotor.

Section 3 to 4), one in the rising part of the pulse and the other in the falling one. As was explained in the case of the nozzles, the absolute pressure at the impeller inlet and outlet are different in the two cases. Since the pressure ratio in the rotor is greater than in the nozzles (for this particular VGT position) the difference is more noticeable. Two conclusions can be extracted from a comparison of the images in Fig. 6.8. First, even though the flow at the rotor channels inlet is very different, the flow at the outlet is similar in terms of the direction of the velocity vectors and thus the effective section. This explains the reduced hysteretic behavior shown in Fig. 6.4, since the corrected mass-flow only depends on the effective area. The second comment is about the very different flow pattern at the rotor inlet. Although the pressure ratio is the same, the inflow conditions are very different. Due to this effect the blade loading will be different, and thus the generated torque. This effect would not be appreciated if the pressure outlet boundary condition had been directly imposed close to the rotor outlet, since a given pressure ratio will necessarily mean a unique inlet pressure. The disagreement mentioned in the previous section concerning the quasi-steady behavior of torque found by Aymanns et

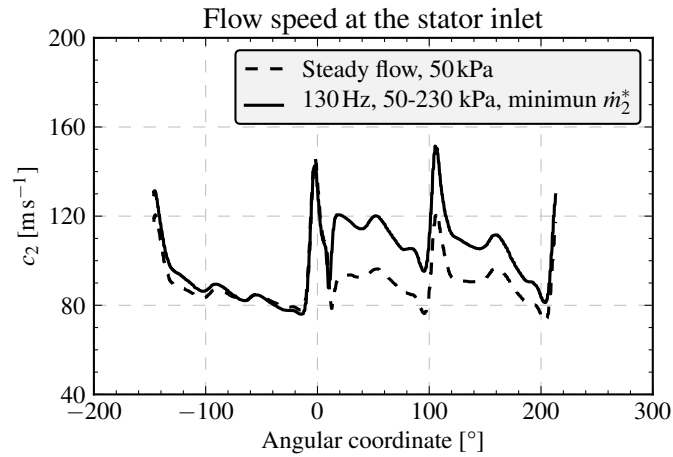


Figure 6.6: Evolution of the velocity magnitude with the angular coordinate at the volute outlet.

al. [8] is the consequence of imposing constant pressure at the turbine outlet, close to the impeller. From this point of view, it is advisable to separate the outlet boundary condition from the rotor if the hysteretic effect in the torque needs to be analyzed, particularly if the turbine under study does not have a considerable expansion at the rotor outlet.

The quasi-steady assumption is not fulfilled if the evolution of rotor torque with local pressure ratio is considered. However, it can be seen that torque can correlate better with inflow conditions at the rotor inlet. In Figure 6.9, the torque evolution with the blade speed ratio at the rotor inlet is presented for the two 130 Hz pulses. The blade speed ratio σ is computed as blade velocity divided by incident flow velocity. In this chapter, the blade speed is obtained at the impeller inlet and the flow velocity is the average velocity magnitude in Section 3. It should be remembered that the blade to speed ratio is generally calculated from the isentropic velocity obtained when expanding the flow from the turbine inlet conditions to the outlet pressure, since the impeller inlet pressure is not usually measured.

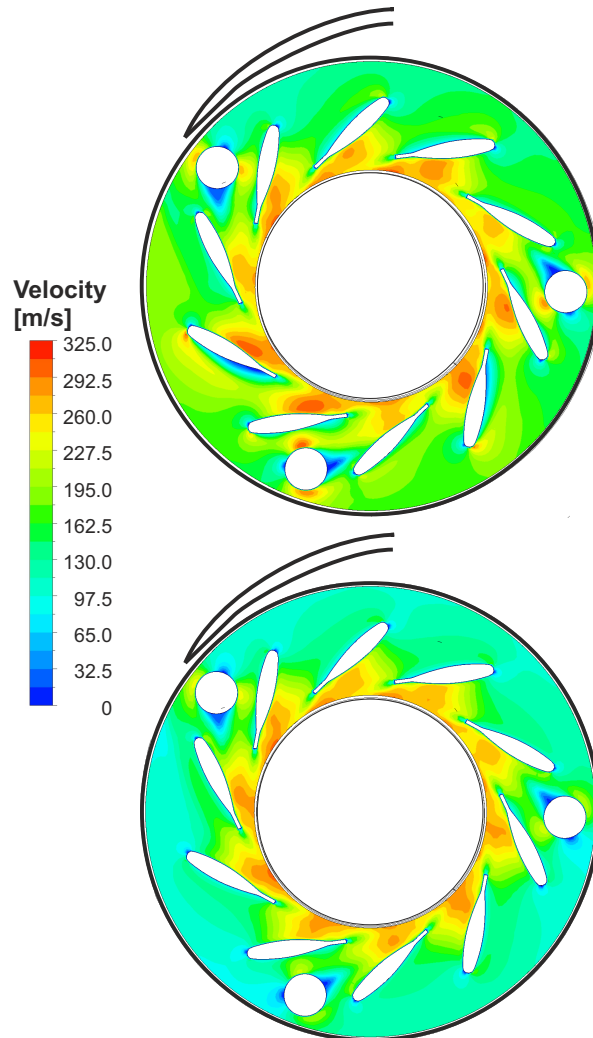


Figure 6.7: Velocity flow fields in the stator for two points of the pulse (130 Hz, 50-230 kPa) with the same pressure ratio ($\pi_{2t3s} \simeq 1.25$). In the upper one the pressure ratio is decreasing and it is increasing in the lower one.

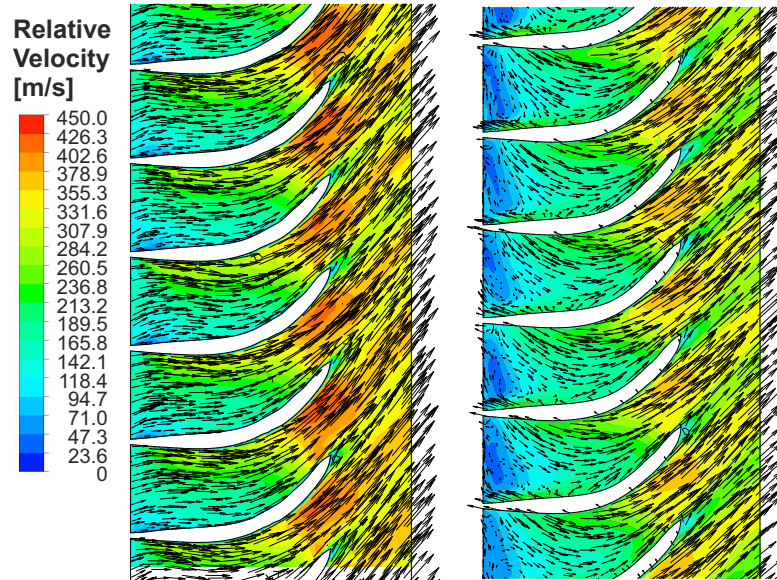


Figure 6.8: Relative velocity flow fields in the rotor for two points of the pulse (130 hz, 50-230 kpa) with the same pressure ratio ($\pi_{3t4s} \simeq 2.42$). In the left image the pressure ratio is increasing, in the right image it is decreasing.

6.5 Application to engine modeling

The analysis described in the preceding section gives some hints on which phenomena can be calculated with a simpler 1D or 0D model. The use of 1D engine gas dynamic models is commonplace because they allow one to predict engine performance with reasonable accuracy and limited computational cost. The use of turbocharger submodels implemented in the complete engine model is one of the key points in the development of boosting systems. Some recommendations can be given on this topic based on the analysis performed in this work, after which a turbine model covering the stator and rotor regions will be developed.

As presented in the literature [93], it is necessary to use a 1D or 0D element to reproduce the non-quasi-steady volute behavior shown in Figure 6.2. Most

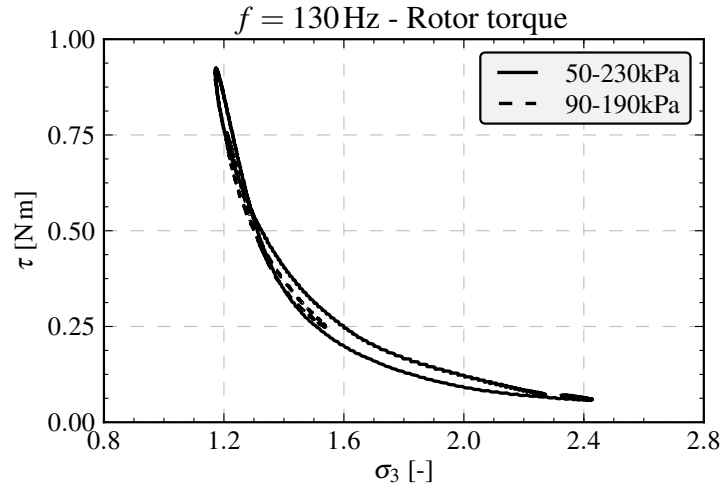


Figure 6.9: Turbine torque vs blade speed ratio at the rotor inlet.

authors have successfully used a constant section 1D pipe with half of the volute length, which accounts for the accumulation and wave transmission effects. However, the non-uniformity of the flow in the volute outlet section during the pulse transmission plotted in Figure 6.6 cannot be captured with such a model. This could be done with a quasi-2D model of the volute, in which the tangential and radial components are calculated by imposing conservation of angular momentum, similar to the work presented by Bozza et al. [19] for a centrifugal compressor.

In this chapter, the conclusion for the vaned stator is that there is a small hysteretic result partly produced by aerodynamic effects. This variation causes the flow angle at the outlet of the nozzle to change throughout the pulse. However, since the hysteresis is small it is considered to be negligible for the current development of the turbine model. As stated in the preceding section, it was observed that rotor flow capacity behaves in a quasi-steady manner, so that it could be computed using a zero-dimensional throat model. In the case of the generated torque, it does not behave as quasi-steady if it is presented versus the pressure ratio, since it depends on the conditions at the impeller inlet.

6.5.1 Proposed model

A new radial turbine model is here proposed, based on the results of the previous sections. The model will work with the instantaneous values of the total pressure and temperature at the stator inlet (Section 2) and the static pressure at the rotor outlet (Section 4). The model is broken up into three submodels: one simulating the stator, one for the rotor, and the intermediate deposit to decouple the response of the other two. This procedure is similar to the one used in a previous model developed by the authors' group [99]. The different thermo-fluid-dynamic processes considered in the model are shown in the h-s diagram presented in Fig. 6.10.

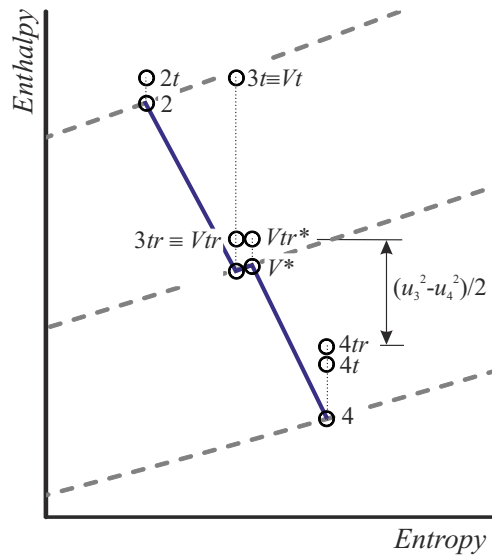


Figure 6.10: Enthalpy-entropy diagram of the thermo-fluid-dynamic processes considered in the model. The notation used in the diagram is described throughout section 6.5.

The numeration of the intersections varies due to the intermediate deposit. To clarify the subscripts notation followed in this section it should be remarked that:

- Section 3 corresponds to the stator outlet and Section 4 to the rotor outlet.

- The flow entering the plenum is at the same conditions as in section 3.
- The flow at the rotor inlet is at the conditions in the deposit (indicated with a V).

The different submodels are presented below.

6.5.1.1 Stator nozzle

The turbine stator will be treated in a similar way as in the previous model. Polytopic expansion will be considered for the evolution of the flow in the nozzle. In the current development, the value of the polytopic coefficient, k , is obtained from the steady computation at 140 kPa (the mean value of pressure). The effective area will be computed from the geometric area of the stator section and the flow angle:

$$A_{3_{eff}} = 2\pi R_3 \cdot h_3 \cdot \cos \alpha_3, \quad (6.2)$$

where α_3 is the angle between the flow velocity and the radial direction and, as previously mentioned, it changes during the pulse. To simplify this model, as a first approach, this angle is kept constant with the value extracted from the 140 kPa steady simulation. The mass flow rate passing through the stator nozzle is therefore related to the pressure ratio in the nozzle as

$$\dot{m}_3 = A_{3_{eff}} \frac{p_{2t}}{RT_{2t}} \left(\frac{p_V}{p_{2t}} \right)^{\frac{1}{k}} \sqrt{2 \frac{\gamma}{\gamma - 1} RT_{2t} \left[1 - \left(\frac{p_V}{p_{2t}} \right)^{\frac{k-1}{k}} \right]}, \quad (6.3)$$

where p_V is the pressure of the intermediate reservoir. Equation (6.3) is valid while the pressure ratio is lower than the critical one, $\left(\frac{\gamma+1}{2} \right)^{\frac{k}{k-1}}$. Once the critical pressure ratio is exceeded, the nozzle will be choked and corrected mass-flow will therefore no longer increase. It is worth mentioning that the discharge pressure, p_3 , will be the pressure in the intermediate deposit p_V , and the discharge velocity can also be computed from the pressure ratio.

6.5.1.2 Intermediate deposit

As mentioned above, the aim of the deposit is to decouple the behavior of rotor and stator, and at the same time to simulate the hysteretic effects in the

turbine. More precisely, it takes into account filling-and-emptying effects of the turbine, which are accomplished by the variation with time of the gas contained in the intermediate deposit. Additionally, due to the different inertia of energy and mass conservation, the plenum introduces some time shift between the pressure and temperature of the flow inside it. The volume of the deposit will be of the same order as the volume of the turbine. In order to model the deposit, it is necessary to define its behavior. The deposit receives the mass flow from the stator (Section 3) and supplies flow to the rotor inlet. In the current work, the conservation of the flow speed in the deposit is considered, $c_V = c_3$. This hypothesis can be assumed because in the flow between stator and rotor there is no sudden increase of area that could decelerate the flow. This hypothesis differs from the one followed in the previous model, in which the flow in the deposit was assumed to be stationary ($c_V = 0$).

In order to model the flow in the deposit, the accumulation effects will be considered by means of the mass conservation equation:

$$\frac{dM_V}{dt} = \dot{m}_3 - \dot{m}_4 \quad (6.4)$$

which are respectively: total mass of the air in the deposit, M_V ; and the mass flow rate from the stator, \dot{m}_3 , and to the rotor, \dot{m}_4 . The energy conservation equation applied to the flow in the deposit establishes that:

$$\frac{d}{dt} \left[M_V \left(c_v T_V + \frac{c_V^2}{2} \right) \right] = \dot{m}_3 \left(c_p T_3 + \frac{c_3^2}{2} \right) - \dot{m}_4 \left(c_p T_V + \frac{c_V^2}{2} \right). \quad (6.5)$$

The flow entering the deposit comes from the stator (3) while the flow leaving the deposit (V) will pass through the rotor. Additionally, the ideal gas equation is needed to compute the pressure inside the deposit, provided that its volume is known.

6.5.1.3 Rotor section

As previously mentioned, only a small hysteretic effect was found in the mass flow through the impeller, as shown in Fig. 6.4. In this case, the throat will be placed in a *rotating channel* and therefore has to be treated in a different way than the stator nozzle, since conservation equations have to be applied in the relative reference frame. Rothalpy is conserved in a rotating passage provided that: the flow is steady in the rotating frame, no friction from the casing has

to be considered, and the wall of the turbine can be considered adiabatic [33]. This approach is different from the one followed in the previous model [99], in which the nozzle equation was directly used. Following the same criteria as in the case of the stator (Eq. (6.2)), the effective area of the rotor throat will be the geometric annular area multiplied by the cosine of the angle at the rotor outlet:

$$A_{4_{eff}} = A_{4_{geom.}} \cdot \cos \alpha_4. \quad (6.6)$$

The conservation of energy in the rotating frame establishes that

$$c_p T_V + \frac{w_V^2}{2} - \frac{u_3^2}{2} = c_p T_4 + \frac{w_4^2}{2} - \frac{u_4^2}{2}, \quad (6.7)$$

where w is the relative velocity and u the blade speed or tangential velocity of the rotor, which can be expressed in terms of the rotational velocity. Mass flow rate through the rotor can be computed as

$$\dot{m}_4 = \rho_4 w_4 A_{4_{eff}}. \quad (6.8)$$

The evolution of flow in the rotor can be taken as polytropic, and n is taken as its polytropic coefficient. Therefore, the mass flow rate through the rotor section can be computed as:

$$\frac{\dot{m}_4 \sqrt{RT_{Vtr}}}{A_{4_{eff}} p_{Vtr}} = \left(\frac{p_4}{p_{Vtr}} \right)^{\frac{1}{n}} \sqrt{\frac{2\gamma}{\gamma-1} \left[1 - \left(\frac{p_4}{p_{Vtr}} \right)^{\frac{n-1}{n}} \right] - \frac{(u_3^2 - u_4^2)}{RT_{Vtr}}}, \quad (6.9)$$

where T_{Vtr} is the total relative temperature in the plenum, that means that the total temperature is calculated referring to the relative speed (w) instead of the absolute one (c). The rotation of the channel increases the critical pressure ratio of the rotor at which choked conditions exist, due to the last term inside the square root of equation (6.9). The difference between the squares of the tangential velocity of the rotor can be expressed in terms of the rotational speed of the turbine as:

$$u_3^2 - u_4^2 = \left(\frac{\pi N}{60} \right)^2 (D_3^2 - D_4^2). \quad (6.10)$$

In Eq. (6.10), D_4 represents the diameter of the rotor outlet. Since the section is annular, an appropriated effective diameter should be defined. For the current computations, the following definition was used:

$$D_4 = \sqrt{\frac{D_{max}^2 + D_{min}^2}{2}}. \quad (6.11)$$

As previously mentioned, the angle at the stator outlet varies during the pulse, thus changing the incident angle at the rotor inlet. In order to consider the incident losses in the rotor, a simple model is used [75], which is based on neglecting the contribution of the tangential velocity to the rotor expansion. Since the radial component is the same for relative and absolute velocity, the following equation holds:

$$w_{3rad} = c_{3rad} = c_3 \cdot \cos \alpha_3. \quad (6.12)$$

This means that while the relative total temperature at the rotor inlet (which is the one at the deposit) can be calculated as:

$$T_{Vtr} = T_V + \frac{w_V^2}{2c_p} = T_V + \frac{w_3^2}{2c_p}, \quad (6.13)$$

for the total relative pressure only the radial component of the relative velocity takes part, that is:

$$p_{Vtr} = p_V \left(\frac{T_{Vtr}^*}{T_V} \right)^{\frac{\gamma}{\gamma-1}} = p_V \left(1 + \frac{w_{3rad}^2}{2c_p T_V} \right)^{\frac{\gamma}{\gamma-1}}. \quad (6.14)$$

6.5.1.4 Turbine power

The power output from the turbine can be computed as:

$$P = \dot{m}_4 c_p (T_{Vt} - T_{4t}), \quad (6.15)$$

T_{Vt} being the total temperature at the deposit and T_{4t} the total temperature at the rotor outlet. The total temperature at the intermediate deposit can be computed as:

$$T_{Vt} = T_V + \frac{c_V^2}{2c_p}. \quad (6.16)$$

The total temperature at the rotor outlet is expressed as:

$$T_{4t} = T_4 + \frac{c_4^2}{2c_p}, \quad (6.17)$$

where T_4 can be obtained from the polytropic expression of the flow in the rotor, and c_4 , the absolute flow velocity, can be obtained from the values of the relative velocity w_4 , the blade velocity u_4 , and the flow angle β_4 .

6.5.2 Model calibration

Up to this point, the different submodels for the stator and rotor section of the radial turbine have been presented. As inputs to the model, apart from the geometric data (areas), the polytropic coefficient in stator, k , and rotor, n , and the flow angle, β , at stator outlet and the rotor outlet are needed. The boundary conditions applied to the model are the temporal evolution of the total pressure and temperature at the stator inlet, and the static pressure at the rotor outlet.

The objective of this model is to be able to simulate the pulsating behavior of a radial turbine. It is clear that in order to obtain the exact response, the temporal evolution of polytropic coefficients and flow angles is needed. However, this approach would reduce the model's usefulness, since it could only be used when the evolutions are known. As previously commented, the values used are those of the steady simulation with a pressure of 140 kPa. Another option would be to use the angle directly from the blades (both at the stator and rotor section), neglecting the fluid-dynamic effects. However, this approach presented a greater error.

The model was implemented in Python, using an explicit Euler time integration scheme for the equations describing the behavior of the deposit (Eqs. (6.4) and (6.5)). The time step size was selected to match the one used during the RANS simulations. The chosen volume of the intermediate plenum is $3.04 \cdot 10^{-5} \text{ m}^3$, representing the real volume of the fluid domain of the stator and rotor zones.

To evaluate the behavior of the calibrated model, it has been used to reproduce the operating conditions of the simulations with steady boundary conditions. The results obtained with the model and the difference with the CFD results are presented in the following Tab. 6.2.

The results of the model have been obtained with the model calibrated using the values of the 140 kPa simulation. The results show the suitability of the model to reproduce the behavior of the stator and rotor sections of the turbine. It is worth mentioning that the biggest error is found in the low pressure region, in which the magnitude of the turbine power is smaller and therefore the difference has less effect in the overall value.

Table 6.2: ASSESSMENT OF THE MODEL UNDER STEADY FLOW CONDITION.

Case	Mass flow rate ($\text{kg}\cdot\text{s}^{-1}$)		Power (W)	
	Model result	Error %	Model result	Error %
50 kPa	0.0367	8.56 %	884.16	2.68 %
100 kPa	0.0692	0.049 %	6393.69	3.76 %
120 kPa	0.0789	0.53 %	8221.37	3.46 %
140 kPa	0.0877	0.69 %	9925.27	2.29 %
160 kPa	0.0957	1.57 %	11504.28	1.37 %
180 kPa	0.102	1.13 %	13466.450	2.15 %
210 kPa	0.112	1.27 %	15590.25	0.45 %

6.5.3 Pulsating results

Figure 6.11 shows the comparison of the flow capacity obtained from the simplified model and that obtained using the 3D-CFD code. Good agreement is found between the results, recovering the hysteretic loop, with only a few discrepancies found in the region of smaller pressure ratios. This difference is probably due to the variation of the flow angle at the stator outlet.

The power developed by the turbine can be computed by means of the simplified model as the difference between total enthalpy in the outlet and the inlet, using Eq.(6.15). The comparison between the results from the model and those from the three-dimensional CFD computations is shown in Fig. 6.12.

Good agreement is found in the power results. A small discrepancy is found in the upper curve of the loop in which power is over-predicted by the model. The difference between the energy computed in a whole pulse cycle for the model and the CFD is about 2.75 %. Once again, the value of the torque developed by the turbine can be easily estimated from the power computation since the rotational speed remains constant.

In view of these results, the model described in this section is able to reproduce the pulsating behavior of the stator and rotor on a radial turbine. Similar results are obtained for other pulses simulated. Figures 6.13, 6.14 and 6.15 show the comparison of the result obtained with the model and the ones from CFD for the pulses with 50 Hz, 90 Hz and 130 Hz.

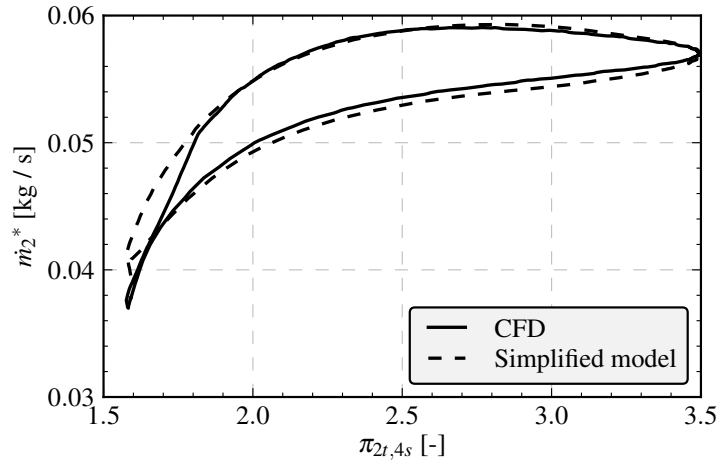


Figure 6.11: Comparison of the turbine flow capacity taking into account the stator and rotor sections by means of CFD and the proposed model. These results are obtained for a 130 Hz pulse with the highest amplitude considered (50-230 kPa).

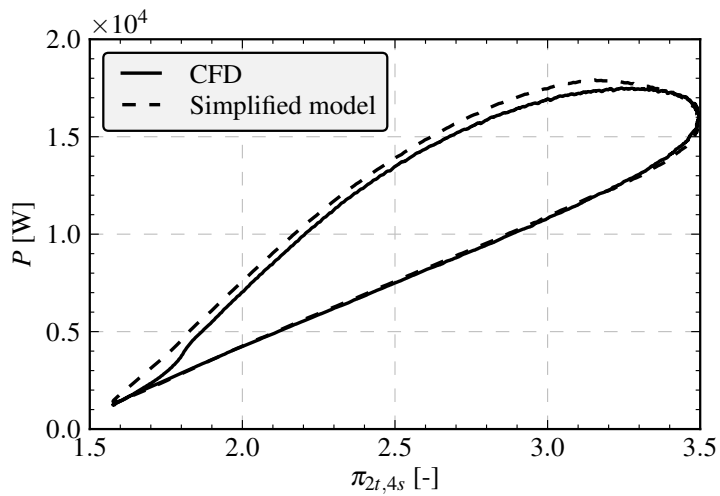


Figure 6.12: Comparison of power as computed by the model and that obtained from the CFD computations. These results are obtained for a 130 Hz pulse with the highest amplitude considered (50-230 kPa).

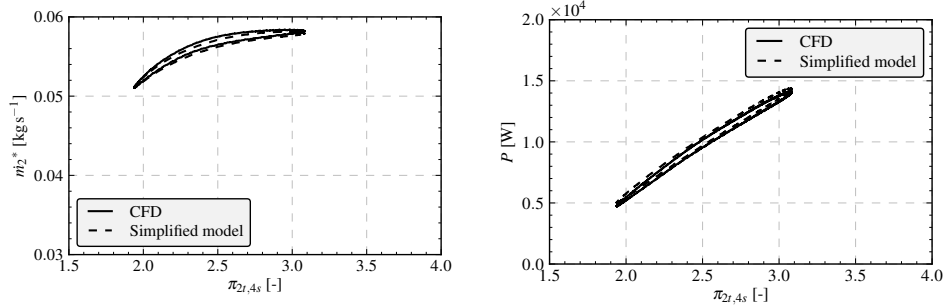


Figure 6.13: Comparison of the results of the model and CFD for the pulse of 50 Hz and the 90-190 kPa amplitude.

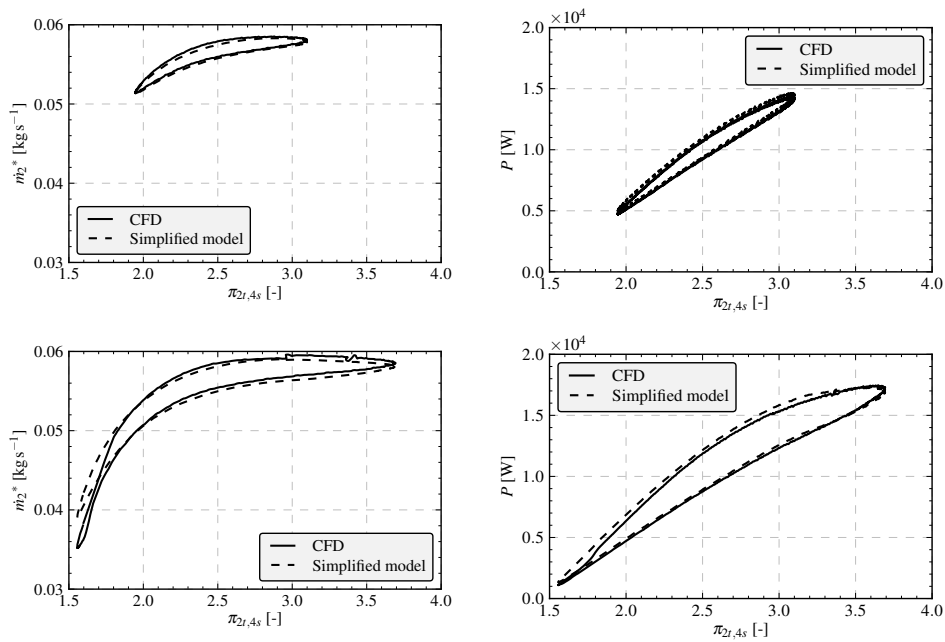


Figure 6.14: Comparison of the results of the model and CFD for the two pulse of 90 Hz (both amplitudes).

In terms of the elements used, the proposed model is similar to the model previously developed by the authors' group [99]. However, there are some im-

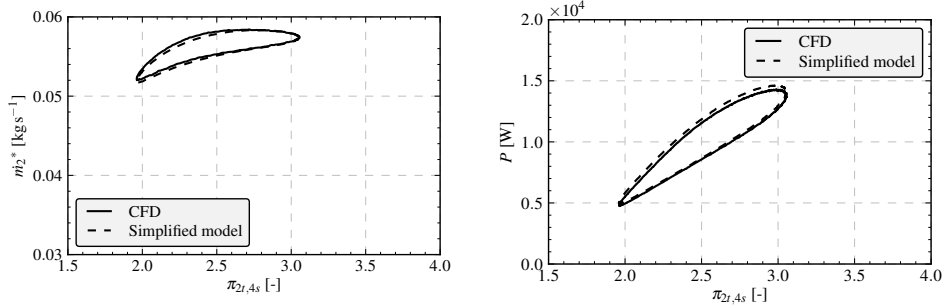


Figure 6.15: Comparison of the results of the model and CFD for the pulse of 130 Hz and the 90-190 kPa amplitude.

portant differences, e.g. in computing the mass flow rate in the rotor section. Instead of a nozzle, the authors suggest the use of a rotating channel in which rothalpy is conserved. This would result in an effective section less dependent on turbine speed and pressure ratio. The proposed formulation for the intermediate deposit is also different: in the new model the intermediate deposit is assumed to conserve the kinetic energy of the flow, while in the previous model the flow was considered to be stationary inside the deposit.

Information from a steady case is needed to calibrate the proposed model, i.e. the flow angle at the rotor and stator outlets and the polytropic coefficient of the evolution of the flow inside them. This means that the pulsating behavior could be recovered from information from a single CFD case with steady boundary conditions. Alternatively, the required information could be obtained from experimental data. On the other hand, the previous model needed the efficiency curve and the turbine map as input, in order to interpolate the results during the pulse. Thus, since the formulation of the new model is more physically-based, it has the advantage of not needing the complete map to describe its behavior.

Although the objective of this model is to analyze the turbine in pulsating conditions, it can also be used to extrapolate the turbine performance from a given point. The advantages of this type of model have been described by Payri et al. [90].

6.6 Conclusions

This chapter describes a CFD analysis of the behavior of a radial turbine under steady and pulsating flow conditions. The main objective was to evaluate separately the non-steady effects in the volute, nozzles and impeller. The comparison with steady experimental results shows that the sliding mesh technique to simulate rotor movement is more suitable than the frozen rotor for this application, probably due to the nozzle-rotor interaction.

The analysis of the pulsating results shows that most of the time-shift in the mass flow occurs in the volute. This shift varies slightly with pulse amplitude and frequency. For the same reason the volute shows significant hysteretic behavior as pulse amplitude and frequency increase. The volute also exhibits an additional unsteady behavior, reducing the peak-to-valley amplitude due to non-uniform flow along the volute outlet section.

The flow in the nozzle section presents a limited hysteretic behavior in its pulsating flow capacity. This effect could be influenced by various aspects. In the first place, even though the characteristic length (wave action) and the accumulation effects of the stator can be neglected, when compared to those of the volute, there is a certain influence when the stator behavior is analyzed. Secondly, the averaging effect of the volute, which reduces the amplitude of the transmitted pulses, causes the pulsating flow capacity curve of the nozzle to shrink before reaching the equivalent steady values. Finally, the detachment and reattachment process of the flow in the nozzle vanes and screws and other aerodynamic effects have some influence on the hysteretic behavior. These aerodynamic transient phenomena change the flow angle at the stator outlet and therefore the instantaneous effective area of the nozzle.

The behavior of the impeller is even less affected by wave action and accumulation effects than the stator, due to its smaller size. In view of the two flow fields at the same pressure ratio obtained from the CFD simulations, it can be established that, even though the flow patterns in the rotor channels vary enormously, the flow in the smallest section (outlet) is quite similar regardless of the flow conditions at the channels inlet. This explains the small degree of hysteretic behavior when dealing with flow capacity in this region. However, the rotor inlet conditions have a huge impact on torque and therefore pulsating torque does not correlate with instantaneous corrected mass flow or pressure ratio, but correlates better with the impeller inflow conditions

(velocity magnitude, blade speed ratio).

As a conclusion of the CFD analysis, a simplified model is proposed that would include a one-dimensional or quasi-two-dimensional element to represent the volute, a nozzle to represent the vaned stator, a small zero-dimensional element to represent the hysteresis in the stator, and a rotating channel in which rothalpy is conserved to represent the flow in the rotor.

In this chapter, a simplified model to simulate the behavior between the stator and rotor has been implemented. Although the implementations of the volute and outlet duct are not included in this simple model, they could be computed using a one-dimensional code. The performance of the stator and rotor model has been evaluated for a pulsating simulation, showing good agreement with the CFD results. The proposed model, due to the physically-based formulation, just needs information from one steady point obtained from a CFD computation.

Chapter Bibliography 6

- [8] R. Aymanns, J. Scharf, T. Uhlmann, and D. Lückmann. “A revision of Quasi Steady Modelling of Turbocharger Turbines in the Simulation of Pulse Charged Engines”. In: *16th SUPERCHARGING CONFERENCE*. 2011 (cit. on pp. 127, 128, 133, 137).
- [12] N.C. Baines. “Turbocharger turbine pulse flow performance and modelling - 25 years on”. In: *Proceedings of the 9th Conference Turbochargers and Turbocharging*. 2010, pp. 347–362 (cit. on pp. 126, 158).
- [19] F. Bozza, V. De Bellis, S. Marelli, and M. Capobianco. “1D Simulation and experimental analysis of a turbocharger compressor for automotive engines under unsteady flow conditions”. In: *SAE Paper 4.2011-01-1147* (2011), pp. 1365–1384. DOI: 10.4271/2011-01-1147 (cit. on p. 140).
- [22] M. Capobianco and A. Gambarotta. “Unsteady flow performance of turbocharger radial turbines”. In: *C405/017, Proceeding of the Institute of Mechanical Engineers, Fourth International Conference, Turbocharging and Turbochargers*. 1990, pp. 123–132 (cit. on p. 126).
- [23] M. Capobianco and S. Marelli. “Waste-gate turbocharging control in automotive SI engines: effect on steady and unsteady turbine perfor-

- mance”. In: *14th Asia Pacific Automotive Engineering Conference*. 2007, pp. 01–3543 (cit. on p. 128).
- [26] C. D. Copeland, R. Martinez-Botas, and M. Seiler. “Comparison Between Steady and Unsteady Double-Entry Turbine Performance Using the Quasi-Steady Assumption”. In: *Journal of Turbomachinery* 133 (2011), pp. 031001–1/031001–10 (cit. on pp. 2, 126, 130).
- [27] A. Costall and R.F. Martinez-Botas. “Fundamental characterization of turbocharger turbine unsteady flow behavior”. In: *Proceedings of the ASME Turbo Expo*. GT-2007-28317. 2007 (cit. on p. 129).
- [33] S. L. Dixon and C. Hall. *Fluid mechanics and thermodynamics of turbomachinery*. Butterworth-Heinemann, 2010 (cit. on pp. 114, 144).
- [40] J. Galindo, P. Fajardo, R. Navarro, and L. M. García-Cuevas. “Characterization of a radial turbocharger turbine in pulsating flow by means of CFD and its application to engine modeling”. In: *Preprint submitted to Applied Energy* (Date of submission 01/03/2012) (cit. on pp. 126, 167).
- [50] F. Hellström. “Numerical computations of the unsteady flow in turbochargers”. PhD thesis. Royal Institute of Technology KTH Mechanics, 2010 (cit. on pp. 25, 129).
- [52] F. Hellstrom and L. Fuchs. “Numerical Computation of the Pulsatile Flow in a Turbocharger With Realistic Inflow Conditions From an Exhaust Manifold”. In: *Proceedings of ASME Turbo Expo 2009: Power for Land, Sea and Air*. GT2009-5961. ASME. 2009 (cit. on pp. 44, 126, 158).
- [57] T. Kawakubo. “Unsteady Rotor-Stator Interaction of a Radial-Inflow Turbine With Variable Nozzle Vanes”. In: *Proceedings of ASME Turbo Expo 2010: Power for Land, Sea and Air*. ASME. 2010 (cit. on pp. 44, 126, 129, 158).
- [59] J. K. W. Lam, Q. D. H. Roberts, and G. T. McDonnell. “Flow modelling of a turbocharger turbine under pulsating flow”. In: *ImechE Conference Transactions from 7th International Conference on Turbochargers and Turbocharging*. 2002, pp. 14–15 (cit. on pp. 24, 44, 126, 158).

- [64] Z. Liu and D.L. Hill. “Issues surrounding multiple frames of reference models for turbo compressor applications”. In: *Fifteenth International Compressor Engineering Conference*. Purdue University. 2000 (cit. on pp. 24, 44, 127, 129).
- [66] S. Marelli and M. Capobianco. “Steady and pulsating flow efficiency of a waste-gated turbocharger radial flow turbine for automotive application”. In: *Energy* 36 (2011), pp. 459–465. ISSN: 0360-5442 (cit. on pp. 126, 129, 130, 132).
- [75] H. Moustapha, M. F. Zelesky, N. C. Baines, and D. Japikse. *Axial and radial turbines*. Concepts NREC, 2003 (cit. on p. 145).
- [81] D. Palfreyman, R. F. Martinez-Botas, and N. Karamanis. “Computational and experimental investigation of the aerodynamics of turbocharger mixed-flow turbines”. In: *ImechE Conference Transactions from 7th International Conference on Turbochargers and Turbocharging, 14-15 May London UK*. 2002, pp. 45–59 (cit. on pp. 15, 126, 131, 158).
- [82] D. Palfreyman and RF Martinez-Botas. “The pulsating flow field in a mixed flow turbocharger turbine: An experimental and computational study”. In: *Journal of Turbomachinery* 127 (2005), p. 144 (cit. on pp. 24, 44, 127).
- [89] F. Payri, J. Galindo, J. R. Serrano, and M. A. Reyes-Belmonte. “Experimental methodology to a comprehensive characterization of automotive turbochargers”. In: *EAEC2011-A17*. Valencia, 2011 (cit. on pp. 16, 128).
- [90] F. Payri, J. R. Serrano, P. Fajardo, M. A. Reyes-Belmonte, and R. Gozalbo-Belles. “A physically based methodology to extrapolate performance maps of radial turbines”. In: *Energy Conversion and Management* 55 (2012), pp. 149–163 (cit. on pp. 126, 150).
- [93] F. Piscaglia, A. Onorati, S. Marelli, and M. Capobianco. “Unsteady Behavior in Turbocharger Turbines: Experimental Analysis and Numerical Simulation”. In: *Proceedings of the Eighth International Conference on Engines for automobiles*. SAE Paper 2007-24-0081. 2007 (cit. on p. 139).
- [97] S. Rajoo and R. Martinez-Botas. “Mixed flow turbine research: A Review”. In: *Journal of Turbomachinery* 130 (2008), p. 044001 (cit. on pp. 15, 126).

- [99] J. R. Serrano, F. J. Arnau, V. Dolz, A. Tiseira, and C. Cervelló. “A model of turbocharger radial turbines appropriate to be used in zero-and one-dimensional gas dynamics codes for internal combustion engines modelling”. In: *Energy Conversion and Management* 49.12 (2008), pp. 3729–3745 (cit. on pp. 4, 120, 141, 144, 149).
- [102] A. T. Simpson, S. W. T. Spence, and J. K. Watterson. “A comparison of the flow structures and losses within vaned and vaneless stators for radial turbines”. In: *Journal of Turbomachinery* 131 (2009), p. 031010 (cit. on pp. 14, 15, 23, 27, 44, 47, 129, 158).

Chapter 7

Conclusions and future works

Contents

7.1	Conclusions	158
7.2	Original contributions	165
7.3	Future works	167
	Chapter 7 Bibliography	170

7.1 Conclusions

OVER THE LAST YEARS, researchers have focused in trying to understand the fluid dynamic processes in turbomachinery. Several works have been performed in analyzing the flow behavior by means of computational fluid dynamics [31, 51, 53, 102]. Some of this works are performed under steady in-flow conditions [81, 57]. However, when the turbine is set on an engine, the turbine receives the pulsating flow coming from the cylinders [59, 52]. The research of the effect of pulsating flow in the behavior of radial turbines is being subject of study [12]. Nevertheless, this is the first thesis in CMT-Motores Térmicos in which its main core deals with computations in turbomachinery.

In the present thesis, a numerical characterization of a turbocharger variable geometry radial turbine has been performed. The final goal of the analysis is the understanding of the turbine behavior under pulsating engine-like conditions. In this last chapter the main ideas that have arisen during the work are summarized. Also, the accomplished achievements are outlined, highlighting the more relevant ones.

The work performed in this thesis can be divided in three parts related with the objectives established at the beginning of this document. The first one deals with the development of a methodology for characterizing a radial turbine by means of numerical computations. The second part is focused on the development and implementation of new boundary conditions for their use in CFD with the aim of reducing the computational cost. In the last part, the radial turbine is analyzed under unsteady flow pulsating conditions, these results are used to implement a turbine model to be used in engine modeling. In the following the methodology followed in each of the chapters and the main achievements are described.

7.1.1 Computational methodology: Case configuration

As it was stated in the objectives section 1.2, this is the first thesis in CMT-Motores Térmicos in which the main core has been the numerical characterization of turbomachinery. Therefore, the main objective has been the development of a methodology to characterize a radial turbine by means of CFD. An important effort has been done in optimizing the case configuration in order to obtain the best results as possible with the computational resources

available. Three different aspects have been considered and are going to be described in the following points: analysis of the mesh, solver configuration, and the experimental validation of the methodology.

7.1.1.1 Mesh analysis

The geometry used in the analysis is taken from a real variable geometry turbine. The use of a real geometry makes difficult the appropriate meshing of the domain. In this work a non-conformal mesh built using a mixed polyhedral and extruded-polygonal elements has been used. The computational domain composing the turbine was divided in different zones: volute, stator, rotor, and outlet section. Radial turbines are typically tested on test rigs which include long straight inlet and outlet straight ducts. Additionally, the boundary conditions are separated for the turbine, thus minimizing their influence in the solution. The ducts are not included in the mesh analysis and are meshed using a Cooper scheme.

Whenever a numerical simulation is performed to obtain the fluid dynamic behavior of a system a mesh independence analysis is required in order to prove that the solution does not depend of the cell size. Generally, the mesh independence analysis is performed by increasing the number of cells in the whole domain. It is clear that not all the regions of the domain have the same requisites in terms of the cell size and there are zones in which a smaller cell size could be more profitable than in other. This procedure gives an idea of the medium cell size needed, but it does not give any information about the proper cell distribution.

In this thesis, the idea of performing a local mesh independence analysis has been developed. This analysis gives an idea of the most adequate cell distribution. The analysis is performed in each one of the turbine sections separately, hence comes the name of the analysis. The cell size of a given zone is reduced and the current region is replaced in the new mesh, in which the remainder zones are taken from a reference case. A simulation is performed with this mesh and the refinement continues until the independence of the current region was achieved. The process continues with the following region.

The results of the mesh independence show that for the studied turbine the minimum cell size was needed in the stator and rotor sections, for those an average cell volume of 0.017 mm^3 was used. The total number of cells in

the domain were 2777122. The final distribution has 23.3% of the cells in the volute, 39.5% in the stator, 23.6% in the rotor, and 7.5% in the outlet section. Finally, the inlet duct represents 1.2% of the total amount of cells, while the outlet one has 4.9%.

7.1.1.2 Solver configuration

In this thesis the 3D CFD simulations have been performed using the commercial code ANSYS-FLUENT. Once the mesh has been defined, the different options in the case configuration should be assessed, since they influence on the results and computational time. The different CFD models used have been described. The viscous model, all the turbomachinery simulations have been performed using the $\kappa - \omega$ SST, which has proved to give good results in several works analyzed from the literature. A comparison of the two solver schemes, pressure based coupled solver (PBCS) and density based (DB) solver, has been performed. The two procedures give different results, but the relative error decreases as the number of cells in the mesh increases. The conclusion is that the differences in the results, if the mesh is adequate, does not justify the computational cost of using a DB solver time consumption.

One of the main topics of discussion when dealing with turbomachinery simulations is the rotor motion procedure. The two main models, multiple reference frame and sliding mesh, have been evaluated. The main advantage of the multiple reference frame is its low computational cost; this model gives a good approximation (about a 7% error in torque) if the operating point is close to the design conditions, thus it has been applied to obtain the characteristics curves of the turbine. However, if the transient effects as the rotor-stator interaction become more important, as it happens in off-design points, the error increases. To capture these effects a fully transient simulation with a rotating the mesh is required.

In the case of a transient simulation, two approaches can be followed concerning the temporal discretization: explicit or implicit formulation. Due to the cell size, the explicit formulation leads to a time-step size of the order of 10^{-9} seconds, which will make the simulation too long. Therefore an implicit formulation is proposed. The last analysis performed in terms of the case configuration, deals with the influence of the time step size on the solution. Finally, a time step size of $1.6576 \cdot 10^{-6}$ was selected, which corresponds to

200 time steps per rotor revolution.

7.1.1.3 Experimental validation

With the objective of validating the numerical methodology, some experimental data were acquired in a turbocharger test rig. A description of the experimental facility and the measurement sensors used was presented. The main difficulty found in this procedure was the correct setting of the stator angle. Since the analysis is performed in a variable geometry turbine, the stator angle can be varied. However the positioning mechanism has an important mechanical play, especially at low temperature, and thus to set the correct aperture is quite a challenge. In fact, it is known for gas-stand testing engineers that if measurement are taken setting the vanes at a given position, and then the facility is stopped and started again, the measured variables can differ.

Measurements have been taken at different nozzles apertures to analyze its influence in the behavior of the turbine. When the numerical results are compared with the experimental data, the curves obtained follow the same trend. Therefore the differences can be laid to a different stator position. As final comment it is convenient to remember than only global measurements were achievable with the experimental resources available, and therefore only a validation of the global turbine behavior was possible.

7.1.2 Developed boundary conditions

The calculation of a complex system usually requires including pipes or one dimensional elements in the computational domain. This is the case of the turbine installed on the engine or in the gas-stand. The calculation of these elements as 3D increases the computational cost. Following with the objective of reducing the computational cost, two boundary conditions based on the method of characteristics have been developed.

7.1.2.1 1D-3D Coupling boundary condition

The first boundary condition allows to perform a coupled 1D-3D simulation, thus reducing the computational time in the ducts but achieving a good geometric resolution (3D) where required. The boundary condition uses the method of characteristics for the exchange of information between the two domains. The boundary condition has been implemented in a 3D commercial code, with the difficulties inherent to this process due to the lack of accessibility of those kind of codes.

Two different cases have been used to validate the behavior of the boundary condition: a theoretical Sod's problem and a simulation based on the experimental test in an impulse test rig. The comparison shows that the 1D-3D boundary condition predicts properly the information transfer between the codes, although the 1D code does not account for dissipative flow effects. The reduction in the required computational resources is dependent on the relative sizes of the pipes and system meshes.

7.1.2.2 Anechoic boundary condition

The goal of the second boundary condition was to reproduce the behavior of an infinite duct without the need of connecting the 3D and 1D domains. In this frame, a new formulation of an anechoic condition based on the method of characteristics has been proposed and implemented for its use in ANSYS-FLUENT. The behavior of the boundary condition has been evaluated using a Sod's shock tube problem, showing better performances in non-homoeotropic flows than the non-reflecting conditions available in ANSYS-FLUENT. As second validation procedure, the boundary condition has been successfully applied to the acoustic characterization of an exhaust silencer. The numerical results obtained using the new implementation have been compared with that obtained using the former methodology and also with experimental measurements taken on an impulse test rig. For that particular application, the use of the anechoic condition allows to reduce the computational time in about a 67.5%.

7.1.2.3 Additional considerations and applications

The implemented boundary conditions were based on the assumption of 1D inviscid and adiabatic flow of a perfect gas. In order to be able to use them in a turbomachinery simulation, the influence of three real flow effects including non-perfect gas behavior, viscous flow and swirling flow, have been analyzed. Concerning non-perfect gas behavior a solution has been proposed, and it has been shown to improve significantly the performance of the non-reflecting BC. The implications of dealing with viscous flow have been investigated. The effect of wall friction can be introduced by means of a modification of the Riemann variables and a correlation for the friction factor. However, as it has been pointed out, when an incoming pressure waves passes through a given section, the infinite duct does send information backwards. This behavior can not be reliably reproduced using an anechoic end and the simulation of the 1D duct will be needed. One of the main characteristics of the flow at the outlet of a turbine is the existence of swirl, therefore this effect was evaluated. A procedure to obtain the transversal pressure profile has been developed assuming the flow to be in radial equilibrium.

The anechoic condition has been proved to give good results in inviscid flows or viscous flows with null main velocity in which the viscous effects are lower. Even though it has been stated that in high velocity viscous flows the BC does not behave as an long duct, a reduction of the reflections is achieved and thus it could still be used to reduce the time required to reach a periodic result in a transient simulation. If the duct needs to be reproduced, then a coupled 1D-3D simulation is required. Another possible application of the coupling BC is the calculation of the turbine mounted on engine using the 1D-3D connection, the methodology needed to perform this kind of computations have been described.

7.1.3 Pulsating flow

7.1.3.1 Analysis of pulsating flow

Radial turbines usually work set on an ICE, and therefore the internal flow at the turbine inlet is dominated by the pulses from the cylinders. Some work has been performed to characterize the turbine behavior under this operating conditions by analyzing the behavior of the different turbine components. The

analysis has been performed in terms of flow capacity versus total to static pressure ratio and power developed by the turbine.

If the mass flow at different sections is compared, it can be stated that most of the time-shift in mass-flow is due to the effect of the volute due to its shape and volume. When the flow capacity is presented versus the pressure ratio, a hysteretic cycle appear, presenting two different flow capacities for a given pressure ratio. The volute presents an important hysteretic behavior as the pulses amplitude and frequency increase. An additional unsteady behavior which reduces the peak-to-valley amplitude is found. This can be understood because of the not uniform flow along the volute outlet section.

A limited hysteretic behavior is found in the pulsating flow capacity of the nozzle section. The behavior is produced by various effects as the wave action (characteristic length) and mass accumulation, which, although they can be neglected when compared with those in the volute, still have some influence. Additionally, the *averaging effect* occurring at the volute outlet, reduces the amplitude of the transmitted pulse, thus making the wings of the flow capacity curve to shrink, not reaching the the equivalent steady values. Another effect that influences the hysteretic behavior is the detachment and reattachment process of the flow in the nozzle vanes and screws and other aerodynamic losses. These aerodynamic transient phenomena modify the flow angle at the stator outlet, and therefore the instantaneous effective area of the nozzle section.

Due to the smaller size of the impeller, the wave action and accumulation effects are even smaller than in volute and stator sections. Two images of the flow field with the same pressure ratio but in different positions in the pulse observing important difference in the velocity patterns at the inlet, while the flow in the outlet are similar. This explains the reduced hysteretic effect in the flow capacity. Nevertheless, the condition at the rotor inlet have a huge impact on the generated torque and therefore it does not correlate well with the instantaneous pressure ratio or corrected mass flow. On the contrary, torque correlates better with the impeller inflow conditions (velocity magnitude, blade speed ratio).

7.1.3.2 Turbine model

A simplified model for the turbine is proposed using the results of the pulsating simulations. The model would include a one-dimensional or quasi-two-dimensional element to represent the volute, a nozzle to represent the vaned stator, a small zero-dimensional element to represent the hysteresis in the stator, and a rotating channel in which rothalpy is conserved to represent the flow in the rotor.

As contribution to engine modeling in this thesis, a simplified model to simulate the behavior between the stator and rotor sections has been implemented. Although the implementation of the volute and outlet duct are not included in this simple model, they could be computed using a one-dimensional code. The performance of the stator and rotor model has been evaluated for a pulsating simulation, showing good agreement with the CFD results. The proposed model, due to the physically-based formulation, just needs information from one steady point obtained from a CFD computation.

7.2 Original contributions

Since this is the first thesis in CMT-Motores Térmicos in which the main core is the numerical simulation of turbomachinery, the main objective has been the development of a methodology to perform numerical simulations of radial turbomachinery. In this section, the main contribution and results of the thesis are highlighted.

- A local mesh independence procedure has been developed. Generally, the independence analysis is performed globally in the whole domain and does not give information about the most adequate cells distribution. The new procedure allows to evaluate the distribution in the different turbine components, namely: volute, stator, rotor and outlet section.
- Concerning the case configuration, a controversial point is the approach followed to reproduce the impeller motion. In this work, simulations using the multiple reference frame, in which the mesh is not actually moved, and the sliding mesh approach have been compared. The results show that the relative error between the two approaches is relatively

low (about a 7 % in torque) for cases in the design operating region. However if off-design points are considered, this error increases and the use of a fully transient simulation, including mesh motion, is required. Experimental measurements taken in a turbocharger gas-stand are used to evaluate the results from steady numerical simulation,

- A coupling 1D-3D boundary condition has been developed. The implementation of the boundary condition has been done in a commercial code with the difficulties that this arises. The transfer of information of the developed BC ANSYS-FLUENT works better than the built-in ANSYS-FLUENT-GT Power. The use of the coupling BC could reduce the computational cost of a system in which an important part of the domain can be simulated using a 1D approximation. Additionally, taking advantage of a 1D code as OpenWAM to simulate a whole engine, the turbine can be simulated in real conditions as set on an engine.
- A new formulation for an anechoic BC has been developed. The intention of the anechoic end is to behave as a long duct. The boundary condition was implemented in ANSYS-FLUENT and has shown to have better performances than the built-in non-reflecting boundary conditions of ANSYS-FLUENT in non-homoeotropic cases. The performance of the new anechoic condition has been compared with the one previously used in CMT-Motores Térmicos, showing better results.
- The effect of non-perfect gas and swirling flow have been evaluated and a solution is proposed to accurately reproduce their effect. However, the anechoic condition does not represent the behavior of a long duct if viscous flow is considered and the simulation of the duct will be required. The BC could still be used to reduce the reflection of the pressure waves at the boundary and thus facilitate the convergence of a transient case.
- Pulsating simulations have been performed to analyze the behavior of the turbine in engine-like conditions. In this thesis the use of CFD allows to evaluate the performance of each of the turbine components in a separate way. This procedure allows to evaluate the relative importance of the pulsating effects and in this way contribute to model them. The pulsating analysis has shown that most of the time-shift occurred is due to the wave propagation and accumulation effects in the volute. A limited hysteretic loop is found in the stator nozzles. In the case of the impeller no hysteresis is found concerning flow capacity. The generated

torque presents a loop as a function of the pressure ratio or corrected mass flow, but disappear of it is plotted against the conditions at the rotor inlet. These facts have been analyzed from images of the flow field.

- A enhanced model for the stator and rotor section has been proposed. The model is more physically based than the previously used ones, for example the rotor passages are now modeled as rotating channel, which leads to require less information as input to perform the calculation. The new model is particularly suitable for simulating the turbine in pulsating conditions.

The main scientific results of the thesis have been published or accepted for publication in [46, 115, 45] or are being considered for publication as [40].

7.3 Future works

From the developments of the present thesis a series of task on the extension and improvement of the current thesis are presented. Those works can be classified in different topics:

1. Experimental measurement techniques. Although the present thesis did not deal with experimental work. In chapter 2 some measurements were used as validation of the numerical methodology. However, with the techniques that are currently in use in CMT-Motores Térmicos only a global validation was possible. Therefore, an advance in the measurement techniques used to allow local measurements of the flow variables would be interesting. An example could be the use of Kulites as local pressure sensor for the internal flow in a turbomachine. Also the correct positioning of the stator aperture system should be assessed.
2. Simulation of the turbine set on engine. In chapter 5, the application of the coupling boundary condition to connect the 3D turbine model with the OpenWAM code was described. Since OpenWAM is capable of simulating a whole engine, a coupled simulation computing the turbine as set on engine was proposed. The main difficulties rely on the initialization of the OpenWAM domains and the computational time required.

3. Pulsating analysis. In this thesis the analysis of three different pulse frequencies (50, 90, and 130 Hz.) and two amplitudes (90-190 kPa and 50-230 kPa). However, some simulations are being performed to analyze the effect of the stator aperture and the impeller rotational speed, and their analysis is kept as future work.
4. The frequencies considered in the current analysis were selected to match the dominant frequency at the outlet of an internal combustion engine at three typical rotational speeds. However only the first harmonic has been considered. Therefore, two different approaches are proposed: simulating higher frequency pulse to analyze its behavior or directly imposing a real pulse which excite a wider range of frequencies. Additionally, the simulation of the kind of experimental pulses used when a turbine is tested on a test-bench could be interesting since it could allow to compare with the experimental measurements.
5. The stator and rotor model implemented in this thesis has been proved to have good performance under pulsating conditions. However, this model should be enhance with additional submodels as the representation of the volute and the outlet section of the turbine. One these submodels are implemented, the model will acquire a predictive behavior, just requiring the pressure pulse at the inlet and not at the outlet. For the volute, a quasi-2D model of the volute where the tangential and radial components are calculated imposing conservation of angular momentum is proposed.

Chapter Bibliography 7

- [12] N.C. Baines. “Turbocharger turbine pulse flow performance and modelling - 25 years on”. In: *Proceedings of the 9th Conference Turbochargers and Turbocharging*. 2010, pp. 347–362 (cit. on pp. 126, 158).
- [31] G. Decombes, J. F. Pichouron, F. Maroteaux, N. Moreno, and J. Julien. “Simulation of the performance of a variable geometry turbocharger for Diesel engine road propulsion”. In: *International Journal of Thermodynamics* 5.3 (2010), pp. 139–149 (cit. on pp. 14, 158).
- [40] J. Galindo, P. Fajardo, R. Navarro, and L. M. García-Cuevas. “Characterization of a radial turbocharger turbine in pulsating flow by means of CFD and its application to engine modeling”. In: *Preprint submitted*

- to *Applied Energy* (Date of submission 01/03/2012) (cit. on pp. 126, 167).
- [45] J. Galindo, A. Tiseira, P. Fajardo, and R. Navarro. “Analysis of the influence of different real flow effects on computational fluid dynamics boundary conditions based on the method of characteristics”. In: *Mathematical and Computer Modelling* Published online (2012). cited By (since 1996) 0; Article in Press. URL: <http://www.scopus.com/inward/record.url?eid=2-s2.0-84857202860&partnerID=40&md5=d266cfaf6a34fe6010607ad916e6bdd2> (cit. on pp. 108, 167).
- [46] J. Galindo, A. Tiseira, P. Fajardo, and R. Navarro. “Coupling methodology of 1D finite difference and 3D finite volume CFD codes based on the Method of Characteristics”. In: *Mathematical and Computer Modelling* 54.7-8 (2011), pp. 1738–1746. DOI: <http://dx.doi.org/10.1016/j.mcm.2010.11.078> (cit. on pp. 6, 15, 62, 81, 88, 93, 112, 118, 167).
- [51] F. Hellstrom and L. Fuchs. “Effects of inlet conditions on the turbine performance of a radial turbine”. In: *PROCEEDINGS OF THE ASME TURBO EXPO 2008: Power for Land, Sea and Air*. Berlin: New York: AMER SOC MECHANICAL ENGINEERS, 2008 (cit. on pp. 14, 15, 47, 158).
- [52] F. Hellstrom and L. Fuchs. “Numerical Computation of the Pulsatile Flow in a Turbocharger With Realistic Inflow Conditions From an Exhaust Manifold”. In: *Proceedings of ASME Turbo Expo 2009: Power for Land, Sea and Air*. GT2009-5961. ASME. 2009 (cit. on pp. 44, 126, 158).
- [53] H. Hiereth and P. Prenninger. *Charging the internal combustion engine*. Ed. by SpringerWienNewYork. Springer Verlag, 2007 (cit. on pp. 14, 158).
- [57] T. Kawakubo. “Unsteady Rotor-Stator Interaction of a Radial-Inflow Turbine With Variable Nozzle Vanes”. In: *Proceedings of ASME Turbo Expo 2010: Power for Land, Sea and Air*. ASME. 2010 (cit. on pp. 44, 126, 129, 158).
- [59] J. K. W. Lam, Q. D. H. Roberts, and G. T. McDonnell. “Flow modelling of a turbocharger turbine under pulsating flow”. In: *ImechE Conference Transactions from 7th International Conference on Turbochargers and Turbocharging*. 2002, pp. 14–15 (cit. on pp. 24, 44, 126, 158).

- [81] D. Palfreyman, R. F. Martinez-Botas, and N. Karamanis. “Computational and experimental investigation of the aerodynamics of turbocharger mixed-flow turbines”. In: *ImechE Conference Transactions from 7th International Conference on Turbochargers and Turbocharging, 14-15 May London UK*. 2002, pp. 45–59 (cit. on pp. 15, 126, 131, 158).
- [102] A. T. Simpson, S. W. T. Spence, and J. K. Watterson. “A comparison of the flow structures and losses within vaned and vaneless stators for radial turbines”. In: *Journal of Turbomachinery* 131 (2009), p. 031010 (cit. on pp. 14, 15, 23, 27, 44, 47, 129, 158).
- [115] A. J. Torregrosa, P. Fajardo, A. Gil, and R. Navarro. “Development of a non-reflecting boundary condition for its application in 3D computational fluid dynamic codes”. In: *Engineering Applications of Computational Fluid Mechanics* (Accepted for publication 16/04/2012) (cit. on pp. 80, 108, 110, 120, 167).

Global bibliography

- [1] M. Abidat, M. K. Hamidou, M. Hachemi, and M. Hamel. “Design and flow analysis of radial and mixed flow turbine volutes”. In: *European Conference on Computational Fluid Dynamics*. 2006 (cit. on p. 14).
- [2] J. Andersen, E. Karlsson, and A. Gawell. “Variable turbine geometry on SI engines”. In: *SAE 2006 World Congress*. SAE 2006-01-0020. 2006 (cit. on pp. 3, 16).
- [3] ANSYS Inc. *Ansys Fluent 12.0 User’s Guide*. Canonsburg, PA 15317, 2009 (cit. on pp. 24, 27, 28, 47, 83, 85).
- [4] ANSYS Inc. *ANSYS FLUENT Theory Guide*. 2011 (cit. on pp. 17, 40, 41, 46).
- [5] E. Arcaklioglu and I. Çelikten. “A diesel engine’s performance and exhaust emissions”. In: *Applied Energy* 80.1 (2005), pp. 11–22 (cit. on p. 2).
- [6] A. Arnone and R. Pacciani. “Rotor-stator interaction analysis using the Navier–Stokes equations and a multigrid method”. In: *Journal of Turbomachinery* 118 (1996), p. 679 (cit. on p. 14).
- [7] O. V. Atassi. “Nonreflecting boundary conditions for the time-dependent convective wave equation in a duct”. In: *Journal of Computational Physics* 197.2 (2004), pp. 737–758. ISSN: 0021-9991 (cit. on pp. 6, 81, 108).
- [8] R. Aymanns, J. Scharf, T. Uhlmann, and D. Lückmann. “A revision of Quasi Steady Modelling of Turbocharger Turbines in the Simulation of Pulse Charged Engines”. In: *16th SUPERCHARGING CONFERENCE*. 2011 (cit. on pp. 127, 128, 133, 137).

- [9] N. C. Baines. “A meanline prediction method for radial turbine efficiency”. In: *6th International Conference on Turbocharging and Air Management Systems, I Mech E*. C554-6. Concepts ETI, Inc. Institution of Mechanical Engineers, 1998 (cit. on p. 3).
- [10] N. C. Baines. “Radial Turbines - An Integrated Design Approach”. In: *6th European Conference on Turbomachinery - Fluid Dynamics and Thermodynamics*. Lille, France, 2005 (cit. on p. 15).
- [11] N. C. Baines, G. B. Ingénieur-mécanicien, N. C. Baines, and N. C. Baines. *Fundamentals of turbocharging*. Ed. by Concepts NREC. Concepts NREC, 2005 (cit. on p. 14).
- [12] N.C. Baines. “Turbocharger turbine pulse flow performance and modelling - 25 years on”. In: *Proceedings of the 9th Conference Turbochargers and Turbocharging*. 2010, pp. 347–362 (cit. on pp. 126, 158).
- [13] R. S. Benson, R. D. Garg, and D. Woollatt. “A numerical solution of unsteady flow problems”. In: *International Journal of Mechanical Sciences* 6.1 (1964), pp. 117–144. DOI: 10.1016/0020-7403(64)90009-8 (cit. on pp. 68, 87, 109).
- [14] R. S. Benson, J. H. Horlock, and D. E. Winterbone. *The thermodynamics and gas dynamics of internal combustion engines*. Ed. by Oxford University Press. Vol. 1. Oxford University Press, 1982 (cit. on pp. 68, 89, 109).
- [15] V. Bermúdez, J. R. Serrano, P. Piqueras, and O. García-Afonso. “Assessment by means of gas dynamic modelling of a pre-turbo diesel particulate filter configuration in a turbocharged HSDI diesel engine under full-load transient operation”. In: *Proceedings of the Institution of Mechanical Engineers, Part D, Journal of Automobile Engineering* 225.9 (2011), pp. 1134–1155 (cit. on p. 93).
- [16] E. Blanco-Marigorta, J. Fernández-Francos, J. González-Pérez, and C. Santolaria-Morros. “Numerical flow simulation in a centrifugal pump with impeller-volute interaction”. In: *ASME 2000 Fluids Engineering Division Summer Meeting*. 2000, pp. 1–6 (cit. on p. 15).
- [17] C. Bogey and C. Bailly. “Three-dimensional non-reflective boundary conditions for acoustic simulations: far field formulation and validation test cases”. In: *Acta Acustica united with Acustica* 88 (2002), pp. 463–471. ISSN: 1436-7947 (cit. on p. 81).

- [18] D. Bohn, T. Heuer, and K. Kusterer. “Conjugate flow and heat transfer investigation of a turbo charger”. In: *Journal of engineering for gas turbines and power* 127 (2005), p. 663 (cit. on p. 23).
- [19] F. Bozza, V. De Bellis, S. Marelli, and M. Capobianco. “1D Simulation and experimental analysis of a turbocharger compressor for automotive engines under unsteady flow conditions”. In: *SAE Paper* 4.2011-01-1147 (2011), pp. 1365–1384. DOI: 10.4271/2011-01-1147 (cit. on p. 140).
- [20] A. Broatch, X. Margot, A. Gil, and F. D. Denia. “A CFD Approach to the Computation of the Acoustic Response of Exhaust Mufflers”. In: *Journal of Computational Acoustic* 13.2 (2005), pp. 301–316. DOI: 10.1142/S0218396X05002682 (cit. on pp. 3, 6, 72, 80, 95, 97).
- [21] M. Brück, B. Michaelis, M. Awasthi, and R. Reinelt. “1D/3D-Coupling GT-POWER/FLUENT to Predict Species Transport in Exhaust Oxygen Sensors at Engine Operating Conditions”. In: *European Automotive CFD Conference*. 2007 (cit. on p. 64).
- [22] M. Capobianco and A. Gambarotta. “Unsteady flow performance of turbocharger radial turbines”. In: *C405/017, Proceeding of the Institute of Mechanical Engineers, Fourth International Conference, Turbocharging and Turbochargers*. 1990, pp. 123–132 (cit. on p. 126).
- [23] M. Capobianco and S. Marelli. “Waste-gate turbocharging control in automotive SI engines: effect on steady and unsteady turbine performance”. In: *14th Asia Pacific Automotive Engineering Conference*. 2007, pp. 01–3543 (cit. on p. 128).
- [24] C. Cervelló. “Contribución a la Caracterización Experimental y al Modelado de Turbinas de Geometría Variable en Grupos de Sobrealimentación”. PhD thesis. Tesis Doctoral UPV, 2005 (cit. on p. 17).
- [25] H. Chen. “Turbine wheel design for Garrett advanced variable geometry turbines for commercial vehicle applications”. In: *8th International Conference on Turbochargers and Turbocharging, Institution of Mechanical Engineers*. 2006 (cit. on pp. 3, 16).
- [26] C. D. Copeland, R. Martinez-Botas, and M. Seiler. “Comparison Between Steady and Unsteady Double-Entry Turbine Performance Using the Quasi-Steady Assumption”. In: *Journal of Turbomachinery* 133 (2011), pp. 031001–1/031001–10 (cit. on pp. 2, 126, 130).

- [27] A. Costall and R.F. Martinez-Botas. “Fundamental characterization of turbocharger turbine unsteady flow behavior”. In: *Proceedings of the ASME Turbo Expo*. GT-2007-28317. 2007 (cit. on p. 129).
- [28] J. Dai, N. Ijichi, H. Tange, H. Shibata, H. Tamaki, and S. Yamaguchi. “Comparison of internal flow field between experiment and computation in a radial turbine impeller”. In: *JSME International Journal Series B* 47.1 (2004), pp. 48–56 (cit. on p. 15).
- [29] J. R. Dea, F. X. Giraldo, and B. Neta. “High-order non-reflecting boundary conditions for the linearized 2-D Euler equations: No mean flow case”. In: *Wave Motion* 46.3 (2009), pp. 210–220 (cit. on pp. 6, 81, 108).
- [30] J. W. Deardorff. “A numerical study of three-dimensional turbulent channel flow at large Reynolds numbers”. In: *Journal of Fluid Mechanics* 41.02 (1970), pp. 453–480 (cit. on p. 25).
- [31] G. Decombes, J. F. Pichouron, F. Maroteaux, N. Moreno, and J. Julien. “Simulation of the performance of a variable geometry turbocharger for Diesel engine road propulsion”. In: *International Journal of Thermodynamics* 5.3 (2010), pp. 139–149 (cit. on pp. 14, 158).
- [32] F. D. Denia, J. Albelda, F. J. Fuenmayor, and A. J. Torregrosa. “Acoustic behaviour of elliptical chamber mufflers”. In: *Journal of Sound and Vibration* 241.3 (2001), pp. 401–421. ISSN: 0022-460X (cit. on p. 95).
- [33] S. L. Dixon and C. Hall. *Fluid mechanics and thermodynamics of turbomachinery*. Butterworth-Heinemann, 2010 (cit. on pp. 114, 144).
- [34] L. W. Dorodnicyn. “Artificial Boundary Conditions for High-Accuracy Aeroacoustic Algorithms”. In: *SIAM Journal on Scientific Computing* 32.4 (2010), pp. 1950–1979 (cit. on p. 81).
- [35] A. M. Elfaghi, W. Asrar, and A. A. Omar. “Higher order compact-flowfield dependent variation (HOC-FDV) solution of one-dimensional problems”. In: *Engineering Applications of Computational Fluid Mechanics* 4.3 (2010), pp. 434–440 (cit. on p. 84).
- [36] B. Engquist and A. Majda. “Absorbing Boundary Conditions for the Numerical Evaluation of Waves”. In: *Math. of Comp.* 31.139 (1977), pp. 629–651 (cit. on p. 81).

- [37] T. Esch and FR Menter. “Heat transfer predictions based on two-equation turbulence models with advanced wall treatment”. In: *Proceedings of the 4th international symposium on turbulence, heat & mass transfer, Antalya, Turkey*. 2003, pp. 614–621 (cit. on p. 28).
- [38] FLUENT. *FLUENT 6.3 Validation Guide*. 2006 (cit. on pp. 27, 40).
- [39] *Fluent 6.3 Getting Started Guide*. Fluent Inc. 2006 (cit. on p. 110).
- [40] J. Galindo, P. Fajardo, R. Navarro, and L. M. García-Cuevas. “Characterization of a radial turbocharger turbine in pulsating flow by means of CFD and its application to engine modeling”. In: *Preprint submitted to Applied Energy* (Date of submission 01/03/2012) (cit. on pp. 126, 167).
- [41] J. Galindo, J. R. Serrano, F. J. Arnau, and P. Piqueras. “Description of a Semi-Independent Time Discretization Methodology for a One-Dimensional Gas Dynamics Model”. In: *Journal of Engineering for Gas Turbines and Power* 131 (2009), p. 034504. DOI: 10.1115/1.2983015 (cit. on pp. 64, 69, 98).
- [42] J. Galindo, J. R. Serrano, F. J. Arnau, and P. Piqueras. “High-frequency response of a calculation methodology for gas dynamics based on Independent Time Discretisation”. In: *Mathematical and Computer Modelling* 50.5-6 (2009), pp. 812–822. DOI: 10.1016/j.mcm.2009.05.011 (cit. on pp. 64, 69).
- [43] J. Galindo, J. R. Serrano, C. Guardiola, and C. Cervelló. “Surge limit definition in a specific test bench for the characterization of automotive turbochargers”. In: *Experimental thermal and fluid science* 30.5 (2006), pp. 449–462 (cit. on p. 14).
- [44] J. Galindo, JR Serrano, H. Climent, and A. Tiseira. “Experiments and modelling of surge in small centrifugal compressor for automotive engines”. In: *Experimental Thermal and Fluid Science* 32.3 (2008), pp. 818–826 (cit. on p. 4).
- [45] J. Galindo, A. Tiseira, P. Fajardo, and R. Navarro. “Analysis of the influence of different real flow effects on computational fluid dynamics boundary conditions based on the method of characteristics”. In: *Mathematical and Computer Modelling* Published online (2012). cited By (since 1996) 0; Article in Press. URL: <http://www.scopus.com/inward/record.url?eid=2-s2.0-84857202860&partnerID=40&md5=d266cfaf6a34fe6010607ad916e6bdd2> (cit. on pp. 108, 167).

- [46] J. Galindo, A. Tiseira, P. Fajardo, and R. Navarro. “Coupling methodology of 1D finite difference and 3D finite volume CFD codes based on the Method of Characteristics”. In: *Mathematical and Computer Modelling* 54.7-8 (2011), pp. 1738–1746. DOI: <http://dx.doi.org/10.1016/j.mcm.2010.11.078> (cit. on pp. 6, 15, 62, 81, 88, 93, 112, 118, 167).
- [47] D. Givoli. “High-order local non-reflecting boundary conditions: a review”. In: *Wave Motion* 39.4 (2004), pp. 319–326 (cit. on p. 81).
- [48] G. Guderley. *Nonstationary gas flow in thin pipes of variable cross section*. Tech. rep. Washington: NASA Technical Memorandum N.1196, 1948 (cit. on p. 108).
- [49] S. I. Hagstrom T. & Hariharan. “Accurate Boundary Conditions for Exterior Problems in Gas Dynamics”. In: *Mathematics of Computation* 51.184 (1988), pp. 581–597 (cit. on p. 81).
- [50] F. Hellström. “Numerical computations of the unsteady flow in turbochargers”. PhD thesis. Royal Institute of Technology KTH Mechanics, 2010 (cit. on pp. 25, 129).
- [51] F. Hellstrom and L. Fuchs. “Effects of inlet conditions on the turbine performance of a radial turbine”. In: *PROCEEDINGS OF THE ASME TURBO EXPO 2008: Power for Land, Sea and Air*. Berlin: New York: AMER SOC MECHANICAL ENGINEERS, 2008 (cit. on pp. 14, 15, 47, 158).
- [52] F. Hellstrom and L. Fuchs. “Numerical Computation of the Pulsatile Flow in a Turbocharger With Realistic Inflow Conditions From an Exhaust Manifold”. In: *Proceedings of ASME Turbo Expo 2009: Power for Land, Sea and Air*. GT2009-5961. ASME. 2009 (cit. on pp. 44, 126, 158).
- [53] H. Hiereth and P. Prenninger. *Charging the internal combustion engine*. Ed. by SpringerWienNewYork. Springer Verlag, 2007 (cit. on pp. 14, 158).
- [54] K. Hillewaert and RA Van den Braembussche. “Numerical simulation of impeller–volute interaction in centrifugal compressors”. In: *Journal of Turbomachinery* 121 (1999), p. 603 (cit. on p. 24).
- [55] D. Japikse and N. C. Baines. *Introduction to turbomachinery*. Ed. by Oxford University Press. Concepts Eti, 1997 (cit. on p. 14).

- [56] WP Jones and B.E. Launder. “The prediction of laminarization with a two-equation model of turbulence”. In: *International Journal of Heat and Mass Transfer* 15.2 (1972), pp. 301–314 (cit. on p. 26).
- [57] T. Kawakubo. “Unsteady Rotor-Stator Interaction of a Radial-Inflow Turbine With Variable Nozzle Vanes”. In: *Proceedings of ASME Turbo Expo 2010: Power for Land, Sea and Air*. ASME. 2010 (cit. on pp. 44, 126, 129, 158).
- [58] T. Kreuz-Ihli, D. Filsinger, A. Schulz, and S. Wittig. “Numerical and experimental study of unsteady flow field and vibration in radial inflow turbines”. In: *Journal of Turbomachinery* 122 (2000), pp. 247–254 (cit. on pp. 15, 47).
- [59] J. K. W. Lam, Q. D. H. Roberts, and G. T. McDonnell. “Flow modelling of a turbocharger turbine under pulsating flow”. In: *ImechE Conference Transactions from 7th International Conference on Turbochargers and Turbocharging*. 2002, pp. 14–15 (cit. on pp. 24, 44, 126, 158).
- [60] K. S. Lee, K. Y. Kim, and A. Samad. “Design optimization of low-speed axial flow fan blade with three-dimensional RANS analysis”. In: *Journal of mechanical science and technology* 22.10 (2008), pp. 1864–1869 (cit. on p. 27).
- [61] H. Li. “Fluid flow analysis of a single-stage centrifugal fan with a ported diffuser”. In: *Engineering Applications of Computational Fluid Mechanics* 3 (2009), pp. 147–163 (cit. on p. 28).
- [62] J. M. Lindquist, B. Neta, and F. X. Giraldo. “A spectral element solution of the Klein-Gordon equation with high-order treatment of time and non-reflecting boundary”. In: *Wave Motion* 47.5 (2010), pp. 289–298 (cit. on p. 81).
- [63] Q. Liu and O. V. Vasilyev. “Nonreflecting boundary conditions based on nonlinear multidimensional characteristics”. In: *International Journal for Numerical Methods in Fluids* 62.1 (2010), pp. 24–55. ISSN: 1097-0363 (cit. on p. 81).
- [64] Z. Liu and D.L. Hill. “Issues surrounding multiple frames of reference models for turbo compressor applications”. In: *Fifteenth International Compressor Engineering Conference*. Purdue University. 2000 (cit. on pp. 24, 44, 127, 129).

- [65] J. M. Luján, V. Bermúdez, J. R. Serrano, and C. Cervelló. “Test bench for turbocharger groups characterization”. In: *SAE Paper* 2002-01-0163 (2002) (cit. on pp. 21, 82).
- [66] S. Marelli and M. Capobianco. “Steady and pulsating flow efficiency of a waste-gated turbocharger radial flow turbine for automotive application”. In: *Energy* 36 (2011), pp. 459–465. ISSN: 0360-5442 (cit. on pp. 126, 129, 130, 132).
- [67] F. R. Menter. “Two-equation eddy-viscosity turbulence models for engineering applications”. In: *AIAA journal* 32.8 (1994), pp. 1598–1605 (cit. on p. 26).
- [68] F. R. Menter, M. Kuntz, and R. Langtry. “Ten years of industrial experience with the SST turbulence model”. In: *Turbulence, heat and mass transfer* 4 (2003), pp. 625–632 (cit. on p. 27).
- [69] F. R. Menter, R. Langtry, and T. Hansen. “CFD simulation of turbomachinery flows—verification, validation and modeling”. In: *European Congress on Computational Methods in Applied Sciences and Engineering, ECCOMAS*. 2004 (cit. on p. 27).
- [70] FR Menter. “Influence of freestream values on k-omega turbulence model predictions”. In: *AIAA journal* 30 (1992), pp. 1657–1659 (cit. on p. 26).
- [71] K. Mollenhauer and H. Tschoeke. *Handbook of Diesel Engines*. Springer, 2010 (cit. on p. 2).
- [72] G. Montenegro and A. Onorati. “Modeling of Silencers for IC Engine Intake and Exhaust Systems by Means of an Integrated 1D-multiD Approach”. In: *SAE International Journal of Engines* 1.1 (2009), p. 466. DOI: 10.4271/2008-01-0677 (cit. on pp. 3, 62, 80).
- [73] G. Montenegro, A. Onorati, F. Piscaglia, and G. D’Errico. *Integrated 1D-Multi-D Fluid Dynamic Models for the Simulation of ICE Intake and Exhaust Systems*. Tech. rep. 2007-01-0495. SAE Technical Paper Series, 2007. DOI: 10.4271/2007-01-0495 (cit. on p. 62).
- [74] J. A. Moríñigo and J. J. Salvá. “Robust non-reflecting boundary conditions for the simulation of rocket nozzle flow”. In: *Aerospace Science and Technology* 14 (2010), pp. 429–441. ISSN: 1270-9638 (cit. on p. 81).
- [75] H. Moustapha, M. F. Zelesky, N. C. Baines, and D. Japikse. *Axial and radial turbines*. Concepts NREC, 2003 (cit. on p. 145).

- [76] G. F. Mucklow and A. J. Wilson. “Wave-action in gases: the attenuation and reflection of compression waves propagated in pipes”. In: *Proc. I. Mech. Eng.* 1955, pp. 69–80 (cit. on p. 83).
- [77] M. L. Munjal. *Acoustics of ducts and mufflers with application to exhaust and ventilation system design*. Wiley-Interscience, 1987. ISBN: 0471847380 (cit. on pp. 3, 95).
- [78] A. Onorati, G. Montenegro, and G. D’Errico. *Prediction of the Attenuation Characteristics of IC Engine Silencers by 1-D and Multi-D Simulation Models*. Tech. rep. 2006-01-1541. SAE Technical Paper Series, 2006. DOI: 10.4271/2006-01-1541 (cit. on pp. 62, 64, 81).
- [79] OpenWAM. CMT- Motores Térmicos. Universidad Politécnica de Valencia. URL: <http://www.OpenWAM.org> (cit. on pp. 4, 14, 63, 87, 98).
- [80] M.H. Padzillah, Rajoo S., and Martinez-Botas R.F. “Numerical Assessment of Unsteady Flow Effects on a Nozzled Turbocharger Turbine”. In: *Proceedings of ASME Turbo Expo 2012*. GT2012-69062. 2012 (cit. on p. 47).
- [81] D. Palfreyman, R. F. Martinez-Botas, and N. Karamanis. “Computational and experimental investigation of the aerodynamics of turbocharger mixed-flow turbines”. In: *ImechE Conference Transactions from 7th International Conference on Turbochargers and Turbocharging, 14-15 May London UK*. 2002, pp. 45–59 (cit. on pp. 15, 126, 131, 158).
- [82] D. Palfreyman and RF Martinez-Botas. “The pulsating flow field in a mixed flow turbocharger turbine: An experimental and computational study”. In: *Journal of Turbomachinery* 127 (2005), p. 144 (cit. on pp. 24, 44, 127).
- [83] S.V. Patankar. *Numerical heat transfer and fluid flow*. Hemisphere Pub, 1980 (cit. on p. 46).
- [84] A. R. Patil, P. R. Sajjanpawar, and V. V. Masurekar. *Acoustic Three-Dimensional Finite Element Analysis of a Muffler*. Tech. rep. 960189. SAE Technical Paper Series, 1996 (cit. on p. 80).
- [85] F. Payri and J. M. Desantes, eds. *Motores de combustión interna alternativos*. Reverté, 2011 (cit. on p. 2).

- [86] F. Payri, J. M. Desantes, and A. Broatch. “Modified impulse method for the measurement of the frequency response of acoustic filters to weakly nonlinear transient excitations”. In: *The Journal of the Acoustical Society of America* 107 (2000), p. 731 (cit. on pp. 82, 95).
- [87] F. Payri, J. M. Desantes, and A. J. Torregrosa. “Acoustic boundary condition for unsteady one-dimensional flow calculations”. In: *Journal of Sound and Vibration* 188.1 (1995), pp. 85–110. ISSN: 0022-460X (cit. on pp. 6, 15, 83, 87, 108).
- [88] F. Payri, J. Galindo, J. R. Serrano, and F. J. Arnau. “Analysis of numerical methods to solve one-dimensional fluid-dynamic governing equations under impulsive flow in tapered ducts”. In: *International Journal of Mechanical Sciences* 46.7 (2004), pp. 981–1004 (cit. on pp. 14, 72).
- [89] F. Payri, J. Galindo, J. R. Serrano, and M. A. Reyes-Belmonte. “Experimental methodology to a comprehensive characterization of automotive turbochargers”. In: *EAEC2011-A17*. Valencia, 2011 (cit. on pp. 16, 128).
- [90] F. Payri, J. R. Serrano, P. Fajardo, M. A. Reyes-Belmonte, and R. Gozalbo-Belles. “A physically based methodology to extrapolate performance maps of radial turbines”. In: *Energy Conversion and Management* 55 (2012), pp. 149–163 (cit. on pp. 126, 150).
- [91] K. S. Peat, A. J. Torregrosa, A. Broatch, and T. Fernández. “An investigation into the passive acoustic effect of the turbine in an automotive turbocharger”. In: *Journal of Sound and Vibration* 295.1-2 (2006), pp. 60–75 (cit. on p. 3).
- [92] R. Pecnik, J. A. S. Witteveen, and G. Iaccarino. “Uncertainty quantification for laminar-turbulent transition prediction in RANS turbomachinery applications”. In: *49th AIAA Aerospace Sciences Meeting including the New Horizons Forum and Aerospace Exposition*. AIAA 2011-660. 2011 (cit. on p. 27).
- [93] F. Piscaglia, A. Onorati, S. Marelli, and M. Capobianco. “Unsteady Behavior in Turbocharger Turbines: Experimental Analysis and Numerical Simulation”. In: *Proceedings of the Eighth International Conference on Engines for automobiles*. SAE Paper 2007-24-0081. 2007 (cit. on p. 139).

- [94] T. J. Poinso and S. K. Lele. “Boundary conditions for direct simulations of compressible viscous flows”. In: *Journal of Computational Physics* 101.1 (1992), pp. 104–129 (cit. on p. 84).
- [95] A. Qamar, N. Hasan, and S. Sanghi. “A new spatial discretization strategy of the convective flux term for the hyperbolic conservation laws”. In: *Engineering Applications of Computational Fluid Mechanics* 4.4 (2010), pp. 593–611 (cit. on p. 84).
- [96] S. Rajoo and R. M. Botas. “Variable geometry mixed flow turbine for turbochargers: an experimental study”. In: *International Journal of Fluid Machinery and Systems* 1.1 (2008), pp. 155–168 (cit. on p. 14).
- [97] S. Rajoo and R. Martinez-Botas. “Mixed flow turbine research: A Review”. In: *Journal of Turbomachinery* 130 (2008), p. 044001 (cit. on pp. 15, 126).
- [98] L. Selle, F. Nicoud, and T. Poinso. “Actual impedance of non-reflecting boundary conditions: implications for computation of resonators”. In: *AIAA journal* 42.5 (2004), pp. 958–964 (cit. on p. 84).
- [99] J. R. Serrano, F. J. Arnau, V. Dolz, A. Tiseira, and C. Cervelló. “A model of turbocharger radial turbines appropriate to be used in zero-and one-dimensional gas dynamics codes for internal combustion engines modelling”. In: *Energy Conversion and Management* 49.12 (2008), pp. 3729–3745 (cit. on pp. 4, 120, 141, 144, 149).
- [100] J. R. Serrano, F. J. Arnau, P. Piqueras, A. Onorati, and G. Montenegro. “1D gas dynamic modelling of mass conservation in engine duct systems with thermal contact discontinuities”. In: *Mathematical and Computer Modelling* 49.5-6 (2009), pp. 1078–1088. DOI: 10.1016/j.mcm.2008.03.015 (cit. on pp. 2, 64, 69).
- [101] S. Shaaban and J. Seume. “Analysis of turbocharger non-adiabatic performance”. In: *ImechE Conference Transactions from 8th International Conference on Turbochargers and Turbocharging*. 2006, pp. 119–130 (cit. on p. 23).
- [102] A. T. Simpson, S. W. T. Spence, and J. K. Watterson. “A comparison of the flow structures and losses within vaned and vaneless stators for radial turbines”. In: *Journal of Turbomachinery* 131 (2009), p. 031010 (cit. on pp. 14, 15, 23, 27, 44, 47, 129, 158).

- [103] J. Smagorinsky. “General circulation experiments with the primitive equations”. In: *Monthly weather review* 91.3 (1963), pp. 99–164 (cit. on p. 25).
- [104] E.M. Smirnov. “Recent Progress in Numerical Simulation of Highly Three-Dimensional Turbulent Flows and Endwall Heat Transfer in Turbine Blade Cascades”. In: *Heat Transfer Research* 42.1 (2011), pp. 25–44 (cit. on p. 23).
- [105] G. A. Sod. “A survey of several finite difference methods for systems of nonlinear hyperbolic conservation laws”. In: *Journal of Computational Physics* 27.1 (1978), pp. 1–31. DOI: 10.1016/0021-9991(78)90023-2 (cit. on pp. 71, 84).
- [106] S. W. T. Spence, R. S. E. Rosborough, D. Artt, and G. McCullough. “A direct performance comparison of vaned and vaneless stators for radial turbines”. In: *Journal of Turbomachinery* 129 (2007), p. 53 (cit. on p. 14).
- [107] M. Strelets. “Detached eddy simulation of massively separated flows”. In: *In 39th AIAA Aerospace Sciences Meeting and Exhibit*. AIAA 2001-0879. American Institute of Aeronautics & Astronautics, 2001 (cit. on p. 25).
- [108] D. R. Stull. *JANAF thermochemical tables*. Tech. rep. DTIC Document, 1971 (cit. on p. 110).
- [109] *Supercharging Testing Standards*. Engine Power Test Code Committee, Issued August, 1995. (Cit. on p. 18).
- [110] M. Tancrez, J. Galindo, C. Guardiola, P. Fajardo, and O. Varnier. “Turbine adapted maps for turbocharger engine matching”. In: *Experimental Thermal and Fluid Science* 35.1 (2011), pp. 146–153. DOI: 10.1016/j.expthermflusci.2010.07.018 (cit. on p. 2).
- [111] C. K. W. Tarn. “Computational aeroacoustics: issues and methods”. In: *AIAA Journal* 33.10 (1995), pp. 1788–1796 (cit. on p. 81).
- [112] A. Thakker and F. Hourigan. “Computational fluid dynamics analysis of a 0.6 m, 0.6 hub-to-tip ratio impulse turbine with fixed guide vanes”. In: *Renewable energy* 30.9 (2005), pp. 1387–1399 (cit. on pp. 14, 15).
- [113] K. W. Thompson. “Time-dependent boundary conditions for hyperbolic systems”. In: *Journal of Computational Physics* 68 (1987), pp. 1–24 (cit. on pp. 81, 84).

- [114] K. W. Thompson. “Time-dependent boundary conditions for hyperbolic systems, II”. In: *Journal of Computational Physics* 89.2 (1990), pp. 439–461. ISSN: 0021-9991 (cit. on pp. 81, 84).
- [115] A. J. Torregrosa, P. Fajardo, A. Gil, and R. Navarro. “Development of a non-reflecting boundary condition for its application in 3D computational fluid dynamic codes”. In: *Engineering Applications of Computational Fluid Mechanics* (Accepted for publication 16/04/2012) (cit. on pp. 80, 108, 110, 120, 167).
- [116] A. M. Tousi, A. Tourani, et al. “Comparison of turbulence methods in CFD analysis of compressible flows in radial turbomachines”. In: *Aircraft Engineering and Aerospace Technology: An International Journal* 80.6 (2008), pp. 657–665 (cit. on p. 26).
- [117] M. Tritthart and D. Gutknecht. “Three-dimensional Simulation of Free-Surface Flows using Polyhedral Finite Volumes”. In: *Engineering Applications of Computational Fluid Mechanics* 1 (2007), pp. 1–14 (cit. on p. 27).
- [118] T. Tsuji, T. Tsuchiya, and Y. Kagawa. “Finite element and boundary element modelling for the acoustic wave transmission in mean flow medium”. In: *Journal of Sound and Vibration* 255.5 (2002), pp. 849–866. ISSN: 0022-460X (cit. on p. 80).
- [119] H. K. Versteeg and W. Malalasekera. *An introduction to computational fluid dynamics: the finite volume method*. Prentice Hall, 2007 (cit. on pp. 14, 25, 28, 72).
- [120] B. Wang and H. Xu. “A method based on Riemann problem in tracking multi-material interface on unstructured moving grids”. In: *Engineering Applications of Computational Fluid Mechanics* 1.4 (2007), pp. 325–336 (cit. on p. 84).
- [121] D. C. Wilcox. *Turbulence Modeling for CFD (Hardcover)*. Dcw Industries, Incorporated; 3rd edition, 2006 (cit. on pp. 25, 26).
- [122] D. E. Winterbone and R. J. Pearson. *Theory of Engine Manifold Design : Wave Action Methods for IC Engines*. John Wiley & Sons, 2000 (cit. on pp. 108–110).
- [123] S. Yedidiah. *Centrifugal pump user’s guidebook: problems and solutions*. Kluwer Academic Publishers, 1996 (cit. on p. 15).

- [124] P.K. Zachos, N. Grech, B. Charnley, V. Pachidis, and R. Singh. “Experimental and numerical investigation of a compressor cascade at highly negative incidence”. In: *Engineering Applications of Computational Fluid Mechanics* 5.1 (2011), pp. 26–36 (cit. on p. 28).

UDF Code

```
/* Breve explicacion de la UDF*/
/*Para que aparezcan mensajes, y asi facilitar el debugging,
basta eliminar los asteriscos asociados a los ini y end */

/* Advertencia: Buscar aquellas variables en cuyos
comentarios aparezca "CAMBIAR" e introducir los valores
concretos de la simulacion*/

/*Se tiene que ejecutar Fluent desde la carpeta de Fluent,
por los relative paths usados*/

/*La condición de radial equilibrium, requiere tener creado
un archivo radial_eq.xy, de la CFF "rho*v_theta^2 / r", que
es la que aparece en el equilibrio radial.*/

/*Además es necesario usar un EXECUTE COMMANDS, de forma que
se actualice este perfil en cada paso de tiempo para calcular
el perfil de presioens*/

#include "udf.h"
#include <unistd.h>

#ifdef FALSE
#define FALSE 0
#endif
#ifdef TRUE
#define TRUE 1
```

```

#endif

#define R_gas 287.038 /* specific gas constant */
#define rehook_ts 0 /* CAMBIAR - number of timesteps at
which you rehook this UDF*/
#define p_op 101325 /* CAMBIAR - operating pressure
set in Fluent */
#define p_ref 100000 /* CAMBIAR - presion de referencia
usada en WAM para calcular los niveles de entropia */
#define frac_aire_limpio 1.0
#define frac_aire_quemado 0.0
#define cociente_time_steps 1 /* CAMBIAR - Cociente moc/cfd
time steps - Si se usa Fluent explicit-explicit, poner 1*/

/*variables necesarias para el radial equilibrium*/
#define MAX_LEN 200 /*CAMBIAR-maximum length of a line*/
#define profile_length 15 /*CAMBIAR-number of elements of
radial_eq.xy*/
#define x_center 1 /*coordinates of the outlet's center
(radial equilibrium)*/
#define y_center 0
#define z_center 0

double cfd_time_step=2e-06; /* CAMBIAR - time-step of
CFD computation*/
double moc_time_step=2e-06; /* CAMBIAR - method of
characteristics' time-step */

FILE *f_u_beta;
FILE *f_a_beta;
FILE *f_gamma_beta;
FILE *f_p_beta;
FILE *f_u_lambda;
FILE *f_a_lambda;
FILE *f_gamma_lambda;
FILE *f_p_lambda;
FILE *f_p_nivel_entropia_entrada;
FILE *f_a_nivel_entropia_entrada;

```



```

FILE *f_gamma_nivel_entropia_entrada;
FILE *f_p_nivel_entropia_salida;
FILE *f_a_nivel_entropia_salida;
FILE *f_gamma_nivel_entropia_salida;
FILE *f_wam;
FILE *f_fluent;
FILE *f_output;
FILE *f_rehook;
FILE *f_radial_eq;
FILE *f_radial_eq_comprob;

double lambda_cc;
double lambda_cc_sin_corregir;
double a_lambda_cc;
double nivel_entropia_lambda_cc;
double beta_cc;
double beta_cc_ant=471.90298; /* CAMBIAR -
inicializacion de beta_cc_ant para el caso
de condicion anecoica*/;

double beta_cc_sin_corregir;
double a_beta_cc;
double nivel_entropia_beta_cc;
double nivel_entropia_entrada_cc;
double nivel_entropia_salida_cc;
double nivel_entropia_cc;
double gamma_cc=1.3990006; /* CAMBIAR - tomamos el
del paso de tiempo anterior, ya que no queremos que
el sistema de ecs sea implicito */

double cp;
double a_cc;
double a_cc_ant=509.51596; /* CAMBIAR - inicializacion
de a_cc_ant para el caso de condicion anecoica*/;
double u_cc;
double p_cc;
double M_cc;
double T_cc;

```

```

double p_tot_cc_gauge;
double T_tot_cc;

double u_cc_ant=188.53598; /* CAMBIAR - u_cc en el paso de
tiempo anterior, para saber si cambia de direccion el flujo*/
double nivel_entropia_cc_ant=502.43622; /* CAMBIAR - nivel_
entropia_cc en el paso de tiempo anterior, para utilizarlo
si cambia de direccion el flujo*/

double beta_vector[cociente_time_steps];
double a_beta_vector[cociente_time_steps];
double nivel_entropia_beta_vector[cociente_time_steps];
double nivel_entropia_lambda_vector[cociente_time_steps];
double lambda_vector[cociente_time_steps];
double a_lambda_vector[cociente_time_steps];
double nivel_entropia_entrada_vector[cociente_time_steps];
double nivel_entropia_salida_vector[cociente_time_steps];
double flow_time_rehook_vector[cociente_time_steps];

double ft_interpolar[2]={0,0}; /* vector de dos posiciones que
almacena los flowtimes de wam.txt que se usan para interpolar,
de forma que ft_interpolar[0]=ft anterior al actual y
ft_interpolar[1]=ft posterior al actual*/

double beta_interpolar[2];
double nivel_entropia_beta_interpolar[2];
double a_beta_interpolar[2];
double lambda_interpolar[2];
double nivel_entropia_lambda_interpolar[2];
double a_lambda_interpolar[2];
double nivel_entropia_entrada_interpolar[2];
double nivel_entropia_salida_interpolar[2];
double current_ts_presion;

int contador;
long int posicion_f_wam=0; /* CAMBIAR - Para que empiece
leyendo la 1a linea de Datos.1d y luego almacene la posicion
posterior a la ultima linea correctamente leida*/

```

```

int zone_ID=2; /* CAMBIAR - ID de la cara en la que se quiere
imponer la bc */

int BC_node_id=-10; /* inicializacion en un valor que no
se puede dar para la ID */

int last_ts=0; /*Porque fluent12 parece no hacer caso al
profile update interval...*/

int last_ts_presion=0; /*variables para que fluent12 solo
haga el Define profile en cada caso de tiempo y no iteración*/

/* Variables "booleanas" para controlar cuando se debe
ejecutar o no una parte del codigo */

int calcular_NRBC_llamada_por_pres=FALSE;
int calcular_NRBC_llamada_por_temp=FALSE;
int entrada=0; /*CAMBIAR - 1 si la UDF se coloca en una
superficie de entrada (flujo a priori entrante al dominio
de FLUENT) o 0 si es de salida*/

int radial=1; /*CAMBIAR - (0 si las condición de contorno
es uniforme, 1 si se aplica la condición de equilibrio
radial (hay que tener en cuenta que las variables deben
sacarse en el eje en este caso)*/

int anecoica_o_wam_o_fluent=2; /*CAMBIAR - (2 si la BC es
una salida anecoica, 1 si el acoplamiento es con WAM o 0
si es con fluent)*/

int explicit_o_implicit=0; /*CAMBIAR - (1 si fluent es
explicit (paso de tiempo vble) o 0 si es implicit
(paso de tiempo fijo y conocido a priori))*/

int cp_cte_o_variable_fluent=0; /*CAMBIAR - (0 para cp
cte calorificamente perfecto (1006.43); 1 para cp según
polinomio fluent*/

```

```

int variables_a_leer;
int inicializar_WAM=0; /*CAMBIAR - (0 para no inicializar;
1 para inicializar WAM)*/

int calcula_NRBC () {

    int current_ts;
    double current_ft;
    current_ft=CURRENT_TIME;
    double basura;
    double basura2;
    double u_beta;
    double gamma_beta;
    double p_beta;
    double u_lambda;
    double gamma_lambda;
    double p_lambda;
    double p_nivel_entropia_entrada;
    double a_nivel_entropia_entrada;
    double gamma_nivel_entropia_entrada;
    double p_nivel_entropia_salida;
    double a_nivel_entropia_salida;
    double gamma_nivel_entropia_salida;
    double comprobar_wam;
    double eps=1E-15; /*para que no haya problemas de lectura
de la ultima cifra y se estanquen en el mismo paso de
tiempo tanto WAM como Fluent*/

    if (explicit_o_implicit==1) {
        /*Si es explicito, los pasos de tiempo del cfd y del
moc son iguales, y valen el paso de tiempo actual.
Lo malo es que en el momento en el que se ejecuta
la UDF el paso de tiempo no esta actualizado.
Ademas, los pasos de tiempo son iteraciones */

        current_ts=N_ITER+1; /*Porque aun no ha actualizado
el numero de iteraciones*/
    }
}

```

```

if ( current_ts-rehook_ts>1) {
    cfd_time_step=CURRENT_TIMESTEP;
    moc_time_step=CURRENT_TIMESTEP;
}
current_ft=current_ft+cfd_time_step; /*Porque aun
no ha actualizado el flowtime. Se estima con el
paso de tiempo anterior*/

} else current_ts=N_TIME;
if (current_ts!=last_ts) {
last_ts=current_ts;
if ( current_ts-rehook_ts==1 &&
anecoica_o_wam_o_fluent!=2) {

/* Para que no entre a leer el monitor de Fluent
cuando impones interactivamente las BC ni en la
1a iteracion (no existe hasta que precisamente
calcula esa iteracion), ni cuando estas utilizando
la condicion anecoica */

/*Lectura del valor de lambda proporcionado por WAM */

/* Se asume que WAM tendra un paso de tiempo siempre
mayor que el de Fluent, y que su ejecucion es mas
rapida. Asi, cuando fluent este calculando un paso
de tiempo, wam ya habra calculado su paso de tiempo,
generado las lambdas y Aa correspondientes entre el
ft actual y el ft+delta_T de wam y estara esperando a
que fluent llegue hasta ese ft. Por lo tanto, esta
UDF en fluent puede leer la linea siguiente del
archivo de lambdas y Aas de wam sabiendo que va a
existir. */

f_wam=NULL;
while (f_wam==NULL)

if (entrada==1) f_wam=fopen("./entrada/Datos.1d","r");

```

```

else f_wam=fopen("./salida/Datos.1d","r");
    }

    if ( current_ts-rehook_ts > 1) {

/* se desplaza el vector de variables de Riemann del dominio
y se deja hueco para el ultimo valor, que se calculo en el
paso de tiempo anterior, y que se leera ahora */

for (contador=0;contador<cociente_time_steps-1;contador++) {
    if (entrada==1) {
        beta_vector[contador]=beta_vector[contador+1];
        a_beta_vector[contador]=a_beta_vector[contador+1];
        nivel_entropia_beta_vector[contador]=
        nivel_entropia_beta_vector[contador+1];
        nivel_entropia_entrada_vector[contador]=
        nivel_entropia_entrada_vector[contador+1];
    } else {
        lambda_vector[contador]=lambda_vector[contador+1];
        a_lambda_vector[contador]=a_lambda_vector[contador+1];
        nivel_entropia_lambda_vector[contador]=
        nivel_entropia_lambda_vector[contador+1];
        nivel_entropia_salida_vector[contador]=
        nivel_entropia_salida_vector[contador+1];
    }
}

/*Lectura de la variable de Riemann obtenido por la
isosurface de FLuent.*/

/*Se va a hacer para paso de tiempo cte y conocido en FLuent.
Si se utilizara un DB explicit-explicit o un vble time step,
habria que generar en la UDF un fichero que guardara timestep
(num) delta_time (s), para saber cuando llega a la CC la
beta obtenida*/

if (entrada==1) {
    /*Calculo de beta*/

```

```

        if ( current_ts-rehook_ts == 2 )
        {
            f_u_beta=fopen("u_beta.out","r");
            f_a_beta=fopen("a_beta.out","r");
            f_gamma_beta=fopen("gamma_beta.out","r");
            f_p_beta=fopen("p_beta.out","r");
        }

        fscanf(f_u_beta, "%lg %lg", &basura, &u_beta);
        fscanf(f_a_beta, "%lg %lg", &basura,
            &a_beta_vector[cociente_time_steps-1]);
        fscanf(f_gamma_beta, "%lg %lg", &basura, &gamma_beta);
        fscanf(f_p_beta, "%lg %lg", &basura, &p_beta);
        beta_vector[cociente_time_steps-1]=
        a_beta_vector[cociente_time_steps-1]-(gamma_beta-1)
        /2*u_beta;

        nivel_entropia_beta_vector[cociente_time_steps-1]=
        a_beta_vector[cociente_time_steps-1]*
        pow((p_ref/(p_beta+p_op)),((gamma_beta-1)
        /(2*gamma_beta)));

/*Calculo de nivel de entropia - entrada*/

        if ( current_ts-rehook_ts == 2 )
        {
            f_p_nivel_entropia_entrada=
            fopen("p_stat-nivel_ent_in.out","r");
            f_a_nivel_entropia_entrada=
            fopen("a-nivel_ent_in.out","r");
            f_gamma_nivel_entropia_entrada=
            fopen("gamma-nivel_ent_in.out","r");
        }
        fscanf(f_p_nivel_entropia_entrada, "%lg %lg",
            &basura, &p_nivel_entropia_entrada);
        fscanf(f_a_nivel_entropia_entrada, "%lg %lg",
            &basura, &a_nivel_entropia_entrada);
        fscanf(f_gamma_nivel_entropia_entrada, "%lg %lg",

```

```

        &basura, &gamma_nivel_entropia_entrada);

nivel_entropia_entrada_vector[cociente_time_steps-1]=
    a_nivel_entropia_entrada*
    pow((p_ref/(p_nivel_entropia_entrada+p_op)),
        ((gamma_nivel_entropia_entrada-1)
        /(2*gamma_nivel_entropia_entrada)));

    } else { /*salida*/

if ( current_ts-rehook_ts == 2 )
{
    f_u_lambda=fopen("u_lambda.out","r");
    f_a_lambda=fopen("a_lambda.out","r");
    f_gamma_lambda=fopen("gamma_lambda.out","r");
    f_p_lambda=fopen("p_lambda.out","r");
}

fscanf(f_u_lambda, "%lg %lg", &basura, &u_lambda);
fscanf(f_a_lambda, "%lg %lg", &basura,
        &a_lambda_vector[cociente_time_steps-1]);

fscanf(f_gamma_lambda, "%lg %lg", &basura, &gamma_lambda);
fscanf(f_p_lambda, "%lg %lg", &basura, &p_lambda);

lambda_vector[cociente_time_steps-1]=
    a_lambda_vector[cociente_time_steps-1]
    +(gamma_lambda-1)/2*u_lambda;

    nivel_entropia_lambda_vector[cociente_time_steps-1]=
    a_lambda_vector[cociente_time_steps-1]*
    pow((p_ref/(p_lambda+p_op)),((gamma_lambda-1)
    /(2*gamma_lambda)));

/*Calculo de nivel de entropia - salida*/

if ( current_ts-rehook_ts == 2 )
{

```



```

f_p_nivel_entropia_salida=
fopen("p_stat-nivel_ent_out.out","r");
f_a_nivel_entropia_salida=
fopen("a-nivel_ent_out.out","r");
f_gamma_nivel_entropia_salida=
fopen("gamma-nivel_ent_out.out","r");
}

fscanf(f_p_nivel_entropia_salida, "%lg %lg",
      &basura, &p_nivel_entropia_salida);
fscanf(f_a_nivel_entropia_salida, "%lg %lg",
      &basura, &a_nivel_entropia_salida);
fscanf(f_gamma_nivel_entropia_salida, "%lg %lg",
      &basura, &gamma_nivel_entropia_salida);
nivel_entropia_salida_vector[cociente_time_steps-1]
=a_nivel_entropia_salida*
pow((p_ref/(p_nivel_entropia_salida+
p_op)),((gamma_nivel_entropia_salida-1)/
(2*gamma_nivel_entropia_salida)));
}

/*Escritura de las variables de Riemann para WAM*/
/*Cuando la velocidad no vaya en el sentido propio
del nivel de entropia para la entrada o salida, se
entendera por nivel de entropia aquel que existia en
la CC en el paso de tiempo anterior*/

/*Tal y como esta planteado ahora, se necesitan poner
"cociente_time_steps" lineas de rehook en el fluent.txt,
para que exista un desfase de cociente_time_steps entre
el valor que lee la otra UDF (que se usa para calcular
la CC) y el valor que se escribe en esta (que se genero
en el paso de tiempo anterior, se escribe en este y se
usa "cociente_time_steps" pasos de tiempo mas tarde
respecto del paso de tiempo anterior ) */

if (entrada==1) {
f_fluent=fopen("./entrada/Datos.cfd","a");

```

```

if (u_cc_ant > 0) {
    /*Se comprueba con u_cc_ant porque son los monitores
    generados en el paso de tiempo anterior*/
    nivel_entropia_entrada_vector[cociente_time_steps-1]=
    nivel_entropia_cc_ant;

    /*Si la vel es positiva, el nivel de entropia de la parte
    de la entrada no tiene significado fisico, porque se ha
    definido con el modulo de la velocidad. Por eso se pasa
    el del paso de tiempo anterior, por si hubiera un cambio
    de sentido del flujo*/
}

    fprintf(f_fluent, "%.16lg %.16lg %.16lg %.16lg %.16lg %.16lg
    %.16lg\n", current_ft-cfd_time_step+moc_time_step,
    beta_vector[cociente_time_steps-1],
    a_beta_vector[cociente_time_steps-1],
    nivel_entropia_beta_vector[cociente_time_steps-1],
    nivel_entropia_entrada_vector[cociente_time_steps-1],
    frac_aire_quemado, frac_aire_limpio);

    /*le restas un cfd_time_step porque generaste las variables
    en el paso de tiempo anterior*/
    } else {
        /*salida*/
f_fluent=fopen("./salida/Datos.cfd","a");

if (u_cc_ant < 0) {
nivel_entropia_salida_vector[cociente_time_steps-1]=
    nivel_entropia_cc_ant;
}

    fprintf(f_fluent, "%.16lg %.16lg %.16lg %.16lg %.16lg
    %.16lg %.16lg\n", current_ft-cfd_time_step+moc_time_step,
    lambda_vector[cociente_time_steps-1],
    a_lambda_vector[cociente_time_steps-1],
    nivel_entropia_lambda_vector[cociente_time_steps-1],
    nivel_entropia_salida_vector[cociente_time_steps-1],

```

```

frac_aire_quemado, frac_aire_limpio);
}

fclose(f_fluent);
}
if ( current_ts > rehook_ts ) {
    if ( anecoica_o_wam_o_fluent!=2) {
        /*Lectura del Datos.1d*/

while (ft_interpolar[1]+eps<current_ft) {
    usleep(100000);
    ft_interpolar[0]=ft_interpolar[1];
    if (entrada==1) {
        lambda_interpolar[0]=lambda_interpolar[1];
        nivel_entropia_salida_interpolar[0]=
            nivel_entropia_salida_interpolar[1];

        if (anecoica_o_wam_o_fluent==0) {
            a_lambda_interpolar[0]=a_lambda_interpolar[1];
            nivel_entropia_lambda_interpolar[0]=
                nivel_entropia_lambda_interpolar[1];
        }
        } else {
        beta_interpolar[0]=beta_interpolar[1];
        nivel_entropia_entrada_interpolar[0]=
            nivel_entropia_entrada_interpolar[1];

        if (anecoica_o_wam_o_fluent==0) {
            a_beta_interpolar[0]=a_beta_interpolar[1];
            nivel_entropia_beta_interpolar[0]=
                nivel_entropia_beta_interpolar[1];
        }
    }
}
comprobar_wam=0;
    while (comprobar_wam != variables_a_leer) {
        usleep(100000);
        fseek(f_wam, posicion_f_wam, SEEK_SET);
        if (entrada==1) {

```

```

/*ENTRADA*/
if (anecoica_o_wam_o_fluent==1) {
/*WAM*/
comprobar_wam=fscanf(f_wam,"%lg %lg %lg %lg
%lg", &ft_interpolar[1], &lambda_interpolar[1],
&nivel_entropia_salida_interpolar[1], &basura,
&basura2);
} else {
/*FLUENT*/
comprobar_wam=fscanf(f_wam,"%lg %lg %lg %lg %lg
%lg %lg", &ft_interpolar[1], &lambda_interpolar[1],
&a_lambda_interpolar[1],
&nivel_entropia_lambda_interpolar[1],
&nivel_entropia_salida_interpolar[1],
&basura, &basura2);
}
/*if (comprobar_wam == EOF) sleep (5);*/
} else {
/*SALIDA*/
if (anecoica_o_wam_o_fluent==1) {
/*WAM*/
comprobar_wam=fscanf(f_wam,"%lg %lg %lg %lg
%lg", &ft_interpolar[1], &beta_interpolar[1],
&nivel_entropia_entrada_interpolar[1],
&basura, &basura2);
} else {
/*FLUENT*/
comprobar_wam=fscanf(f_wam,"%lg %lg %lg %lg %lg
%lg %lg", &ft_interpolar[1], &beta_interpolar[1],
&a_beta_interpolar[1], &nivel_entropia_beta_interpolar[1],
&nivel_entropia_entrada_interpolar[1], &basura, &basura2);
}
/*if (comprobar_wam == EOF) sleep (5);*/
}
if (comprobar_wam == variables_a_leer) posicion_f_wam=
ftell(f_wam); /*Para que salve la posicion solo si
ha realizado una lectura correcta*/
}

```

```

}
if (ft_interpolar[0]==0) {
  if (entrada==1) {
    lambda_interpolar[0]=lambda_interpolar[1];
    nivel_entropia_salida_interpolar[0]=
    nivel_entropia_salida_interpolar[1];
    if (anecoica_o_wam_o_fluent==0) {
      a_lambda_interpolar[0]=a_lambda_interpolar[1];
      nivel_entropia_lambda_interpolar[0]=
      nivel_entropia_lambda_interpolar[1];
    }
  } else {
    beta_interpolar[0]=beta_interpolar[1];
    nivel_entropia_entrada_interpolar[0]=
    nivel_entropia_entrada_interpolar[1];
    if (anecoica_o_wam_o_fluent==0) {
      a_beta_interpolar[0]=a_beta_interpolar[1];
      nivel_entropia_beta_interpolar[0]=
      nivel_entropia_beta_interpolar[1];
    }
  }
} /*para el 1er paso de tiempo, en el que no
tiene definidos unos valores para ft_interpolar[0]*/

/*Interpolacion en tiempo*/

if (entrada==1){
lambda_cc=lambda_interpolar[0]+(lambda_interpolar[1]
-lambda_interpolar[0])/(ft_interpolar[1]-
ft_interpolar[0])*(current_ft-ft_interpolar[0]);

nivel_entropia_salida_cc=
nivel_entropia_salida_interpolar[0]+
(nivel_entropia_salida_interpolar[1]-
nivel_entropia_salida_interpolar[0])/(ft_interpolar[1]
-ft_interpolar[0])*(current_ft-ft_interpolar[0]);
  if (anecoica_o_wam_o_fluent==0) {
    lambda_cc_sin_corregir=lambda_cc;
  }
}

```

```

a_lambda_cc=a_lambda_interpolar[0]+(a_lambda_interpolar[1]
-a_lambda_interpolar[0])/(ft_interpolar[1]-ft_interpolar[0])
*(current_ft-ft_interpolar[0]);
nivel_entropia_lambda_cc=nivel_entropia_lambda_interpolar[0]
+(nivel_entropia_lambda_interpolar[1]-
nivel_entropia_lambda_interpolar[0])
/(ft_interpolar[1]-ft_interpolar[0])
*(current_ft-ft_interpolar[0]);
}
}
else {
beta_cc=beta_interpolar[0]+(beta_interpolar[1]
-beta_interpolar[0])/(ft_interpolar[1]
-ft_interpolar[0])*(current_ft-ft_interpolar[0]);

nivel_entropia_entrada_cc=
nivel_entropia_entrada_interpolar[0]+
(nivel_entropia_entrada_interpolar[1]-
nivel_entropia_entrada_interpolar[0])
/(ft_interpolar[1]-ft_interpolar[0])
*(current_ft-ft_interpolar[0]);

if (anecoica_o_wam_o_fluent==0) {
beta_cc_sin_corregir=beta_cc;
a_beta_cc=a_beta_interpolar[0]+(a_beta_interpolar[1]-
a_beta_interpolar[0])/(ft_interpolar[1]-ft_interpolar[0])
*(current_ft-ft_interpolar[0]);
nivel_entropia_beta_cc=nivel_entropia_beta_interpolar[0]+
(nivel_entropia_beta_interpolar[1]-

nivel_entropia_beta_interpolar[0])
/(ft_interpolar[1]-ft_interpolar[0])
*(current_ft-ft_interpolar[0]);
}
}
/* Se asignan los valores de los vectores de vbles de
Riemann procedentes de fluent que se van a usar para
calcular la BC en este paso de tiempo */

```

```

/* Decision del nivel de entropia que se debe utilizar,
   en funcion del sentido de flujo en la condicion de contorno
   actual y en la del paso de tiempo anterior*/

/*Hipotesis y confirmacion de las distintas configuraciones
del flujo (entrante, saliente, cambio de sentido) en funcion
de u_cc y u_cc_ant. Como se calcula u_cc, ya no se necesita
recalcular luego*/

if (entrada==1) {
    nivel_entropia_entrada_cc=
    nivel_entropia_entrada_vector[0];
    if (u_cc_ant > 0 ) {
nivel_entropia_cc=nivel_entropia_salida_cc;
beta_cc=beta_vector[0]+a_beta_vector[0]*
log(nivel_entropia_cc/nivel_entropia_beta_vector[0]);

        if (anecoica_o_wam_o_fluent==0) {
lambda_cc=lambda_cc_sin_corregir+a_lambda_cc*
log(nivel_entropia_cc/nivel_entropia_lambda_cc);
        } /*Hay que corregir lambda porque viene de
           fluent y no de wam*/
u_cc=(lambda_cc-beta_cc)/(gamma_cc-1);
        if (u_cc_ant*u_cc < 0 ) {
            nivel_entropia_cc=nivel_entropia_cc_ant;
            beta_cc=beta_vector[0]+a_beta_vector[0]*
            log(nivel_entropia_cc/
            nivel_entropia_beta_vector[0]);

            if (anecoica_o_wam_o_fluent==0) {
lambda_cc=lambda_cc_sin_corregir+a_lambda_cc*
                log(nivel_entropia_cc/nivel_entropia_lambda_cc);
            }
            u_cc=(lambda_cc-beta_cc)/(gamma_cc-1);
        }
    } else if (u_cc_ant < 0 ) {
        nivel_entropia_cc=nivel_entropia_entrada_cc;
    }
}

```

```

beta_cc=beta_vector[0]+a_beta_vector[0]*
    log(nivel_entropia_cc/nivel_entropia_beta_vector[0]);

if (anecoica_o_wam_o_fluent==0) {
    lambda_cc=lambda_cc_sin_corregir+a_lambda_cc*
        log(nivel_entropia_cc/nivel_entropia_lambda_cc);
    }
u_cc=(lambda_cc-beta_cc)/(gamma_cc-1);
if (u_cc_ant*u_cc < 0 ) {
    nivel_entropia_cc=nivel_entropia_cc_ant;
    beta_cc=beta_vector[0]+a_beta_vector[0]*
        log(nivel_entropia_cc/nivel_entropia_beta_vector[0]);

        if (anecoica_o_wam_o_fluent==0) {
lambda_cc=lambda_cc_sin_corregir+a_lambda_cc
*log(nivel_entropia_cc/nivel_entropia_lambda_cc);
    }
    u_cc=(lambda_cc-beta_cc)/(gamma_cc-1);
    }
} else {
    nivel_entropia_cc=nivel_entropia_cc_ant;
    beta_cc=beta_vector[0]+a_beta_vector[0]*
        log(nivel_entropia_cc/nivel_entropia_beta_vector[0]);
    if (anecoica_o_wam_o_fluent==0) {
        lambda_cc=lambda_cc_sin_corregir+a_lambda_cc*
            log(nivel_entropia_cc/nivel_entropia_lambda_cc);
        }
    u_cc=(lambda_cc-beta_cc)/(gamma_cc-1);
    }
} else {
    nivel_entropia_salida_cc=
        nivel_entropia_salida_vector[0];

    if (u_cc_ant > 0 ) {
        nivel_entropia_cc=nivel_entropia_salida_cc;
        lambda_cc=lambda_vector[0]+a_lambda_vector[0]*
            log(nivel_entropia_cc/nivel_entropia_lambda_vector[0]);
        if (anecoica_o_wam_o_fluent==0) {

```



```

        beta_cc=beta_cc_sin_corregir+a_beta_cc*
            log(nivel_entropia_cc/nivel_entropia_beta_cc);
    }
    u_cc=(lambda_cc-beta_cc)/(gamma_cc-1);

    if (u_cc_ant*u_cc < 0 ) {
nive_l_entropia_cc=nive_l_entropia_cc_ant;
        lambda_cc=lambda_vector[0]+a_lambda_vector[0]*
            log(nivel_entropia_cc/nivel_entropia_lambda_vector[0]);

if (anecoica_o_wam_o_fluent==0) {
        beta_cc=beta_cc_sin_corregir+a_beta_cc*
            log(nivel_entropia_cc/nivel_entropia_beta_cc);
    }
    u_cc=(lambda_cc-beta_cc)/(gamma_cc-1);
    }
    } else if (u_cc_ant < 0 ) {
nive_l_entropia_cc=nive_l_entropia_entrada_cc;
        lambda_cc=lambda_vector[0]+a_lambda_vector[0]*
            log(nivel_entropia_cc/nivel_entropia_lambda_vector[0]);

if (anecoica_o_wam_o_fluent==0) {
        beta_cc=beta_cc_sin_corregir+a_beta_cc*
log(nivel_entropia_cc/nivel_entropia_beta_cc);
    }
    u_cc=(lambda_cc-beta_cc)/(gamma_cc-1);

        if (u_cc_ant*u_cc < 0 ) {
nive_l_entropia_cc=nive_l_entropia_cc_ant;
        lambda_cc=lambda_vector[0]+a_lambda_vector[0]*
            log(nivel_entropia_cc/nivel_entropia_lambda_vector[0]);

        if (anecoica_o_wam_o_fluent==0) {
beta_cc=beta_cc_sin_corregir+a_beta_cc*
            log(nivel_entropia_cc/nivel_entropia_beta_cc);
        }
    u_cc=(lambda_cc-beta_cc)/(gamma_cc-1);
    }
}

```

```

    } else {
    nivel_entropia_cc=nivel_entropia_cc_ant;
    lambda_cc=lambda_vector[0]+a_lambda_vector[0]*
    log(nivel_entropia_cc/nivel_entropia_lambda_vector[0]);

        if (anecoica_o_wam_o_fluent==0) {
beta_cc=beta_cc_sin_corregir+a_beta_cc*
    log(nivel_entropia_cc/nivel_entropia_beta_cc);
        }
        u_cc=(lambda_cc-beta_cc)/(gamma_cc-1);
    }
}
} else {
/*Salida anecoica*/

/*Se asume que u_cc, u_cc_ant son positivas (si no,
no podria ser una salida anecoica). Asi,
nivel_entropia_cc=nivel_entropia_salida[0]
Se impone beta_cc=beta_cc_ant + correccion por nivel
de entropia, con lo que no hace falta leer el Datos.1d*/

/*Crear a_cc_ant y beta_cc_ant y aplicar correccion de seg.
orden. Cuando WAM este cambiado, hacerlo tambien en el caso
general*/

nivel_entropia_cc=nivel_entropia_salida_vector[0];

/*Aproximacion de 2o orden*/
a_cc=(lambda_vector[0]+beta_cc_ant+a_lambda_vector[0])/2*
log(nivel_entropia_cc/nivel_entropia_lambda_vector[0])+
a_cc_ant/2*log(nivel_entropia_cc/nivel_entropia_cc_ant))
/(2-0.5*(log(nivel_entropia_cc/
nivel_entropia_lambda_vector[0])
+log(nivel_entropia_cc/nivel_entropia_cc_ant)));

lambda_cc=lambda_vector[0]+(a_lambda_vector[0]+a_cc)/2*
log(nivel_entropia_cc/nivel_entropia_lambda_vector[0]);

```

```

beta_cc=beta_cc_ant+(a_cc_ant+a_cc)/2*
log(nivel_entropia_cc/nivel_entropia_cc_ant);

u_cc=(lambda_cc-beta_cc)/(gamma_cc-1);
}

/* Calculo de la CC */

/* Para que no repita la misma linea cuando se haga un
rehook en el udf_output ni acceda cuando impones
interactivamente la BC (porque, en ese instante,
current_ts=rehook_ts) */

/*ini Message("\nAhora empieza a calcular la BC\n"); end*/

if (anecoica_o_wam_o_fluent != 2) {
    a_cc=(lambda_cc+beta_cc)/2;
    /*Porque para BC anecoica he mo utilizado una
    aproximacion de  $2i_j^{\frac{1}{2}}$  orden*/
}

p_cc=p_ref*pow((a_cc/nivel_entropia_cc),
(2*gamma_cc/(gamma_cc-1)));

/*ini Message("\n p_cc (si radial en el eje)
vale %lg\n", p_cc); end*/

M_cc=u_cc/a_cc;
T_cc=pow(a_cc,2)/(gamma_cc*R_gas);

/* Vamos a imponer solo 2 de los 3 parametros, xq es una CC
y no un punto interior al fluido. Tal vez seria interesante
usar mass-flow inlet, xq forzaria la velocidad en vez de
la presion total */

p_tot_cc_gauge=p_cc*pow((1+(gamma_cc-1)/2*pow(M_cc,2)),
(gamma_cc/(gamma_cc-1)))-p_op;

```

```

/* calcular absolute total pressure y restar operating
   pressure para enviar a Fluent la gauge total pressure */

T_tot_cc=T_cc*(1+(gamma_cc-1)/2*pow(M_cc,2));

/*ini Message("\nSe impone en la BC el valor p=%lf y
T=%lg\n",p_tot_cc_gauge,T_tot_cc); end*/

/*"Actualizar" valores*/
  if (cp_cte_o_variable_fluent==1) {
cp=1161.482*pow(T_cc,0)-2.368819*pow(T_cc,1)+
0.01485511*pow(T_cc,2)-0.00005034909*pow(T_cc,3)+
0.00000009928569*pow(T_cc,4)-
0.0000000001111097*pow(T_cc,5)+
0.00000000000006540196*pow(T_cc,6)-
1.573588E-017*pow(T_cc,7) ; /*Polinomio FLUENT*/
}else{
cp=1006.43;
}
gamma_cc=cp/(cp-R_gas);
u_cc_ant=u_cc;
nivel_entropia_cc_ant=nivel_entropia_cc;
beta_cc_ant=beta_cc;
a_cc_ant=a_cc;

/*ini Message("\nPara el siguiente paso de tiempo
se usara un gamma_cc %lg, correspondiente a la
temperatura %lg\n", gamma_cc, T_cc); end*/

/* Escritura de los resultados */

if (entrada==1) f_output=fopen("./entrada/udf_output.txt","a");
else f_output=fopen("./salida/udf_output.txt","a");

fprintf(f_output,"%d %.16lg %.16lg %.16lg %.16lg %.16lg
%.16lg %.16lg %.16lg %.16lg %.16lg\n", current_ts,
p_tot_cc_gauge, T_tot_cc, p_cc, T_cc, u_cc , a_cc, cp,
gamma_cc, lambda_cc, beta_cc, nivel_entropia_cc);

```

```

fclose(f_output);
}
}
return TRUE;
}

DEFINE_PROFILE(p_inlet,thread,var) {
if (myid==BC_node_id) {
    face_t face;
    calcular_NRBC_llamada_por_pres=FALSE;
    if((calcular_NRBC_llamada_por_pres==FALSE)
    && (calcular_NRBC_llamada_por_temp==FALSE) ) {
        calcular_NRBC_llamada_por_pres=calcula_NRBC();
    }

/* Imposicion de la BC de presion en la
entrada del calculo 3D*/

begin_f_loop(face,thread) {
/* Entrada */
    if (u_cc >= 0) {
F_PROFILE(face,thread,var)=p_tot_cc_gauge;
    } else {
F_PROFILE(face,thread,var)=p_cc-p_op;
    }
    }end_f_loop(face,thread)
}
}

DEFINE_PROFILE(p_outlet,thread,var) {
if (myid==BC_node_id) {
    face_t face;
    calcular_NRBC_llamada_por_pres=FALSE;
    if((calcular_NRBC_llamada_por_pres==FALSE)
    && (calcular_NRBC_llamada_por_temp==FALSE) ) {
        calcular_NRBC_llamada_por_pres=calcula_NRBC();
    }
}
}

```

```

        /* Imposicion de la BC de presion en la
        salida del calculo 3D*/
        if (radial==0) {
            begin_f_loop(face,thread) {
/* Salida */

                if (u_cc >= 0) {
F_PROFILE(face,thread,var)=p_cc-p_op;
                } else {
F_PROFILE(face,thread,var)=p_tot_cc_gauge;
                }
            }end_f_loop(face,thread)
        }else { /*radial equilibrium*/
            int i;
            double face_centroid[ND_ND];
            char string[MAX_LEN];
            double rho_v_theta_r[profile_length+1];
            /*[profile_length+1] para tener en cuenta
            el valor en 0, que sale del MoC*/

            double radial_coord[profile_length+1];
            double pres_radial_eq[profile_length+1];
            double pressure_face;
            double radius;

            current_ts_presion=N_TIME;

if (current_ts_presion!=last_ts_presion) {
            last_ts_presion=current_ts_presion;
            f_radial_eq=fopen("radial_eq.xy","r");
            /*Posicionamiento tras las 4 lineas de cabecera*/
            for (i=0;i<4;i++)
                fgets (string ,MAX_LEN , f_radial_eq);
                radial_coord[0]=0; /*la posición 0 no se usa*/
                rho_v_theta_r[0]=0;
/*Lectura del profile.xy*/
                for (i=1;i<profile_length+1;i++) {
fscanf(f_radial_eq, "%lg %lg",

```

```

&radial_coord[i], &rho_v_theta_r[i]);
}
fclose(f_radial_eq);

radial_coord[1]=0;
rho_v_theta_r[1]=0;

if (u_cc >= 0) {
    pres_radial_eq[0]=p_cc-p_op;
} else {
    pres_radial_eq[0]=p_tot_cc_gauge;
}

/*CALCULAR Perfil de presiones segun radial equilibrium*/
for (i=1;i<profile_length+1;i++) {
    pres_radial_eq[i]=pres_radial_eq[i-1]+
        (rho_v_theta_r[i]+rho_v_theta_r[i-1])/2*
        (radial_coord[i]-radial_coord[i-1]);
}
/* Imposicion del perfil de presiones en el outlet segun
radial equilibrium*/

begin_f_loop(face,thread) {
F_CENTROID(face_centroid,face,thread);
radius=pow(pow(face_centroid[0]-x_center,2)+
    pow(face_centroid[1]-y_center,2),0.5);
    /*change taking into account the direction of
    the surface*/
    i=0;
while (radius>radial_coord[i]) {
i++;
}
    pressure_face=pres_radial_eq[i-1]+
        (pres_radial_eq[i]-pres_radial_eq[i-1])/
        (radial_coord[i]-radial_coord[i-1])*
        (radius-radial_coord[i-1]);

F_PROFILE(face,thread,var)=pressure_face;

```

```

}end_f_loop(face,thread)
}
}
}
}

DEFINE_PROFILE(T_tot,thread,var) {
  if (myid==BC_node_id) {
    face_t face;
    calcular_NRBC_llamada_por_temp=FALSE;
    if((calcular_NRBC_llamada_por_pres==FALSE)
    && (calcular_NRBC_llamada_por_temp==FALSE) ) {
      calcular_NRBC_llamada_por_temp=calcula_NRBC();
    }
    /* Imposicion de la BC de temperatura total en el
    calculo 3D, que se utiliza solo si el flujo es
    entrante al dominio*/

begin_f_loop(face,thread) {
  F_PROFILE(face,thread,var)=T_tot_cc;
  }end_f_loop(face,thread)
}
}

DEFINE_ON_DEMAND(inicializar) {
/*el corchete de esta funcion no puede ir en
la misma linea que la cabecera*/

Domain *domain;
Thread *thread;
face_t face;
double basura;
double current_ft;
current_ft=CURRENT_TIME;
Message("\nEl FLOW_TIME de inicializacion de
WAM es, %f\n", current_ft);
domain = Get_Domain(1);
thread = Lookup_Thread(domain,zone_ID);

```



```

begin_f_loop(face,thread) {
if (PRINCIPAL_FACE_P(face,thread)) BC_node_id=myid;

}end_f_loop(face,thread)

#if !RP_HOST
  if (myid==BC_node_id) {
    /* CAMBIAR - Numero de vbles por timestep que
    se leen de Datos.1d dependiendo de si se
    acopla con WAM o con fluent*/

    if (anecoica_o_wam_o_fluent==1) variables_a_leer=5;
    /*WAM*/
    else variables_a_leer=7; /*Fluent*/

    if (entrada==1) {
/*ENTRADA*/

f_fluent=fopen("./entrada/Datos.cfd","a");
f_rehook=fopen("./entrada/rehook.txt","r");
for (contador=0;contador<cociente_time_steps;
contador++) {

fscanf(f_rehook, "%lg %lg %lg %lg %lg %lg %lg",
&flow_time_rehook_vector[contador],
&beta_vector[contador], &a_beta_vector[contador],
&nivel_entropia_beta_vector[contador],
&nivel_entropia_entrada_vector[contador],
&basura, &basura);

fprintf(f_fluent, "%.16lg %.16lg %.16lg %.16lg
%.16lg %.16lg %.16lg\n",
flow_time_rehook_vector[contador],
beta_vector[contador], a_beta_vector[contador],
nivel_entropia_beta_vector[contador],
nivel_entropia_entrada_vector[contador],
frac_aire_quemado, frac_aire_limpio);

```

```

}
fclose(f_rehook);
} else {

/*SALIDA*/
    f_fluent=fopen("./salida/Datos.cfd","a");
    f_rehook=fopen("./salida/rehook.txt","r");
    for (contador=0;contador<cociente_time_steps;
    contador++) {
        fscanf(f_rehook, "%lg %lg %lg %lg %lg %lg %lg",
        &flow_time_rehook_vector[contador],
        &lambda_vector[contador], &a_lambda_vector[contador],
        &nivel_entropia_lambda_vector[contador],
        &nivel_entropia_salida_vector[contador],
        &basura, &basura);

        fprintf(f_fluent, "%.16lg %.16lg %.16lg %.16lg %.16lg
        %.16lg %.16lg\n", flow_time_rehook_vector[contador],
        lambda_vector[contador], a_lambda_vector[contador],
        nivel_entropia_lambda_vector[contador],
        nivel_entropia_salida_vector[contador],
        frac_aire_quemado, frac_aire_limpio);

        if (inicializar_WAM==1){
            fprintf(f_fluent, "%.16lg %.16lg %.16lg %.16lg
            %.16lg %.16lg %.16lg\n", current_ft,
            lambda_vector[contador], a_lambda_vector[contador],
            nivel_entropia_lambda_vector[contador],
            nivel_entropia_salida_vector[contador],
            frac_aire_quemado, frac_aire_limpio);
        }
    }
    fclose(f_rehook);
}
fclose(f_fluent);
}
#endif
}

```

OpenWAM CFD connection

```
// -----  
  
#pragma hdrstop  
  
#include "TCFDConnection.h"  
#include <math.h>  
#include "TTubo.h"  
#include <dos.h>  
#include <sys/stat.h>  
  
// -----  
  
fastcall TCFDConnection::TCFDConnection(nmTypeBC TipoCC,  
int numCC, nmTipoCalculoEspecies SpeciesModel,  
int numeroespecies, nmCalculoGamma GammaCalculation,  
bool ThereIsEGR) : TCondicionContorno(TipoCC,  
numCC, SpeciesModel, numeroespecies, GammaCalculation,  
ThereIsEGR) {  
  
    FirstTime = true;  
    FUpdateTime = 0;  
    FExistFile = false;  
    FSpecieCFD.resize(numeroespecies, 0.);  
}  
  
__fastcall TCFDConnection::~TCFDConnection() {  
}
```

```

void TCFDConnection::ReadBoundaryData(char *FileWAM,
fpos_t &filepos, int NumberOfPipes, TTubo **Pipe) {

FTuboExtremo = new stTuboExtremo[1];
FTuboExtremo[0].Pipe = NULL;

int i = 0;
while (FNumeroTubosCC < 1 && i < NumberOfPipes) {
if (Pipe[i]->getNodoIzq() == FNumeroCC) {
FTuboExtremo[FNumeroTubosCC].Pipe = Pipe[i];
FTuboExtremo[FNumeroTubosCC].TipoExtremo = nmIzquierda;
FCC = &(FTuboExtremo[FNumeroTubosCC].Beta);
FCD = &(FTuboExtremo[FNumeroTubosCC].Landa);
FNodoFin = 0;
FIndiceCC = 0;
FNumeroTubosCC++;
}
if (Pipe[i]->getNodoDer() == FNumeroCC) {
FTuboExtremo[FNumeroTubosCC].Pipe = Pipe[i];
FTuboExtremo[FNumeroTubosCC].TipoExtremo = nmDerecha;
FCC = &(FTuboExtremo[FNumeroTubosCC].Landa);
FCD = &(FTuboExtremo[FNumeroTubosCC].Beta);
FNodoFin = FTuboExtremo[FNumeroTubosCC].Pipe->getNin() - 1;
FIndiceCC = 1;
FNumeroTubosCC++;
}
i++;
}

FILE *fich = fopen(FileWAM, "r");
fsetpos(fich, &filepos);

char TMP[256];
fscanf(fich, "%s ", &TMP);
FCFDModel = TMP;
FCFDout = new char[(int)strlen(FCFDModel)];
GetName(FCFDModel, FCFDout, ".1d");

```

```

// GetName(FCFDModel, FCFDout, ".cfd"); //< CFD
FCFDin = new char[(int)strlen(FCFDModel)];
GetName(FCFDModel, FCFDin, ".cfd");
// GetName(FCFDModel, FCFDin, ".1d"); //< CFD

// fscanf(fich, "%d ", &FCFDTiemStep);

fgetpos(fich, &filepos);
fclose(fich);

FFraccionMasicaEspecie = new double[FNumeroEspecies - FIntEGR];
for (int i = 0; i < FNumeroEspecies - 1; i++) {
FFraccionMasicaEspecie[i] = FTuboExtremo[0].Pipe->
GetFraccionMasicaInicial(i);
}
if (FHayEGR) {
FFraccionMasicaEspecie[FNumeroEspecies - 1] =
FTuboExtremo[0].Pipe->GetFraccionMasicaInicial
(FNumeroEspecies - 1);
}
}

void TCFDConnection::CalculaCondicionContorno(double Time) {

struct stat buf;

FILE *fileout;
FILE *filein;

double FraccionMasicaAcum = 0.;
double comprobar_filein; /*variable para controlar
que realiza una lectura valida del fichero filein*/

if (FirstTime) {
fileout = fopen(FCFDout, "r");
if (fileout != NULL) {
fclose(fileout);
remove(FCFDout);
}
}
}

```

```

}
FirstTime = false;
}

for (int j = 0; j < FNumeroEspecies - 2; j++) {
FFraccionMasicaEspecie[j] = FTuboExtremo[0].Pipe->
GetFraccionMasicaCC(FIndiceCC, j);
FraccionMasicaAcum += FFraccionMasicaEspecie[j];
}
FFraccionMasicaEspecie[FNumeroEspecies - 2] =
1. - FraccionMasicaAcum;
if (FHayEGR)
FFraccionMasicaEspecie[FNumeroEspecies - 1] =
FTuboExtremo[0].Pipe->GetFraccionMasicaCC
(FIndiceCC, FNumeroEspecies - 1);

fileout = fopen(FCFDout, "a");
/*cout << "version actual" << endl; */
fprintf(fileout, "%.16lg %.16lg %.16lg %.16lg %.16lg\n",
Time, *FCC * ARef, FTuboExtremo[0].Entropia * ARef,
FFraccionMasicaEspecie[0], FFraccionMasicaEspecie[1]);

fclose(fileout);

if (!FExistFile) {
filein = fopen(FCFDin, "r");

while (filein == NULL) {
cout << "INFO: Waiting for the file creation" << endl;
sleep(30);
filein = fopen(FCFDin, "r");
}
fclose(filein);
FExistFile = true;
}

// stat(FCFDin, &buf);
//

```

```

// while (difftime(buf.st_mtime, FUpdateTime) == 0) {
// sleep(30);
// stat(FCFDin, &buf);
// }

double t0 = 0.;
double t1 = 0.;
double b0 = *FCC;
double b1 = *FCC;
double AA0 = FTuboExtremo[0].Entropia;
double AA1 = FTuboExtremo[0].Entropia;
double nivel_entropia_CDO=FTuboExtremo[0].Entropia;
double nivel_entropia_CD1=FTuboExtremo[0].Entropia;
double a_CDO=ARef;
double a_CD1=ARef;
filein = fopen(FCFDin, "r");
while (t1 < Time-1e-16) {

t0 = t1;
b0 = b1;
AA0 = AA1;
nivel_entropia_CDO=nivel_entropia_CD1;
a_CDO=a_CD1;

comprobar_filein=EOF;
/*cout << "\ndatos del primer while: t1 "
<< t1 << " Time " << Time-1e-16 << "\n"; */

while (comprobar_filein==EOF) {

/*comprobar_filein=fscanf(filein, "%lg %lg %lg",
&t1, &b1, &AA1);
for (int j = 0; j < FNumeroEspecies - 1; j++) {
comprobar_filein=fscanf(filein, "%lg", &FSpecieCFD[j]);
}
if (FHayEGR)
comprobar_filein=fscanf(filein, "%lg",
&FSpecieCFD[FNumeroEspecies - 1]);

```

```

fscanf(filein, "\n");          */
comprobar_filein=fscanf(filein,"%lg %lg %lg %lg %lg
%lg %lg", &t1, &b1, &a_CD1, &nivel_entropia_CD1, &AA1,
&FSpecieCFD[0], &FSpecieCFD[1]);

/*cout << "\nLeo los valores " << t1 << "\n y
comprobar_wam vale " << comprobar_filein; */

if ((t1 < Time-1e-16) && (comprobar_filein==EOF)) {
    stat(FCFDin, &buf);
    while (difftime(buf.st_mtime, FUpdateTime) == 0) {
        cout << "INFO: Waiting for an update" <<
difftime(buf.st_mtime, FUpdateTime) << endl;
        sleep(3);
        stat(FCFDin, &buf);
    }
    FUpdateTime = buf.st_mtime;
}

}

}

}

fclose(filein);
double TimeStep = t1 - t0;
double DeltaTime = Time - t0;

double Beta = Interpola(b0, b1, TimeStep, DeltaTime);
double AA = Interpola(AA0, AA1, TimeStep, DeltaTime)/ARef;
double a_CD = Interpola(a_CD0, a_CD1, TimeStep, DeltaTime);
double nivel_entropia_CD = Interpola(nivel_entropia_CD0,
nivel_entropia_CD1, TimeStep, DeltaTime)/ARef;

double Ucc_ant=FTuboExtremo[0].Pipe->GetVelocity1(FNodoFin);
double AA_ant=FTuboExtremo[0].Pipe->GetEntropy1(FIndiceCC);
double signo_Ucc;

if (FIndiceCC==1) {          /*tubo salida*/

```



```

if (Ucc_ant>0) {      /*la corriente salia por el tubo
de salida en el pasoanterior*/

/* nivel_entropia_cc es el de WAM,
por lo que no hay que tocarlo*/

*FCD = Beta / ARef +
a_CD*log(FTuboExtremo[0].Entropia/nivel_entropia_CD)/ARef;

    signo_Ucc=(*FCC-*FCD);

if (Ucc_ant*signo_Ucc < 0 ) {
/*hay cambio de signo, tomamos
el del paso anterior*/

    FTuboExtremo[0].Entropia= AA_ant;
*FCD = Beta / ARef +
a_CD*log(FTuboExtremo[0].Entropia/nivel_entropia_CD)/ARef;
}
} else if (Ucc_ant<0) {
FTuboExtremo[0].Entropia= AA;
*FCD = Beta / ARef +
a_CD*log(FTuboExtremo[0].Entropia/nivel_entropia_CD)/ARef;

signo_Ucc=(*FCC-*FCD);

if (Ucc_ant*signo_Ucc < 0 ) {
/*hay cambio de signo, tomamos el del paso anterior*/
FTuboExtremo[0].Entropia= AA_ant;
*FCD = Beta / ARef +
a_CD*log(FTuboExtremo[0].Entropia/nivel_entropia_CD)/ARef;
}

} else {

/*hay cambio de signo, tomamos el del paso anterior*/
FTuboExtremo[0].Entropia= AA_ant;

```

```

*FCD = Beta / ARef +
a_CD*log(FTuboExtremo[0].Entropia/nivel_entropia_CD)/ARef;
}
}

if (FIndiceCC==0) {      /*tubo entrada*/

if (Ucc_ant<0) {
/*la corriente salia por el tubo de salida
en el pasoanterior*/

/* nivel_entropia_cc es el de WAM, por lo que
no hay que tocarlo*/

*FCD = Beta / ARef +
a_CD*log(FTuboExtremo[0].Entropia/nivel_entropia_CD)/ARef;

signo_Ucc=(*FCC-*FCD);

if (Ucc_ant*signo_Ucc < 0 ) {
/*hay cambio de signo, tomamos el del paso anterior*/
FTuboExtremo[0].Entropia= AA_ant;

*FCD = Beta / ARef +
a_CD*log(FTuboExtremo[0].Entropia/nivel_entropia_CD)/ARef;
}

} else if (Ucc_ant>0) {
FTuboExtremo[0].Entropia= AA;
*FCD = Beta / ARef +
a_CD*log(FTuboExtremo[0].Entropia/nivel_entropia_CD)/ARef;
signo_Ucc=(*FCC-*FCD);

if (Ucc_ant*signo_Ucc < 0 ) {
/*hay cambio de signo, tomamos el del paso anterior*/
FTuboExtremo[0].Entropia= AA_ant;

*FCD = Beta / ARef +

```

```

a_CD*log(FTuboExtremo[0].Entropia/nivel_entropia_CD)/ARef;
}

} else {
/*hay cambio de signo, tomamos el del paso anterior*/
FTuboExtremo[0].Entropia= AA_ant;

*FCD = Beta / ARef +
a_CD*log(FTuboExtremo[0].Entropia/nivel_entropia_CD)/ARef;
}
}

// ! Flow from de pipe to the cfd model
}
#pragma package(smart_init)

```

